

**IMPLANTABLE BIOMEDICAL DEVICES FOR LOCALIZED BREAST CANCER
DRUG DELIVERY**



DISSERTATION

Submitted to the Graduate Faculty

In Partial Fulfillment of the Requirement for the

Degree of **Doctor of Philosophy** in the

Department of Materials Science and Engineering

African University of Science and Technology, Abuja-Nigeria

By:

DANYUO YIPORO (ID No: 70083)

October, 2015.

PhD Dissertation Committee:

Prof. Wole Soboyejo, Chair (Princeton University, NJ, USA)

Dr. O. Shola Odusanya (SHESTCO, Abuja, Nigeria)

Dr. Karen Malatesta (Princeton University, NJ, USA)

Associate Prof. Steve A. Adeshina (Nigerian Turkish Nile University, Abuja, Nigeria)


**IMPLANTABLE BIOMEDICAL DEVICES FOR LOCALIZED BREAST CANCER
DRUG DELIVERY**

By:
Danyuo Yiporo


A THESIS APPROVED BY THE MATERIALS SCIENCE AND ENGINEERING
DEPARTMENT


RECOMMENDED:


Supervisor, Professor Wole Soboyejo


.....
Co-supervisor, Dr. O. Shola Odusanya


.....
Committee Member: Dr. Karen Malatesta


.....
Committee Member: Associate Prof. Steve A. Adeshina


.....
Head, Dept. of Materials Science and Engineering: Prof. Azikiwe Peter Onwualu


.....
Vice President of Academic: Professor Charles E. Chidume, FAS

16th October, 2015.
Date:

Copyright by Danyuo Yiporo, @ October 2015.
All Rights Reserved.

DEDICATION

This thesis is dedicated to my late father; Ottuor James Danyuo, whose countless effort in my academia cannot be forgotten. May his gentle soul, the soul of my stepmother, Danyuo Yirtunona Eunice and all the faithful departed rest in peace. Amen.

ABSTRACT

This thesis focused on an implantable encapsulated structures that can deliver localized heating and controlled released of prodigiosin (PG) (a cancer drug) synthesized by bacteria (*Serratia marcescens* (subsp. *marcescens*)). Prototypical poly-dimethyl-siloxane (PDMS) packages, containing well-controlled micro-channels and drug storage compartments, were fabricated along with a drug-storing polymer produced by free radical polymerization of Poly(N-isopropylacrylamide)(PNIPA)-based gels. The mechanisms of drug diffusion of P(NIPA)-based gels were elucidated. Scanning electron microscopy (SEM) and optical microscopy were used to study the heterogeneous porous structure of the P(NIPA)-based gels. The release exponents, n , of the gels were found to be between 0.5 and 0.81. This is in the range expected for Fickian diffusion ($n = 0.5$). Deviation from Fickian diffusion was also observed ($n > 0.5$). The gel diffusion coefficients were shown to vary between $2.1 \times 10^{-12} \text{ m}^2/\text{s}$ and $4.8 \times 10^{-6} \text{ m}^2/\text{s}$. Statistical analyses were carried out on the variations of the data presented using Minitab software package 16. HPLC analysis on the purity of prodigiosin synthesized was determined to be 92.8%. The effects of localized release of PG and paclitaxel (PT) on cell viability were elucidated via clonogenic assay testing on MDA-MB-231 breast cancer cell line. The results were validated using models to establish the effective diffusivity of PG and bromophenol blue (BB) released from the devices into a surrounding scaffold that mimicked cancer tissue. Degradable implants made from poly(lactic-glycolic-acid) (PLGA) were also studied to determine their potential application for drug delivery. Degradation rates and drug release kinetics were elucidated. Implications in the results were discussed for localized treatment of breast cancer via controlled drug delivery systems combined with localized hyperthermia.

Keywords: localized drug delivery, biomedical device, hydrogels, prodigiosin, biodegradable devices, degradation rate, cancer drug delivery, cell viability and statistics.

Table of Contents

Pages

All Rights Reserved.....	ii
DEDICATION.....	iii
ABSTRACT.....	iv
Table of Contents.....	v
Acknowledgements.....	x
Publications in PhD Focus.....	xii
Other Publications and Conference Presentations.....	xiii
List of Figures.....	xiv
List of Tables.....	xix
CHAPTER ONE.....	1
1.0 Background and Introduction.....	1
1.1 Introduction.....	1
1.2.1 Implantable Biomedical Devices.....	3
1.2.2 Cancer and Cancer Statistics.....	4
1.2.3 Major Causes of the High Incidence of Breast Cancer.....	6
1.2.3 Stages in Cancer Development.....	8
1.2.4. Metastasis.....	9
1.2.4 Microenvironment Promoting Tumor Migration.....	11
1.4 The Primary Goal.....	13
1.5 Scope of Work.....	13
1.6 Bibliography.....	15
2.1 Introduction.....	19
2.2 Cancer Statistics.....	21
2.3 The Symptoms of Breast Cancer.....	21
2.4 Challenges with Current Cancer Treatment.....	22

2.5.0 Cancer Drugs	23
2.5.1 Paclitaxel TM (PT)	23
2.5.2 Prodigiosin (PG)	24
2.6 Cancer Drug Delivery	26
2.8 Drug Delivery Polymers	29
2.9 Hydrogels	29
2.9.1 Poly(N-Isopropyl acrylamide) (PNIPA)-based Hydrogels	30
2.9.2 Polyacrylamide-based Composite	33
2.10 Biodegradable Polymers	35
2.11 Mechanism of Polymer Degradation	37
2.12 Polydimethylsiloxane (PDMS)	40
2.13.0 Characteristics of P(NIPA)-based Hydrogels	41
2.13.1 Swelling Kinetics	41
2.13.2 De-Swelling Kinetics	43
2.13.3 Equilibrium Swelling Measurements	43
2.14.0 Kinetics of Swollen Hydrogels	44
2.14.1 Free Energy	44
2.14.2 Swelling Characteristics of Ionic Hydrogels	44
2.14.3 Factors Affecting the Swelling Characteristics of Ionic Hydrogels	46
2.15 Strain on Hydrogels Due to Swelling	47
2.16 The Goals of Drug Delivery	48
2.17 Drug and Tumor Transport Mechanisms	49
2.18 Hydrogels and their Drug Release Mechanisms	50
2.19 Determination of Drug Concentration in Tumors	52
2.22 Effective Diffusion in Porous Media	55
2.23 Hyperthermia and Heat Cycles for Cancer Treatment	57
2.24 Nanoparticles for Drug Delivery	58

2.24.1 Magnetic nanoparticles.....	58
2.24.2 Magnetic Nanoparticles Heating	59
2.25.0 Biomaterials and Tissue Integration	60
2.25.1 Cell/ Surface Interactions	60
2.25.2 PDMS Surface and Cell Adhesion	61
2.25.3.0 Techniques for PDMS Surface Modification	62
2.25.3.1 Boiling Water Approach.....	62
2.25.3.2 Ultra-Violet (UV)/Ozone (O) Treatment of PDMS.....	63
2.25.3.3 FTIR-ATR Measurements.....	63
2.26 Conclusion	65
2.27 Bibliography	65
3:0 Swelling of Poly(N-isopropyl acrylamide) (PNIPA)-Based Hydrogels with Bacterial-Synthesized Prodigiosin for Localized Cancer Drug Delivery.....	75
3.1 Introduction	75
3.2.0 Materials and Methods	76
3.2.1 Materials	76
3.2.2 Preparation of P(NIPA)-Based Hydrogels	77
3.2.3 Prodigiosin (PG) Extraction	79
3.2.4 Determination of the Purity of Prodigiosin Extracted	80
3.2.5 Phase Transition Temperature Measurements.....	81
3.2.6 Fluid/Drug Concentrations	82
3.2.7 Swelling Ratios and Transport Measurement.....	82
3.2.8 Strain Induced in Hydrogels Due to Swelling	83
3.2.9 Drug/Fluid Release from PNIPA-based Hydrogels.....	84
3.2.10 Statistical Analysis	85
3.3.0 Results and Discussion	86
3.3.1 Gel Characterization.....	86

3.3.2 Swelling Characteristics	87
3.3.3 LCSTs of P(NIPA)-based Hydrogels	89
3.3.4 Gel Swelling and PG Release.....	90
3.3.5 Strains (ϵ) Induced in Hydrogels Due to Swelling	92
3.3.6 Purity of Extracted Prodigiosin	92
3.4 Summary and Concluding Remarks.....	93
3.5 Bibliography	94
4.0 Prodigiosin Release from an Implantable Biomedical Device: Kinetics of Localized Cancer Drug Release	110
4.1 Introduction	110
4.2 Experimental Materials and Procedures	111
4.2.1 Materials and Methods	111
4.2.2 Preparation of P(NIPA)-Based Hydrogels	111
4.2.3 Poly (Di-methyl-Siloxane) (PDMS) Fabrication.....	113
4.2.4 Encapsulation of P(NIPA) into PDMS Capsules	114
4.3.0 Results and Discussion.....	115
4.3.1 Gel Morphology	115
4.3.2 Swelling and Re-swelling Ratios.....	115
4.3.3 Swelling and Re-swelling Characteristics	116
4.3.4 Diffusion and Swelling Mechanisms.....	117
4.3.5 Modeling of Fluid Release	119
4.3.6 Effect of Drug Diffusion across Channel Lengths	121
4.4 Implications	122
4.5 Conclusions	124
4.6 Bibliography	125
5.0 Prodigiosin Release from an Implantable Biomedical Device: Effect on Cell Viability	142
5.1 Introduction	142

5.2.0 Materials and Methods	143
5.2.1 Materials	143
5.2.2 P(NIPA)-based Scaffold	144
5.2.3 Implantable Device.....	144
5.2.4 Cell Culture	145
5.2.5 Clonogenic Assay	146
5.2.6 Scaffold Diffusion Experiment.....	147
5.2.7 Diffusion Model	148
5.3.0 Results and Discussion	151
5.3.1 Cancer Cells and Colony Growth.....	151
5.3.2 Effects of Drug Release on Cell Viability	152
5.3.3 Effect of Temperature on Cell Viability.....	152
5.3.4 Effect of Temperature and Drug Release on Cell Viability	153
5.3.5 Cytotoxicity of the PG and PT	154
5.3.6 Statistical Testing on Cell Viability.....	155
5.4 Effective Diffusivity of Drug Release into Scaffolds	155
5.5 Implications	157
5.6 Conclusions	159
5.7 Bibliography	160
6.0 Pulsated Drug Release from PLGA-Based composites for Extended Delivery	171
6.1.0 Introduction	171
6.2.0 Materials and Methods.	172
6.2.1 Materials	172
6.2.2 Preparation of Drug Concentrations	173
6.2.3 Dissolution of Polymers	173
6.2.4 Formation of PLGA-Based Minirods	174
6.2.3 Characterization of Samples	174

6.2.4.0 Degradation and Drug Release	175
6.3.0 Results and Discussion	178
6.3.1 Characterization and Morphological Changes.....	178
6.3.2 Water Absorption and Mass Loss.....	180
6.3.3 Drug Diffusion and Reaction Rates	181
6.3.4 Thermal Analysis.....	183
6.4 Implications	184
6.5 Conclusion.....	185
6.6 Bibliography	186
7.0 Perspectives and Conclusions	196
7.1.0 Recommendations for Future Work	199
7.1.1 Surface Modification and Cell Adhesion.....	199
7.1.2 Mechanical Characterization of Polymers.....	199
7.1.3 Design of a Novel Degradable Implant.....	200
7.1.4 Animal Trials.....	200
7.2 Bibliography	201

Acknowledgements

I am very grateful to the World Bank STEP-B program (grand No. 4304-UNI), the World Bank African Centres of Excellent Project (the Pan-African Materials Institute (PAMI) with grand No. P126974), the African Development Bank (ADB) with grand No. 2100155014816 (Support to Network of African Institutions of Science and Technology project) and the African Capacity Building Foundation with Grant No. 292 (Capacity Building Initiative for African Universities in Science and Technology project) for the financial support. The authors are also grateful to the Nelson Mandela Institute (NMI) and the African University of Science and Technology (AUST) for the scholarships given to me. Lastly, we are grateful to Suleman Nasiru from the University for Development Studies, Ghana, for his assistance in the statistical analysis.

Appreciation is also extended to Prof. Eric Garfunkel (Rutgers University) and Dr. Adeoye Soyemi (Eastbourne General Hospital, Eastbourne, England) for useful technical discussions on cancer treatment. I do appreciate my PhD Dissertation Committee: Prof. Wole Soboyejo, Dr. O. Shola Odusanya, Dr. Steve A. Adeshina (Assoc. Prof.) and Dr. Karen Malatesta for their countless support and guidance.

The best thing that has ever happen to me was to have Prof. Wole Soboyejo as my Ph.D. advisor. His supervision was incredible. I also appreciate the effort of my editorial team (Prof. Wole Soboyejo, Dr. O. Shola Odusanya, Dr. Yusuf Oni, Dr. Nicolas Anuku and Dr. Karen Malatesta) for their useful comments and suggestions.

My sincere gratitude goes to the Biomedical Research Group at the African University of Science and Technology, Abuja-Nigeria and the African Materials Research Society (AMRS) for their useful suggestions.

Finally, I am very grateful to the entire Danyuo's family for their time and support.

Publications in PhD Focus

1. **Y. Danyuo**, S. Dozie-Nwachukwu, J. D. Obayemi, C. J. Ani, O. S. Odusanya, Y. Oni, N. Anuku, K. Malatesta and W. O. Soboyejo. "Swelling of Poly(N-isopropyl acrylamide) (PNIPA)-Based Hydrogels With Bacterial-Synthesized Prodigiosin for Localized Cancer Drug Delivery". Publisher (ELSEVIER); Journal of Materials Science and Engineering C (MSEC), Vol. 59 (2016) pp19-29. (available online, 28 September 2015). Doi:10.1016/j.msec.2015.09.090.
2. **Y. Danyuo**, J. D. Obayemi, S. Dozie-Nwachukwu, C. J. Ani, O. S. Odusanya, Y. Oni, N. Anuku, K. Malatesta and W. O. Soboyejo. "Prodigiosin Release From an Implantable Biomedical Device: Kinetics of Localized Cancer Drug Release". Publisher (ELSEVIER); Journal of Materials Science and Engineering C (MSEC), Vol. 42 (2014) pp734-745. Doi:10.1016/j.msec.2014.06.008.
3. **Y. Danyuo**, O. Oberaifo, J. D. Obayemi, S. Dozie-Nwachukwu, C. J. Ani, O. S. Odusanya, M. G. Zebaze Kana, K. Malatesta and W. O. Soboyejo. "Pulsated Drug Release from PLGA-Based composites for Extended Delivery". Journal of Bioactive and Compatible Polymers (JBCP) (Submitted, October, 2015).
4. **Y. Danyuo**, C. J. Ani, J. D. Obayemi, S. Dozie-Nwachukwu, O. S. Odusanya, Y. Oni, N. Anuku, K. Malatesta and W. O. Soboyejo. Book: "Advanced Materials for Energy, Biomedical and Multifunctional Structures", Chapter Titles: Prodigiosin Release from an Implantable Biomedical Device: Effect on Cell Viability. Trans Tech Publications Ltd., Switzerland. Conference book of proceedings (2015) (Under Review).

Other Publications and Conference Presentations

1. J. D. Obayemi, S. Dozie-Nwachukwu, **Y. Danyuo**, O. S. Odusanya, N. Anuku, K. Malatesta and W. O. Soboyejo. “Biosynthesis and the Conjugation of Magnetite Nanoparticles With Luteinizing Hormone Releasing Hormone (LHRH)”. ELSEVIER; J. of Mater. Sci. and Engr. C (MSEC), Vol. 46 (2015) pp482-496. DOI: 10.1016/j.msec.2014.10.081.
2. J. D. Obayemi, **Y. Danyuo**, S. Dozie-Nwachukwu, O. S. Odusanya, N. Anuku, K. Malatesta, W. Yu, K. E. Uhrich and W. O. Soboyejo. “Injectable Biodegradable Prodigiosin-Loaded Microparticles for Localized Cancer Drug Delivery”. Publisher (ELSEVIER); Journal of Materials Science and Engineering C (MSEC) (under review). Manuscript Number: MSEC-D-15-00246R1.
3. **Y. Danyuo**, O. Oberiafor, O. S. Odusanya, M. G. Zebaze Kana and W. O. Soboyejo. “Prodigiosin Loaded PLGA-Based composites: for Extended Localized Drug Release”. 14th International Union of Materials Research Societies (IUMRS) - International Conference on Advanced Materials October 25 ~ 29 (2015), ICC JEJU, KOREA.
4. **Danyuo Yiporo**, Winston Wole Soboyejo and O. S. Odusanya. Implantable Biomedical Devices for Localized Breast Cancer Drug Delivery. AUST PhD Colloquium 2015. Book of Proceedings. 22nd January 2015.
5. **Y. Danyuo**, J. D. Obayemi, S. Dozie-Nwachukwu, C. J. Ani, O. S. Odusanya, Y. Oni, N. Anuku, K. Malatesta and W. O. Soboyejo. Biomedical Implants for Localized Cancer Treatment: Experiments and Models. The 7th International African Materials Research Society, Addis-Ethiopia, (07-14th December, 2013).
6. **Y. Danyuo**, J. D. Obayemi, S. Dozie-Nwachukwu, C. J. Ani, O. S. Odusanya, Y. Oni, N. Anuku, K. Malatesta and W. O. Soboyejo. Biomedical Implants for Localized Cancer Treatment: Experiments and Models. A Joint Presentation at the 1st International Conference of the NANOMEDICINE Society of Nigeria and the Nigerian Engineered Materials Conference at AUST-Abuja.”. (25th – 29th November, 2013).
7. **Y. Danyuo**, J. D. Obayemi, S. Dozie-Nwachukwu, C. J. Ani, O. S. Odusanya, Y. Oni, N. Anuku, K. Malatesta and W. O. Soboyejo. Implantable BIOMEMS for localized cancer drug delivery. Nigerian Engineered Materials Conference at Obafemi Awolowo University, Ile Ife. (20th – 24th November, 2012).
8. **Y. Danyuo** and S. Dozie-Nwachukwu. “Nanoparticles and BioMEMS for Cancer Detection and Treatment”. Presentation at AUST, During the Visit of World Bank Vice President, 2012.
9. **Danyuo Yiporo**, S.O. Dozie-Nwachukwu, G.A. Etuk-Udo, O. Oberiafor, M. C. Ilouno., T. M. Meshack, A. Agwu, O. S. Odusanya and W. O. Soboyejo. BIOMEMS for breast cancer drug delivery. Nigerian Engineered Materials Conference at Akure (20th – 24th November, 2011).

List of Figures

Figure 1.1: Drug concentration following absorption of therapeutic agent as a function of time..	3
Figure 1.2: Shows the growth rate of cancer cells compared with the normal cell growth.....	5
Figure 1.3: Stages in Cancer Development.....	9
Figure 1.4: Steps in the Metastasis Process	10
Figure 1.5: The tumor microenvironment and its role in promoting tumor growth	11
Figure 1.6: polymer implants loaded with BCNU are lined in a human brain tumor resection cavity.....	13
Figure 2.1: Illustrating the anatomy of a woman’s breast: (a) without tumor and (b) with tumor located within the breast..	20
Figure 2.2: Summary of the mechanisms underlying liposome-based drug delivery to tumors for the heat-sensitive liposome system.....	23
Figure 2.3: (a) The Chemical Structure of PT, (b) Nomenclature of PT and (c) Complex of α , β Tubulin Subunits and PT is shown as Yellow Stick.	24
Figures 2.4: Prodigiosin: (a) Chemical Structure of Prodigiosin, (b) synthesized prodigiosin from <i>Serratia marcescens</i> at Sheda Science and Technology Complex, Abuja, Nigeria. (c) Fractions of Purified Prodigiosin.	25
Figure 2.5: Optimum conditions required for maximum production of prodigiosin concentration were achieved (at time 30 h, 30°C and pH 8.0).	26
Figure 2.6a: A variety of different delivery strategies that are currently being used or in testing stage to treat human cancers.	27
Figure 2.6b: Multi-well silicon-based drug-release device, adapted.	27
Figure 2.7: Schematic illustration of transdermal drug delivery system	28
Figure 2.8: Phase Diagram for P(NIPA)-based Hydrogel in Water	32
Figure 2.9: Shows the Polymer Unit Structures of PGA, PLA, PLGA and PLGA-PEG:Polymer Unit Structures: Typical Synthetic Route of a PLGA-PEG Diblock Copolymer.....	36
Figure 2.10: Shows a Linear Poly-dimethyl-siloxane (PDMS).....	40
Figure 2.11: Illustration of Mesh Size in a Hydrogel at; (A) Swollen State and (B) De-Swollen State.....	42

Figure 2.12: Scheme of Drug Release and Local Drug Concentration from Three Theoretical Implant Types.	49
Figure 2.13: Schematics of Drug Release Profiles Resulting from Diffusion Controlled Release; (a) from a Matrix Type Device (B) From a Diffusion through a Controlled Channel.	52
Figure 2.14: Average doxorubicin concentration in rabbit liver tumors as a function of distance from an implant for 4 days after tumor treatment.	53
Figure 2.15: Simplified scheme of drug transport from an implant centrally placed in a liver tumor	54
Figure 2.16: Illustrate the Iron Oxide Crystal Structure Showing the Arrangement of Fe ⁺² and Fe ⁺³ ions on the FCC structure of magnetite.	58
Figure 2.17: Schematic Representation of Cell or Surface Interaction of Cell Adhesion to A Biomaterial Substrate.....	60
Figure 2.18: FTIR-ATR spectra from: (I) Sylgard-184 treated for UVO equal to 0 min (A), 10 min (B) and 60 min (C). (II) Extracted poly(vinyl methyl siloxane) (PVMS) samples treated with UVO for various times ranging from 0 to 30 min	64
Figure 3.1: LCD Microscopy Analysis of PNIPA-Based Hydrogels: (a) Homopolymer (100 mol% of NIPA and (b) 95 mol% of P(NIPA)-5 mol% of AM; (c) 90 mol% of P(NIPA)-10 mol% of AM; and (d) P(NIPA) with 85 mol% of P(NIPA)-15 mol% of AM.	97
Figure 3.2: Microscopy Analysis of P(NIPA)-Based gels: (a) P(NIPA-co-AM-co-BMA) (90:5:5 mol%); (b) P(NIPA-co-AM-co-BMA) (85:5:10 mol%)(imaged with Celestron Microscope); (c) P(NIPA-co-AM-co-BMA) (90:5:5 mol%) and (d) P(NIPA-co-AM-co-BMA) (85:5:10 mol%)(Imaged with Nikon Inverted Microscope).....	98
Figure 3.3: Average Swelling Ratios of P(NIPA)-based Hydrogels at 28°C (room temperature) for 30 hrs.	99
Figure 3.4: Effect of Temperature on the Average Swelling Ratio of P(NIPA)-Based Hydrogels in 2.5 mg/ml 30 hrs in PG.....	99
Figure 3.5: Swelling Ratio of PNIPA-Based Hydrogels in Different Fluids (5 ml of 2 µg/ml of drug solutions) or distilled water at 28°C.	100
Figure 3.6: Equilibrium Volume Ratio of PNIPA-Based Hydrogels Soaked in Prodigiosin at 28°C.....	101
Figure 3.7: Effects of PG on the LCSTs of P(NIPA)-based Hydrogels.	101
Figure 3.8: Fraction of Drug (20 µg/ml of Prodigiosin) Release from P(NIPA)-Based Hydrogels Versus Int (s) at 37°C.	102
Supplimentary Data (Figures)	107

Figure 4.1: Schematic Diagrams of Mold and PDMS Components; (a) Aluminium slab; (b) Brass slab with Central Cylindrical rod; (c) Fabricated Mold; (d) Encapsulated Biomedical Device with Microchannels for Drug Elution; and 1(e) Hyperthermia System with a PID Temperature Controller.	128
Figure 4.2: SEM Image of P(NIPA)-Based Hydrogels: (a) Homopolymer and (b) P(NIPA)-Composite (With 15 mol% of acrylamide (AM)), (c) P(NIPA)-Copolymer (5 mol% of AM and 5 mol% of BMA) and (d) P(NIPA)-Copolymer (5 mol% of AM and 10 mol% of MA).	129
Figure 4.3: Swelling Ratio of P(NIPA)-Based Hydrogels and P(NIPA)-Based Copolymers in Different Fluids at 28°C. Error Bars Show 95% Confidence Interval of the Mean.	130
Figure 4.4: Swelling Ratios of PNIPA-based Hydrogels in Prodigiosin at 28°C. Error Bars Show 95% Confidence Interval of the Mean.	130
Figure 4.5: Swelling and Reswelling Ratios of PNIPA-based Homopolymer in aqueous medium: (a) Distilled Water; (b) Prodigiosin; (c) Paclitaxel TM and (d) Bromophenol Blue. Error Bars Show 95% Confidence Interval of the Mean.	131
Figure 4.6: Swelling and Reswelling Ratios of P(NIPA)-based copolymer (95 mol% of P(NIPA)-co-5 mol% of AM) in aqueous medium: (a) Distilled Water; (b) Prodigiosin; (c) Paclitaxel TM and (d) Bromophenol Blue.	132
Figure 4.7: Swelling and Reswelling Ratios of P(NIPA)-based copolymer (90 mol% of P(NIPA)-co-10 mol% of AM) in aqueous medium: (a) Distilled Water; (b) Prodigiosin; (c) Paclitaxel TM and (d) Bromophenol Blue.	133
Figure 4.8: Swelling and Reswelling Ratios of P(NIPA)-based copolymer ((85 mol% of P(NIPA)-co-15 mol% of AM) in aqueous medium: (a) Distilled Water; (b) Prodigiosin; (c) Paclitaxel TM and (d) Bromophenol Blue.	134
Figure 4.9: Plots: (a) Fluid Flow Via Channel Length (cm) Against Travel Time at 43°C; (b) Estimation of the effective diffusivity from L^2 versus Time.	135
Figure 4.10: Diffusion Fits for Bromophenol Blue Dye Obtained From; Plots of $\ln(mt/m_0)$ Versus $\ln(t)$ (s) for P(NIPA)-Based gels Hydrogels at 28°C, 37°C, 41°C, 43°C, 45°C and 48°C.	136
Figure 4.11: Release Rates of Bromophenol Blue at 41°C: (a) Homopolymer; (b) Hydrophilic Copolymer (Containing 15 mol% of Acrylamide).	137
Figure 4.12: Plots of $\ln D$ versus $1/T$ (K ⁻¹): (a) Homopolymer, and (b) Co-polymer (With 15 mol % of AM).	137
Figure 4.13: Release Rates of Bromophenol Blue Dye at 37°C: (a) Homopolymer, (b) Hydrophilic Copolymer (With 15 mol% of Acrylamide), (c) Release Profiles of P(NIPA)-Based Hydrogels at 41°C and (d) Moles of Prodigiosin Release Per Gram of Polymers (P(NIPA)).	138
Figure 4.14: Fluid/Drug Elution in P(NIPA) Copolymers.	139

Figure 5.1: (a) Schematic Diagram of Encapsulated Biomedical Device with Microchannels for Drug Elution, (b) PID Temperature Controller (Used to Set and Monitor Local Temperatures). ...	163
Figure 5.2: Transport of Anticancer Drug Species Delivered from an Implantable Biomedical Device: (a) Schematic Diagram for a Typical Tissue, (b) Schematic PNIPA-based Scaffold Model.	163
Figure 5.3: MDA-MB-231 Breast Cancer Cells in Culture Flask: (b) Cells Floats on Growth Media Immediately after Detachment; (c) Detached Cells Adhered to Flask after 2 hours; (a) Cells Adhered on the flask after Several Days.	164
Figure 5.4: Growth Curve of Viable Cells Versus Time (days). Error Bars Show 95% Confidence Interval of the Mean.	165
Figure 5.5: Colonies of MDA-MB-231 breast cancer cells on flask: (a) 7 days of culture; (b) 14 days of culture.	165
Figure 5.6: Cell Viability (MDA-MB-231 Cell Line): (a) Effect of drugs (Prodigiosin and Paclitaxel™) after 72 hrs; (b) Effect of Temperature on Cell Viability after 72 hrs; (c) Combined Effect of Drug Release and Temperature on Cell Viability.	166
Figure 5.8: Effective Diffusivities of Dye Elution versus Time in a P(NIPA)-Based Scaffold.	167
Figure 5.9a-b: (a) Contour of drug concentration along the length of the geometry (x-coordinate) (b) Exponential Decay of Drug Concentration Eluted along the length of the geometry (x-coordinate) at 37°C.	168
Figure 5.10: Comparing the Experimental and Simulation: (a) Models and Experiment along the Geometry Length from the implanted device boundary at 96 hrs. (b) Percentage of Drug Release from an Implantable Biomedical Device into a Scaffold.	168
Figure 6.1: Standard Curve for Drug Released from PLGA-based Polymer (PLGA 65:35): (a) PG Released from PLGA-Based millirods and (b) PT Released from PLGA-based Millirods.	188
Figure 6.2 (a-c): Optical Images of PLA:PGA During Degradation and Drug Release at 37°C, pH 7.4, 60 rpm; (a) PLA:PGA (50:50)-Based Mini rods Loaded with PG, (b) PLA:PGA (65:35)-Based Mini rods Loaded with PG and (c) PLA:PGA (75:25)-Based Mini rods Loaded with PT.	189
Figure 6.2 (d-f): Poros SEM Images of PLA:PGA During Degradation and Drug Release at 37°C, pH 7.4, 60 rpm Mini rods Loaded with PT.	190
Figure 6.3: First Order Estimation of Rate Constant and Drug half-life from Drug Loaded PLGA-based Mini rods: (a) PLGA (50:50)-PG, (b) PLGA (65:35)-PG, (c) PLGA (75:25)-PG and (d) PLGA (85:15)-PG.	191
Figure 6.4: Cumulative Drug Release from PLGA, Drug-Based Mini rods Incubated at 37°C, pH 7.4 and under a mechanical agitation of 60 rpm.	191

Figure 6.5: Drug Release Versus Degradation of PLGA Drug-based Mini-rods at 37°C, pH 7.4, 60 rpm. 192

Figure 6.6: Polymer Degradation Rate: (a) Polymer Mass Loss versus Time and (b) Effect of Degradation Rate on Polymer Half-life. 192

Figure 6.7: Determination of the initial Diffusion Rate from PLGA-based Polymers; (a) Encapsulated with PG and (b) Encapsulated with PT. 193

Figure 6.8: Thermal Characteristics of PLGA-based mini-rods incubated in PBS at 37°C Under Mechanical Shaking (60 rpm): (a) PLGA 50:50 Loaded with PG for 24 days and (b) Decrease in Thermal Properties with Increase in Incubation Time..... 193

Figure 7.1: Schematics of Novel Biodegradable Drug Delivery Systems..... 200

List of Tables

Table 1.1: World 10 Most frequent cancer in men and women in 2008 .	6
Table 2.1: Monomers Used in Synthesizing Temperature-Sensitive Hydrogels/Micorgels.....	31
Table 2.2: Structures of Some Temperature Sensitive Polymers	32
Table 2.3: Polymerization of PNIPA-Based Gel, copolymerized with BMA.	34
Table 2.4: List of biodegradable polymers and their polymer repeated unit structures.	36
Table 2.5: Summary of Release Exponents Associated with Diffusion Mechanisms in Drugs Eluting from Polymeric Films of Different Geometries	51
Table 3.1: Gel Materials and their Role in Gel Polymerization	103
Table 3.2: Displays the ANOVA Test for the Effect of the Different Polymer Ratio on the Swelling Ratios	103
Table 3.3A: Displays the Analysis of Variance (ANOVA) Test of the Effect of Temperature on the Swelling Ratios.	103
Table 3B: Least Significant Difference (LSD) Test	104
Table 3.4: Repeated ANOVAs for the Swelling Ratios of P(NIPA)-based Hydrogels in Different Fluids (5 ml of 2 µg/mL of drug solutions) or distilled water at 28°C.	105
Table 3.5: Activation Energy and LCST of PNIPA-Based Hydrogels in Distilled Water	105
Table 3.6: The Values of n, k and D at 37°C from PG Release.....	106
Table 3.7: Strain Induced on Hydrogels Due to Swelling.	106
Appendix A. Supplementary Data	107
Table 4.1: Gel Materials and their Role in Gel Polymerization.	139
Table 4.2: P(NIPA)-Based Hydrogel Configuration and their Compositions.	140
Table 4.3: Diffusivity, D, of P(NIPA)-loaded Prodigionsin, Drug Release Exponent (n), and Geometric Constant of P(NIPA)-Based Hydrogels (K) at 37°C	140

Table 4.4: Diffusion Values of P(NIPA)-loaded Prodigiosin at Different Temperatures..	141
Table 4.5: Diffusion Coefficients for the Hydrogels in Different Fluids Were Compared at 37°C.	141
Table 5.1: P(NIPA)-based Scaffolds Configuration and Compositions.	169
Table 5.2: Transport Properties of P(NIPA)-based Scaffolds.	169
Table 5.3: Diffusive and Permeability Data.	170
Table 6.1A: Preparation of Drugs Solutions into Working Concentrations.	194
Table 6.1B: Ratios of Polymer, Drug and PVP Used in PLGA-Drug-Based Mini rods Formation.	194
Table 6.2: Polymer Degradation and Drug Diffusion Terms at 37°C in PBS pH “7.4”.	194
Table 6.3: Summary of Encapsulation Efficiencies and Drug Loading for PLGA-Based Polymer.	195
Table 6.4: Initial Diffusion Terms for the Initial Burst Release of PG and PT from PLGA-based Polymers.	195

CHAPTER ONE

1.0 Background and Introduction

1.1 Introduction

The increasing incidence of cancer [1] has stimulated research on the development of novel implantable devices for the localized treatment of cancer [2-4]. Cancer is currently the second leading cause of death worldwide after cardiovascular disease [5, 6]. Current trends also suggest that cancer will become the leading cause of death by 2030 [5, 7]. Furthermore, standard treatment methods, such as bulk systemic chemotherapy [1, 4, 8] and radiotherapy [9-11], have shown severe side effects. There is, therefore, the need to develop localized cancer treatment methods to mitigate these side effects.

One approach that can be used to reduce the potential side effects of cancer treatments is to use localized drug delivery that can reduce the higher concentrations of cancer drugs in a tissue. This can be achieved by using implantable drug eluting devices for the localized delivery of drugs [4, 12]. Such approaches can also be combined with localized hyperthermia in cancer treatment [13, 14]. Recent research by Yaoming *et al.*, (2012) [12], has also shown that haematoporphyrin based-photodynamic therapy, combined with hyperthermia, provides an effective therapeutic vaccine against colon cancer growth in mice.

The uptake, storage and delivery of cancer drugs can be facilitated by the use of gels [16-18]. These include environment-sensitive gels that can respond to local stimuli, such as temperature, pH, electric fields and solvent composition [2, 19-21]. The swelling and controlled release of cancer drugs [22, 23] from such gels can, therefore, provide the basis for the design of implantable biomedical systems for the localized treatment of cancer. However, such controlled release requires a good basic understanding of phase transitions [22, 23], swelling and diffusion-controlled release from smart hydrogels.

Thermo-sensitive hydrogels have been explored for their potential use in drug delivery [4, 12, 24, 25]. These include poly(N-Isopropyl acrylamide) P(NIPA), which is a thermo-sensitive hydrogel. PNIPA has a lower critical solution temperature (LCST) of about 32°C in aqueous solution, especially when it has been cross-linked [12, 26]. P(NIPA) is produced by reacting TEMED with P(NIPA)-based gels through free radical polymerization. The process is terminated by exposing the samples to air. Freezing the samples below 9°C also helps to produce heterogeneous microporous hydrogels with interconnected pores. It has also been reported that the LCST of P(NIPA) is dependent on the pH, with the LCST increasing with increasing pH [27].

Furthermore, crosslinking P(NIPA) with acrylamide helps to effectively increase the LCST, while cross-linking with butyl-methylacrylate decreases the LCST [4]. Such control of the LCST makes P(NIPA)-based gels attractive for potential applications in drug delivery systems. However, there is a need for further research to prepare NIPA-based gels for potential applications in drug delivery systems for the localized treatment of diseases such as cancer.

This thesis presents the results of an experimental study of the kinetics of cancer drug release (bacterial-synthesized prodigiosin drug release) from an implantable device in which prodigiosin (PG) is soaked in encapsulated P(NIPA) gels. The P(NIPA)-based gels were encapsulated in a poly-di-methyl-siloxane (PDMS) biocompatible package with micro-channels that facilitate the delivery of cancer drugs such as paclitaxelTM (PT) and prodigiosin. Control experiments were also performed in which gel swellings and drug release kinetics was studied at temperatures that are relevant to hybrid treatments that involve chemotherapy and hyperthermia. This study also conducted the effect of cancer drugs (PG and PT) on cell viability. The implications of the results are then discussed for the design of implantable biomedical structures for the localized treatment of breast cancer.

The field of controlled release has since been borne out of this motivation to develop systems that release drugs in a controlled and effective manner. This can be appreciated by examining *Figure 1.1*. It shows the changes in the blood plasma levels following a single dose administration of a therapeutic agent. This figure shows the blood plasma level rises rapidly and later decays exponentially as drug is metabolized and excreted from the body [8]. Moreover, the figure shows drug concentrations above which the drug produces undesirable/toxic side effects. The therapeutic window is the difference between these two levels, which is usually based on a dose-response of the median 50% of a population [28].

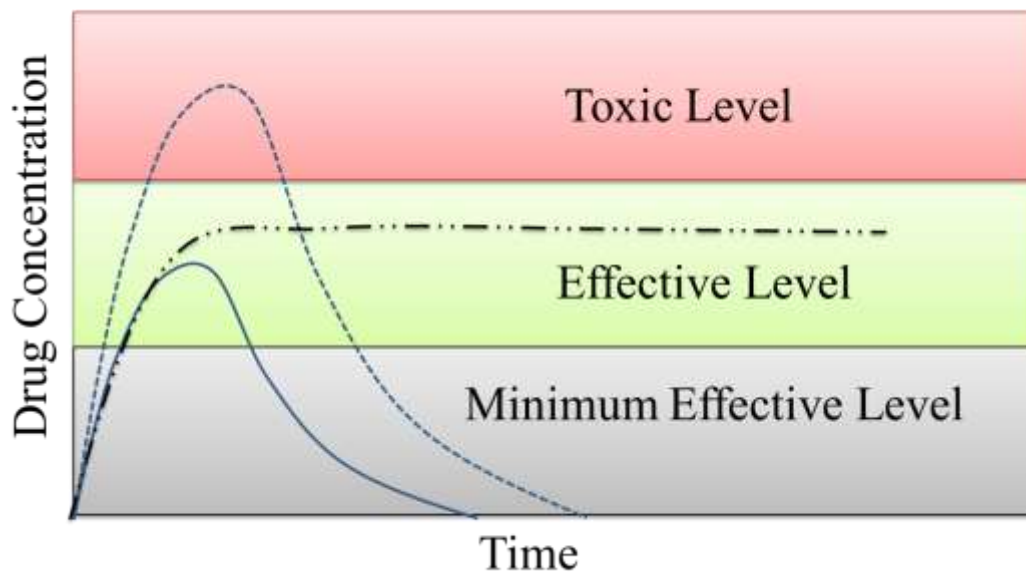


Figure 1.1: Drug concentration following absorption of therapeutic agent as a function of time. Redrawn after Roseman and Yalkowsky, 1976 [29].

1.2.1 Implantable Biomedical Devices

Implantable biomedical devices represent a new class of devices that can be used to provide localized cancer drug delivery [30]. They can be inserted in regions that surround cancer tissue, and to deliver surgical drugs, in ways that reduce the short and long term effects of bulk

chemotherapy. Implantable biomedical devices typically contain a drug reservoir that can be used to provide drugs locally to tumor sites [28].

The delivery can be achieved by a number of mechanisms. They include:

- a) Polymer drug release can be developed by incorporating swelling hydrogels as the membrane covers for the micro reservoirs;
- b) Generate sufficient pressure to move the drugs;
- c) Obtain enough displacement to achieve a desired flow rate and electromechanical response of a polymer material to an external source. The drug release kinetics relates to the surface properties, liquid uptake behavior and, swelling diffusion.

1.2.2 Cancer and Cancer Statistics

According to the National Cancer Institute, cancer can be thought of as an uncontrolled cellular growth that is caused by the malfunction of specific genes that are responsible for regulating cell growth and division (*Fig. 1.2*). This malfunction is attributed to changes in deoxyribonucleic acid (DNA) sequence, and mutation of the genes. It is projected by World Health Organization (WHO) that global cancer rates could increase by 50 % to 15 million by 2020 [31].

The incidence of different types of cancer that are observed in men and women are summarized in Table 1.1 [32]. Breast cancer is not only the most common form of cancer in women but also the second leading cause of death in women diagnosed with cancer. One in eight women will actually have breast cancer during their lifetimes. Forecasted changes in population demographics in the next two decades suggest that even if current global cancer rates remain unchanged, the estimated incidence of 12.7 million new cancer cases in 2008 [32]

will continue to rise to 21.4 million by 2030, with almost two thirds of all cancer diagnoses occurring in low- and middle-income countries [32].

Recent reports from the American Cancer Society researchers estimated 1,529,560 new cancer cases and 569,490 deaths from cancer in 2010 [33]. In the United States, the incidence of breast cancer in women is on the increase. This was released following successful screening exercise done in some developed nations [34], including the United Kingdom, Denmark, the Netherlands, and Norway [35].

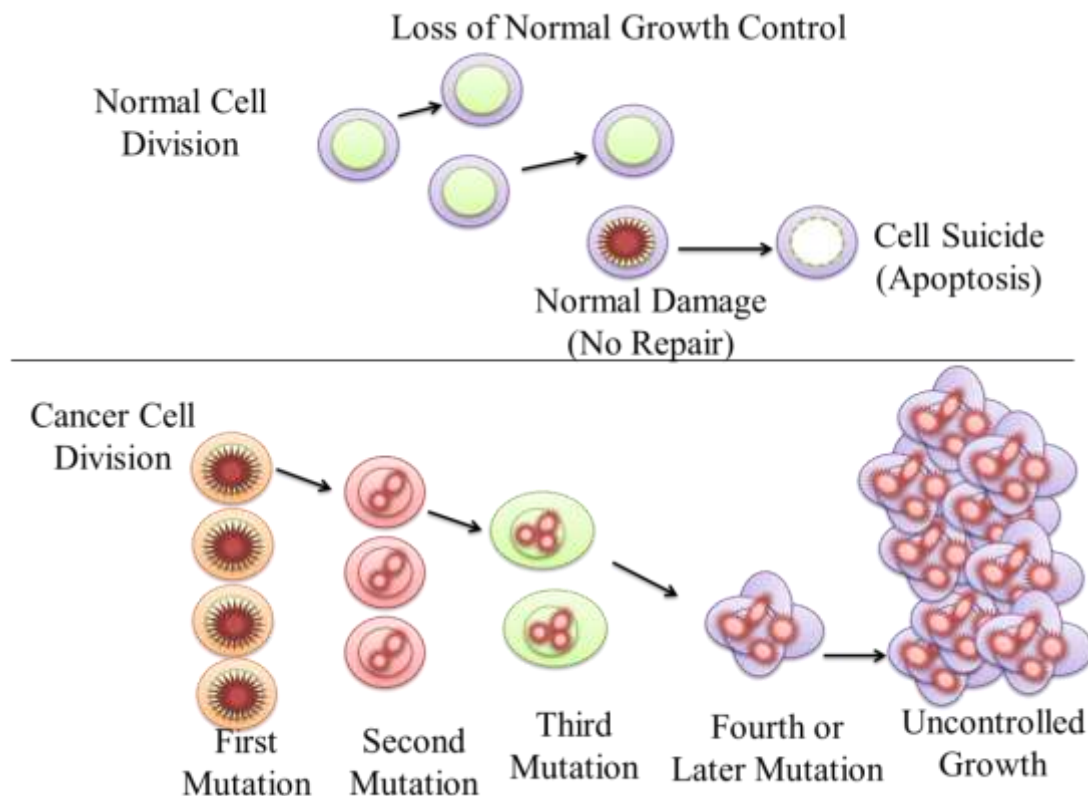


Figure 1.2: Shows the growth rate of cancer cells compared with the normal cell growth. (Redrawn from Ferley et al., 2010) [32].

Table 1.1: World 10 Most frequent cancer in men and women in 2008 [32].

Commonest in Men			Commonest in Women			Both Cases		
<i>Type of cancer</i>	<i>Number</i>	<i>%</i>	<i>Type of cancer</i>	<i>Number</i>	<i>%</i>	<i>Type of cancer</i>	<i>Number</i>	<i>%</i>
Lung	1,095,000	16.5	Breast	1,383,000	22.9	Lung	1,608,000	12.7
Prostrate	913,000	13.8	Colorectum	570,000	9.4	Breast	1,383,000	10.9
colorectum	663,000	10.0	Cervix uteri	529,000	8.8	Colorectum	1,233,000	9.7
Stomach	640,000	9.6	Lung	513,000	8.5	Stomach	989,000	7.8
Liver	522,000	7.9	Stomach	349,000	5.8	Prostrate	913,000	7.2
Oesophagus	326,000	4.9	Corpus uteri	287,000	4.8	Liver	748,000	5.9
Bladder	297,000	4.5	Ovary	225,000	3.7	Cervix uteri	529,000	4.2
Non-Hodgkin's lymphoma	199,000	3.0	Liver	225,000	3.7	Oesophagus	482,000	3.8
Leukaemia	195,000	2.9	Thyroid	163,000	2.7	Bladder	386,000	3.0
Liporal cavity	170,000	2.6	Non-Hodgkin's lymphoma	156,000	2.6	Non-Hodgkin's lymphoma	355,000	2.8

1.2.3 Major Causes of the High Incidence of Breast Cancer

Breast cancer incidence in women who obtained mammograms increased from 32 to 63 % in ages ranging from 40 to 49 between 1987 and 1998. Also, for women between the ages of 50 and 64, the incidence of breast cancer increased from 31 to 73 %, upon receiving a mammogram, during the period between 50 and 64 [36].

The increased incidence of breast cancer is attributed partly to risk factors such as smoking [37], fatty diets and or obesity [38, 39], the use of hormones for birth control [40], delay or

refraining from child birth in the Western or developed countries [41, 42], oral contraceptives [43], excessive alcohol consumption [44-46], genetic factors [47, 48], and previous exposure to radiation treatments [49].

Breast cancer has been recently reported as the second leading cause of cancer death among women [50]. Low doses of alcohol consumption (for example, ≤ 1 drink/day) increase the risk of breast cancer to about 4% [51], while heavy alcohol intake (for example, ≥ 3 drink/day) is reported to increase risk from 40-50% [52,53]. Moreover, regular high alcohol intake has also been reported to increased breast cancer mortality [54].

The role of epigenetic mechanisms in alcohol-related breast cancer has also been investigated. In a recent study by Christensen and coworkers (2010) [55], methylation profiles of 1,413 cytosines showed a strong trend toward decreased DNA methylation with increasing alcohol intake, and a trend toward increased methylation with increasing dietary folate. Other studies have shown altered methylation patterns for several genes associated with alcohol consumption, including hypermethylation of the estrogen receptor (ER- α) [56] and E-cadherin genes [57] and also hypomethylation of protein 16 (p16) [57].

In addition, sequential higher estrogen exposure is capable of inducing aberrant DNA methylation which is associated with breast carcinogenesis in both *in vivo* and *in vitro* conditions [58]. These elucidations suggest possible mechanisms of alcohol-induced carcinogenesis in breast cancer. Therefore, a woman is at risk of getting breast cancer depending on her overall exposure to estrogen across her life span. Earlier menstruations among women in addition to those who reach menopause at an older age have a higher cumulative estrogen exposure. This explains that, such women have a high risk of getting breast cancer than women with a shorter menstrual life. Postmenopausal alcoholic women have higher estrogen levels than women who are not alcoholic, increasing their overall estrogen exposure, which may in turn increase breast cancer risk [58].

However, in the case of developing countries, where the lifestyles are different, reasons for the increased incidence of cancer are not fully understood. However, it is anticipated that the incidence of breast cancer will continue to increase in developing nations, as they experience economic growth that increases incidence of the risk factors associated with the lifestyles in developed nations.

1.2.3 Stages in Cancer Development

Cancer begins when a cell breaks free from the normal restraints on cell division and begins proliferation indefinitely. The stages of malignant tumor development over time are shown in *Figure 1.3*. Tumors develop due to approximately four types of mutations though the number of mutations involved in different types of tumors differs. The exact number of mutations required for a normal cell to fully undergo malignancy cell is not known. It has been predicted that the number probably could be less than ten [59].

Generally, a tumor begins to develop when a cell experiences mutation in specific genes that control cell division. This makes the cell more readily divide than is normally the case. Moreover, because of this mutation, the altered cell and its descendants develop and divide more often to a condition termed as hyperplasia.

At some point, one of these cells experiences other mutations which further increase its tendency to divide. This cell's descendants divide excessively and also look abnormal, a condition called dysplasia.

Over time, one of these cells experiences yet another mutation. This cell and its descendants are very abnormal in both growth and appearance. If the tumor formed from these cells is still contained within its tissue of origin, then it is called *in situ* cancer which may remain indefinitely in the body. Any additional mutations to this *in situ* cancer cell grant the tumor the ability to invade neighboring tissues and also shed cells into the blood or lymph, which causes the tumor

to be malignant. This stage is very difficult as cells may escape to establish new tumors (metastases) at other locations in the body.

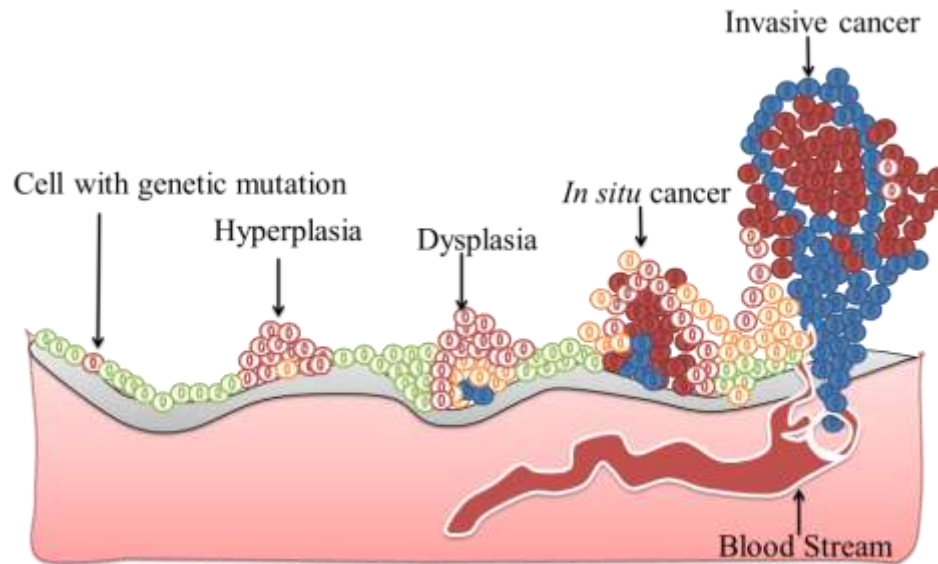


Figure 1.3: Stages in Cancer Development (Modified after referece [59]).

1.2.4. Metastasis

Metastasis occurs due to the adaptation of cancer cells to tissue microenvironments at distances from the primary tumor [60]. Metastasis involves several stages: first, cancer cells break away from the primary tumor to invade the host stroma, intravasate and moved into the lymphatic or blood vessels. These cells then spread to the capillary bed of distant organs, where they basically invade the new surrounding tissues and proliferate to form secondary tumors [61, 62] leading to colonization [63-65].

Detection at an early stage, before cells begins to spread can often be treated successfully by conventional cancer therapies such as surgery, chemotherapy and local irradiation [60]. Metastatic diffusion of cancer cells remains the most important clinical problem and late detection before cells metastasize renders treatment to be less successful [63]. The ability of

tumor cells to is dependent on their ability to exit from the blood circulation, to colonize distant organs, and to grow in distant organs.

However, only a very small number of tumor cells in the blood stream survive to reach the target organ [64-67]. Although several carcinoma cell enters the circulatory system, most of them die during transportation with only 1-5% of viable cells which later lead to the formation of secondary deposits in distinct sites [64-67]. Steps in the metastasis process are shown in Figure 1.4.

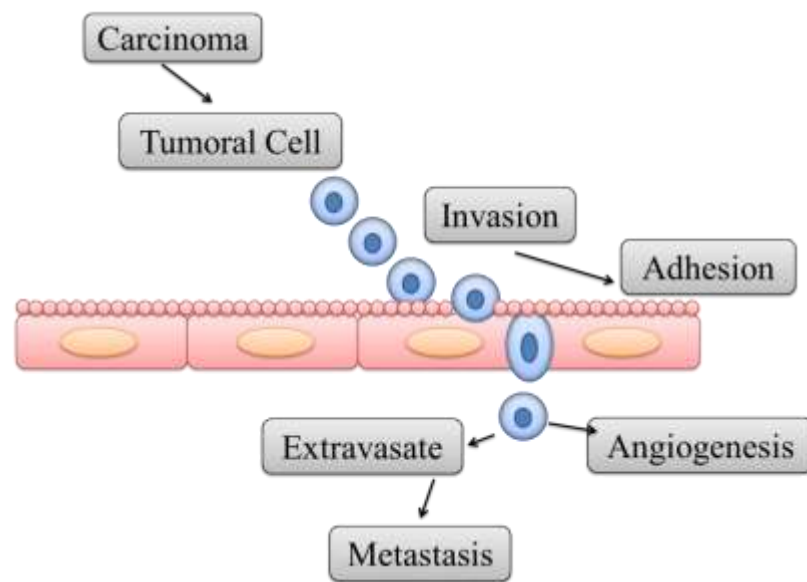


Figure 1.4: Steps in the Metastasis Process (Redrawn after Esquivel et al., 2013) [60].

Cell-cell interactions and adhesion between tumor and the endothelium cells in distant tissues aid metastasis [68-70]. Significant contributions to the adhesion of cancer cells include; direct tumor cell interactions with platelets, fibroblasts and monocytes/macrophages, polymorphonuclear cells, soluble components, cytokines, chemokines, proteins of the extracellular matrix, growth factors including other molecules secreted by host cells, extravasation, and the establishment of metastatic lesions [71-74]. Metastatic cancer cells require conducive-microenvironments to adapt to their continued proliferation and survival [63-65].

My discussion with Dr. Karen from Princeton University revealed the importance of Caderin genes in cancer development, especially in metastasis. Cadherins genes make cells to adhere to one another. When a cancer cell escapes from the primary tumor site, the cadherins changes to enable the cell to leave its original site and then move into other tissues and loacations in the body.

1.2.4 Microenvironment Promoting Tumor Migration

Tumor microenvironment is composed of stromal fibroblasts, myofibroblasts, myoepithelial cells, macrophages, endothelial cells as well as leucocytes/extracellular matrix (ECM) and soluble factors derived from tumor cells [60]. The inflammatory environment surrounding a tumor promotes the breaking of the basal membrane, a process required for the invasion and migration of metastatic cells [75]. Tumor cells produce cytokines and chemokines to facilitate evasion of the immune system and also help to establish the development of metastasis (Fig.1.5).

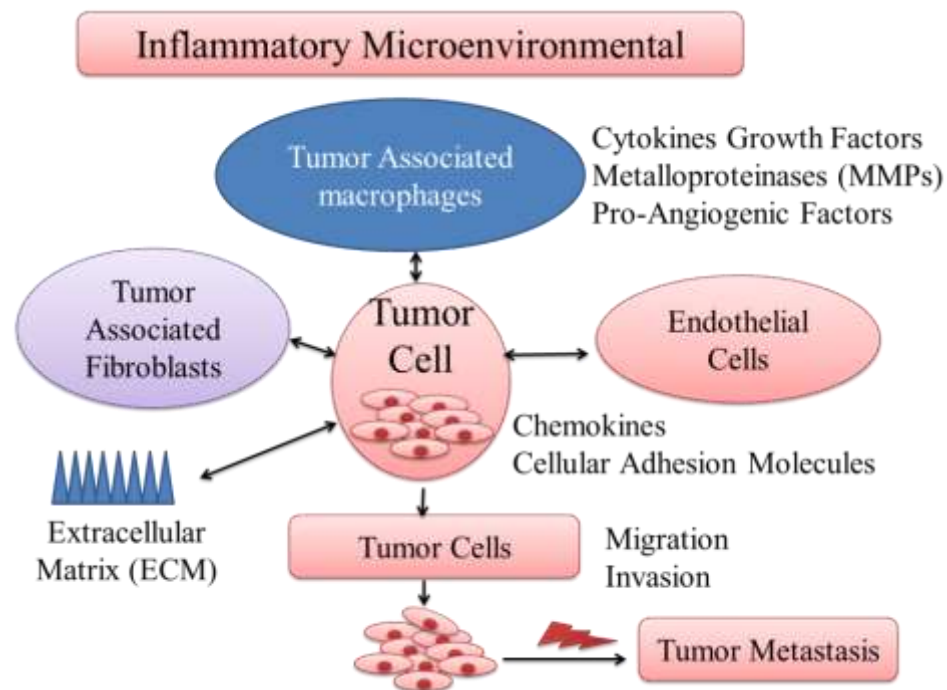


Figure 1.5: The tumor microenvironment and its role in promoting tumor growth (Redrawn from César Esquivel et al., 2013) [60].

The increase of tumor-associated macrophages (TAMs) is associated with poor prognosis through various mechanisms. This includes; a) release by macrophage IL-10 and prostaglandin E2 which suppress antitumor response, b) easy to release angiogenic factors such as vascular endothelial growth factor (VEGF), endothelial growth factor (EGF), endothelin-2 plasminogen activator promote tumor growth, and c) to facilitate cell invasion metastasis by releasing matrix metalloproteinase [76, 77]. The tumor microenvironment and its role in promoting tumor growth is shown (Fig. 1.5).

1.3 Controlled Drug Delivery

One way of managing the increased incidence of breast cancer is to reduce the side effects associated with bulk systemic chemotherapy. This may be achieved by introducing an implantable drug delivery system into a region in which cancer tissue has been removed by surgery (Fig. 1.6). The loaded drug is gradually released when polymer wafers dissolve away [1]. The drug delivery system can then release cancer drugs locally into the tissue surrounding the device. In this way, any remaining cancer cells or tissue can be killed, as the eluted drug flows into the surrounding tissue. Since the delivery of the drug is localized, the total quantity of drug, that is needed to have a therapeutic effect, is reduced significantly. Hence, the potential side effects associated with localized cancer drug delivery should be much lower than those associated with bulk systemic chemotherapy [4]. In addition, since less drug is used for localized treatment, the cost of treatment should be decreased.

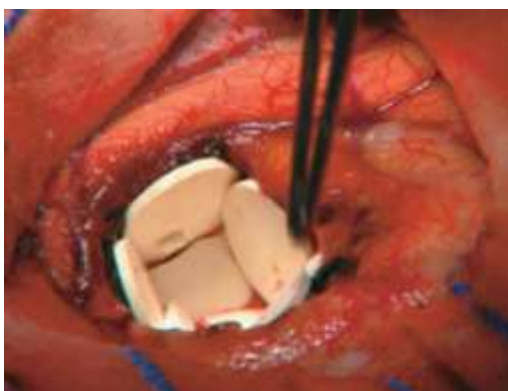


Figure 1.6: polymer implants loaded with BCNU are lined in a human brain tumor resection cavity. (Moses et al., 2003) [78].

1.4 The Primary Goal

Diseases such as cancer require repeated administration of drugs over long periods of time, ranging from months to years with precise control for reasons of safety and efficacy. There are challenges for delivery due to the inaccessibility of the target tissue or organ. In view of this, the current work is focused on fabricating fully implantable, self-controlled drug delivery system to treat breast cancer. The goal is to produce an implantable biomedical device for localized breast cancer drug delivery within Africa and the world.

The main advantage of localized delivery is that it reduces the amount of drug that is needed to have a therapeutic effect [79]. Hence, localized drug delivery can reduce the side effects associated with chemotherapy. These can be further reduced by the synergy that can be engineered between localized hyperthermia and localized chemotherapy.

1.5 Scope of Work

The primary objective of this work was to develop implantable biomedical devices for localized treatment of breast cancer. The materials that would be effective for localized drug release were elucidated. The research was carried out in the following steps:

- ❖ Poly-di-methyl-siloxane packages with well-controlled micro-channels and drug storage compartments were fabricated along with drug storing polymers that were produced from non-resorbable poly(N-isopropyl acrylamide) (P(NIPA)) and monomers of (acrylamide (AM) and resorbable poly(lactic) acid-co-poly(glycolic) acid.
- ❖ The swelling and fluid release characteristics of the polymers and polymer composites were studied using the cancer drugs prodigiosin and paclitaxelTM and also bromophenol blue as a control. The mechanisms of drug release were elucidated at temperatures that are relevant to cancer treatment.
- ❖ The localized release of prodigiosin, paclitaxelTM and bromophenol blue were studied under *in-vitro* conditions. The experiments establish the drug release rates from micro-channels, of different lengths. A combination of diffusion and micro-fluidics concept was then used to model the fluid flow through the micro-channels in an implantable cancer drug delivery device.
- ❖ This study also considered the kinetics of prodigiosin release from implantable biomedical devices for localized cancer drug release.
- ❖ Then the effects of prodigiosin release from an implantable biomedical device on cell viability were also studied.
- ❖ This work also presents studies of biodegradable drug delivery systems for localized cancer drug delivery. Drug release kinetics, drug loading efficiency, encapsulation efficiency, degradation mechanisms, drug release rates, half-lives of drugs and polymer. These were studied at 37°C in phosphate buffer saline solution (PBS) (pH 7.4) under mechanical agitation of 60 revolutions per minute (rpm) within an incubator shaker.
- ❖ This work recommended the release of prodigiosin/paclitaxel on tumor shrinkage from laboratory rats for future work. This is clearly the challenge for future work.

1.6 Bibliography

- [1] B. Hildebrandt and P. Wust in: W. P. Ceelen (Ed). Peritoneal Carcinomatosis: A Multidisciplinary Approach, Springer, New York. (2007) 185.
- [2] A. Afrassiabi, A. S. Hoffman and L. A. Cadwell. Effect of Temperature on the Release Rate of Biomolecules from Thermally Reversible Hydrogel. *Membrane Sci.* 33 (1987) 191-200.
- [3] S. Allan, A. S. Hoffman and J. Heller. An Introduction to Materials in Medicine, 2nd Edition. Elsevier Inc. (2004) 628-637.
- [4] Y. Oni, C. Theriault, A. V. Hoek and W. O. Soboyejo. Effects of Temperature on Diffusion from PNIPA-Based Gels in a BioMEMS Device for Localized Chemotherapy and Hyperthermia. *Mater. Sci. and Eng. C.* 31 (2011) 67-76.
- [5] P. Boyle and B. Levin. The World Cancer Report. World Health Organization, International Agency for Research on Cancer (IARC) Press, Lyon. (2008) 112.
- [6] J. Mackay and G. A Mensah. The atlas of disease and stroke, published by the world health organization in collaboration with the centers for disease control and prevention (2004). ISBN-13 97892415.
- [7] D. Gutierrez. Cancer Facts and Figures. 2nd Edition. America Cancer Society. (2008) 50.
- [8] D. Needhama, M. W. Dewhirst. The development and testing of a new temperature-sensitive drug delivery system for the treatment of solid tumors. *Advanced Drug Delivery Reviews.* ELSEVIER. 53 (2001) 285-305.
- [9] M. C. Perry. Approach to the Patient with Cancer. In: L. Goldman and A. I. Schafer, Eds. Cecil Medicine, 24th Ed. Philadelphia, Pa: Saunders Elsevier. chap 182 (2011).
- [10] D. Brain, R. D. Kavanagh, D. B. Kavanagh and D. R. Timmerman. editors. Stereotactic Body Radiation Therapy. Lippincott W. and Wilkins, Philadelphia, PA, USA (2005).
- [11] J. A. Del Regato. Radiological oncologists: the unfolding of a medical specialty. Reston (VA): Radiology Centennial. 268 (1993) 167-176.
- [12] G. Fu and W. O. Soboyejo. Swelling and diffusion characteristics of modified poly (N-isopropylacrylamide) hydrogels. *Materials Science and Engineering C.* 30 (1) (2010) 8-13.
- [13] A. Chilkoti, M. R. Dreher, D. E. Meyer and D. Raucher. Targeted drug delivery by thermally responsive polymers. *Adv. Drug Delivery Rev.* 54 (2002) 613-630.
- [14] Theriault C., Barkey C., Chandrasekar R., Paetzell E., Oni Y., Soboyejo W. O. An *in-vitro* study of the effects of temperature on breast cancer cells: Experiments and models. *Mat. Sci. and Eng. C.* 32(8) (2012) 2242-2249.
- [15] H. Yaoming, G. Haiyan and L. Shuping. Haematoporphyrin Based Photodynamic Therapy Combined with Hyperthermia Provided Effective Therapeutic Vaccine Effect against Colon Cancer Growth in Mice, *Int. J. Med. Sci.* 9 (2012) 627-633.
- [16] Catarina G., Paula P., and Miguel G. Self-Assembled Hydrogel Nanoparticles for Drug Delivery Applications. *J. Materials* 3 (2010) 1420-1460.
- [17] J. Jennifer, D. KangVand F. M. William. Thermoresponsive Hydrogels as a New Ocular Drug Delivery Platform to the Posterior Segment of the Eye. *Transactions of the American Ophthalmological Society.* 106 (2008) 206-214.
- [18] Todd R. H., Daniel S. K. Hydrogels in drug delivery: Progress and challenges. *J. Polymer* 49 (2008) 1993-2007.
- [19] T. G. Farmer, T. F. Edgar and N. A. Peppas. In Vivo Simulations of pH-Responsive Cationic Hydrogels in Diabetic Patients. *Ind. and Eng. Chem. Res.* 47 (2008) 10053-10063.
- [20] N. A. Peppas, P. Bures, W. Leobandung and H. Ichikawa. Hydrogels in pharmaceutical formulations. *Europ. J. of Pharmaceutics and Biopharmaceutics.* 50(1) (2000) 27-46.
- [21] J. D. Schmaljohann, Thermo- and pH-responsive Polymers in Drug Delivery, *Advanced*

- Drug Delivery Reviews. 58 (2006) 1655-1670.
- [22] B. Jeong and A. Gutowska, Lessons from Nature: Stimuli-Responsive Polymers and their Biomedical Applications, *Trends in Biotechnology*. 20 (7) (2002) 305-311.
- [23] K. S. Soppimath, T. M. Aminabhavi, A. M. Dave, S. G. Kumbar and W. E. Rudzinski. Drug Development and Industrial Pharmacy. 28 (2002) 957-963.
- [24] H. A. De Las, C. Alexander and S. Pennadam. Stimuli Responsive Polymers for Biomedical Applications. *Chemical Society Reviews*. 34 (2005) 276-285.
- [25] Q. Yong and K. Park, Environment-Sensitive Hydrogels for Drug Delivery, *Wiley Periodicals. Inc. Appl. Polym. Sci.* 99 (2005) 37-44.
- [26] H. G. Schild. Poly(N-isopropylacrylamide): Experiment, Theory And Application. *Progress in Polymer Science*. 17(2) (1992) 163-249.
- [27] M. K. Yoo, Y. K. Sung, Y. M. Lee and C. S. Cho. Effect of Polyelectrolyte on The Lower Critical Solution Temperature of Poly(N-Isopropyl Acrylamide) in the Poly(Nipaam-Co-Acrylic Acid) Hydrogel. *Polymer*. 41(15) (2000) 5713-5719.
- [28] S. Allan, A. S. Hoffman and J. Heller. *An Introduction to Materials in Medicine*, 2nd Edition. Elsevier Inc. (2004) 628-637.
- [29] T. J. Roseman and S. H. Yalkowsky. Controlled Release Polymeric Formulations, D. R. Paul and F. W. Harris (eds.). ACS Symposium Series 33, American Chemical Society, Washington DC. (1976) 33-52.
- [30] Y. Oni and W. O. Soboyejo. Swelling and Diffusion of PNIPA-Based Gels for Localized Chemotherapy and Hyperthermia. *Mater. Sci. and Eng. C*. 32 (2012) 24-30.
- [31] P. Kleihues, G. H. Brundtland, B. W. Steward. International Agency for Research on Cancer (IARC), WHO media centre, World Cancer Report (2003), p351.
- [32] J. Ferlay, H. R. Shin, F. Bray, D. Forman, C. D. Mathers and D. M. Parkin. Estimates of Worldwide Burden of Cancer in 2008: GLOBOCAN 2008. *International Journal of Cancer*. 127 (2010) 2893-2917.
- [33] J. Ahmedin, R. Siegel, J. Xu, E. Ward. Cancer Statistics, 2010. *CA Cancer J. Clin.* 60(5) (2010) 277-300.
- [34] H. K. Weir, M. J. Thun, B. F. Hankey, L. A. G. Ries, H. L. Howe, P. A. Wingo, A. J. E. Ward, R. N. Anderson and B. K. Edwards. Annual Report to the Nation on the Status of Cancer, 1975-2000, Featuring the Uses of Surveillance Data for Cancer Prevention and Control. *J. of the Nat'l Cancer Institute*. 95(17) (2003) 1276-1299.
- [35] D. M. Parkin, F. I. Bray and S. S. Devesa. Cancer Burden in the Year 2000. The Global Picture. *Eur. J. Cancer*. 37(8) (2001) S4-S66.
- [36] A. Logomasini. The Cancer Trend. The Competitive Enterprise Institute. Washington, DC. (2008) 202-331-1010.
- [37] M. Varela-Rey, A. Woodhoo, M-L. Martinez-Chantar, J.M. Mato, and C. S. Lu. Alcohol, DNA Methylation, and Cancer. *Alcohol Research: Current Reviews*. 25-36. <http://pubs.niaaa.nih.gov/publications/> (Accessed on 28th Jan. 2015, 2:00 am).
- [38] International Agency for Cancer Research (IARC)(2002). IARC Handbook of Cancer Prevention, Volume 6: Weight control and physical activity. Lyon: IARC Press. (2002).
- [39] K. Kerlikowske, R. Walker, D. L. Miglioretti, A. Desai, R. Ballard-Barbash, D. S. Buist DS Obesity, mammography use and accuracy, and advanced breast cancer risk", *J Natl. Cancer Inst.* 100(23) (2008) 1724-1733.
- [40] R. T. Chlebowski, L. H. Kuller, R. L. Prentice et al. Breast Cancer after Use of Estrogen Plus Progestin in Postmenopausal Women. *N Engl J Med*. 360(6) (2009) 573-587.
- [41] G. Albrektsen, I. Heuch, S. Hansen and G. Kvale. Breast Cancer Risk by Age at Birth, Time since Birth and Time Intervals Between Births: Exploring Interaction Effects. *Br J Cancer*. 92 (2005) 167-75.

- [42] M. Lambe, C. Hsieh, D. Trichopoulos, A. Ekbom, M. Pavia and H. O. Adami. Transient Increase in the Risk of Breast Cancer after Giving Birth. *N Engl J Med.* 331 (1994) 5-9.
- [43] Collaborative Group on Hormonal Factors in Breast Cancer. Breast cancer and hormonal contraceptives: collaborative analysis of individual data on 53,297 women with breast cancer and 100,239 women without breast cancer from 54 epidemiological studies. *Lancet.* 347(9017) (1996)1713-1727.
- [44] R. Baan, K. Straif, Y. Grosse et al). Carcinogenicity of alcoholic beverages. *Lancet Oncol,* 8(4) (2007)292-293.
- [45] L. H. Kushi, T. Byers, C. Doyle et al. American Cancer Society Guidelines on Nutrition and Physical Activity for cancer prevention: reducing the risk of cancer with healthy food choices and physical activity. *CA Cancer J Clin.* 56(5) (2006) 254-281.
- [46] S. R. Cummings, J. A. Tice, S. Bauer et al. Prevention of Breast Cancer In Postmenopausal Women: Approaches to Estimating and Reducing Risk. *J Natl Cancer Inst.* 101(6) (2009) 384-398.
- [47] P. Lichtenstein, N .V. Holm, P. K. Verkasalo et al., Environmental and Heritable Factors in the Causation of Cancer-analyses of Cohorts of Twins from Sweden, Denmark, and Finland”, *N Engl J Med.* 343(2) (2000) 78-85.
- [48] S. Chen and G. Parmigiani. Meta-analysis of BRCA1 and BRCA2 penetrance. *J. Clin Oncol.* 25 (2007) 1329-1333.
- [49] American Cancer Society (ACS). *Cancer Facts & Figures 2009*, Atlanta, GA: American Cancer Society (2009).
- [50] C. DeSantis, R. Siegel, P. Bandi and A. Jemal. Breast Cancer Statistics. *CA. A Cancer Journal for Clinicians.* 61(6) (2011) 409-418.
- [51] N. Hamajima, K. Hirose, K. Tajima et. al. Alcohol, Tobacco and Breast Cancer- Collaborative Reanalysis of Individual Data from 53 Epidemiological Studies, Including 58,515 Women With Breast Cancer and 95,067 Women without The Disease. *British Journal of Cancer.* 87(11) (2002) 1234-1245.
- [52] C. Pelucchi, I. Tramacere, P. Boffetta et al. Alcohol Consumption and Cancer Risk. *Nutrition and Cancer* 63(7) (2011) 983-990.
- [53] H. K. Seitz, C. Pelucchi, V. Bagnardi and C. La Vecchia. Epidemiology and Pathophysiology of Alcohol and Breast Cancer: Update 2012. *Alcohol and Alcoholism.* 47(3) (2012) 204-212.
- [54] C. Allemani, F. Berrino, V. Krogh et. al. Do Pre-Diagnostic Drinking Habits Influence Breast Cancer Survival? *Tumori.* 97(2) (2011) 142-148.
- [55] B. C. Christensen, K. T. Kelsey, S. Zheng et al. Breast Cancer DNA Methylation Profiles are Associated with Tumor size and Alcohol Folate Intake. *Plos Genetics.* 6(7) (2010) E1001043.
- [56] K. Zhu, N.E. Davidson, S. Hunter et al. Methyl-group Dietary Intake and Risk of Breast Cancer among African-American Women: a Case-Control Study by Methylation status of the Estrogen Receptor Alpha Genes. *Cancer Causes and Control.* 14(9) (2003) 827-836.
- [57] M. H. Tao, C. Marian, P. G. Shields et al. Alcohol Consumption in Relation to Aberrant DNA Methylation in Breast Tumors. *Alcohol* 45(7) (2011) 689-699, 2011.
- [58] S. V. Fernandez, J. Andrus. Estrogen and Xenoestro-Gens in Breast Cancer. *Toxicologic Pathology.* 38(1) (2010)110-122.
- [59] <http://science.education.nih.gov/supplements/nih1/cancer/guide/understanding1.htm>. Date accessed 1/18/2015, time; 5pm.
- [60] C. Esquivel-Chirino, J. Esquivel-Soto, J. A. Morales-González, D. M. Sánchez, J. L. Ventura-Gallegos, L. E. Hernández-Mora and A. Zentella-Dehesa. Inflammatory Environmental, Oxidative Stress in Tumoral Progression. Chapter 8. INTECH (2013) 188-

208.

- [61] Bendas, G, & Borsig, L. Cancer cell adhesion and metastasis: selectins, integrins, and the inhibitory potential of heparins. *Int J Cell Biol.* (2012) 676-731.
- [62] Chambers, A. F., Groom, A. C., & Mac Donald, I. C. Dissemination and growth of cancer cells in metastatic sites. *Nature Reviews Cancer.* 2(8) (2002). 563-572.
- [63] Calorini, Lido, & Bianchini, Francesca. Environmental control of invasiveness and metastatic dissemination of tumor cells: the role of tumor cell-host cell interactions. *Cell Communication and Signaling.* 8 (2010) 24.
- [64] H. Rubin, Contact interactions between cells that suppress neoplastic development: can they also explain metastatic dormancy? *Adv. Cancer Res.* 100 (2008). 159-202.
- [65] Aguirre-Ghiso, J. A. (2007). Models, mechanisms and clinical evidence for cancer dormancy. *Nat Rev Cancer,* 7, 834-846.
- [66] Nicolson, G. L. (1993). Cancer Progression and Growth: Relationship of Paracrine and Autocrine Growth Mechanisms to Organ Preference of Metastasis. *Exp Cell Res,* 204, 171-80.
- [67] G. J. Gasic. Role of Plasma, Platelets and Endothelial Cells in Tumor Metastasis. *Cancer Metastasis Rev,* 3 (1986) 99-116.
- [68] De Visser, K. E., Korets, L. V., & Coussens, L. M. (2005). De novo carcinogenesis promoted by chronic inflammation is B lymphocyte dependent. *Cancer Cell,* 7, 411-423.
- [69] E. Di Carlo, G. Forni, P. Lollini, M. P. Colombo, A. Modesti and P. Musiani. The intriguing role of polymorphonuclear neutrophils in antitumor reactions. *Blood,* 97 (2001) 339-345.
- [70] J. E. De Larco, B. R. Wuertz and L. T. Furcht. The potential role of neutrophils in promoting the metastatic phenotype of tumors releasing interleukin-8. *Clin Cancer Res.* 10 (2004) 4895-4900.
- [71] T. Silzle, G. J. Randolph, M. Kreutz and L. A. Kunz-Schughart. The Fibroblast: Sentinel Cell and Local Immune Modulator in Tumor Tissue. *Int J Cancer.* 108 (2004) 173-180.
- [72] R. Kalluri and M. Zeisberg. Fibroblasts in Cancer. *Nat Rev Cancer.* 6 (2006) 392-401.
- [73] G. L. Nicolson. Cancer Progression and Growth: Relationship of Paracrine and Autocrine Growth Mechanisms to Organ Preference of Metastasis. *Exp Cell Res.* 204 (1993) 171-80.
- [74] P. Mehlen and A. Puisieux Metastasis: a question of life or death *Nat. Rev. Cancer,* 6 (2006) 449-458.
- [75] F. Colotta, P. Allavena, A. Sica, C. Garlanda and A. Mantovani. Cancer-related Inflammation, the Seventh Hallmark of Cancer: Links to Genetic Instability. *Carcinogenesis.* 30 (2009) 1073-1081.
- [76] T. Kawaguchi. Cancer Metastasis: Characterization and Identification of the Behavior of Metastatic Tumor Cells and the Cell Adhesion Molecules, Including Carbohydrates. *Curr Drug Targets Cardiovasc Haematol Disord.* (2005) 39-64.
- [77] R. F. Thorne, J. W. Legg and C. M. Isacke. The Role of the CD44 Transmembrane and Cytoplasmic Domains in Coordinating Adhesive and Signaling Events. *J Cell Sci.* 117 (2004) 373-380.
- [78] M. A. Moses, H. Brem and R. Langer. *Cancer Cell.* 4 (2003) 337-341.
- [79] A. Montazeri. Health-Related Quality Of Life in Breast Cancer Patients, Iranian Center for Breast Cancer and Iranian Institute of Health Sciences Research. *Journal of Experimental and Clinical Cancer Research.* (2008).

2.0 Literature Review

2.1 Introduction

The development of drug delivery devices, a part of which this work addresses, has been the focal point of research in recent years [1,2]. In recent years, significant efforts have been made to develop devices for the localized treatment of cancer [3].

It has been reported that cancer is currently responsible for 20,000 deaths per day and 7.6 million incidences per year across the globe [4]. In addition, 2.9 million new cases are expected to occur in the developed world and 4.7 million new cases are expected to occur in the less developed countries. According to the American Cancer Society (ACS); breast, colorectal, and lung cancer are the most common forms of cancer in women in developed countries [5], while in developing countries, breast cancer still remains as the most common form of cancer among women, followed by cervical, and stomach cancer. Among cancers in men, the most prominent type in developed nations is prostate cancer, followed by lung, and colorectal cancers, whereas stomach, lung, and liver cancers are the most common forms of cancer among men in the less developed world [5].

This chapter presents a review of prior work and the underlying materials concepts that are relevant to the development of drug delivery devices for cancer treatment. These include: cancer statistics, challenges in cancer treatments, controlled drug delivery, mechanisms of drug release, biomedical implants, swelling characteristics of hydrogels, and drug release kinetics that are relevant to implantable drug delivery systems, as well as heat diffusion for localized hyperthermia. The chapter also presents work on drug delivery devices, the use of micro-fluidics and hydrogels in localized cancer drug delivery, and the use of poly(lactic-acid) (PLA)/ Poly(glycolic-acid) (PGA) composites in localized cancer treatment. Finally, the role of surface

coatings and surface textures were reviewed for the development of implantable devices that can adhere and integrate well with biological tissues.

Prior work [6] has shown that breast cancer typically starts in the breast, within thin tubes called the ducts. Early stages of breast cancer are within the breast or inside the glands under the arms known to be the lymph nodes (Figure 2.1a, b). During breastfeeding, breast milk is carried by the ducts, from the milk-producing glands, to the nipple. In the case of invasive breast cancer, cancer cells spread beyond the ducts and are found in the fatty tissues of the breast. The cancer eventually spreads throughout the body, when it breaches the cell membranes (basement membranes). When this occurs, cancer cells can be carried in the bloodstream to induce metastases, especially in the lungs and in the bone [6]. Most breast cancers usually arise from the lining of the milk ducts, or from the milk glands found within the breast lobes. The most common site is the upper outer part of the breast.

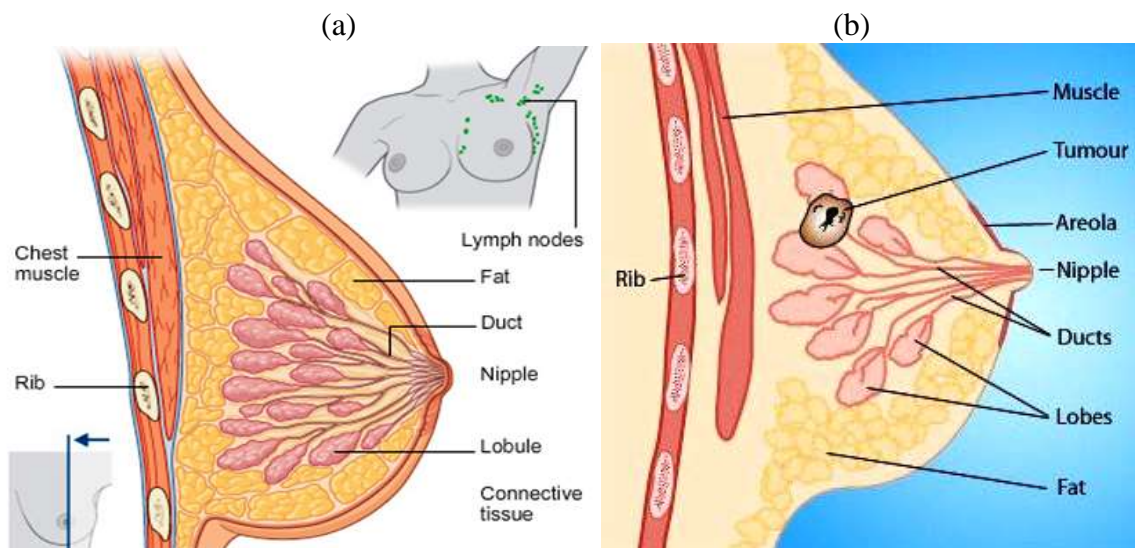


Figure 2.1: Illustrating the anatomy of a woman's breast: (a) without tumor and (b) with tumor located within the breast. (a) Adapted from (Paul Crea, St. Vincent's Clinic (2007) and (b) ABC Health and Wellbeing (2005).

2.2 Cancer Statistics

Cancer is reported to be increasing causing morbidity and mortality in all regions across the globe [7]. The increasing population growth suggested that, even if the current trends in cancer should remain unchanged, cancer would still contribute to 21.7 million new cases in 2008 [8]. Moreover, the statistics indicated that two thirds of the entire global incidence of cancer would occur in low and middle-income nations [8].

The ACS report in 2008 projected 715,700 new cancer cases in Africa, 1,034,300 cases in Western Europe, 3,720,700 new cases in Eastern Asia, South-Eastern Asia is 725,600, South-Central Asia, indicating 1,423,100, out of 12,667,500 worldwide estimates contributing to one death in eight. Hence, cancer deaths will be more than the deaths due to AIDS, tuberculosis, and malaria combined [8].

2.3 The Symptoms of Breast Cancer

Although the origin of cancer is not fully understood, cancer is generally associated with an acceleration of cell growth, and errors in the replication of deoxyribonucleic acid (DNA), which changes the sequence of DNA. It is very unusual for breast cancer to produce symptoms in its early stage. This results in late detection and treatment, and becomes a challenge when cancer reaches the metastasis stage. Early detection and secondary prevention via screening are therefore the keys to early detection of pre-cancerous cells or tissue. The symptoms of breast cancer include;

- Lymph thickening of breast tissue
- Swelling in the armpit or around the collar bone
- Changes in size or shape of the breast

- Changes in skin texture such as puckering or dimpling
- Discharge from nipples such as blood
- Constant pain in breast or armpit
- An inverted nipple (changes in the nipple where the nipple is pulled back into the breast)
- Redness or a rash on the skin or around the nipple

2.4 Challenges with Current Cancer Treatment

The existing bulk systemic cancer treatment methods include; surgery, radiotherapy, hyperthermia, chemotherapy, hormone therapy, and immunotherapy. However, the side effects of these current treatments are severe. Although surgery has been recognized as one way of treating cancer, it can disfigure the patient. Furthermore, there are no guarantees that all of the cancer cells or tissue will be successfully removed by surgery. Radiation on the other hand can be damaging to the local healthy organs and tissues as well as to the cancer. The use of bulk systemic chemotherapy as a method for cancer treatment also has some major challenges [9]. This is because only one tenth of one percent of the injected drugs reaches the desired tumor sites. Hence, most of the injected drugs kill or damage healthy cells or tissues that do not require chemotherapy [10].

Gregoriadis (1976) [11] explored the potential of liposomes to serve as cancer drug carriers [9]. Conventional liposomes have been evaluated chemically and are used in treating Kaposi sarcoma (Fig. 2.2). However, they failed to release drugs in a controllable manner to tumors [9].

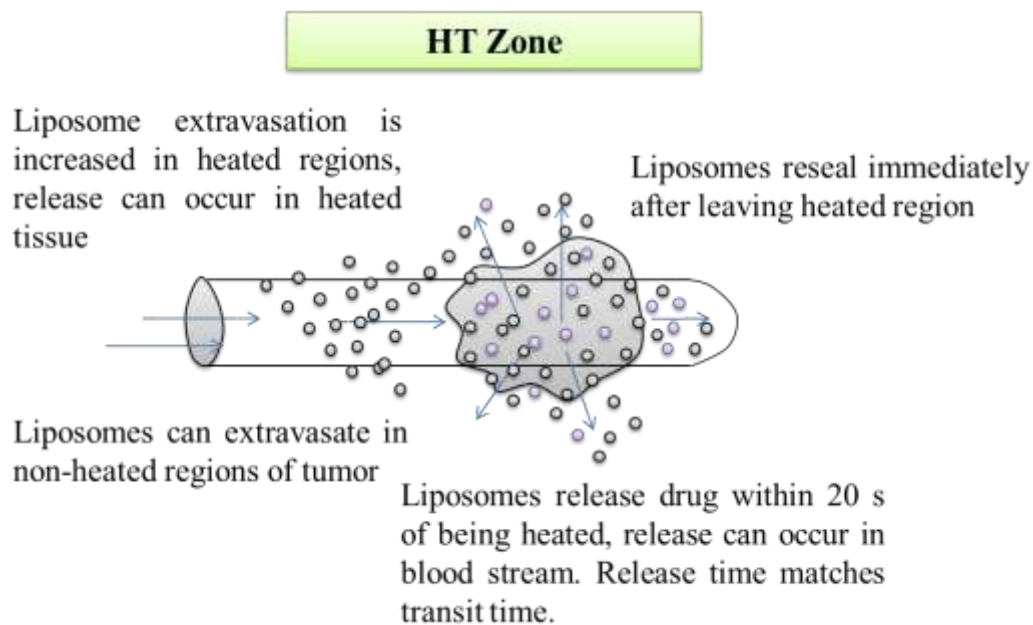


Figure 2.2: Summary of the mechanisms underlying liposome-based drug delivery to tumors for the heat-sensitive liposome system (Modified after David and Mark, 2001) [9].

2.5.0 Cancer Drugs

There exist many drugs that are used to manage/treat cancer. However, this study is aimed to test prodigiosin, a drug synthesized by bacteria, against the known cancer drug, PaclitaxelTM (PT).

2.5.1 PaclitaxelTM (PT)

PaclitaxelTM is a chemically-synthesized form of Taxol[®], which is produced from the bark of the Pacific Yew tree (an antileukemic and antitumor agent from *Taxus brevifolia*) [12]. But PT can also be obtained from a taxane precursor from the needles of the European yew in a semi-synthetic process. PT has anti-neoplastic property results from its ability to stabilize microtubules [13]. This, however, disrupts the normal cell division in the G2 and M phases during cell cycle [14] when microtubule function is required. PT is also a substrate for P-glycoprotein which is a factor that is most likely responsible for multiple drug resistance of

tumor cells [15]. Even though the permeability of tumor capillaries is higher than that of the normal capillaries, P-glycoprotein actually reduces the concentration of PT in the neoplastic tissues [16].

The chemical structure of PT is a taxane ring (Fig. 2.3) together with a side chain at position C-13 (Fig. 2.3c). The C-13 side chain of the PT structure has been identified as the most vital site for biological activity (Horwitz, 1992) [17].

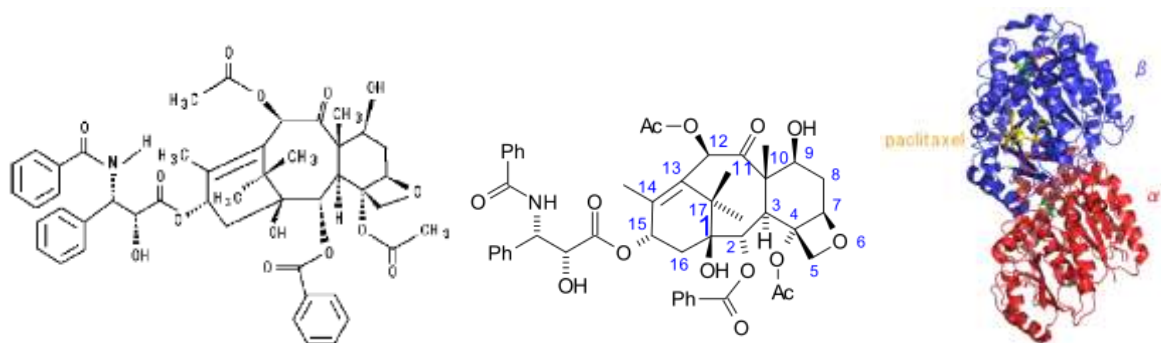


Figure 2.3: (a) The Chemical Structure of PT, (b) Nomenclature of PT and (c) Complex of α , β Tubulin Subunits and PT is shown as Yellow Stick.

2.5.2 Prodigiosin (PG)

Prodigiosin (PG) is a tripyrrole red pigment that is biologically synthesized by bacteria, *Serratia marcescens* (MS) as well as other bacteria. Recent studies have shown that, PG could be used as a drug agent for; anticancer, antiproliferative, cytotoxic, antibacterial and also for immunosuppressive activities [18-20]. PG has been reported to effectively induce apoptosis in hematopoietic cancer cells as well as cells derived from other human cancers (e.g. gastric and colon cancers), with no marked toxicity in nonmalignant cell lines [19,21,22].

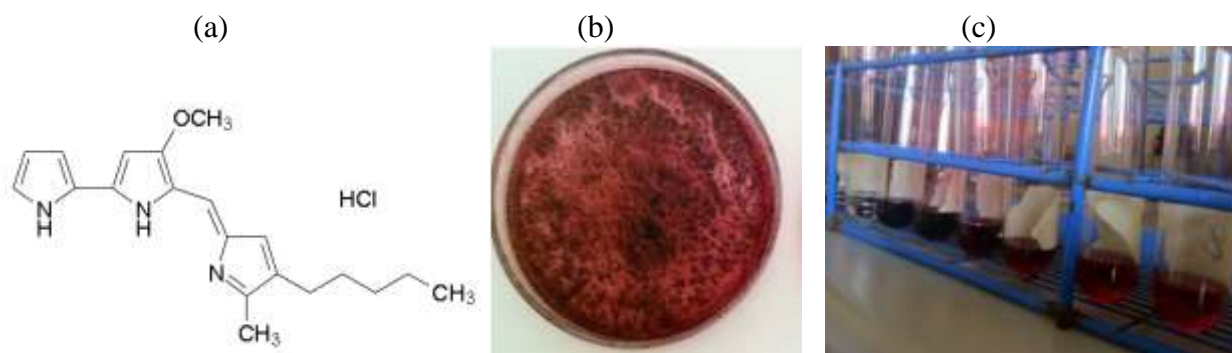
Moreover, Francisco and coworkers (2003) [23] reported the effect and mechanisms of action of PG against different human neuroblastoma cell lines (i.e. SH-SY5Y, LAN-1, IMR-32 (N-type) and SK-N-AS (S-type)). PG was described as a proton sequestering agent that has the ability to destroy the intracellular pH gradient. The cytotoxic effect of PG was allied with its

action on the mitochondria, thereby exerting uncoupling effects on the electronic chain transport of protons to mitochondrial Adenosine triphosphate (ATP) synthesis. This action causes the production of ATP to be reduced without any decrease in oxygen consumption. This action is unique from those induced by the conventional chemotherapy drugs, showing the possibilities of the use of PG as an antitumor agent in the treatment of neuroblastoma.

Morphological study of cells treated with PG confirms that PG induces cell shrinkage, chromatin condensation, reorganization of actin microfilament architecture and detachment of cells from substrates [24]. Moreover, other activities of PG includes; induction of single-and-double strand DNA breaks modulation of pH, regulation of mitogen-activated protein kinase, and inhibition of cell cycle progression [22].

PG is soluble in acetonitrile, methanol, chloroform and dimethyl sulfoxide (CH₃)₂SO (DMSO) and insoluble in water. Solutions of PG are stable in acidic pH and unstable under alkaline conditions. Solutions, at 2 mg/ml in DMSO or methanol, are stable for at least 6 months at -20 °C. The chemical structure of PG including synthesized prodigiosin from *Serratia marcescens* at Sheda Science and Technology Complex, Abuja-Nigeria, are presented (Fig. 2.4).

Sumathi and co-workers (2014) [25] presented the optimum conditions required for maximum production of prodigiosin were achieved at 30 h, 30°C, pH 8 and 3% substrate concentration (Fig. 2.5).



Figures 2.4: Prodigiosin: (a) Chemical Structure of Prodigiosin, (b) synthesized prodigiosin from *Serratia marcescens* at Sheda Science and Technology Complex, Abuja, Nigeria. (c) Fractions of Purified Prodigiosin.

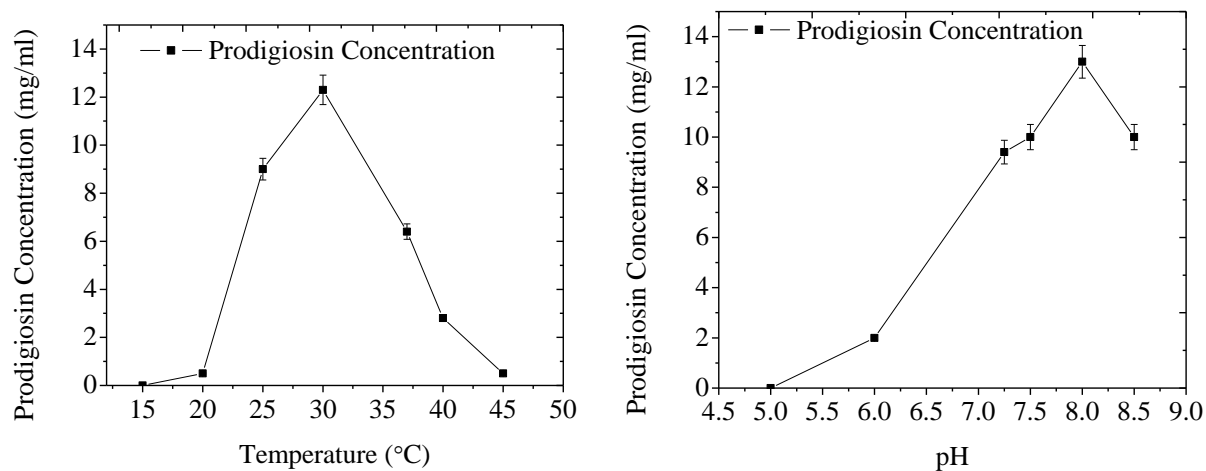


Figure 2.5: Optimum conditions required for maximum production of prodigiosin concentration were achieved (at time 30 h, 30°C and pH 8.0). Replotted from [25].

2.6 Cancer Drug Delivery

Substantial progress has been made to develop drug delivery systems for localized cancer treatment. Meanwhile, the drawbacks accompanying bulk systemic chemotherapy have inspired current efforts toward the development of new approaches to enhance localized chemotherapy [2]. This section presents a review of drug delivery approaches that are relevant to localized treatment. Current developed drug delivery devices include: local chemotherapy; controlled cancer therapeutics; liposomal systems; transdermal drug delivery patches; microchips; micro-pumps; microspheres; polymer conjugates (Figure 2.6a), and a multi-well silicon-based drug-release device (Figure 2.6b).

However, these approaches of drug delivery lack specificity and consistency and also expose drugs to nontarget cells/tissues to drugs. These approaches also lack the ability to deliver controlled amounts of drugs to selected tissues. The primary objective of this work is to develop implantable biomedical devices for localized treatment of breast cancer. The materials issue associated with localized drug release will also be elucidated.

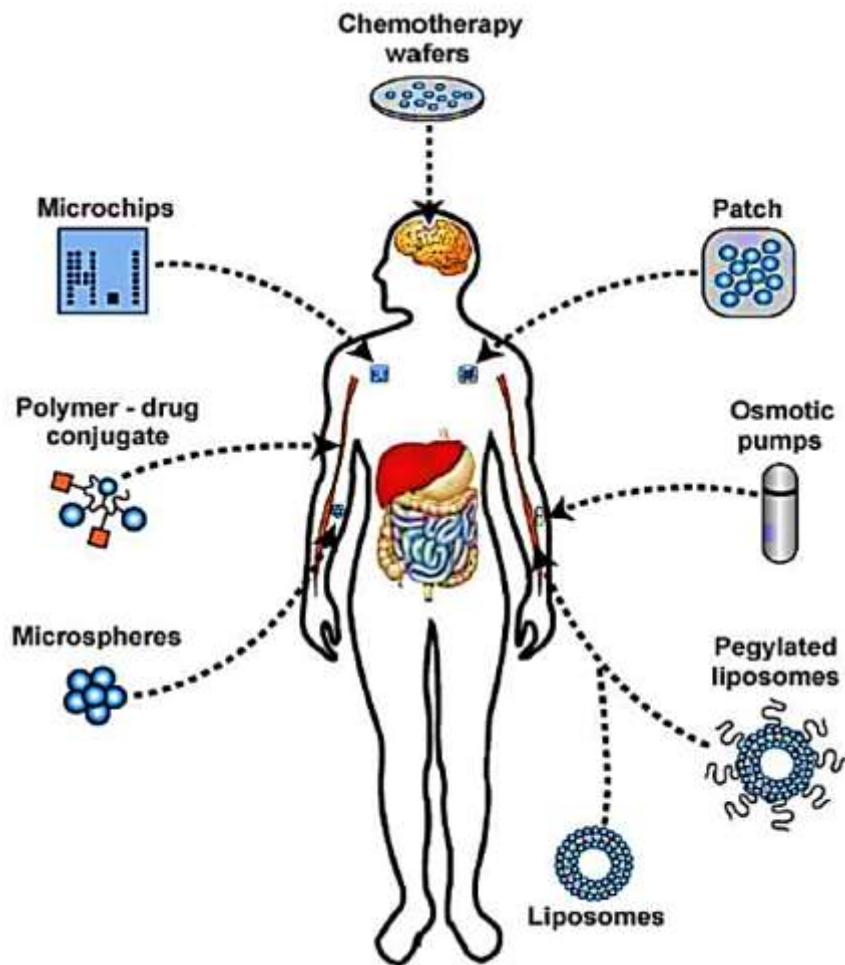


Figure 2.6a: A variety of different delivery strategies that are currently being used or in testing stage to treat human cancers (Hildebrandt et al., 2007) [26].

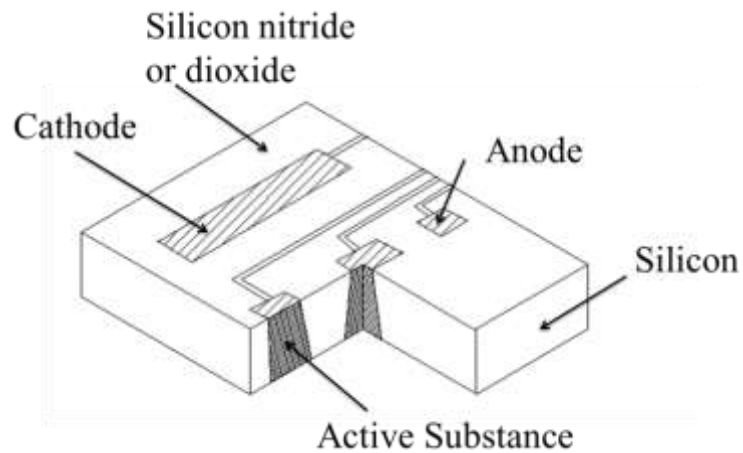


Figure 2.6b: Multi-well silicon-based drug-release device, adapted (Modified from Santini et al., 1999) [27].

2.7 Micropumps

Micropumps, as well as microneedles, are microfluidic products used in the biomedical field, especially in drug delivery [28]. Micropumps are classified into two groups, depending on the actuation mechanisms involved in the device operation. For instance, there are those that operate mechanically, and others that are non-mechanical. A comprehensive review of prior work on micropumps has been presented by Ashraf et al., in 2011 [28]. This summarizes microfluidic design approaches, their performance parameters, working principles, fabrication techniques, and safety issues. Flow is usually controlled, although some devices may rely on natural driving forces (such as diffusion and osmosis) to deliver drug concentrations locally within the therapeutic window.

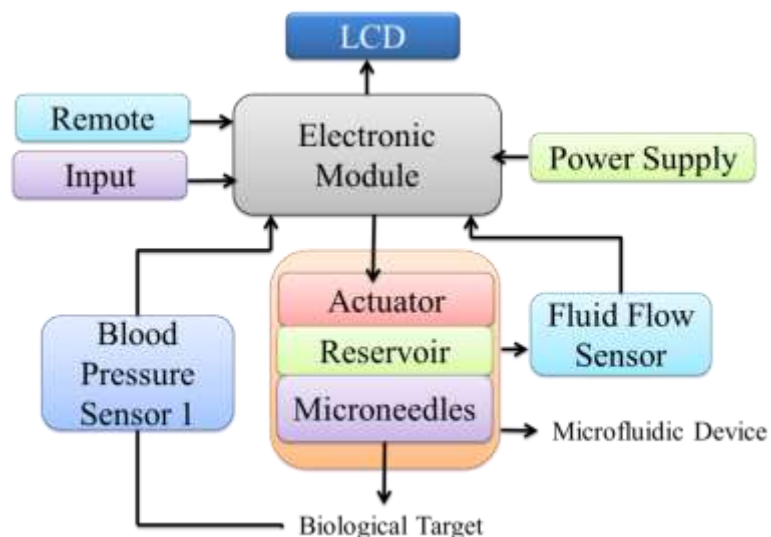


Figure 2.7: Schematic illustration of transdermal drug delivery system: Redrawn from (Ashraf, et al., 2011) [28].

There has been progress in recent times toward developing micro-fluid transdermal drug delivery devices [29]. A schematic illustration of a transdermal drug delivery system is shown (Fig. 2.7) above. In such a device, the actuator provides the necessary force required for fluid to

flow in the device. The valve also plays a significant role in micro-pumps, as it controls the flow of fluid through the device and closes when necessary.

2.8 Drug Delivery Polymers

In recent years, there have been increasing efforts to develop biodegradable polymers for drug delivery systems [30-33]. These have favor because such systems do not require surgical removal, once the drug supply is depleted. There are efforts by major chemical companies to make monomers and polymers that are readily more accessible. The mechanism controlling biodegradation of a polymer is basically hydrolysis of the ester linkages, which gives an idea on the role played in *in vivo* performance of the lactide or glycolide materials. Moreover, the crystallinity of the materials and the intake of water are also factors that can determine the rates of the *in vivo* degradation of the polymer.

Poly-caprolactone and its copolymers have been explored for controlled drug delivery [34,35]. Natural and Synthetic polymers mostly are used for drug delivery because they have minimal effect on the biological systems after their integration into the body. Degradation *in vivo* is at a well-defined rate to nontoxic compounds, and this has been long explored to have readily excreted degradation products [36]. But a natural polymer remains more attractive since they are readily available. More to the point, the natural polymers are relatively inexpensive and they can be chemically modified.

2.9 Hydrogels

Hydrogels are three-dimensional polymeric materials with enormous swelling capacity in aqueous medium due to their water-swollen network (Cross-linked structures) of hydrophilic homopolymers or copolymers [37,38]. Weaker forces such as Van der Waals forces and

hydrogen bonds serve as cross-links to create the swollen network. Polymeric material in its dry state is called a xerogel, regardless of the nature of its swelling medium.

Thus: Xerogel + water \rightarrow hydrogel (2.1)

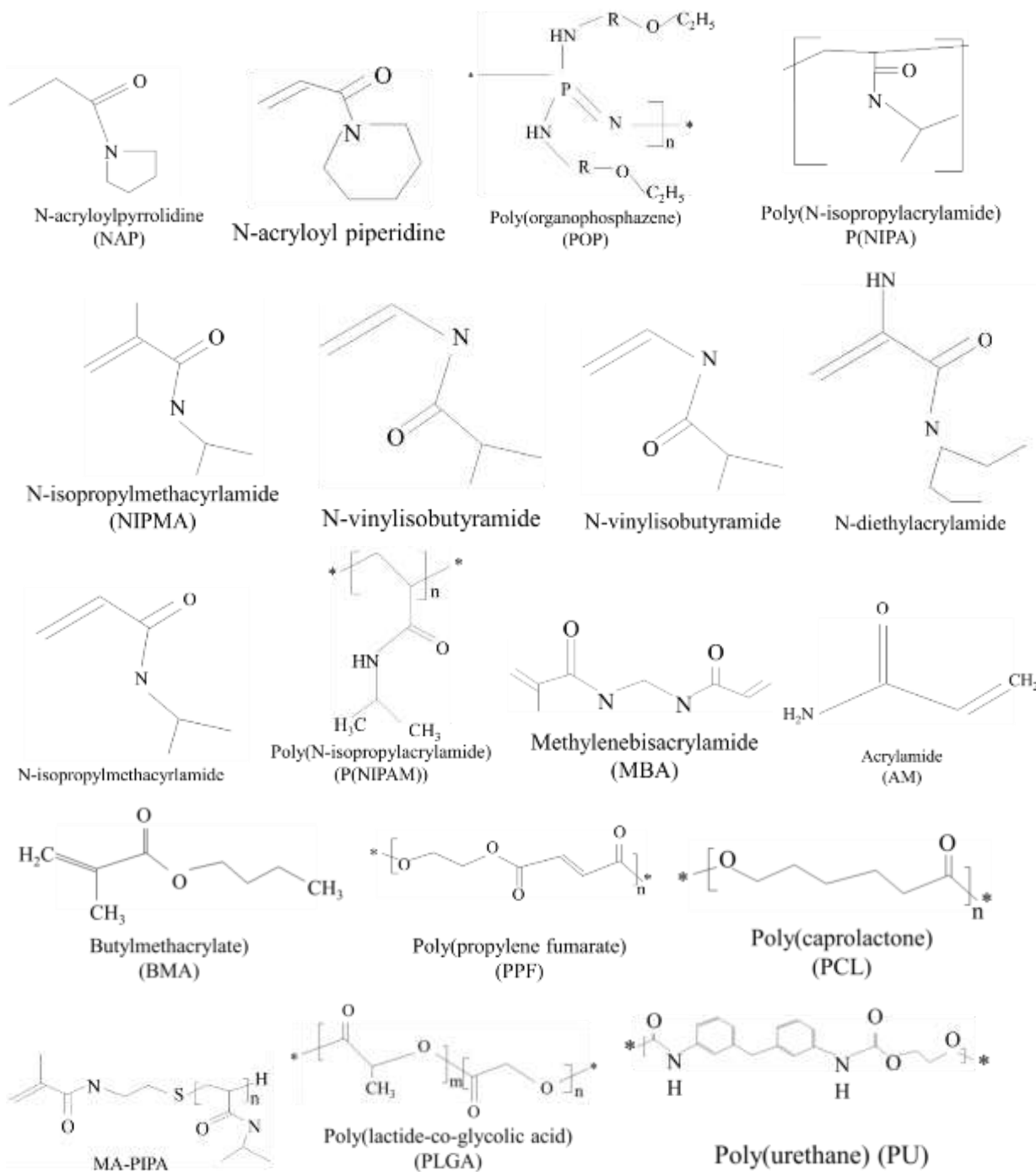
Hydrogels can undergo structural changes due to changes in pH, temperature and environment [39]. Hydrogels are covalently bonded polymeric networks that contain water. They are formed by simply reacting one or more co-monomers [2,40]. Hydrogels can also be physically cross-linked from entanglements, associated bonds such as hydrogen bonds or strong Van der Waals interactions between chains [37].

2.9.1 Poly(N-Isopropyl acrylamide) (PNIPA)-based Hydrogels

Considerable progress has been made in understanding P(NIPA)-based hydrogels [3,41,42]. Smart hydrogels have been studied in recent years to harness their swelling behaviors and the release of fluids from the polymer matrix in response to environmental stimuli such as temperature, pH, electric field and solvent composition [1,43,44]. P(NIPA)-based hydrogels can be used to store and release controlled amounts of drugs. They have the potential to be used for applications in drug delivery systems [45,46]. One drawback to P(NIPA) hydrogels is that they are not biocompatible, but that problem can be solved.

Thermo-sensitive hydrogels have recently been explored for their potential in drug delivery [2,40,47]. The [table \(2.1\)](#) below shows some common monomers used in synthesizing temperature-sensitive hydrogels/microgels.

Table 2.1: Monomers Used in Synthesizing Temperature-Sensitive Hydrogels/Micorgels.



PNIPAA is a thermo-sensitive hydrogel with a lower critical solution temperature (LCST) (Fig. 2.8) of about 32°C in an aqueous solution especially when it is cross-linked with other monomers [48].

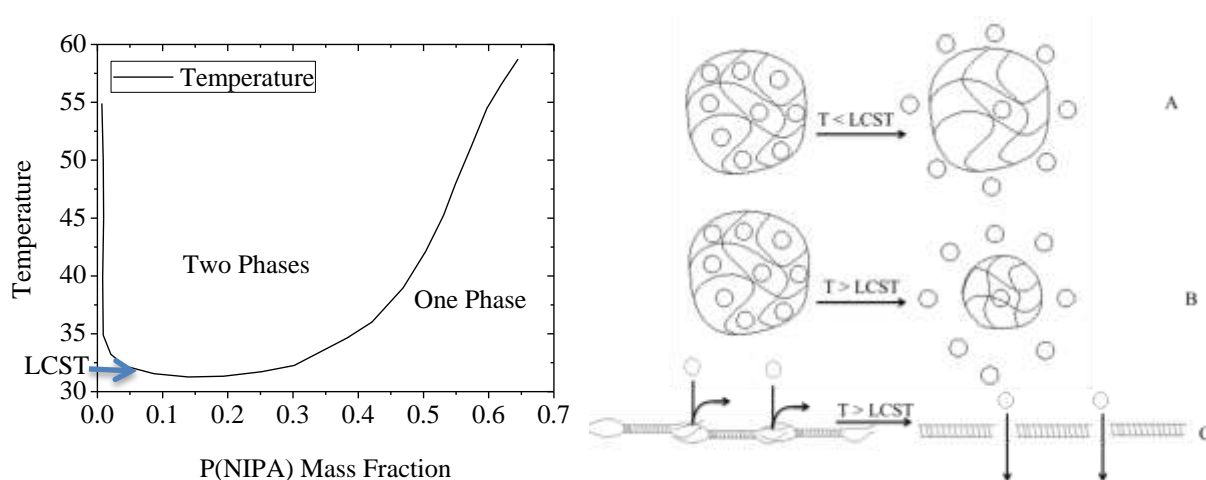
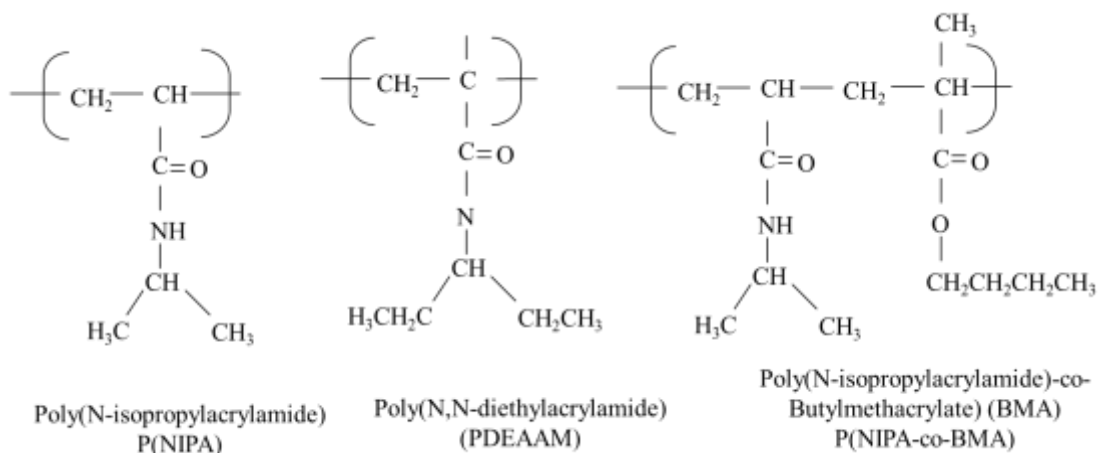


Figure 2.8: Phase Diagram for P(NIPA)-based Hydrogel in Water (first figure from left); (a) when the application temperature is less than the lower critical solution temperature (LCST), (b) when the application temperature is greater than the LCST and (c) drug molecules will be released from the hydrogel if $T > LCST$ through the loosely bonded gel structure or will not if $T < LCST$.

P(NIPA)-based hydrogels exhibit swelling transitions around 32°C [49] although 33°C [40] and 34°C [2] were reported in recent studies for P(NIPA)-based homopolymers. Examples of some temperature-sensitive hydrogels have been presented (Table 2.2).

Table 2.2: Structures of Some Temperature Sensitive Polymers



It is also noted that the LCST can be modified through copolymerization/crosslinking to achieve LCSTs closed to the physiological human body temperature ($\sim 37^\circ\text{C}$). This makes P(NIPA)-based hydrogels attractive for potential applications in controlled drug release. A recent

study shows that polyelectrolytes can affect the LCSTs of P(NIPA)-based hydrogels [50]. It has also been reported that the LCSTs of P(NIPA) is dependent on pH and its LCSTs increase with an increase in pH [50]. Moreover, crosslinking NIPA with acrylamide helps to effectively increase the LCST [2,40].

When P(NIPA) is heated above a critical temperature of 32°C-35°C in water, it undergoes a reversible temperature phase transition from a swollen hydrated state to a shrunken dehydrated state, thereby losing about 90% of its mass [2,40,48]. The ability of P(NIPA)-based hydrogel to store and release incorporated drugs/fluids motivated many to investigate the possible applications of P(NIPA) to be used in controlled drug-delivery [2,40,51].

However, further work is needed to explore new ways of improving the swelling and drug release kinetics of P(NIPA)-based hydrogels [2,52,53,54]. This could help to obtain smart hydrogels for sensitive drug delivery systems. Other works improved upon the swelling performance of P(NIPA)-based hydrogels by forming interpenetration polymer networks inside the hydrogel [55].

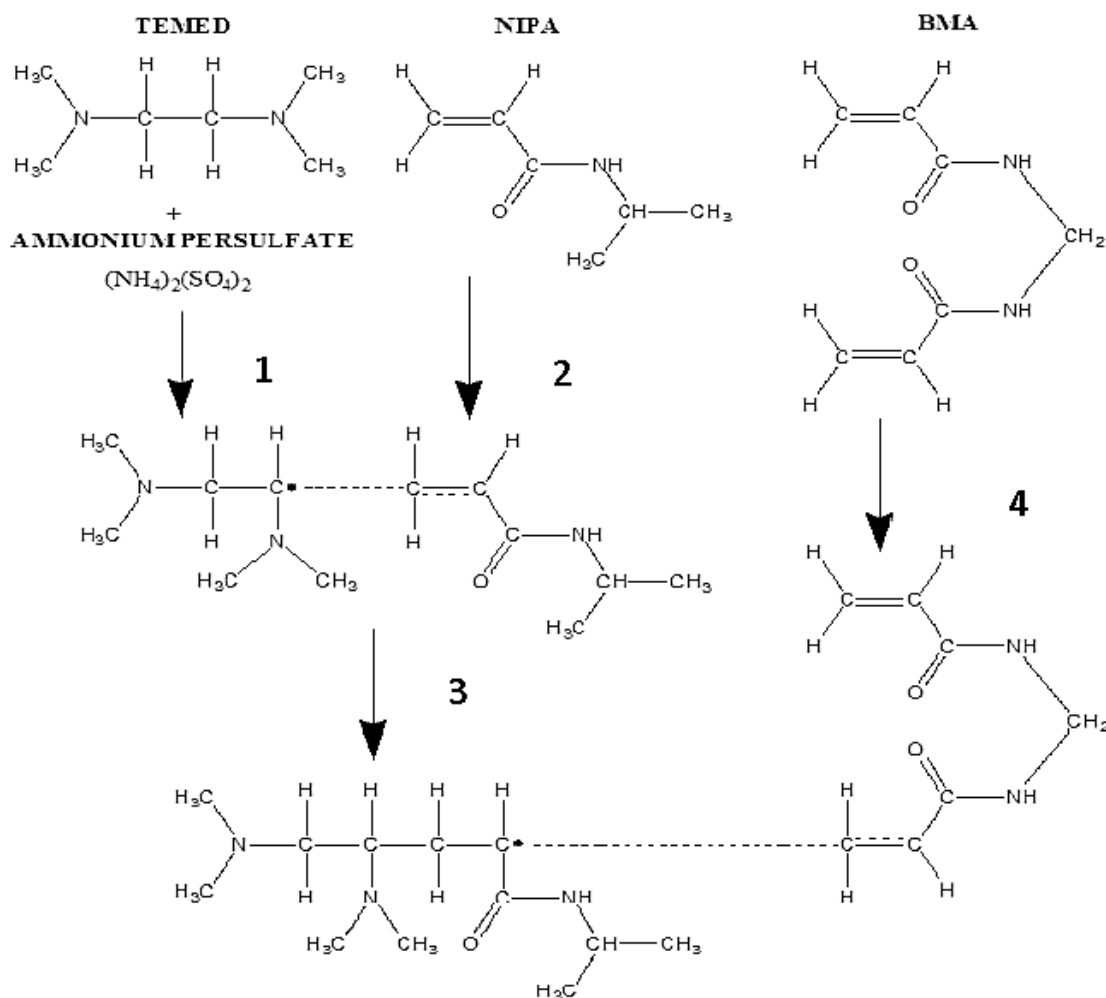
In spite of the numerous advantages of hydrogels, they offer poor mechanical properties as earlier reported by Flory [39] including low strength and low modulus, especially in the swollen state. This has led to the development of new gel composites that consist of polyurethane foams and P(NIPA) [39].

2.9.2 Polyacrylamide-based Composite

Acrylamide (AM) monomer can be cross-linked with small amounts of methylene-bis-acrylamide (MBA) by polymerization. MBA is used as a cross-linking agent because of its two acrylamide molecules linked by a methylene group. The AM monomer usually polymerizes in a head-to-tail manner into long chains which contribute to building growing chains. This also

initiates other sites for chains to extend. The polymerization of AM is characterized by free-radical catalysis [56], hence ammonium persulfate (APs) and the base *N,N,N',N'*-tetra-methylene-diamine (TEMED) can serve as initiators (catalysis) for the process (Table 2.3).

Table 2.3: Polymerization of PNIPA-Based Gel, copolymerized with BMA.

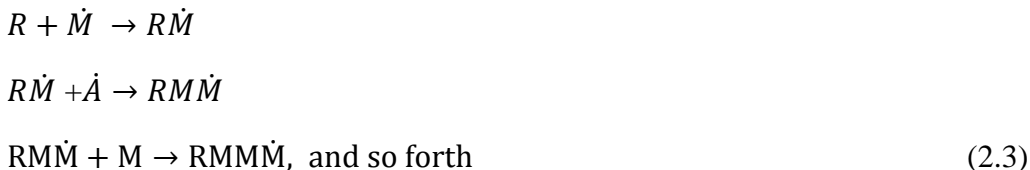


¹Initiation, ²Propagation (free radicals are very reactive causing structural change), ³Polymerization stage, ⁴Crosslinking with MBA. TEMED catalyzes the decomposition of the persulfate ion to give a free radical (i.e. a molecule with an unpaired electron).

Furthermore, TEMED catalyzes the decomposition of the persulfate ion to give a free radical (i.e. a molecule with an unpaired electron) [57].



The polymerization can be represented by equation (2.3). Suppose we let as \dot{R} represent the free radical and M represent the acrylamide monomer molecule. This implies:



where \dot{A} is an unpaired electron, \dot{M} is a radical of acrylamide molecule, while $R\dot{M}$, $RM\dot{M}$ and $RMMM\dot{M}$ represents the growth of long chains until the polymerization process is terminated. This develops longer acrylamide chains, especially when an MBA molecule is introduced into the solution. Butyl-methyl-acrylamide (BMA) can also be used as a hydrophobic co-monomer for copolymerization. Figure (2.9), illustrates a polymerization step for P(NIPA)-based hydrogel copolymerized with BMA.

2.10 Biodegradable Polymers

Biodegradable polymers studied in recent times belong to the polyester family: poly(lactic acid) (PLA) and poly(glycolic acid) (PGA). PLA, PGA, and their copolymers have countless clinical applications [58,59]. The polymer chains can degrade hydrolytically and or enzymatically. PGA is normally synthesized by rigid opening of glycolide. PGA is a highly insoluble polymer and it is unremarkable when used as a copolymer with PLA. The table below (Table 2.4) shows a list of biodegradable polymers and their repeated unit structures [60]. PLGA can also be copolymerized with other monomers such as polyethylene glycol (Fig. 2.9) for biomedical applications [60-62].

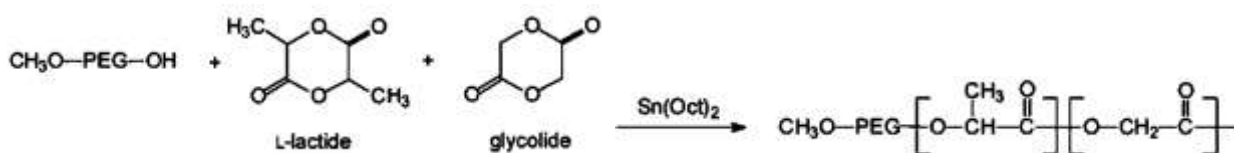
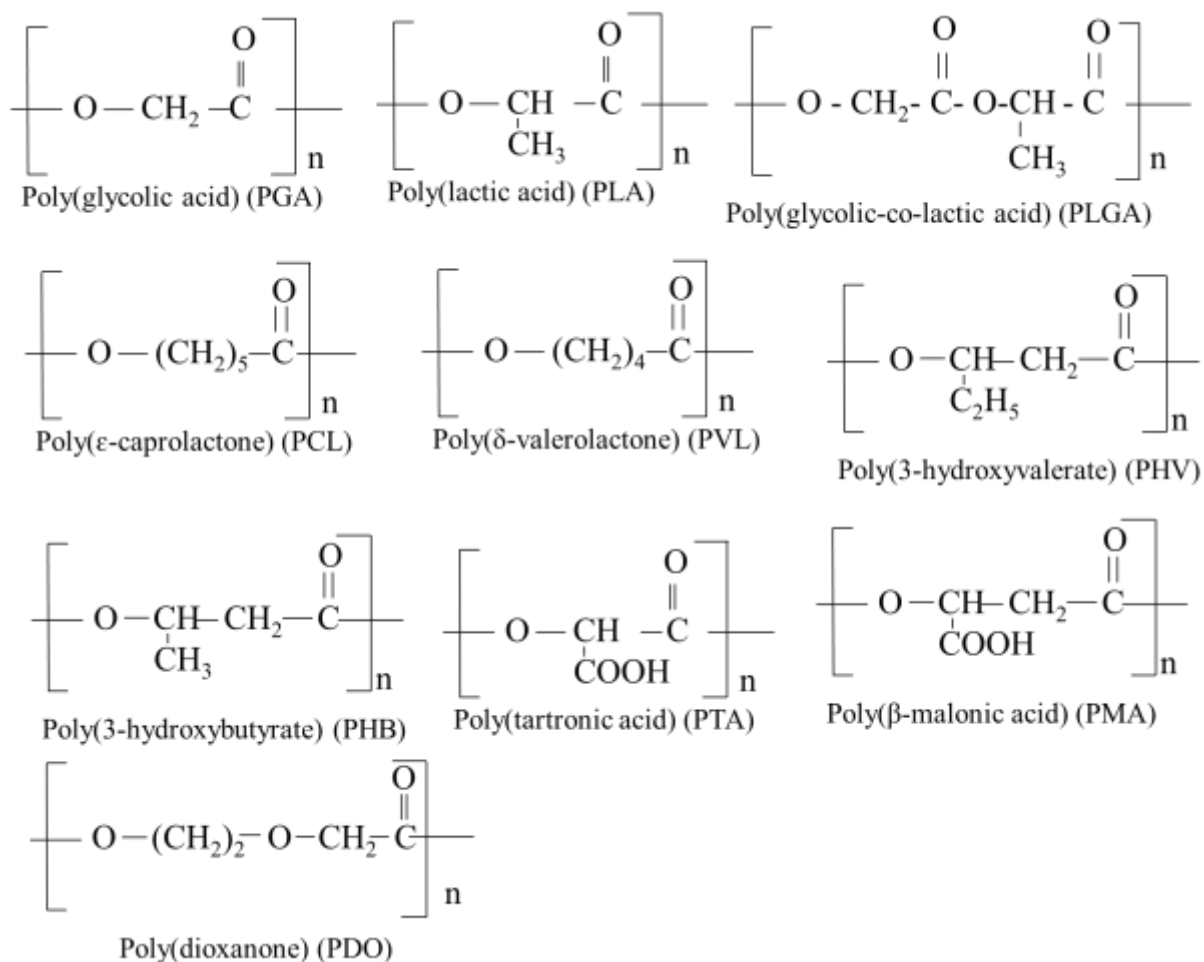


Figure 2.9: Shows the Polymer Unit Structures of PGA, PLA, PLGA and PLGA-PEG: Polymer Unit Structures: Typical Synthetic Route of a PLGA-PEG Diblock Copolymer.

Table 2.4: List of biodegradable polymers and their polymer repeated unit structures.



Biodegradable microparticles have also been formulated from PLAs or PLGAs for controlled drug release [31]. PLAs or PLGAs have shown greater biocompatibility and biodegradability [32,33] than P(NIPA)-based hydrogels. By altering a number of factors such as polymer composition, molecular weight, size and surface characteristics, well-defined degradation rates can be achieved to control the release of encapsulated therapeutic agents [30].

The largest application of PLA/PGA polymers is in drug-delivery systems, resorbable sutures, and other orthopedic fixation devices such as pins, rods, and screws [63,64]. PGA is also known to be a rigid thermoplastic material with a high crystallinity (40-50 %). Its glass transition temperature and melting temperature are 36°C and 225°C, respectively [65].

2.11 Mechanism of Polymer Degradation

Degradation is a chemical process which alters both the chemical composition of the polymer as well as its physical parameters. These include; the polymer color, crystallinity, chain flexibility, cross-linking, chain conformation, molecular weight distribution and branching [66]. The nature of weak links and polymer end groups has an effect on the stability of a polymer [66]. Polymer degradation involves chain scission by cleavage of bonds between the monomers in the polymer backbones [66]. There exist four major modes of polymer degradations. These include; photo-degradation, mechanical degradation, thermal-degradation and chemical degradation. Predominantly, biodegradation of polymers occurs by chemical degradation where hydrolysis depicts the mode of chemical degradation [67]. Polymer degradation is characterized by weight loss when soaked in water/phosphate buffer saline (PBS). The weight change can be observed using:

$$\frac{M_t}{M_i} = \sqrt{t} \quad (2.4)$$

where M_t is the mass of the polymer at time t , M_i is the initial mass of the polymer, and t is the degradation time. The concentration of the solvent in the polymer is then determined from:

$$C(t) = \frac{W_w - W_d}{W_{sat}} \quad (2.5a)$$

$$W_{sat} = \rho V \quad (2.5b)$$

where W_d is the dry weight of the polymer, W_w is the weight when immersed in a fluid for control duration, W_{sat} is the saturated polymer weight, ρ is the density of the water/PBS used and V is the volume of the sample. Moreover, the chemical reactions can be estimated from the reaction kinetics:

$$\frac{dC}{dt} = -kC^n \quad (2.6)$$

where k is the reaction rate constant, n is the order of reaction, C is the concentration of drug release at time t . Therefore, for a first order ($n = 1$) and at $t = 0$, $C = C_0$. This gives an exponential time dependent of drug concentration and equation (2.7) becomes:

$$C(t) = C_0 e^{-kt} \quad (2.7)$$

In addition to the mass loss, the molecular mass change can be obtained using gel permeation chromatography, while thermal analyses are obtained using differential scanning calorimetry (DSC) and morphological features are obtained with scanning electron microscopes (SEM) and optical microscopes or similar techniques. The effect of the average molecular weight change due to the presence of moisture causes hydrolytic degradation as presented below [66]:

$$M'_n = \frac{M_n}{[1+x(M_n/1800)]} \quad (2.8)$$

where M_n is the initial average molecular weight of the polymer, M'_n is the average molecular weight after reaction with water and x is the water content (weight %). The rate of polymer melt degradation is generally represented by the equation [66]:

$$\frac{1}{N} = \frac{1}{N_0} + k_0 e^{(-E/RTt)} \quad (2.9)$$

where N_0 and N are the initial and final number average degree of polymerization, respectively. Moreover, k_0 is degradation rate constant, E is activation energy, R is the universal gas constant,

T is the degradation temperature (K) and t is the time (m). However, due to the difficulty in obtaining the degree of polymerization, the intrinsic viscosity, η is often related to the polymerization using Mark Howink equation:

$$\eta = bN^\beta \quad (2.10)$$

$$C_\eta = kM_n^\alpha = C_\eta \cdot e^{-\alpha kt} \quad (2.11)$$

where η is the intrinsic viscosity, b and β are constants which depend on the type of polymer, and α is the Mark-Houwink exponent which depends on the solvent in which the polymer degrades. The rate of degradation of the polymer melts then becomes [66]:

$$\frac{1}{\eta^{1/\beta}} = \frac{1}{\eta_0^{1/\beta}} + k_o \left(1/b\right)^{(1/\beta)} e^{(-E/RTt)} \quad (2.12)$$

where η_0 and η are the initial and final intrinsic viscosities, E is the activation energy of the polymer, while b and β are constants which depend on the type of polymer.

The rate of polymer erosion can also be given as:

$$\frac{dM}{dt} = -k \quad (2.13)$$

where M is the polymer mass at any time, t and k is the kinetic rate constant of the degradation.

For a 1-D erosion and constant density of fluid, $\frac{dM}{dt} = -k$ can be rearranged as:

$$\frac{dl}{dt} = -k' \quad (2.14)$$

where l is the dimension of the polymer in the direction of degradation front at any given time t, and k' is the adjusted rate constant ($l = l_0 - k't$).

Metters *et al.*, [61,62] devised statistical kinetic models to predict polymer degradation behavior, which says that the probability (P) of any random PLA unit been hydrolyzed is given by:

$$P = 1 - f_{PLA} = 1 - e^{-k't} \quad (2.15)$$

where f_{PLA} is the total fraction of polymer hydrolyzed (equal to the ratios of polymer concentration C/C_0 for before and after polymer degradation).

2.12 Polydimethylsiloxane (PDMS)

Polydimethylsiloxane (PDMS) is a silicon-based organic polymer (Fig. 2.10) with unusual rheological properties. It is optically clear, and it is also considered to be inert, non-toxic, and biocompatible. PDMS has been approved by the U. S. Food and Drug Administration (FDA) as a biocompatible polymer for applications in implantable biomedical devices in humans [68-70], following several toxicity studies [71-73]. Biocompatible and inexpensive polymers, such as PDMS, are often the materials of choice for the fabrication of microfluidic devices [3].

Sylgard-184 kit is an elastomeric PDMS kit and its curing agents are manufactured by Dow Corning Corporation. These comprise mainly the constituents of a reaction mixture having vinyl endcapped oligomeric dimethyl-siloxane, a methyl hydrosiloxane as crosslinking agent, and a platinum complex, which can be used as a catalyst for the hydrosilation reaction (Dow Corning's).

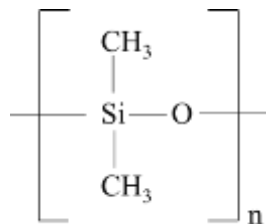


Figure 2.10: Shows a Linear Poly-dimethyl-siloxane (PDMS)

2.13.0 Characteristics of P(NIPA)-based Hydrogels

2.13.1 Swelling Kinetics

The swelling or shrinkage of P(NIPA)-based hydrogels is usually controlled by the diffusion of water molecules through the gel network [74]. Although, this process may be slow, especially near the critical point, the rate of response is inversely proportional to the square of the gel size [75]. Other studies reported that P(NIPA)-based hydrogels exhibit dangling chain structures near the phase transition temperature [76,77]. This implies the hydrogel would easily collapse and expand when an external stimulus is applied, as a result of the free dangling chains on the sides. The adsorption or desorption of fluid/drug solution occurs through interconnected pore structures by convection [78]. The macro-porosity of P(NIPA)-based hydrogels depends on: the phase separation that occurs during cross-linking; gel synthesis parameters such as temperature and crosslinker; monomer concentration, and also the pore-forming agent such as the type of the inert diluents used [79]. However, the gel preparation temperature appears to exert the greatest influence on the macroporosity within the P(NIPA) gel network [78]. This suggests that polymerization below the lower critical solution temperature (LCST) should help achieve the macroporous gel network.

However, prior work [80] has shown a rapid shrinking of P(NIPA) gels when they were prepared at temperatures above their LCST. It is also possible to produce fast responsive P(NIPA) gels at temperatures below freezing point (-18°C). Poly(ethylene-glycol) (PEG) with various molecular weights as a co-monomer to P(NIPA) has shown a great macroporosity in the microstructure P(NIPA)-based hydrogels [81]. Zhang et al., [82] have shown that P(NIPA)-based hydrogels can be prepared to achieve higher degrees of porosity by increasing the cross-linker concentrations. Critical cross-linker concentration possibly caused a heterogeneous macroporous network structure [83].

The swelling ability of a hydrogel is accomplished through direct weighing, prior to soaking the gel in fluid/drug solution at controlled temperatures inside a temperature-controlled water-bath. The swelling ratio is given by:

$$S_R = \frac{W_t - W_o}{W_o} \quad (2.16)$$

where, W_t is the weight of swollen gel at temperature T , and W_o is the weight of the dry gel. In a recent work by [Fu and Soboyejo \[84\]](#), the addition of sodium Alginate to P(NIPA)-based hydrogels influenced the swelling ratios. Sodium alginate is biocompatible and it also enhances the creation of interpenetrating polymer network [\[85\]](#).

Other parameters used to characterize P(NIPA) network structures include; the polymer volume fraction in the swollen state ($v_{2,s}$) as well as the corresponding mesh size ξ , given by [\[86\]](#):

$$\xi = (v_{2,s})^{-\frac{1}{3}} (\bar{r}_0^2)^{\frac{1}{2}} = \alpha N \quad (2.17a)$$

$$\alpha = (v_{2,s})^{-\frac{1}{3}} \text{ and } N = (\bar{r}_0^2)^{\frac{1}{2}} = \left(2lC_n \frac{\bar{M}_c}{M_w} \right) \quad (2.17b)$$

where α is related to the polymer volume fraction ($v_{2,s}$), \bar{M}_c is a measure of the degree of cross-linking, C_n is the Flory characteristic ratio, l is the length of the bond along the polymer backbone and M_w is the molecular weight of the repeating units from which the polymer chain is composed. Schematics of the above parameters are presented below ([Fig. 2.11](#)).

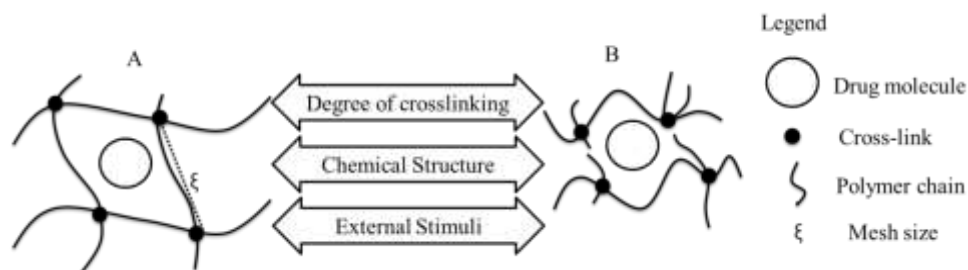


Figure 2.11: Illustration of Mesh Size in a Hydrogel at; (A) Swollen State and (B) De-Swollen State. Modified after Lin and Metters, 2006 [87].

2.13.2 De-Swelling Kinetics

De-swelling kinetics of P(NIPA)-based hydrogels can be determined by first soaking dried gels in fluid/drug solutions at controlled temperature to equilibrium. Then, the de-swelling experiment is carried out by transferring loaded gels into water bath, placed on a filter paper to study fluid/drug release at temperatures of choice. The fluid/drug release in the gels is obtained from the relative gel mass [78]:

$$M_{\text{rel}} = \frac{M_t}{M_s} \quad (2.18)$$

where M_t is the mass of the gel at time, t and M_s is the swollen mass. An inorganic phase was incorporated into P(NIPA)-based gels to give faster de-swelling kinetics and as well as to improve upon the mechanical properties of the gels when prepared under homogeneous conditions [88]. Homogeneous synthesis creates microphase separation of P(NIPA) during polymerization, yielding a highly porous product structure.

2.13.3 Equilibrium Swelling Measurements

Equilibrium swelling is determined by soaking the gels in distilled water at room temperature (25°C) for two weeks [78] or in prodigiosin at 28°C for a week [40]. The equilibrium volume ratio of gels at the swollen state (V_{eq}) is determined from the measured diameters of the hydrogels. This gives:

$$V_{\text{eq}} = \left\{ \frac{\pi D^2}{4} / \frac{\pi D_0^2}{4} \right\} = \frac{D^2}{D_0^2} \quad (2.19)$$

where D_0 and D are the diameters of the hydrogels, for before and after the equilibrium swelling.

2.14.0 Kinetics of Swollen Hydrogels

2.14.1 Free Energy

Flory and Rehner earlier represented the swelling of cross-linked polymer gels by employing a Gaussian distribution model for the polymer chains [89]. They describe the equilibrium degree of cross-linked polymers by hypothesizing that the extent to which a polymer network swelled was structured by the elastic retroactive forces of the polymer chains as well as the thermodynamic compatibility of the polymer and the water molecules. In terms of the free energy of the system, the total free energy change upon swelling was given by:

$$\Delta G = \Delta G_{el} + \Delta G_{mix} \quad (2.20)$$

where ΔG_{el} is the influence of the elastic retroactive forces and ΔG_{mix} is the thermodynamic compatibility of the polymer. By differentiating equation (2.20) with respect to the number of water molecules in the system at constant temperature (T) and pressure (P), we can obtain the change in chemical potential in the water as a result of swelling. This gives:

$$\mu_1 - \mu_{1,0} = \Delta\mu_{el} + \Delta\mu_{mix} \quad (2.21)$$

where μ_1 is the chemical potential of the swelling agent within the gel and $\mu_{1,0}$ is the chemical potential of the pure fluid. The chemical potential of the swelling agent that is inside and outside of the gel must be equal in equilibrium.

2.14.2 Swelling Characteristics of Ionic Hydrogels

The general equations for the free energy (2. 22a) and the chemical potential (2.22b) of ionic hydrogels at equilibrium swelling is given by [90]:

$$\Delta G = \Delta G_{el} + \Delta G_{mix} + \Delta G_{ion} \quad (2.22a)$$

$$\mu_1 - \mu_{1,0} = \Delta\mu_{el} + \Delta\mu_{mix} + \Delta\mu_{ion} \quad (2.22b)$$

where ΔG_{ion} and $\Delta \mu_{ion}$ are the changes in free energy and chemical potential due to ionic contributions of the swelling agent/system.

Through the mixing process, the chemical potential change was obtained from the heat of mixing and the entropy of mixing [91-93] (equation 2.23a). Similarly, the elastic contribution to the chemical potential change was obtained from statistical theory of rubber elasticity [91]. This elastic free energy therefore depends on the number of polymer chains within the network as well as the linear expansion factor in the presence of water (equation 2.23b).

$$\Delta \mu_{mix} = RT [\ln(1 - v_{2,s}) + v_{2,s} + \chi_1 v_{2,s}] \quad (2.23a)$$

$$\Delta \mu_{el} = RT \left(\frac{V_1}{v \bar{M}_c} \right) \left(1 - \frac{2\bar{M}_c}{\bar{M}_n} \right) v_{2,r} \left[\left(\frac{v_{2,s}}{v_{2,r}} \right)^{1/3} - \frac{v_{2,s}}{2v_{2,r}} \right] \quad (2.23b)$$

where v is the specific volume of the polymer, $v_{2,s}$ is the volume fraction of the polymer in the gel, $v_{2,r}$ is the volume fraction of the polymer in the relaxed state, χ_1 is the polymer water interaction parameter [91-93], v_1 is the molar volume of the swelling agent, R is the Boltzmann's constant, T is the reaction temperature, \bar{M}_c is the molecular weight of the polymer chains between junction points, and \bar{M}_n is the molecular weight of the polymer chains if no crosslinks had been introduced.

The swelling of cross-linked networks in the presence of water can be obtained by combining equation (2.23a and 2.23b) above. This gives:

$$\frac{1}{\bar{M}_c} = \frac{2}{\bar{M}_n} - \frac{\left(\frac{v}{V_1} \right) [\ln(1 - v_{2,s}) + v_{2,s} + \chi_1 v_{2,s}]}{v_{2,r} \left[\left(\frac{v_{2,s}}{v_{2,r}} \right)^{1/3} - \frac{v_{2,s}}{2v_{2,r}} \right]} \quad (2.24)$$

where all the symbols have their usual meaning from equations (2.23a and 2.23b).

2.14.3 Factors Affecting the Swelling Characteristics of Ionic Hydrogels

There are several factors affecting the swelling characteristics of ionic hydrogels. The major factors include the degree of ionization in the network, ionization equilibrium and the nature of the counter-ions. Increase in ionic concentration of hydrogels due to environmental stimulus, increases the repulsive forces which make the polymer network more hydrophilic [90].

However, the ionic term in equation (2.22) strongly depends on the ionic strength as well as the nature of ions.

$$\Delta\mu_{ion} = RTV_1\Delta C_{tot} \quad (2.25)$$

where ΔC_{tot} is the difference in the total concentration of mobile ions within the gel network.

Several works have demonstrated the ionic contributions to the swelling of polyelectrolytes [94-96]. Brannon-Peppas and Peppas [96,97] developed the expressions for the ionic contribution to swelling of polyelectrolytes for anionic (equation 2.26a) and cationic (2.26b) materials, respectively:

$$\Delta\mu_{ion} = \frac{RTV_1}{4I} \left(\frac{v_{2,s}^2}{v} \right) \left(\frac{K_a}{10^{-pH} + K_a} \right)^2 \quad (2.26a)$$

$$\Delta\mu_{ion} = \frac{RTV_1}{4I} \left(\frac{v_{2,s}^2}{v} \right) \left(\frac{K_b}{10^{pH-14} + K_b} \right)^2 \quad (2.26b)$$

where I is the ionic strength, and K_a and K_b are dissociation constants for the acid and base, respectively. The degree of swelling for crosslinked anionic polymer gels in water at equilibrium can be obtained by combining equations (2.23a-b) and (2.26a):

$$\frac{V_1}{4I} \left(\frac{v_{2,s}^2}{v} \right) \left(\frac{K_a}{10^{-pH} + K_a} \right)^2 = (\ln(1 - v_{2,s}) + v_{2,s} + \chi_1 v_{2,s}) + \left(\frac{V_1}{v\bar{M}_c} \right) \left(1 - \frac{2\bar{M}_c}{\bar{M}_n} \right) v_{2,r} \left[\left(\frac{v_{2,s}}{v_{2,r}} \right)^{1/3} - \frac{v_{2,s}}{2v_{2,r}} \right] \quad (2.27a)$$

Similarly, the equilibrium degree of swelling is also be obtained by combining equations (2.23a-b and 2.26b):

$$\frac{V_1}{4I} \left(\frac{v_{2,s}^2}{v} \right) \left(\frac{K_b}{10^{pH-14} + K_a} \right)^2 = (\ln(1 - v_{2,s}) + v_{2,s} + \chi_1 v_{2,s}) + \left(\frac{V_1}{v \bar{M}_c} \right) \left(1 - \frac{2\bar{M}_c}{\bar{M}_n} \right) v_{2,r} \left[\left(\frac{v_{2,s}}{v_{2,r}} \right)^{1/3} - \frac{v_{2,s}}{2v_{2,r}} \right] \quad (2.27b)$$

2.15 Strain on Hydrogels Due to Swelling

Brannon-Peppas and Peppas earlier explained the dynamic swelling of ionic hydrogels due to changes in the ionic strength [96]. For a one-dimensional transport, the swelling of ionic gels due to changes in pH, relates to the volume change or change in length. The strain, ε on the gel as a result of swelling, can be calculated at any time during the swelling as:

$$\varepsilon = \frac{l - l_0}{l_0} \quad (2.28)$$

where l is the length at any time and l_0 is the initial length. However, the responses of the strain to inputs were additive and also time-independent of the applied inputs. The time dependent strain is then given by:

$$\varepsilon(t) = \int_0^t L(t - \tau) \frac{\partial I(\tau)}{\partial \tau} d\tau \quad (2.29)$$

where $\frac{\partial I(\tau)}{\partial \tau}$ is the change in pH/ionic strength and $L(t-\tau)$ is the ionic mechanochemical compliance (it is a function of the polymer). For an isotropic swelling, the volume swelling ratios of the gels are given by:

$$Q(t) = \frac{V_s(t)}{V_d} = \frac{l(t)^3}{l_0} = \{1 + \varepsilon(t)\}^3 \quad (2.30)$$

where $V_S(t)$ is the volume of the swollen gel at any time and V_d is the initial volume of the dry polymer. Therefore, combining equations (2.29. and 2.30), we can obtain the swelling of an ionic gel due to a change in the ionic strength [90]. This gives:

$$Q(t) = \left[1 + \int_0^t L(t - \tau) \frac{\partial I(\tau)}{\partial \tau} d\tau\right]^3 \quad (2.31)$$

where all the parameters have their usual meanings.

The diffusional number, De was also given by the ratio of polymer relaxation time to characteristic diffusion time [90]:

$$De = \frac{\text{Relaxation time}}{\text{Diffusion of solvent}} = \frac{\lambda}{\theta} = \frac{\lambda D_{1,2}}{\{\delta(t)\}^2} \quad (2.32)$$

where λ is the characteristic relaxation time for the polymer due to swelling stresses and δ is the time for water to diffuse into the gel [98,99]. Also, δ is related to the square of the half thickness of a thin disc sample divided by the diffusion coefficient of water in the polymer (i. e. $\delta^2/D_{1,2}$).

2.16 The Goals of Drug Delivery

A novel implant device is proposed to provide an optimal drug delivery profile to the tumor. This device should be able to provide effective drug concentration to the desired region over a prolonged period of time. Such intratumoral implants must provide an optimal drug release profile that is characterized by the ability to deliver drug to a large area, to rapidly reach the therapeutic concentration and to maintain the therapeutic concentration for an extended time (Figure 2.12) [103].

Implant “A” exhibits a zero-order release profile at a constant rate above the elimination rate. Local drug concentration could slowly rise, but may take a long time to reach tissue concentrations that are toxic enough to kill the surrounding cancer cells.

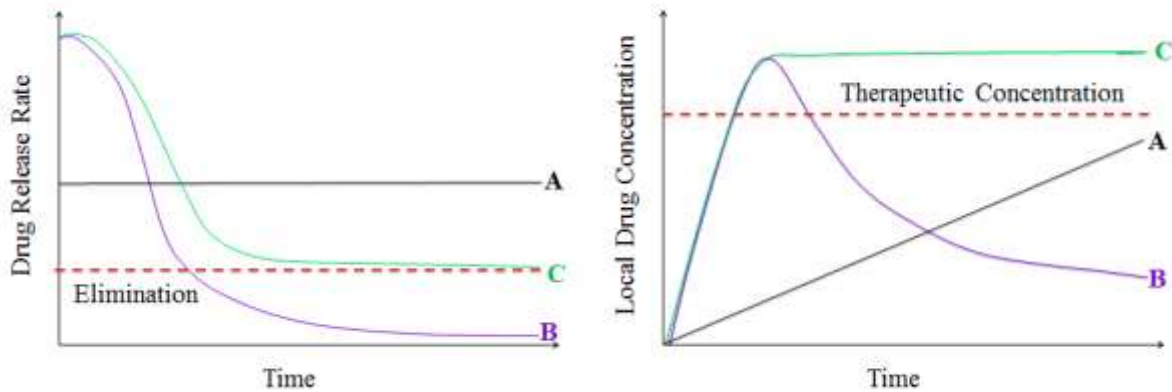


Figure 2.12: Scheme of Drug Release and Local Drug Concentration from Three Theoretical Implant Types (Modified after Weinberg et al., 2008) [100].

Implant “B” delivers a rapid dose of drugs that quickly surpass the effective concentration levels. However, drug release rates after the initial burst are insufficient to maintain this concentration for any extended length of time. Such release rates are undesirable because they allow cancer cells to remain viable and possibly gain drug resistance [101].

The ideal type of implant is “C” [100] that combines the best characteristics of both implants (A and B). Drug delivery rises rapidly to attain the effective dose and then maintains the dose within the therapeutic drug level. Achieving these goals will maximize the treatment success of intra-tumoral implants.

2.17 Drug and Tumor Transport Mechanisms

Mechanisms of drug transport and or drug elimination in a surrounding tumor tissue have a major influence on the approach by which an implant could deliver drugs to a tumor [102].

Localized drug delivery into tumors has several possible problems that could alter the treatment [100].

Drug transport is generally achieved by either diffusion or convection [103-105]. During drug diffusion, drug molecules move from a region of higher concentration to neighboring region of lower concentration at rates proportional to the concentration gradients. The mode of drug release from a localized implant is often by diffusion [106]. However, the transport of drugs with bulk flow of fluid is usually a convection transport process [100].

It is important to note that convection places a vital role in organs with higher rate of interstitial fluid flows. It is through convection that chemotherapy drug agents are transported through the vascular space to the tumor [102]. Chemo-drugs then travel along the same stream that delivers nutrients to the tumor [102]. However, diffusion/convection in drug delivery depends on the delivery system and the type of tissue [100]. For instance, in the brain, where interstitial fluid constantly flow from the ventricles to the surrounding parenchyma, convection has a substantial effect on the scope of drug penetration [107], while in situations with small molecular drugs (with limited flow), diffusion serves as the mechanism for drug transport.

2.18 Hydrogels and their Drug Release Mechanisms

There have been efforts to developed models that can provide insights into the mechanism of drug release in polymeric hydrogels [108, 109]. The released exponent, n and the dependent constant via diffusion system, k can be determined from equation (2.33) [108]:

$$\frac{m_t}{m_o} = kt^n \quad (2.33)$$

where $\frac{m_t}{m_o}$ is the fractional release of fluid/drugs at time t, k is the constant relating the geometry of the controlled release system/device, and n is the release exponent which indicates the mechanism of drug release. Interpretations on the values of release exponents associated with the different geometries are presented below (Table 2.5).

Table 2.5: Summary of Release Exponents Associated with Diffusion Mechanisms in Drugs Eluting from Polymeric Films of Different Geometries [108, 109].

Slab	Cylinder	Sphere	Drug Release Mechanism
0.5	0.45	0.43	Controlled Diffusion (Fickian Diffusion)
$0.5 < n < 1.0$	$0.45 < n < 0.89$	$0.43 < n < 0.85$	Anomalous Transport (Non Fickian Transport)
1.0	0.89	0.85	Controlled Swelling (Case II-Transport)
$n > 1$	$n > 0.89$	$n > 0.85$	Super-Case-II transport

Exemplary illustration of Fick's law of diffusion in one dimension describing drug release profiles from a matrix type device and that of drug diffusion through a controlled channel are presented (Fig. 2.13).

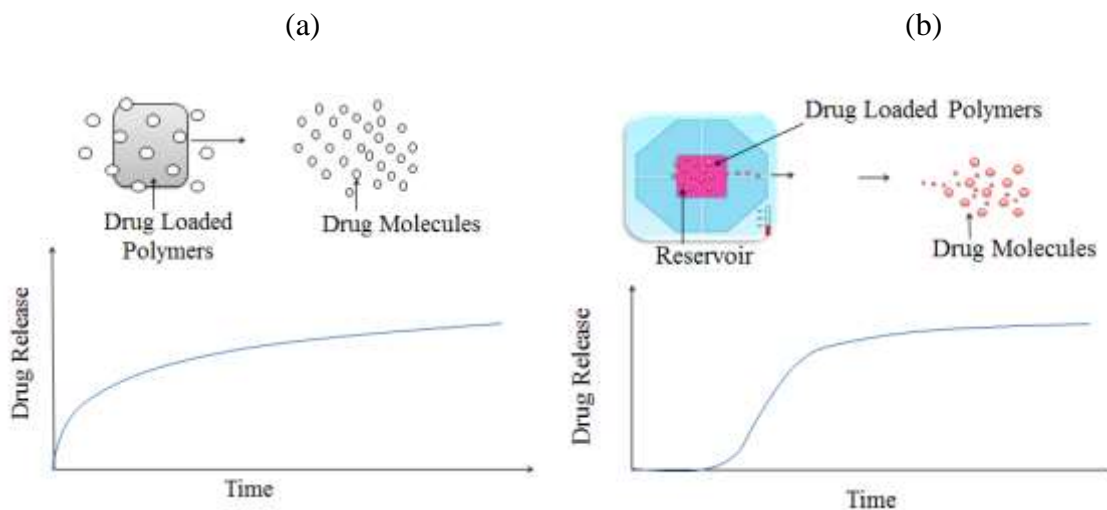


Figure 2.13: Schematics of Drug Release Profiles Resulting from Diffusion Controlled Release; (a) from a Matrix Type Device (B) From a Diffusion through a Controlled Channel.

2.19 Determination of Drug Concentration in Tumors

The concentration of drugs in a tissue could be determined as a function of time. In determining the concentration of drugs in a tumor, the tissue could be mechanically or chemically homogenized. The following are drug detection techniques that could possibly be used; fluorescence detection, high performance liquid chromatograph (HPLC) [111,112], mass spectrometry, and atomic absorption spectroscopy (ASS) [113]. Drug concentrations can also be quantified with a liquid scintigraphy by labeling the targeted drug. Most importantly, the key reasons for measuring drug concentration in tissues are; to obtain definitive drug detection, to achieve a high sensitivity and hence, acquire the ability to detect low doses of drug within the tissue. These techniques are however, limited by spatial resolution and accuracy since measurements are averaged based on the entire piece of tissue [100]. Prior studies have shown that anti-tumor implants delivered drugs to few millimeters from the surface of the implant [100], while tumor ablation prior to drug delivery improved the amount of drug that penetrate (Fig. 2.14).

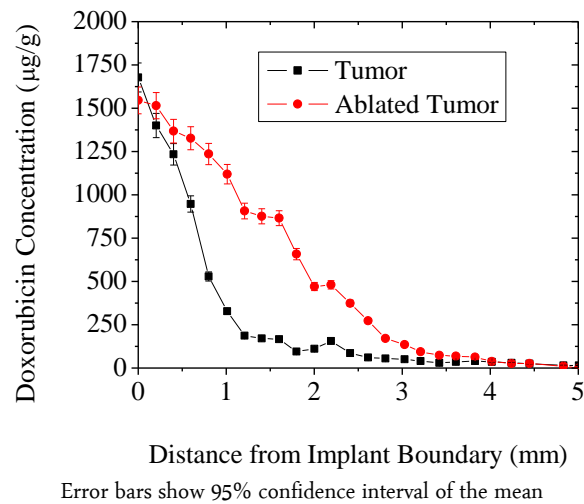


Figure 2.14: Average doxorubicin concentration in rabbit liver tumors as a function of distance from an implant for 4 days after tumor treatment. (Modified after Weinberg, 2008)[100].

2.20 Tumor Drug Elimination

After drugs are delivered, there are several mechanisms that cause drugs to be eliminated from tissues by metabolism. Cells have extraordinary structures such as organelles which work by detoxifying any foreign molecules by way of enzymes or pH-mediated degradation [100].

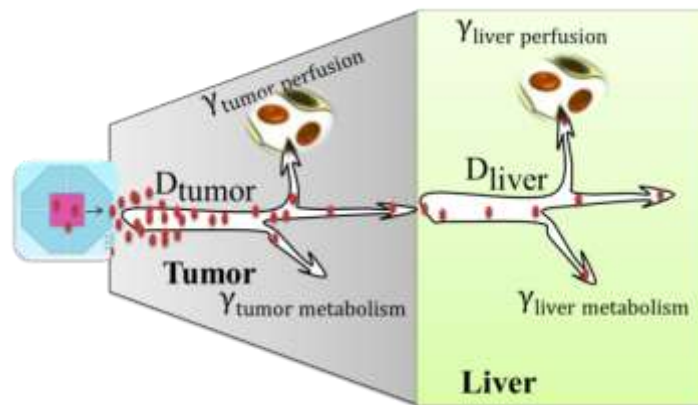
In contrast, cells have protective molecules such as glutathione. Glutathione is specifically designed to bind foreign molecules and as well as to make them more hydrophilic and less effective [114].

Moreover, drugs can also be eliminated from a target tissue via perfusion from the target area of interest [115]. Drug perfusion causes drugs to be transported either by diffusion or convection through the two systematic circulations; the blood and the lymph. Thus, drug elution from an implant can be transported to the tumor tissue depending on the diffusion rate of the tumor [100,115] (Fig.15). The average porosity of a tumor enhances the effective diffusion.

Most chemotherapy drugs exhibit short half-lives in the plasma. When chemotherapy drugs reach the plasma, they are most likely to be eliminated [115]. The approximate rate of drug elimination in first order drug transport in a tissue is determined by the equation:

$$\frac{\partial C}{\partial t} = D \nabla^2 C - \gamma C \quad (2.34)$$

where C is the drug concentration, t is the time, ∇ is the gradient operator, D is the tissue specific rate of diffusion and γ is the elimination constant.



D_{tumor} Diffusion constant of drug in tumor, γ_{tumor} metabolism, γ_{tumor} perfusion Simultaneous modes of elimination, D_{liver} When drugs gets to the surrounding tissue, it continues to diffuse outward into liver tissue. γ_{liver} metabolism, γ_{liver} perfusion Different rates of elimination by metabolism or perfusion.

Figure 2.15: Simplified scheme of drug transport from an implant centrally placed in a liver tumor (Modified after Weinberg, 2008) [100].

2.21 Imaging Techniques in Drug Detection

Imaging an *ex vivo* tissue improves upon the overall spatial resolution of bulk tissue. Usually imaging a tissue requires the tissue to be removed, and then sliced into pieces to enable drug detection in the sliced pieces. Autoradiography and fluorescence are two possible techniques used in drug detection [116]. Autoradiography requires that the drug be radiolabeled. Hence, the drug is detected by exposing the radiolabeled tissues to a flat panel detector [116,117]. This technique provides high sensitivity in drug detection with very low detection limits that gives

overall high resolution. However, autoradiography is limited by the fact that drugs have to be radiolabeled.

Also, fluorescent detection technique can be employed to characterize drug concentration in tissues using fluorescent microscopes or fluorescence scanners. During fluorescent microscopy, drug agents are inherently labeled with a fluorescent tag (e.g. fluorescent isothiocyanate) (FITC) [118]. This method therefore offers low detection limits with a reasonable sensitivity and a good resolution. However, only few drug molecules can fluoresce. Fluorescent labeling of drugs inevitably modifies their transport and efficacy, unlike radiolabeling techniques. Moreover, fluorescent imaging suffers from much greater background noise than radiographic imaging. However, there has been recent development in tomographic fluorescence which offers the potential to reduce the noise and bestow a 3-D localization of drug [119].

Moreover, magnetic resonance imaging (MRI) can also be used to detect drugs. Drug carriers must therefore be labeled with MRI contrast agents (e.g. gadolinium or super-paramagnetic iron oxide (SPIO)). MRI technique offers the potential to noninvasively image anatomical features and drug concentrations, simultaneously [120,121]. Drug concentration can then be approximated by measuring the image intensity [122].

2.22 Effective Diffusion in Porous Media

Localized drug delivery can be achieved when drug is delivered directly at the target site. P(NIPA) gels are thermosensitive hydrogels with hydrophilic networks that are capable of absorbing great amounts of fluid/drug, while maintaining structural integrity [3, 40,54,124].

The network structure and the nature of components play key roles in the diffusional behavior and stability of the incorporated bioactive agent. The use of hydrogels allows not only

delivery of drugs, but also enhances controlled release. The mass transport due to diffusion for isotropic tissues was established [125]:

$$\frac{\partial C}{\partial t} = D^{eff} \nabla^2 C + \frac{\rho}{\varepsilon} = D^{eff} \left[\frac{\partial^2 C}{\partial x^2} + \frac{\partial^2 C}{\partial y^2} + \frac{\partial^2 C}{\partial z^2} \right] + \frac{\rho}{\varepsilon} \quad (2.35)$$

where C is the average concentration of the medium, ρ is the mass density of fluid/drug, ε is the average porosity of the polymer, D^{eff} is the effective diffusivity of fluid/drugs through the porous medium and, t, and is the time for fluid/drug release. The effective diffusivity, D^{eff} for an anisotropic tissue/porous medium was related to the tortuosity of the tissue/porous system (λ).

This gives a general diffusion, equation in the Cartesian coordinates [125]:

$$D^{eff} = \frac{D}{\lambda^2} + \frac{\rho}{\varepsilon} = \left[\frac{D}{\lambda_x^2} \frac{\partial^2 C}{\partial x^2} + \frac{D}{\lambda_y^2} \frac{\partial^2 C}{\partial y^2} + \frac{D}{\lambda_z^2} \frac{\partial^2 C}{\partial z^2} \right] + \frac{\rho}{\varepsilon} \quad (2.36)$$

where D is the coefficient of diffusion and λ is the tortuosity of the system, while the other symbols have their usual meanings. For the case of an isotropic porous medium, the effective viscosity, μ was related to the porosity [126]:

$$\frac{\tilde{\mu}}{\mu} = \frac{1}{\varepsilon} \lambda^* \quad (2.37)$$

where $\tilde{\mu}$ is the effective dynamic viscosity of the medium. Tortuosity also relate to the porosity of packed beds by $\lambda^* = \sqrt{\varepsilon}$ [127].

2.23 Hyperthermia and Heat Cycles for Cancer Treatment

The phrase “hyperthermia” refers to the techniques of applying heat to improve cancer treatment. Hyperthermia could be used in conjunction with conventional techniques to improve the outcomes of cancer treatment. For example, the synergy of hyperthermia combined with chemotherapy can effectively kill cancer cells within the framework of multimodal treatments [128].

Hyperthermia can be done locally or regionally depending on the system. The types of hyperthermia include whole-body hyperthermia (HBH), hyperthermia isolated limb perfusion (HILP), and hyperthermic peritoneal perfusion (HPP) [128]. Prior works gave suggestions on the effectiveness of hyperthermia in the clinical treatment of cancer [128-133].

Hyperthermia on its own has low efficacy in conquering cancer. One aim of this current work is to combine hyperthermia with chemotherapy to deliver drugs locally to the target tumor using loaded thermo-sensitive P(NIPA)-based gels through microchannel-based devices. Experiments with hyperthermia in *in-vitro* experiments and animals have demonstrated effective cell death within temperatures of 41 to 47°C [134-136].

However, the results from *in-vivo* experiments sometimes do not agree well with *in-vitro* observations made even under controlled conditions [137]. This may be due to interactions between different physiological factors that are absent in the *in-vitro* environment. Hyperthermia has been used successfully. Yu and co-workers (2011) [138] used a combination of arterial embolization hyperthermia with arsenic trioxide nanoparticles to treat solid malignancies in rabbit liver.

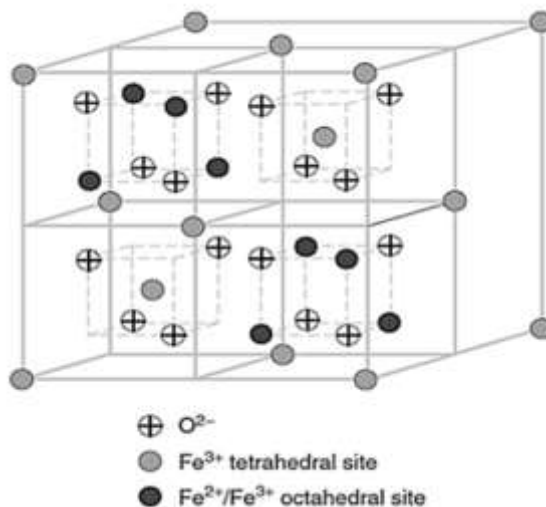
2.24 Nanoparticles for Drug Delivery

2.24.1 Magnetic nanoparticles

There are attractive properties driven from magnetic nanoparticles which render them applicable in the biomedical field. Magnetite is the most magnetic among all naturally occurring minerals on earth [139]. Magnetite forms part of the spinel group, with a standard formula of $A(B)_2O_4$ where the letters; A and B are, receptively different metal ions that occupies specific sites within the crystal structure. Within magnetite (Fe_3O_4), the letters A and B correspond to Fe^{+2} and Fe^{+3} , respectively.

The arrangement of Fe^{+2} and Fe^{+3} enables electron transfer between the different types of iron ions in the structure [140]. This generates magnetic field through an electric field vector.

Figure 2.16 illustrate the arrangement of Fe^{+2} and Fe^{+3} ions on the face centered cubic (FCC) structure of magnetite. The iron ions are located within the tetrahedral and octahedral sites, surrounded by oxygen ions. Maghemite nanoparticles have also been explored for hyperthermia treatment of tumors under a magnetic field [141].



Magnetic Relaxation properties of super paramagnetic particles

Figure 2.16: Illustrate the Iron Oxide Crystal Structure Showing the Arrangement of Fe^{+2} and Fe^{+3} ions on the FCC structure of magnetite [140].

2.24.2 Magnetic Nanoparticles Heating

Hyperthermia treatment of cancer tumor can be induced by generating heat in the tissue due to an alternating magnetic field within a region in which magnetic materials are implanted. The small magnetic nanoparticles within the tissue can induce heating due to hysteresis losses [142]. Hyperthermia by magnetic nanoparticles requires a magnetic material with the best heat evolution. In prior work [143], alternating magnetic fields have been used to induce hyperthermia around Bio-Micro-Electro-Mechanical-Systems (BioMEMS) which were designed to induce both heat diffusion and drug diffusion. Heating was associated with magnetic nanoparticles that were embedded in a PDMS and the fluid within P(NIPA)-based hydrogels.

It is important to relate the energy dissipation of magnetic fluid to the first law of thermodynamics. This gives:

$$dU = dW + \delta Q \quad (2.38)$$

where U is the internal energy, W is the magnetic work done on the system and, Q is the heat added to the system. Therefore, the magnetic work can be estimated from the internal energy for an adiabatic process ($Q = 0$). This is given by:

$$\Delta U = -\mu_o \int M dH \quad (2.39)$$

where M is the magnetization, H is the magnetic field intensity and μ_o is the permeability of free space [144]. The resulting heat can diffuse through the tissue and the implanted device to induce tumor shrinkage and cancer cell death via hyperthermia. Synergy can also be promoted by the combined effect of heat and drug diffusion for localized treatment of cancer.

2.25.0 Biomaterials and Tissue Integration

2.25.1 Cell/ Surface Interactions

Efforts have been made to reduce the factors that caused loosening of an implant [145,146]. These factors include; modifying and or manipulating the surface chemistry as well as modifying the surface texture of the implant. Modifying the surface of an implant is advantageous. It has a greater impact on the multi-scale, which ranges from chemisorption and surface energies within the atomic scale [147] to surface roughness and texture at the micro-to-meso-scale [148].

Experimental studies of surface texture and the interactions of human osteo-sarcoma (HOS) cells with Ti-6Al-4V has been studied using laser microgrooves formation on the surfaces of implants [149] (Fig. 2.7). This shows that contact guidance with improved cell or surface integration can be promoted by laser microgrooves, comparable to the cell size. Surface texture with proteins such as fibronectin, actin, vinculin, and integrin's plays a significant role in cell adhesion [150]. Their interaction also helps to improve cell growth and differentiation [150-152].

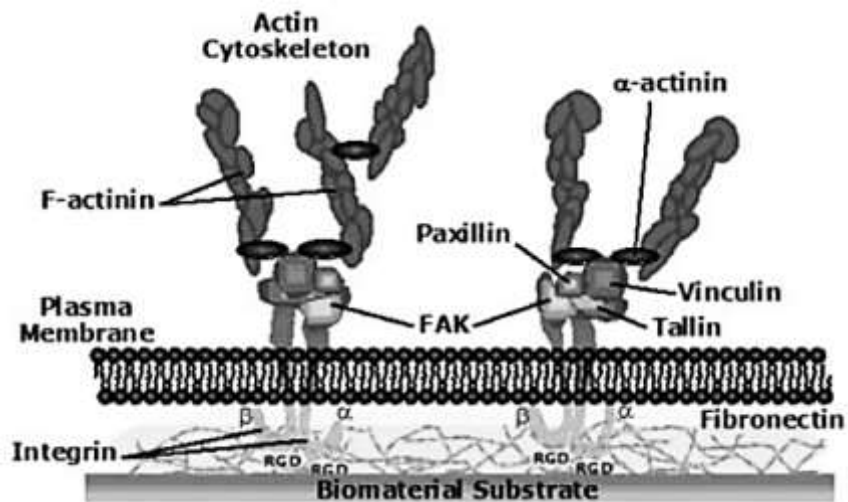


Figure 2.17: Schematic Representation of Cell or Surface Interaction of Cell Adhesion to A Biomaterial Substrate: (Modified from Chen et al, 2006) [149].

2.25.2 PDMS Surface and Cell Adhesion

PDMS have been considerably studied for fabricating microfluidic devices. Microfluidic devices are basically micro and nano-technology-based bioanalytical systems [153]. PDMS substrates possessed a universal appeal over other materials. This includes properties such as; optical transparency, tunable elasticity, biological inertness, inexpensiveness and hence its simplicity to be use in fabrication [153].

However, limited adhesion of cells to substrates suppresses cellular functions or causes cell death. PDMS has a very strong hydrophobic surface which limits cell adhesion and cell growth [154-156]. The hydrophobicity of PDMS makes it nonspecific for protein adsorption [157].

Physicochemical properties of PDMS such as the stiffness and the oxidation states of the surface (hydrophobic to hydrophilic) possibly affect the growth of cells during cell culture [158]. Fabrication condition such as the curing temperature/time and the ratios of base to curing agent (ranging from 5:1 to 100:1) affects the stiffness of PDMS [158]. Weibel and co-worker (2006) [158] presented the effect of different composition of PDMS surfaces in altering cell attachment. The growth rates for primary human umbilical artery endothelial cells, transformed 3T3 fibroblast, osteoblast-like MC3T3-E1 cells and HeLa cells (transformed epithelial cells) were found to improve by the different curing ratios of cured PDMS [159]. Sulfuric acid can also be used to generate hydroxyl groups, followed by vapor plasma methods to enhanced cell adhesion to various polymer surfaces [160].

Mammalian cells usually attached to substrates/scaffolds in order to grow/function [161,162]. The topography and stiffness of PDMS also have an effect on the microenvironment regarding the differentiation of human epidermal stem cells, mesenchymal stem cells, etc. [163-165].

2.25.3.0 Techniques for PDMS Surface Modification

The work of Toworfe et al. (2004) [166] has shown that, coated fibronectin on the surface of PDMS enhances MC3T3-E1 cellular functions which include; cell attachment and spreading on the PDMS surfaces. There are several techniques that can be used to modify the surface of biomaterials. These include: boiling PDMS slabs in deionized water, oxygen plasma treatment, UV-ozone radiation, self-assemble monolayer coating and polymer/peptide grafting techniques

2.25.3.1 Boiling Water Approach

The presence of hydroxyl groups (-OH), on the surface of a substrate helps to promote cell adhesion [167,168]. Recent study conducted [169] proposes a very simple approach that can chemically modify upon the cytophilicity of hydrosilylation cured PDMS elastomers in boiling deionized water. This study involved placing cross-linked PDMS substrate in boiling deionized water for about an hour which generated hydroxyl groups (-OH) on the surface. This was attributed to the remaining SiH functional groups present in the cured elastomer, which then act as good binding sites for cell attachment. The proposed reaction at the near end of the PDMS elastomer surface in boiling water was given by [170]:



The SiOH groups formed simply provide polar “cell-friendly” hydrogen bonding sites that would offer relief from the strong hydrophobic environment of PDMS to promote cell adhesion. It will then be possible to use, Atomic Force Microscopy (AFM), Attenuated Total Reflection Infrared Analysis (ATR-IR), and Fourier transform infrared spectroscopy (FTIR) to analyze the changes in the PDMS surface chemistry. Only then can one determine the formation of hydroxyle groups on the surface of PDMS upon treatment.

2.25.3.2 Ultra-Violet (UV)/Ozone (O) Treatment of PDMS

Among the various techniques for modifying PDMS surfaces, UV [171-173] or UV/ozone exposures (UVO) [174,175] have been extensively explored. UVO treatment is a photosensitized oxidation process in which the molecules of the treated material are excited and then dissociated by the absorption of short-wavelengths from UV radiation [176,177]. Efimenko and co-workers [181] reported that, when PDMS was exposed to UV light or a combination of UV light and ozone, the silicone rubber experienced a drastic surface chemical changes that were very similar to those produced by the oxygen plasma. However, UV-UVO-based modification process were reported to be much slower (about an order of magnitude) than plasma-based modification techniques [176]. Contact angle experiments conducted have shown that UVO modification of PDMS surfaces were polar consisting of -OH groups [175]. During UVO surface modification, atomic oxygen is simultaneously generated when molecular oxygen is dissociated by $\lambda_1 = 184.9$ nm and ozone by $\lambda_2 = 253.7$ nm [176].

2.25.3.3 FTIR-ATR Measurements

Fourier transform infrared spectroscopy (FTIR) is used in the attenuated total reflection (ATR) mode to chemically characterize surfaces of polymers. FTIR-ATR measurements are used to determine the various chemical functionalities present in an unmodified Sylgard-184 PDMS as well as examining the UVO- and UV- treated samples to a depth of several micrometers (Fig. 2.8) [176].

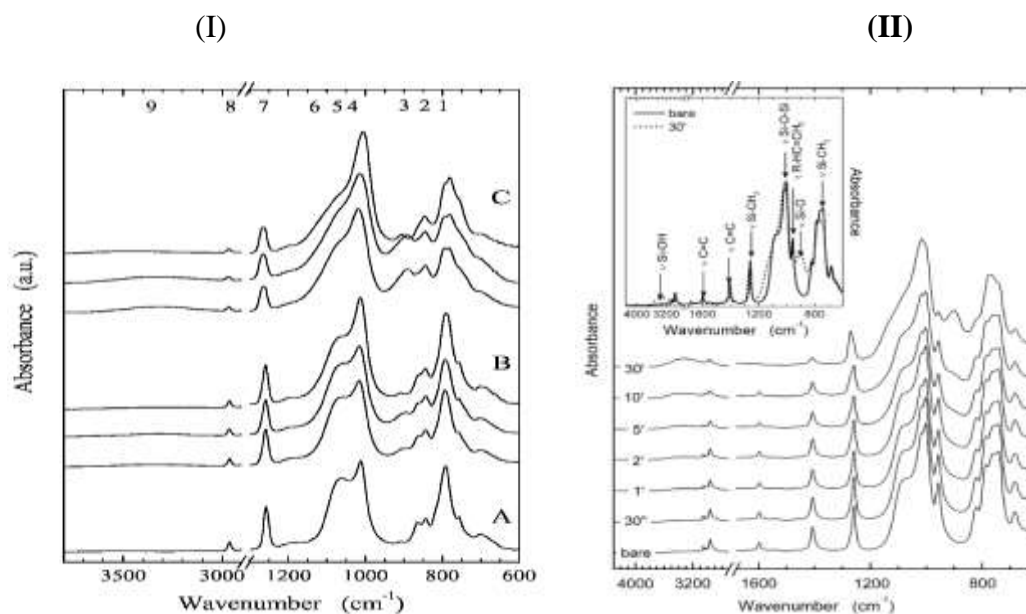


Figure 2.18: FTIR-ATR spectra from: (I) Sylgard-184 treated for UVO equal to 0 min (A), 10 min (B) and 60 min (C). (II) Extracted poly(vinyl methyl siloxane) (PVMS) samples treated with UVO for various times ranging from 0 to 30 min. [176].

2.25.3.4 Near-Edge X-Ray Absorption Fine Structure

Near-edge absorption fine structure (NEAFS) is often used to examine the surface and bulk chemistry as well as bond densities of samples. NEAFS involves the resonance of soft X-ray that excite the K or L shell electrons to vacant low-lying antibonding molecular orbitals of σ symmetry, σ^* , or π symmetry, π^* [178]. The initial state of the K shell excitation gives NEAFS its element specificity, while the final-state of the empty molecular orbitals provide NEAFS with its bonding or chemical selectivity. Determining the intensity of NEAFS spectral features then make it possible for the identification of chemical bonds as well as their relative population densities within the sample [177].

2.26 Conclusion

This chapter presents a review of prior work and the underlying materials concepts that are relevant to the development of drug delivery devices for cancer treatment. Topics covered include: cancer statistics, challenges in cancer treatments, drug delivery systems, mechanisms of drug release, biomedical implants, swelling characteristics of hydrogels, and drug release kinetics that are relevant to implantable drug delivery systems, as well as heat diffusion for localized hyperthermia. The chapter also presents the use of micro-fluidics, hydrogels and liposomes in localized cancer drug delivery. Finally, the role of surface coatings and surface textures were reviewed for the development of implantable devices that can adhere and integrate well with biological tissues.

2.27 Bibliography

- [1] A. Afrassiabi, A. S. Hoffman and L. A. Cadwell. Effect of Temperature on the Release Rate of Biomolecules from Thermally Reversible Hydrogel. *Membrane Sci.* 33 (1987) 191-200.
- [2] Y. Oni, C. Theriault, A. V. Hoek and W. O. Soboyejo. Effects of Temperature on Diffusion from PNIPA-Based Gels in a BioMEMS Device for Localized Chemotherapy and Hyperthermia. *Mater. Sci. and Eng. C.* 31 (2011) 67-76.
- [3] Y. Oni and W. O. Soboyejo. Swelling and Diffusion of PNIPA-Based Gels for Localized Chemotherapy and Hyperthermia. *Mater. Sci. and Eng. C.* 32 (2012) 24-30.
- [4] D. Gutierrez. *Cancer Facts and Figures*. 2nd Edition. American Cancer Society. (2008) 50.
- [5] C. Melissa, R. Siegel, A. Jemal. *Global Cancer facts and figure, 2008*. 2nd Edition. World Health Organization, 2008. Estimated number of new cancer cases by world Area, 2008. American Cancer Society. (2008).
- [6] J. Pollock. National Cancer Institute in 2006; The National Women's Health Information Centre website in 2006. National Breast and Cervical Cancer Early Detection Program, Centers for Disease Control and Prevention in 2006. (2007).
- [7] A. Alwan. *Global Status Report on Noncommunicable Diseases in 2010*. Geneva, Switzerland: World Health Organization (2011) 164.
- [8] J. Ferlay, H. R. Shin, F. Bray, D. Forman, C. D. Mathers and D. M. Parkin. Estimates of Worldwide Burden of Cancer in 2008: GLOBOCAN 2008. *International Journal of Cancer.* 127 (2010) 2893-2917.

- [9] N. David and W. D. Mark. The Development and Testing of a New Temperature-sensitive Drug Delivery System for the Treatment of Solid Tumors. *Advanced Drug Delivery Reviews*, 53 (2001) 285-305.
- [10] D. J. Chaplin, S. A. Hill, K. M. Bell and G. M. Toser. Modication of Tumor Blood Flow: Current States and Future Directions, *Semin. Radiat. Oncol.* 8 (3) (1998) 151-163.
- [11] G. Gregoriadis. The Carrier Potential of Liposomes in Biology and Medicine. *N. Eng. J. Med.* 295 (1976) 704-707.
- [12] M. C. Wani, H. L. Taylor, M. E. Wall, P. Coggon and A. T. McPhail. Plant Antitumor Agents. VI. The Isolation and Structure of Taxol, a Novel Antileukemic and Antitumor Agent from *Taxus Brevifolia*: *J. Am. Chem. Soc.* 93 (1971) 2325-2327.
- [13] V. Bojat, V. Balabanyan and R. Alyautdin. The Entrapment of Paclitaxel in PLGA Nanoparticles Increases its Cytotoxicity against Multiresistant Cell Line. *British Journal of Medicine & Medical Research* 1(4) (2011) 306-319.
- [14] J. Spratlin and M. B. Sawyer. Pharmacogenetics of paclitaxel metabolism. *Crit. Rev. Oncol. Hematol.* 61 (2007) 222-9.
- [15] M. D. Chavanpatil, Y. Patil and J. Panyam. (2006). Susceptibility of Nanoparticle encapsulated Paclitaxel to P-Glycoprotein-Mediated Drug Efflux. *Int. J. Pharm.* 320(1-2) (2006) 150-156.
- [16] J. M. Gallo, S. Li, P. Guo, K. Reed and J. Ma. The effect of P-glycoprotein on Paclitaxel Brain and Brain Tumor Distribution in Mice. *Cancer Res.* 63(16) (2003) 5114-5117.
- [17] J. Horwitz. Alpha-Crystallin Can Function As A Molecular Chaperone. *Proc Natl . Acad Sci. U S A.* Nov 1. 89(21) (1992) 10449-10453.
- [18] S. B. Han, H. M. Kim, Y. H. Kim, C. W. Lee, E. S. Jang, K. H. Son, S. U. Kim, Y. K. Kim. T Cell Specific Immunosuppression by Prodigiosin Isolated from *Serratia Marcescens*. *Int J. Immunopharmacol.* 20 (1998) 1-13.
- [19] B. Montaner, S. Navarro, M. Piqué, M. Vilaseca, M. Martinell, E. Giralt, J. Gil and R. Pérez-Tomás. Prodigiosin from the Supernatant of *Serratia Marcescens* Induces Apoptosis in Hematopoietic Cancer Cell Lines. *British J. Pharmacol.* 131 (2000) 585-593.
- [20] M. J. Song, J. Bae, D. S. Lee, C. H. Kim, J. S. Kim, S. W. Kim and S. I. Hong. Purification and Characterization of Prodigiosin Produced by Integrated Bioreactor from *Serratia Sp.* KH-95. *J. Biosc. Bioeng.* 101 (2006) 157-161.
- [21] B. Montaner and R. Pérez-Tomás. Prodigiosin Induces Caspase-9 and Caspase-8 Activation and Cytochrome. C Release in Jurkat T cells. *Ann. NY Acad. Sci.* 973 (2002) 246-249.
- [22] R. Pérez-Tomás, B. Montaner, E. Llagostera and V. Soto-Cerrato. The Prodigiosins, Proapoptotic Drugs with Anticancer Properties. *Biochem. Pharmacol.* 66 (2003) 1447-1452.
- [23] R. Francisco, R. Perez-Tomas, P. Gimenez-Bonafe, V. Soto-Cerrato, P. Gimenez-Xavier and S. Ambosio. Mechanisms of Prodigiosin Cytotoxicity in Human Neuroblastoma Cell Lines. *European Journal of Pharmacology.* 572 (2-3) (2007) 111-119.
- [24] C. Díaz-Ruiz, B. Montaner and R. Pérez-Tomás. Prodigiosin Induces Cell Death and Morphological Changes Indicative of Apoptosis in Gastric Cancer Cell Line HGT-1. *Histol. Histopathol.* 16 (2001) 415-421.
- [25] C. Sumathi, D. MohanaPriya, S. Swarnalatha, M. G. Dinesh and G. Sekaran. Production of Prodigiosin Using Tannery Fleshing and Evaluating Its Pharmacological Effects. Publishing Corporation. *Scientific World Journal.* Article ID 290327 (2014) 1-8.
- [26] B. Hildebrandt and P. Wust in: W. P. Ceelen (Ed). *Peritoneal Carcinomatosis: A Multidisciplinary Approach*, Springer, New York, (2007) 185.

- [27] J. T. Santini Jr., M. J. Cima and R. A. Langer. Controlled-Release Microchip. *Nature*. 397 (1999) 335-338.
- [28] M. W. Ashraf, S. Tayyaba and N. Afzulpurkar. Micro Electromechanical Systems (MEMS) Based Microfluidic Devices for Biomedical Applications. *Int. J. Mol. Sci.* 12 (2011) 3648-3704.
- [29] M. W. Ashraf, S. Tayyaba, N. Afzulpurkar, A. Nisar. Fabrication and Analysis of Tapered Tip Silicon Microneedles for MEMS Based Drug Delivery System. *Sens. Transducer*. 122 (2010) 158-173.
- [30] E. Walter, K. Moelling, J. Pavlovic and H. P. Merkle, Microencapsulation of DNA using Poly(DL-Lactide-Co-Glycolide): Stability Issues and Release Characteristics; *J. Control. Release* 61 (1999) 361-374.
- [31] P. Johansen, Y. Men, H. P. Merkle, and B. Gander. Revisiting PLA/PLGA Microspheres: an Analysis of their Potential in Parenteral Vaccination; *Eur. J. Pharm. Biopharm.* 50 (2000) 129-146.
- [32] C. Berkland, M. King, A. Cox, K. Kim, and P. W. Pack. Precise Control Of PLG Microsphere Size Provides Enhanced Control Of Drug Release Rate. *J. Control. Release*. 82 (2002) 137-147
- [33] C. Berkland, K. Kim and D.W. Pack. PLG Microsphere Size Control Drug Release Rate through Several Competing Factor. *Pharm. Res.* 20 (2003) 1055-1062.
- [34] G. L. Brode and J. V. Koleske. Poly-caprolactone Polymerization and Properties, *Journal of macromol. Science*. A6. (1972) 1109-1144.
- [35] J. V. Koleske. Blends Containing Poly(ϵ -Caprolactone) and Related Polymers, in *Polymer Blends*. R. Paul and S. Newman, eds. Academic press. New York. 2 (1978).
- [36] M. Chasin and R. Langer (1990), *Biodegradable polymers as drug delivery systems*, p231.
- [37] N. A. Peppas. *Other Biomedical Applications of Hydrogels, Hydrogels in Medicine and Pharmacy. Properties and Applications*, N.A. Peppas, Editor. CRC Press, Boca Raton, FL. 3 (1987) 177-186.
- [38] T. R. Hoare and D. S. Kohane. Hydrogels in drug delivery: Progress and challenges. *Polymer*. 49 (2008) 1993-2007.
- [39] L. Kaifeng, C. Tomothy. Ovaert and J. J. Mason. Preparation and Mechanical Characteristics of a PNIPA Hydrogel Composite. Thesis. University of Notre Dame, USA, Department of Aerospace and Mechanical Engineering (2007).
- [40] Y. Danyuo, J. D. Obayemi, S. Dozie-Nwachukwu, C. J. Ani, O. S. Odusanya, Y. Oni, N. Anuku, K. Malatesta and W. O. Soboyejo. Prodigiosin Release From an Implantable Biomedical Device: Kinetics of Localized Cancer Drug Release. *J. of Mater. Sci. and Eng. C (MSEC)*. 42 (2014) 734-745.
- [41] Y. Hirokawa and T. Tanaka. Volume Phase Transition in a Nonionic Gel. *J. Chem. Physics*. 81(12) (1984) 6379.
- [42] Y. A. Hana, J. H. Choib, D.-J. Parkc, B. C. Jia. Relationship between the Volume Phase Transition and the Surface Area of Poly(N-Isopropylacrylamide) and Poly(N-Isopropyl acrylamide-co-Sodium Methacrylate) Hydrogels. 21(8) (2002).
- [43] J. D. Schmaljohannal, Thermo- and pH-responsive Polymers in Drug Delivery. *Advanced Drug Delivery Reviews*. 58 (2006) 1655-1670.
- [44] T. G. Farmer, T. F. Edgar and N. A. Peppas. *In Vivo* Simulations of pH-Responsive Cationic Hydrogels in Diabetic Patients. *Ind. and Eng. Chem. Res.* 47 (2008) 10053-10063.
- [45] K. S. Soppimath, T. M. Aminabhavi, A. M. Dave, S. G. Kumbar and W. E. Rudzinski. *Drug Development and Industrial Pharmacy*. 28 (2002) 957-963.
- [46] B. Jeong and A. Gutowska, Lessons from Nature: Stimuli-Responsive Polymers and their Biomedical Applications, *Trends in Biotechnology*. 20 (7) (2002) 305-311.

- [47] H. A. De Las, C. Alexander and S. Pennadam. Stimuli Responsive Polymers for Biomedical Applications. *Chemical Society Reviews*. 34 (2005) 276-285.
- [48] H. G. Schild. Poly(N-isopropyl acrylamide): Experiment, Theory and Application. *Progress in Polymer Science*. 17 (2) (1992) 163-249.
- [49] J. Siepmann, R. A. Siegel and J. M. Rathbone (Editors). *Fundamentals and Applications of Controlled Release Drug Delivery*. *Advances in Delivery Science and Technology*. Springer New York. (2006).
- [50] M. K. Yoo, Y. K. Sung, Y. M. Lee and C. S. Cho. Effect of Polyelectrolyte on the Lower Critical Solution Temperature of Poly(N-Isopropyl Acrylamide) in the Poly(NIPAAM-Co-Acrylic Acid) Hydrogel. *Polymer*. 41 (15) (2000) 5713-5719.
- [51] X. Zhang, Y. Yang, T. Chung, K. Ma. Preparation and Characterization of Fast Response Macroporous Poly(N-Isopropyl acrylamide) Hydrogels. *Langmuir*. 17 (2001) 6094-6099.
- [52] T. G. Park. Temperature Modulated Protein Release from pH/Temperature-Sensitive Hydrogels. *Biomaterials*. 20(6) (1999) 517-521.
- [53] R. H. Pelton and P. Chibante. Preparation of Aqueous Lattices with N-isopropyl acrylamide. *Colloids and Surfaces*. 20 (3) (1986) 151-263.
- [54] G. Fu and W. O. Soboyejo. Swelling and Diffusion Characteristics of Modified Poly(N-Isopropyl acrylamide) Hydrogels. *Mater. Sci. and Eng. C*. 30 (2010) 8-13.
- [55] G. Q. Zhang, L. S. Zha, M. H. Zhou, J. H. Ma, B. R. Liang. Preparation and Characterization of pH-and Temperature-Responsive Semi-Interpenetrating Polymer Network Hydrogels Based on Linear Sodium Alginate and Crosslinked Poly(N-Isopropyl acrylamide). *Colloid and Polymer Science* 283 (2005) 431-438.
- [56] T. Tanaka. Gels. *US National Library of Medicine, National Institutes of Health. Sci. Am.* 244 (1) (1981) 124-138.
- [57] J. M. Walker. *The Protein Protocols Handbook*. University of Hertfordshire, Hatfield in UK. Humana press Inc. 63 (1996) 55-56.
- [58] Y. Qiu and K. Park. Environment-sensitive hydrogels for drug delivery. *Departments of Pharmaceutics and Biomedical Engineering, Purdue University, West Lafayette. USA. Advanced Drug Delivery Reviews*. 53 (2001) 321-339.
- [59] A. Gareth Hughes. Nanostructure-mediated drug delivery. *Nanomedicine: Nanotechnology, Biology and Medicine*. 1 (2005) 22-30.
- [60] P. A. Gunatillake and R. Adhikari. Biodegradable Synthetic Polymers for Tissue Engineering. *European Cells and Materials*. 5 (2003) 1-16.
- [61] A. T. Metters, C. N. Bowman and K. S. Anseth. Statistical Kinetic Model for the Bulk Degradation of PLA-b-PEG-b-PLA hydrogel networks. *J. Phys. Chem. B*. 104 (2000) 7043-7049.
- [62] A. T. Metters, C. N. Bowman. A Statistical Kinetic Model for the Bulk Degradation of PLA-b-PEG-b-PLA hydrogel networks; Incorporating Network Non-idealities. *J. Phys. Chem. B*. 104 (2001) 8069-8076.
- [63] E. Behraves, A. W. Yasko, P. S. Engel and A. G. Mikos. Synthetic Biodegradable Polymers for Orthopaedic Applications. *Clin, Orthop. Relat. Res.* 367 (1999) 118-125.
- [64] E. Jr. Middleton, C. Kandaswami, T. C. Theoharides. The Effects of Plant Flavonoids on Mammalian Cells: Implications for Inflammation, Heart Disease and Cancer. *Pharmacol Rev.* 52(4) (2000) 673-751.
- [65] A. G. Pathiraja and A. Raju. Biodegradable Synthetic Polymers for Tissue Engineering. *European Cells and Materials*. 5 (2003) 1-16.
- [66] S. Venkatachalam, S. G. Nayak, J. V. Labde, P. R. Gharal, K. Rao and A. K. Kelkar. Degradation and Recyclability of Poly (Ethylene Terephthalate). *Polyesters. INTECH. Chapter 4*. (2012) 75-76.

- [67] C. Lin. Biodegradable Polymers in Drug Delivery. Chemical Department, College of Environmental Science and Forestry. State University of New York. Lectures Materials. Nov. 29 2005.
- [68] P-J. Wipff, H. Majd, C. Acharya, L. Buscemi, J-J. Meister, B. Hinz. The Covalent Attachment of Adhesion Molecules to Silicone Membranes for Cell Stretching Applications. *Biomaterials*. 30 (2009) 1781-1789.
- [69] S. A. Visser, R. W. Hergenrother, S. L. Cooper. *Polymers Biomaterials Science: An introduction to Materials in Medicine*. San Diego, Calif: Academic Press. (1996) 50-60.
- [70] Dow Corning Healthcare Product Selection Guide. Advancing Healthcare through Material Innovations. U.S. FDA-Registered (CFN 1816403). Form No. 51-988E-01(©2001, 2002, 2003, 2007, 2013 Dow Corning Corporation) 2-19.
- [71] G-H. Hsiue, S-H. Hsu, C-C. Yang, S-H. Lee, I-K. Yang. Preparation of controlled release ophthalmic drops, for glaucoma therapy using thermosensitive poly-N-isopropyl acrylamide. *Biomaterials* 23 (2002) 457-462.
- [72] G-H. Hsiue, R-W. Chang, C-H. Wang, S-H. Lee. Development of in situ thermosensitive drug vehicles for glaucoma therapy. *Biomaterials* 24 (2003) 2423-2430.
- [73] Y. Matsumaru, A. Hyodo, T. Nose, S. Ito, T. Hirano, S. Ohashi. Application of Thermosensitive Polymers as a New Embolic Material for Intravascular Neurosurgery. *J Biomater Sci. Polym Ed.* 7 (1996) 795-804.
- [74] K. S. Oh, J. S. Oh, H. S. Choi, Y. C. Bae. Effect of Crosslinking Density on the Swelling Behavior of NIPA Gel Particles. *Macromolecules*. 31(21) (1998) 7328-7335.
- [75] T. Tanaka, D. J. Fillmore. Kinetics of Swelling of Gels. *J Chem. Phys.* 70 (1979) 1214-1218.
- [76] R. Yoshida, K. Uchida, Y. Kaneko, K. Sakai, A. Kikuchi, Y. Sakurai, T. Okano. Comb-Type Grafted Hydrogels with Rapid De-swelling Response to Temperature Changes. *Nature*. 374 (1995) 240-242.
- [77] Y. Kaneko, K. Sakai, A. Kikuchi, R. Yoshida, Y. Sakurai and T. Okano. Influence of Freely Mobile Grafted Chain Length on Dynamic Properties of Comb-Type Grafted Poly(N-isopropyl acrylamide) Hydrogels. *Macromolecules*. 28(23) (1995) 7717-7723.
- [78] O. Okay and Y. Dogu, Swelling-Deswelling Kinetics of Poly(N-isopropyl acrylamide) Hydrogels Formed in PEG Solutions. Wiley Periodicals. Inc. *J. Appl. Polym. Sci.* 99 (2006) 319-325.
- [79] O. Okay. Macroporous Copolymer Networks. *Prog. Polym. Sci.*, 25 (2000) 711-779.
- [80] S. Takata, K. Suzuki, T. Norisuye, and M. Shibayama. Dependence of Shrinking. *M. Polymer*. 43 (2002) 3101-3107.
- [81] H. Cicek, A. Tuncel. Preparation and Characterization of the Thermoresponsive Isopropylacrylamide-Hydroxyethyl methacrylate Copolymer Gels. *J. Polym. Sci. Part A: Polym. Chem.*, 36 (1998) 527-541.
- [82] Zhang, J-T.; S-X. Cheng, S-W. Huang, R-X. Zhuo. Temperature-Sensitive Poly(N-isopropylacrylamide) Hydrogels with Macroporous Structure and Fast Response Rate. (2003) *Macromol. Rapid Commun.* 24 (7) (2003) 447-451.
- [83] C. Sayil and O. Okay. Macroporous Poly(N-isopropyl acrylamide) Networks. *Polym. Bull.* 48 (2002) 499-506.
- [84] G. Fu and W. O. Soboyejo. Investigation of Swellable Poly (N-Isopropyl acrylamide) Based Hydrogels for Drug Delivery. *Mater. Sci. and Eng. C.* 31 (2011) 1084-1090.
- [85] A. Atala, W. Kim, K.T. Paige, C.A. Vacanti, A.B. Retik. Reflux with a Chondrocyte-alginate Suspension. *Journal of Urology*. 152 (1994) 641-644.
- [86] Peppas, N.A., et al., Hydrogels in pharmaceutical formulations. *European Journal of Pharmaceutics and Biopharmaceutics*. 50(1) (2000) 27-46.

- [87] C. C. Lin and A. T. Metters: Hydrogels in Controlled Release Formulations: Network Design and Mathematical modeling. *Adv. Drug Deliv. Rev.* 58 (2006) 1379-1408.
- [88] B. G. Kabra and S. H. Gehike. Synthesis of Fast-Response, Temperature-Sensitive Poly(N-isopropyl acrylamide) Gel. *Polym. Commun.* 32(11) (1991) 322-323.
- [89] P. J. Flory and J. Rehner. Statistical Mechanics of Cross-Linked Polymer Networks. II. Swelling. *J. Chem. Phys.* 11 (1943a) 521-526. q
- [90] N. A. Peppas. Kinetics of Smart Hydrogel in Reflexive Polymers and Hydrogels: Understanding and Designing Fast-responsive Polymeric Systems. N. Yui, R. Mrsny and K. Park, eds. CRC Press. Boca Raton, FL. (2004) 99-113.
- [91] P. J. Flory and J. Rehner. Statistical Mechanics of Cross-Linked Polymer Networks. I. Rubberlike Elasticity. *J. Chem. Phys.* 11 (1943b) 512-520.
- [92] P. J. Flory. Statistical Mechanics of Swelling of Network Structures, *J. Chem. Phys.* 18 (1950) 108-111.
- [93] P. J. Flory. Principles of Polymer Chemistry. Cornell University Press, Ithaca, NY. (1953).
- [94] J. Ricka and T. Tanaka. Swelling of Ionic Gels: Quantitative Performance of the Donnan theory. *Macromolecule.* 17 (1984) 2916-2921.
- [95] L. Brannon-Peppas and N. A. Peppas. The Equilibrium Swelling Behavior of Porous and Non-Porous Hydrogels, in *Absorbent Polymer Technology*. L. Brannon-Peppas and R.S. Harland, Eds. Elsevier. Amsterdam. (1990) 67-75.
- [96] L. Brannon-Peppas and N.A. Peppas. Equilibrium Swelling Behavior of pH-Sensitive Hydrogels. *Chem. Eng. Sci.* 46 (1991a) 715-722.
- [97] L. Brannon-Peppas and N.A. Peppas, Time-dependent Response of Ionic Polymer Networks to pH and Ionic Strength Changes. *Int. J. Pharm.* 70 (1991b) 53-57.
- [98] J. S. Vrentas, C.M. Jarzelski and J. L. Duda. A Deborah Number for Diffusion in Polymer-Water Systems. *AIChE J.* 21(1975) 894-901.
- [99] N. A. Peppas and N. M. Franson. The Swelling Interface Number As a Criterion for Prediction of Diffusional Solute Release Mechanisms in Swellable Polymers. *J. Polym. Sci. Polym. Phys.* 21(1983) 983-997.
- [100] B. D. Weinberg, E. Blanco and J. Gao. Polymer Implants for Intratumoral Drug Delivery and Cancer Therapy. *Journal of Pharmaceutical Sciences.* 97 (2008) 1681-1702.
- [101] G. Chu. Cellular Responses to Cisplatin. The Roles of DNA-binding Proteins and DNA Repair. *J. Biol. Chem.* 269 (1994) 787-790.
- [102] R-K. Jain. Transport of molecules, particles, and cells in solid tumors. *Annu Rev. Biomed Eng.* 1 (1999) 241-263.
- [103] R-K. Jain. Delivery of molecular and cellular medicine to solid tumors. *Adv. Drug Deliv. Rev.* 46 (2001) 149-168.
- [104] A-B. Fleming and W-M. Saltzman. Pharmacokinetics of the Carmustine Implant. *Clin Pharmacokinet.* 41(2002) 403-419.
- [105] J. Sinek, H. Frieboes, X. Zheng and V. Cristini. Two-dimensional chemotherapy simulations demonstrate fundamental transport and tumor response limitations involving nanoparticles. *Biomed Microdevices.* 6 (2004) 297-309.
- [106] A. Jemal, R. Siegel, E. Ward, T. Murray, J. Xu, C. Smigal and M-J. Thun. 2006. Cancer statistics. *CA Cancer J. Clin.* 56 (2006) 106-130.
- [107] S. Kalyanasundaram, V-D. Calhoun and K-W. Leong. A finite Element Model for Predicting the Distribution of Drugs Delivered Intracranially to the Brain. *Am J. Physiol.* 273 (1997) 1810-1821.
- [108] A.N. Peppas, Analysis of Fickian and Non-Fickian Drug Release from Polymers. *Pharm. Acta. Helv.* 60 (4) (1985) 110-111.

- [109] J. Siepmanna, N.A. Peppas, Modeling of Drug Release from Delivery Systems Based on Hydroxypropyl Methylcellulose (HPMC). *Advanced Drug Delivery Rev.* 48 (2001) 139-157.
- [110] J. Siepmann and F. Siepmann: Mathematical modeling of drug delivery. *Int. J. Pharm.* 364 (2008) 328-343.
- [111] J-R. Haaga, A-A. Exner, Y. Wang, N-T. Stowe and P-J. Tarcha. Combined Tumor Therapy by Using Radiofrequency Ablation and 5-FU-Laden Polymer Implants: Evaluation in Rats and Rabbits. *Radiology.* 237 (2005) 911-918.
- [112] J-H. Zheng, C-T. Chen, J-L. Au and M-G. Wientjes. Time-and Concentration-dependent Penetration of Doxorubicin in Prostate Tumors. *AAPS Pharm Sci.* 3 (2001) E15.
- [113] A. Szymanski-Exner, A. Gallacher, N-T. Stowe, B. Weinberg, J-R. Haaga, J. Gao. Local Carboplatin Delivery and Tissue Distribution in Livers after Radiofrequency Ablation. *J. Biomed Mat. Res.* 67A (2003) 510-516.
- [114] B. Tanner, J-G. Hengstler, B. Dietrich, M. Henrich, P. Steinberg, W. Weikel, R. Meinert, B. Kaina, F. Oesch and P-G. Knapstein. Glutathione, Glutathione S-Transferase Alpha and Pi, and Aldehyde Dehydrogenase Content in Relationship to Drug Resistance in Ovarian Cancer. *Gynecol Oncol* 65 (1997) 54-62.
- [115] F. Qian, G-M. Saidel, D-M. Sutton, A. Exner and J. Gao. Combined modeling and experimental approach for the development of dual-release polymer millirods. *J Control Release* 83 (2002) 427-435.
- [116] J-L. Au, S-H. Jang and M-G. Wientjes. Clinical Aspects of Drug Delivery to Tumors. *J Control Release.* 78 (2002) 81-95.
- [117] J-F. Strasser, L-K. Fung, S. Eller, S-A. Grossman and W-M. Saltzman. Distribution of 1,3-bis (2-chloroethyl)-1-nitrosourea and Tracers in the Rabbit Brain after Interstitial Delivery by Biodegradable Polymer Implants. *J Pharmacol. Exp. Ther.* 275 (1995) 1647-1655.
- [118] Y. Lu, E. Sega, C-P. Leamon and P-S. Low. Folate Receptor-Targeted Immunotherapy of Cancer: Mechanism and Therapeutic Potential. *Adv. Drug Deliv. Rev.* 56 (2004) 1161-1176.
- [119] V. Ntziachristos. Fluorescence Molecular Imaging. *Annu. Rev. Biomed. Eng.* 8 (2006) 1-33.
- [120] H-J. Weinmann, W. Ebert, B. Misselwitz and H. Schmitt-Willich. Tissue-specific MR Contrast Agents. *Eur. J. Radiol.* 46 (2003) 33-44.
- [121] V. Ntziachristos. Fluorescence Molecular Imaging. *Annu. Rev. Biomed. Eng.* 8 (2006) 1-33.
- [122] N. Nasongkla, E. Bey, J. Ren, H. Ai, C. Khemtong, J-S. Guthi, S-F. Chin, A-D. Sherry, D-A. Boothman and J. Gao. Multifunctional Polymeric Micelles as Cancer-Targeted, MRI-Ultrasensitive Drug Delivery Systems. *Nano Lett.* 6 (2006) 2427-2430.
- [123] A-A. Exner, B-D. Weinberg, N-T. Stowe, A. Gallacher, D-L. Wilson, J-R. Haaga and J. Gao. Quantitative Computed Tomography Analysis of Local Chemotherapy in Liver Tissue after Radiofrequency Ablation. *Acad. Radiol.* 11 (2004) 1326-1336.
- [124] N.A. Peppas. *Hydrogels in Medicine and Pharmacy, Fundamentals*, CRC Press, Boca Raton, FL, 1 (1986). 180.
- [125] Nicholson C., *Diffusion and Related Transport Mechanism in Brain Tissue*, Rep. Prog. Phys., 2001; 64, 815-884.
- [126] J. Bear, Y. Bachmat, *Introduction to Modeling of Transport Phenomena in Porous Media*, Kluwer Academic Publishers. Dordrecht. 4 (1990) 553.
- [127] S. Liu and J. H. Masliyah. Non-linear Flows in Porous Media, *J. Non-Newton. Fluid Mech.* 86 (1999) 229-252.

- [128] B. Hildebrandt, P. Wust, O. Ahlers, A. Dieing, G. Sreenivasa, T. Kerner, R. Felix, H. Riess. The cellular and molecular basis of hyperthermia. *Critical Reviews in Oncology/Hematology*. 43 (2002) 33-56.
- [129] B. Hildebrandt, P. Wust, B. Rau, P-M. Schlag, H. Riess. "Regional hyperthermia in rectal cancer". *Lancet*. 356(9231) (2000) 771-772.
- [130] R. Issels, S. W. Prensinger, A. Nagele et al., "Ifosfamide Plus Etoposide Combined with Regional Hyperthermia in Patients with Locally Advanced Sarcomas". *J Clin. Oncol*. 11: (1990) 1818-1829.
- [131] P. Wust, J. Gellermann, B. Rau, J. Löffel, A. Speidel, H. Stahl, H. Riess, Th. J. Vogl and R. Felix, P. M. Schlag. Hyperthermia in the Multimodal Therapy of Advanced Rectal Carcinomas. *Recent Rec Cancer Res*. 142 (1996) 281-309.
- [132] P. Wust, H. Stahl, K. Dieckmann, Peter Wust, Holger Stahl, K. Dieckmann, S. Scheller, J. Löffel, H. Riess, J. Bier, V. Jahnke and R. Felix. Local Hyperthermia of N2/N3 Cervical Lymphnode Metastases: Correlation of Technical/Thermal Parameters and Response. *Int. J. Radiat. Oncol. Biol. Phys.* 34 (1996) 635-646.
- [133] B. Rau, P. Wust, W. Tilly, J. Gellermann, C. Harder, H. Riess, V. Budach, R. Felix, P. M. Schlag. Preoperative Radiochemotherapy in Locally Advanced or Recurrent Rectal Cancer: Regional Radiofrequency Hyperthermia Correlates with Clinical Parameters. *Int. J. Radiat. Oncol. Biol. Phys.* 48(2) (2000) 381-391.
- [134] M. Urano, M. Kuroda, Y. Nishimura. For the Clinical Application of Thermochemotherapy Given at Mild Temperatures. *Int. J. Hyperthermia*. 15 (1999) 79-107.
- [135] W. C. Dewey. Arrhenius Relationships from the Molecule and Cell to the Clinic. *Int. J. Hyperthermia*. 10(4) (1994) 457-83.
- [136] M. W. Dewhirst, L. Prosnitz, D. Thrall, D. Prescott, S. Clegg, C. Charles, J. MacFall, G. Rosner, T. Samulski, E. Gillette, S. LaRue. Hyperthermic Treatment of Malignant Disease: Current Status and a View toward the Future. *Seminars in Oncology*. 24(6) (1997) 616-625.
- [137] I. H. Bicher. The physiological Effects of Hyperthermia. *Radiology*. 137(2) (1980) 511-513.
- [138] H. Yu, G-Y. Zhu, R-Z. Xu, H-Z. Niu, Q. Lu, G-Z. Li, Z-Y. Wang, D-S. Zhang, N. Gu and G-J. Teng. Arterial Embolization Hyperthermia Using AS2O3 Nanoparticles in VX2 Carcinoma-Induced Liver Tumors. *PloS One*. 6(3) (2011) e17926.
- [139] J. H. Richard, E. Rafel Dunin-Borkowski and A. Putuis. Direct Imaging of Nanoscale Magnetic Interaction in Minerals. *Proc. Natl. Acad. Sci. USA*. 99(26) (2002) 165561.
- [140] Y. Gossuin, P. Gillis, A. Hocq, Q. L. Vuong and A. Roch. Magnetic Relaxation Properties of Super paramagnetic Particles, *Wiley Interdisciplinary Reviews: Nanomedicine and Nanobiotechnology*. 1(3) (2009) 299-310.
- [141] X. Ruizhi, Z. Yu, M. Ming, X. Jingguang, L. Jiwei, G. Quanzhong and G. Ning. Measurement of Specific Absorption Rate and Thermal Simulation for Arterial Embolization Hyperthermia in the Maghemite-Gelled Model. *Magnetics. IEEE Transactions*. 43(3) (2007) 1078-1085.
- [142] D. E. Spiers, P. A. Eichen, M. J. Leonard, L. E. Wax, G. E. Rottinghaus, J. E. Williams, D. P. Colling. Benefit of Dietary Seaweed (*Ascophyllum Nodosum*) Extract in Reducing Heat Strain and Fescue Toxicosis: A Comparative Evaluation. *J. Therm. Biol*. 29 (7/8) (2004) 753-757.
- [143] O. Akkaya. An implantable Biomedical Device for localized hyperthermia and drug delivery., Thesis in the Department of Mechanical and Aerospace Engineering, Princeton University. (2011) (Unpublished).

- [144] U. Frisch. Fully. Developed Turbulence and Intermittency. *Annals of the New York Academy of Sciences*. 357 (1980) 359-367.
- [145] J. H. Dumbleton, M. T. Manley A. A. Edidin. A Literature Review of the Association between Wear Rate and Osteolysis in Total Hip Arthroplasty. *J Arthroplasty*. 15 (2002) 649-661.
- [146] H. G. Willert, G. H. Buchhorn. The Biology of the Loosening of Hip Implants. In: R-P. Jakob, P. Fulford, F. Horan, editors. *European Instructional Course Lectures*. London: The British Editorial Society of Bone and Joint Surgery. 4 (1999) 58-82.
- [147] B. Feng, J. Weng, B. C. Yang, J. Y. Chen, J. Z. Zhao, L. He, S. K. Qi, X. D. Zhang. Surface Characterization of Titanium and Adsorption of Bovine Serum Album. *Mater Charact*. 49 (2003) 129-137.
- [148] R. J. Menezes, G. Tomlinson and N. Kreiger. Physical Activity and Risk of Renal Cell Carcinoma. *Int. J. Cancer*. 4 (2003) 642-646.
- [149] J. Chen, S. Mwenifumbo, Langhammer C., J. P. McGovern, M. Li, A. Beye, Soboyejo W. O (2006), Cell/Surface Interactions and Adhesion on Ti-6Al-4V: Effects of Surface Texture Anselme (2000).
- [150] K. Anselme Osteoblast Adhesion on Biomaterials. *Biomaterials*. 21 (2000) 667-681.
- [151] K. Burridge. K. Fath, T. Kelly, G. Nuckolls, C. Turner. Focal Adhesions: Transmembrane Junctions between the Extracellular Matrix and the Cytoskeleton. *Annual Review Cell Biol*. 4 (1988) 487-525.
- [152] D. A. Lauffenberger, A. F. Horwitz. Cell Migration: A Physically Integrated Molecular Process. *Cell*. 84 (1996) 359-369.
- [153] W. Zhong, D. S. Choi, Y. H. Nguyen, J. Chang and L. Qin. Studying Cancer Stem Cell Dynamics on PDMS Surfaces for Microfluidic Devices Design. *Scientific Reports*. 2 (2013) 2332.
- [154] J. J. Linderman, G. Mehta, M. J. Kiel, J. W. Lee, N. Kotov, S. Takayama. Polyelectrolyte-Clay- Protein Layer Film on Microfluidic PDMS Bioreactor Surfaces for Primary Murine Bone Marrow Culture. *Advanced Functional Materials*. 17 (2007) 2701-2709.
- [155] M. N. De Silva, R. Desai, D. J. Odde. Micro-patterning of Animal Cells on PDMS Substrates in the Presence of Serum without Use of Adhesion Inhibitors. *Biomedical Microdevices*. 6 (2004) 219-222.
- [156] J. G. Collier, J. R. Thome. *Convective Boiling and Condensation Oxford Engineering Science Series, 3rd Edition*, Oxford University Press, NY. (1994) 596.
- [157] Wong and C-M. Ho. Surface Molecular Property Modification of Poly(dimethylsiloxane) (PDMS) Based Microfluidic Devices. *Springer-Verlag*. 7(3) (2009) 291-306.
- [158] D. B. Weibel and G. M. Whitesides. Application of Microfluidic in Chemical Biology. *Curr. Opin. Chem. Biol*. 10 (2006) 584-591.
- [159] J. N. Lee, X. Jiang, D. Ryan and G. M. Whitesides. Compatibility of Mammalian Cells on Surface of PDMS. *Langmuir*. 20 (2004) 11684-11691.
- [160] J. H. Lee, J. W. Park, H. B. Lee. Cell-adhesion and Growth on Polymer Surfaces with Hydroxyl-groups Prepared by Water-Vapor Plasma Treatment. *Biomaterials*. 12 (1991) 443-448.
- [161] W. M. Saltzman, P. Paron-Wingertter, K. W. Leong and S. Lin. Fibroblast and hepatocyte behavior on synthetic polymer surfaces. *J. Biomed Mater. Res*. 25 (1991) 741-759.
- [162] J. Folkman and A. Moscona. Role of Cell Shape in Growth Control. *Nature*. 273 (1978) 345-349.
- [163] K. Kurpinski, J. Chu, C. Hashi and S. Li. Anisotropic Mechanosensing by Mesenchymal Stem Cells. *Proc. Natl. Acad. Sci. USA*. 103 (2006) 16095-16100.

- [164] B. Valamehr et al., 2008. Hydrophobic surface for Enhanced Differentiation of Embryonic Stem Cell-Derived Embryoid Bodies. *Proc. Natl. Acad. Sci. USA* 105. (2008) 14459-14464.
- [165] F. Guilak, D. M. Cohen, B. T. Estes, J. M. Gimble, W. Liedtke and C. S. Chen. Control of Stem Cell Fate by Physical Interactions with the Extracellular Matrix Cell. *Stem Cell*. 5(1) (2009) 17-26.
- [166] G. K. Toworfe, R. J. Composto, C. S. Adams, L. M. Shapiro and P. Ducheyne. Fibronectin Adsorption on Surface-activated Poly(dimethyl-siloxane) and its Effect on Cellular Function. *J. Biomed. Mater. Re. Part A* 71A (2004) 449-461.
- [167] A. S. G. Curtis, J. V. Forrester, C. Mcinnes, F. Lawrie. Adhesion of Cells to Polystyrene Surface. *J. of Cell Biology*. 97 (1983) 1500-1506.
- [168] A. S. G. Curtis, J. V. Forrester and P. Clark. Substrate Hydroxylation and Cell-adhesion. *J. of Cell Science*. 86 (1986) 9-24.
- [169] J. Y. Park, D. Ahn, Y. Y. Choi, C. M. Hwang, S. Takayama, S. H. Lee, S-H. Lee. Surface Chemistry Modification of PDMS Elastomers with Boiling Water Improves Cellular Adhesion. *Sensors and Actuators B*. 173 (2012) 765-771.
- [170] M. A. Brook. *Silicon in Organic, Organometallic and Polymer Chemistry*. J. Wiley, New York. (2000) 680.
- [171] V. N. Vasilets, K. Nakamura, Y. Uyama, S. Ogata and Y. Ikada. Improvement of the Micron-Wear Resistance of Silicone by Vacuum Ultraviolet Irradiation. *Polymer*. 39 (1998) 2875-2881.
- [172] M. Ishii, and M. Komatsubara. *Proceedings. 1998 IEEE Conf. on Electrical Insulation and Dielectric Phenomena, Atlanta*. (1998) 134.
- [173] T. S. W. Huck, N. Bowden, P. Onck, T. Pardoen, J. W. Hutchinson and G. M. Whitesides. *Langmuir*. 16 (2000) 3497.
- [174] J. T. Koberstein and C. L. Mirley. U.S. Patent 5,661,092 (1997); J. T. Koberstein and C. L. Mirley. U.S. Patent 5,962,079 (1999).
- [175] M. Ouyang, C. Yuan, R. J. Muisener, A. Boulares and J. T. Koberstein. *Chem. Mater*. 12, (2000) 1591.
- [176] K. Efimenko, W. E. Wallace and J. Genzer. Surface Modification of Sylgard-184 Poly(dimethyl siloxane) Networks by Ultraviolet and Ultraviolet/Ozone Treatment. *Journal of Colloid and Interface Science* 254 (2002) 306-315.
- [177] K. Efimenko, J. A. Crowe, E. Manias, D. W. Schwark, D. A. Fischer, J. Genzer. Rapid formation of soft hydrophilic silicone elastomer surfaces. *Polymer* 46 (2005) 9329-9341
- [178] J. Stöhr. *NEXAFS Spectroscopy*. Springer Series in Surface Sciences. Springer-Verlag. Berlin. 25 (1992) 118.

3:0 Swelling of Poly(N-isopropyl acrylamide) (PNIPA)-Based Hydrogels with Bacterial-Synthesized Prodigiosin for Localized Cancer Drug Delivery

3.1 Introduction

In recent years, the incidence of cancer has increased along with cancer mortality rates across the globe [1]. Hence, in 2008, the World Health Organization estimated that cancer contributed up to 84 million deaths [2]. Should the current trends in cancer remain unchanged, the current data suggest that two thirds of the entire global incidence of cancer will occur in low and middle income countries [3]. Cancers also results in more deaths than AIDS, tuberculosis and malaria combined [4]. The early detection and treatment of cancer are the keys to the management of cancer [5-8]. However, since it is very unusual for most cancers, such as breast cancer, to present clear symptoms at their early stages, late detection and treatment are often conducted when the cancer reaches a metastasis stage.

Current treatment methods, such as bulk systemic chemotherapy [9-12] and radiotherapy [13, 14], result in severe side effects. The uptake, storage and delivery of cancer drugs can be facilitated by the use of gels [15-17]. These include: environmentally-sensitive gels that can respond to local stimuli, such as temperature, pH, electric fields and solvent composition [18-21]. The swelling and controlled release of cancer drugs [22, 23] from such gels can, therefore, provide the basis for the design of implantable biomedical systems for the localized treatment of cancer.

However, such controlled release requires a basic understanding of phase transitions [22, 23], swelling and diffusion-controlled release from smart hydrogels. In an attempt to reduce the side effects of cancer treatment, efforts have been made to develop drug delivery systems for localized cancer treatment [22, 23]. Since poly(N-isopropylacrylamide) (P(NIPA))-based polymers expels their liquid contents at temperatures close to the human body temperature of

~37°C, P(NIPA) has been investigated by several research groups for possible applications in controlled drug delivery [11, 12, 24, 25].

The thermo-sensitive properties of P(NIPA) have been explored for potential applications in drug delivery systems [26, 27]. P(NIPA) is useful because of its lower critical solution temperature (LCST) of about 32°C in aqueous solutions, especially when it is cross-linked [28, 29]. It has also been reported that the LCSTs of P(NIPA) are dependent on pH, with the LCST increasing with increasing pH [30, 31].

Here we present the results of an experimental study of the swelling characteristics of P(NIPA)-based hydrogels for the storage and localized release of a purified biosynthesized PG drug, which is produced from the bacterial, *Serratia marcescens* (SM) subsp. *marcescens* bacteria. The swelling characteristics of the hydrogels were studied using prodigiosin (PG), paclitaxel (PT), aqueous bromophenol blue (BB) and distilled water (DW) as controls over a range of temperatures (28-48°C) that is relevant to implantable devices for the localized treatment of breast cancer via hyperthermia and drug delivery.

3.2.0 Materials and Methods

3.2.1 Materials

The PT that was used in this study was procured from LC Laboratories (Woburn, MA, USA). PT is a chemically-synthesized version of Taxol[®], which was produced originally from the bark of the Pacific yew tree, *Taxus brevifolia*, which has anti-leukemic and anti-tumor activities [32]. PT was dissolved with dimethyl sulfoxide (CH₃)₂SO (DMSO) that was purchased from BDH Chemicals (Poole Dorset, England). Sylgard 184 kit silicon elastomer and a silicon elastomer curing agent (a cross-linker) were used for PDMS encapsulation. They were obtained from Sylgard Dow Corning Krayden Inc. (Midland, Michigan, USA). The materials used in the

P(NIPA) gel synthesis (Table 3.1) were purchased from Sigma Aldrich Co. (St. Louis, MO, USA). They include: N-Isopropylacrylamide (NIPA) (purity = 97 %; Mw = 113.16 g/mol), N,N,N',N'-Tetramethylethylenediamine (TEMED) (purity = 99 %; Mw = 116.2 g/mol), N,N'-Methylenebisacrylamide (MBA) (purity > 99.5 %, Mw = 154.17 g/mol), Acrylamide (AM) (purity > 99.9 %, Mw = 71.08 g/mol), Butyl Methacrylate (BMA) (purity = 99 %, Mw = 142.2 g/mol) and Ammonium Persulfate (APS) (purity = 98 %, Mw = 228.2 g/mol).

During High Performance Liquefied Chromatography (HPLC) analysis of the purity of PG, the followings chemicals were used: methanol (purity = 99.8%, Mw = 32.04 g/mol) and 10 mM triethylamine (purity = 99.5, Mw = 101.19 g/mol) (Sigma Aldrich Co., St. Louis, MO, USA), while pure PG (purity = 95%, Mw = 323.4 g/mol) was procured from Santa Cruz Biotechnology (CA, USA).

3.2.2 Preparation of P(NIPA)-Based Hydrogels

The materials used for P(NIPA) gel synthesis were obtained in powder form, as described above in Section 2.1 (Table 3.1). P(NIPA)-based hydrogels were prepared by free radical polymerization [33]. The concentrations of APS and MBA were 1.91 mol% and 1.15 mol%, respectively. The amount of the cross-linker (MBA) was obtained from:

$$\left(\frac{M_{MBA}}{M_{w(MBA)}} \right) \times 100\% = \text{mol \%} \quad (3.1)$$

where, $M_{w(NIPA)}$ is the molecular weight of the monomer, NIPA $\left(113 \frac{\text{g}}{\text{mol}}\right)$, M_{NIPA} is the initial amount of the monomer (0.87 g), $M_{w(MBA)}$ is the molecular weight of the cross-linker, MBA $\left(154 \frac{\text{g}}{\text{mol}}\right)$ and M_{MBA} is the unknown amount of MBA (g) to be used in the gel polymerization. The mole% of MBA was 1.15 %. The calculated amount of the MBA based on

the 0.87 g of NIPA (monomer) from equation (3.1) was found to be 0.0136 g. Furthermore, the amount of APS was obtained by replacing MBA in equation (3.1) with APS.

P(NIPA)-based homo-polymer, denoted by gel code A, was prepared by mixing 0.87 g of NIPA, 0.0136 g of MBA, and 0.0335 g of APS (samples were weighed with an analytical balance (Mettler AE 100, Mettler-Toledo Ltd., Leicester, UK)). The samples were then dissolved with 7.8 ml of DW, before stirring vigorously until a homogenous mixture was obtained from 4-9°C. The mixing process was exothermic. The solution was then immersed in ice and sonicated, while nitrogen gas was bubbled through for 20 minutes at a pressure of 10 bars to remove all dissolved oxygen. The homo-polymer was initiated with 15 μ l of TEMED. The mixtures were then swirled gently for 5 seconds.

The solutions were later poured into 5 mm diameter cylindrical molds that were opened to terminate the free radical polymerization. The samples inside the cylindrical molds were then left at 24°C in a water bath (Model 2321, Fisher Scientific Inc., Loughborough, Leicestershire, UK) to strengthen the polymerized gels over 12 hr period. They were then washed 10 times with deionized water to remove any chemical residue. The resultant wet gels were then cut into discs and cylindrical samples with diameters of 5 mm and heights of 5 mm. They were then soaked in deionized water, while replacing the deionized water for two weeks. The samples were finally removed from the deionized water. They were subsequently dried in a laboratory environment (29°C) to remove all moistures.

P(NIPA)-based co-polymer hydrogels were also prepared using the same procedure for the fabrication of the P(NIPA) homo-polymer. However, co-monomer species, AM and BMA were co-polymerized with P(NIPA) to form co-polymers gels. Samples of P(NIPA) co-polymer hydrogels which contained 5 or 10 mol% of BMA were initiated with 5 and 10 μ l of TEMED, respectively, while gels that contained 5, 10 and 15 mol% of AM were initiated with 20, 30, 40

μl of TEMED, respectively. Controlled additions of TEMED reduced the turbidity of the hydrogels. It therefore, helped to produce transparent hydrogels.

Since the transport characteristics of conventional P(NIPA)-based gels are largely dependent on the morphologies of the gels inner matrices, an LCD Deluxe digital optical microscope (Celestron #44345, Columbia St., Torrance-USA) was used to study the gel microstructures.

3.2.3 Prodigiosin (PG) Extraction

PG was extracted from the bacterium, SM, at the Biotechnology and Genetic Engineering Advanced Laboratory, Sheda Science and Technology Complex (SHESTCO), Abuja, Nigeria. The process involved a prepared growth media, peptone glycerol agar (PGA) with composition of was 0.5% peptone, 1% glycerol and 15 g/l agar at pH "7". SM was inoculated onto the PGA culture plates and incubated at 28°C for 48 hrs. The SM grew in the culture, producing a characteristic pink and red pigment, associated with the presence of PG [34].

The SM grown on the surface of the media was scooped into 100 ml of absolute ethanol, agitated vigorously to extract the pigment into the ethanol. The 100 ml SM-ethanol solution was filtered using Whatman filter paper (number 1). This was done to remove some debris from the solution. The solution was then centrifuged at 5000 revolutions per minute (rpm) for 10 min to allow the bacteria to sediment. The supernatant containing the pigment, PG was collected and placed in a rotary evaporator (BUCHI, Rotavapor® 114 with Water Bath B-480, Bristol, Wisconsin, USA). This was used to remove the ethanol, leaving the crude extract of PG.

The PG was then purified using column chromatography. The stationary phase was a silica gel (BDH Chemicals, 300624v, Poole Dorset, England), while the mobile phase was a mixture of ethyl acetate, chloroform and methanol in the ratio of 2:1:1, respectively. The PG crude extract

was layered at the top of the gel in the column and fractions were eluted by adding the mobile phase. Then, 5 ml fractions were collected over several minutes.

The collection was followed by UV-Vis spectrophotometric (UV-Vis) measurements of the fractions at a wavelength of 535 nm using a UV-Vis spectrophotometer (Cecil 7500 Series, Buck Scientific Inc., East Norwalk, USA). The fractions that absorbed at this wavelength were pooled together and subsequently dried in a lyophilizer (Labconco, Kansas City, Missouri, USA). 100 mg of dried PG was suspended in 1 mL methanol and stored at -20°C. The PG samples were then stored in the dark, since the efficacy of PG could be affected by ultra-violet radiation [35].

3.2.4 Determination of the Purity of Prodigiosin Extracted

HPLC was carried out using an HPLC system with a dual wavelength absorbance detector (Waters 2695 with 2487 Absorbance Detector, LabX, Midland, ON, Canada). This was used to determine the purity of the extracted samples by producing spectra at 535 nm. Methanol and 10 mM triethylamine (17:3 v/v), with pH adjusted to 6.5 (using phosphoric acid), were used as the mobile phase at a flow rate of 1.0 ml/min through a reverse column at 40°C. The acid was used to improve upon the chromatographic peak shape and also to provide a source of protons in the reverse phase. The concentration of the standard solution was matched to the sample solution to avoid peak mis-assignment due to peak shape effects. 500 µg of each sample; standard PG and the sample PG were separately dissolved in 2 ml of methanol to obtain equal concentrations of 250 µg/ml.

The PG content was determined from the HPLC analysis by comparing the peak areas (normalization), as well as the symmetrical increase of the peak areas, as a function of the retention time. By comparing the retention time and response of the peak in the chromatogram of the standard solution, with the sample chromatogram, the peaks were assigned. The percentage

peak, AP, areas were obtained from [36]:

$$AP = \% \text{ Area of a peak} = \frac{A_i}{\sum_{i=1}^n A_a} \times 100 \quad (3.2)$$

where A_i is the area of a particular peak, A_a is the peak-area of any peak observed on the chromatogram, which also include the peaks of other impurities in the sample. The amount of PG present in the sample (corresponding to a peak area) was obtained from [36]:

$$AA = \text{Amount of analyte in sample}(\mu\text{g/ml}) = \frac{\text{Peak Area}}{\text{Response Factor}} \quad (3.3a)$$

$$\text{where the Response Factor} = \frac{\text{Peak Area of standard sample}}{\text{Standard Amount}(\mu\text{g/ml})} \quad (3.3b)$$

The sample peak indicates some degree of tailing or asymmetrical by deviating slightly from the ideal, symmetrical. The asymmetry factor (A_s) was obtained from:

$$A_s = \frac{b}{a} \quad (3.4)$$

where a and b are the front and back half widths measured at 10% of the peak height [37].

3.2.5 Phase Transition Temperature Measurements

The lower critical solution temperatures (LCSTs) of the P(NIPA)-based hydrogels were determined using a Differential Scanning Calorimeter (DSC) (Perkin Elmer Inc., Waltham, Massachusetts, USA). To determine the LCSTs, samples were obtained from the polymerized P(NIPA)-based gels. They were soaked in DW (as a control) and PG for 5 days, prior to DSC measurement. Fractions of gel were cut carefully and placed into empty hermetically sealed stainless steel containers. Each sample in the steel containers weighed 5 mg. The stainless steel containers were then sealed to prevent the evaporation of DW/PG during the scanning calorimetric measurements.

The DSC scans for the samples were programmed to run for a period of 18 hours. After the complete scans at heating rates of 10°C/min, plots of heat flow and temperature increase rate were obtained. The LCSTs were then determined using a calorimetric technique [38] that provides information on the heat released from the cleavage of hydrogen bonds between the water solvent and the polymer.

3.2.6 Fluid/Drug Concentrations

Each sample of BB, PG and PT was accurately weighed to 0.1 g. The 0.1 g of PG was initially dissolved with 2 ml methanol (100%) to give a stock solution of 5 mg/ml. The 5 mg/ml solution was then adjusted with PBS to give a final concentration of 2.5 mg/ml. The other samples, such as BB and PT, were similarly prepared. However, the initial dissolution of BB and PT were done in 2 ml ethanol and 2 ml DMSO, respectively, while 38 ml PBS was used to adjust each solution to obtain final concentrations of 2.5 mg/ml. The ratios of DMSO:PBS, methanol:PBS, and ethanol:DW, were each 5:95 v/v% in the final drug/sample solutions.

The reactions of DMSO with PBS, as well as methanol with PBS, produced turbid solutions. Drug/sample solutions were filtered twice using Whatman filter paper (number 1) to remove debris. The swelling properties of the hydrogels were then characterized using the final concentrations of 2.5 mg/ml (PG, PT and BB) and DW, as described in section 3.2.7 below.

3.2.7 Swelling Ratios and Transport Measurement

Dried hydrogels were used to determine the swelling ratios of P(NIPA)-based hydrogels in PG, BB and PT. The solvents (PG, BB and PT) were dissolved with aqueous solvents, as presented in section 3.2.6. The swelling ratios of P(NIPA)-based hydrogels were determined by

immersing the hydrogels into 5 ml of the different solutions (2.5 mg/ml of PT, PG and BB) or 5 ml DW, to absorb drugs/fluids. The swelling and release behavior of the loaded gels were then studied. The average swelling ratios (SR_A) were obtained by soaking the P(NIPA)-based hydrogels in DW, PG and BB (at temperatures between 28 - 48°C). These are given by [39]:

$$SR_A = (M_t - M_o)/M_o \quad (3.4)$$

where M_t is the mass of the gel at time t and M_o is the mass of the dried gel at time, $t = 0$.

The fluid/drug uptake in the gels was obtained from the relative gel mass [40]:

$$M_{rel} = M_t/M_s \quad (3.5)$$

where M_s is the swollen mass at a given temperature and M_t is the mass of the hydrogel at time, t . The equilibrium volume ratio was obtained from:

$$V_{eq} = \frac{\left(\frac{\pi D^2}{4}\right)}{\left(\frac{\pi D_o^2}{4}\right)} = \frac{D^2}{D_o^2} \quad (3.6)$$

where D_o and D are the diameters of the hydrogels before and after equilibrium swelling.

3.2.8 Strain Induced in Hydrogels Due to Swelling

Brannon-Peppas and Peppas earlier explained the dynamic swelling of hydrogels [41]. For one-dimensional transport, the swelling of gels were related to the change in lengths. The strain, ε , induced in the gel as a result of swelling, is given by equation (3.7) to be:

$$\varepsilon = \frac{l-l_o}{l_o} \quad (3.7)$$

where l is the length at a given time, t and l_o is the initial length.

3.2.9 Drug/Fluid Release from PNIPA-based Hydrogels

Peppas and co-workers [42] have also developed an equation for the modeling of drug release. This assumes a time-dependent power law function of the form:

$$\frac{m_t}{m_i} = 4 \left(\frac{D}{\pi \delta^2} \right) t^n = k t^n \quad (3.8)$$

where $\frac{m_t}{m_i}$ is the fluid/drug release fraction, k is the geometric constant of the release system, n is the fluid/drug release exponent, depicting the release mechanism, m_i is the initial mass of the swollen hydrogel prior to drug release, m_t is the mass of the hydrogel at time, t during drug elution, δ is the thickness of the gel and D is the diffusion coefficient. Equation (3.8) is applied to systems in which diffusion occurred within the polymeric networks [42]. The constants k and n were obtained from the linear form of equation (3.8). This gives:

$$\ln \left(\frac{m_t}{m_i} \right) = \ln k + n \ln t \quad (3.9)$$

where k and n were obtained, respectively, from the intercepts and slopes of the plots of $\ln(m_t/m_i)$ versus $\ln t$. The intercepts on the $\ln(m_t/m_i)$ axis were equal to $\ln(k)$. The diffusion coefficients, D_s , were obtained from:

$$D_s = \frac{k\pi\delta^2}{4} \quad (3.10)$$

where k, π and δ are the geometric constant of the release system, the mathematical constant reflecting the ratio of a circle circumference to its diameter and the thickness of the gel, respectively. The diffusion coefficients were determined at different temperatures (28-48°C). The activation energies for the different gels were also obtained from the Arrhenius equation. This gives:

$$D = D_o \exp\left(\frac{-E_a}{RT}\right) \quad (3.11a)$$

and

$$\ln D = \ln D_o - \frac{E_a}{RT} \quad (3.11b)$$

where D is the diffusion coefficient, D_o is the diffusion constant at room temperature, R is the universal gas constant, T is temperature and E_a is the gel activation energy. The activation energy for each sample was obtained from the slope of a linear plot of $\ln(D)$ versus $T^{-1}(K^{-1})$.

3.2.10 Statistical Analysis

Statistical analysis for each experiment was carried out for at least at three independent times and the average values \pm standard errors (SE) were reported [43]. The present data were analyzed using Minitab software package (Minitab16, Minitab Inc., State College, PA, USA).

Analysis of variance (ANOVA) tests on the effect of temperature on the swelling ratios (Fig. 3.4) were presented. In order to investigate these differences, a post hoc test was carried out using the least significant difference (LSD) test. ANOVAs tests for the effect of the different polymer ratios on the swelling ratios (Fig. 3.3) were also presented. Significance of the result was determined from the difference in the means. Moreover, repeated ANOVAs were also performed on the effect of different drugs/fluids on the swelling ratios of P(NIPA)-based hydrogels (Fig. 3.5).

Statistical variations of AM on the equilibrium volume ratios of P(NIPA)-based hydrogels (Fig. 3.6) at 95% confidence interval (CI) were also evaluated using student's t -test statistic [43]. The significant difference in the LCSTs due to PG and DW was similarly evaluated (Fig. 3.7). In addition, the differences in strains induced on the P(NIPA)-based hydrogels (due to swelling in

DW and PG) were evaluated along with the effects of polymer ratios on increasing the strains (Table 3.7). The *p*-values less than 0.05 were considered statistically significant or vice versa.

3.3.0 Results and Discussion

3.3.1 Gel Characterization

The optical microscopy images of the gels revealed collapsed walls within an interpenetrating matrix (Figs. 3.1a-d). This suggests that the gels can easily collapse and expand, when an external stimulus is applied. The P(NIPA)-based co-polymer matrices were cracked in multiple locations. The structure of the polymers shows clear evidence of micro-cracks and micro-pores (Fig. 3.1a-d).

The homo-polymer matrix revealed dominant pore sizes of 0.15-10 μm (Fig. 3.1a), interconnecting pores sizes ranging from 0.5-15 μm were observed in P(NIPA-co-AM) (95:5 mol%) (Fig. 3.1b), while spherical micro pores with sizes ranging from 5-25 μm were observed in the P(NIPA-co-AM) (90:10 mol%) (Fig.3.1c). Similarly, micro-voids and micro-pores were also observed in the P(NIPA-co-AM) (85:15 mol%) with pore sizes between 0.5 to 70 μm (Fig. 3.1d).

The gels co-polymerized with AM and BMA had different pores sizes in their structures (Fig. 3.2a-3.2b). The micropores were uniformly distributed in the gel matrices, revealing dominant pore sizes of 0.1 - 17 μm (Fig. 3.2a), 0.12 - 20 μm (Fig. 2b) for P(NIPA) homo-polymer, and co-polymers (with 5 mol% of AM), respectively.

The average porosity of P(NIPA)-based homo-polymer hydrogels was found to be 0.34, while P(NIPA) co-polymers containing AM had average porosities of 0.53, 0.58 and 0.67 for P(NIPA-co-AM) (95:5 mol%), P(NIPA-co-AM) (90:10 mol%) and P(NIPA-co-AM) (85:15 mol%), respectively. However, P(NIPA-co-BMA) (95:5 mol%) had an average porosity of 0.39,

while the P(NIPA-co-BMA) (90:10 mol%) had an average porosity of 0.48. The amount of AM and BMA significantly increases the porosity of the hydrogels, which helps with solution uptake.

3.3.2 Swelling Characteristics

In drug delivery, it is very important to know the mechanism of solute transfer from the gel matrix [44]. Diffusion serves as the main mechanism of solute transport for non-biodegradable gels. However, the mass transfer in hydrogels can be attained from the swelling of the hydrogel. P(NIPA)-based hydrogels were exposed to drug solutions (PG, PT), DW and BB to absorb drugs/fluid. The swelling behaviours of the loaded gels were then studied. When the hydrogels were exposed to the above solutions/fluids, they swelled until dynamic equilibrium conditions were attained at saturation.

At equilibrium, the thermodynamically driven swelling force was counter-balanced by the retractive force of the cross-linked structure, leading to an equilibrium state. This swollen state then allows the gaps between the crosslinks and mesh size to be widened. This facilitates the transfer of different solutes through the gels.

Most hydrogels used in biomedical applications have mesh sizes, ranging from 5-100 nm [45], in their swollen state. Once the gel has imbibed fluid/drug, the mesh size widens, allowing free passage of the solutes. These size scales are much larger than most small molecular weight drugs that are used in pharmaceutical formulations. Hence, the diffusion of such drugs is not hindered in such swollen matrices. The transfer of solutes was controlled by the swelling of the gels. The small hydrodynamic radii of drugs molecules enabled them to diffuse through the gel network. Hence, the knowledge of gel swelling characteristics provides the necessary understanding of the network structure of the gels and their capacity to function as drug carriers.

The results obtained for the average swelling ratios (SRa) of P(NIPA)-based hydrogels, exposed to different fluids at 28°C (room temperature) for 30 h are presented (Fig. 3.3). The differences in the SRa were due to the ion concentrations of the different solutions in which P(NIPA)-based hydrogels were soaked. Table (3.2) displays the ANOVA test for the effect of the different polymer ratios on the SRa (Fig. 3.3). The test revealed there is no significant difference on the effect of the different polymer ratios on SRa. Since there is no significant difference, there was no need for post hoc test.

The dependence of the swelling temperature on the SRa of P(NIPA)-based gels in PG is presented (Fig. 3.4). There is a clear evidence of a reversed temperature response to SRa (Fig. 4). The SRa were higher at room temperature (28°C) (Fig. 3.4), while drastic decreasing trends were observed at higher temperatures above 30°C (Fig. 3.4). The increase in swelling ratios at lower temperatures resulted in greater solution uptake by the hydrogels. This is attributed to the thermo-sensitivity of the P(NIPA)-based hydrogels.

Table (3.3A) displays the result on the analysis of variance (ANOVA) test of the effect of temperature on the SRs. The results revealed there was significant difference on the effect of temperature on the gel swelling. In order to investigate these differences, a post hoc test was carried out using the least significant difference (LSD) test. In table (3B) if you see * on the mean difference it means it is significant. The increase in temperature however, caused the aggregation of polymer networks [46].

Furthermore, the P(NIPA)-based hydrogels experienced rapid uptake of DW, BB, PT and PG during the initial stages of immersing (Figs. 3.5a-3.5d), before attaining equilibrium swelling. Generally, the hydrogels swelled more rapidly, due to large swelling forces generated by electrostatic repulsion among the ionized acid groups and the osmotic pressure. Repeated ANOVAs for the swelling ratios of P(NIPA)-based hydrogels in different fluids (5 ml of 2 µg/ml of drug solutions) or distilled water at 28°C is presented in Table 3.4. For all the polymer ratios

(A, B, C, D) (Fig. 3.5); there is no significant difference on the effect of the drugs on gel swelling ratios. Since there was no significant difference, there was no need for post hoc test.

The osmotic pressures and chemical potential balance within and outside the gel network were contributing factors to the swelling properties of the gels in the different solutions. At equilibrium, the sum of the osmotic pressure for the mixing, rubber elasticity and ion interactions equals to zero. Decrease in the chemical potential of the swelling system directly affects the total volume uptake.

The volume fraction of a hydrogel (in the swollen state) is a measure of the amount of fluid/drug absorbed and retained by the hydrogel. The results (Fig. 3.6) show that the equilibrium volume ratio (V_{eq}) of P(NIPA)-based gels increases linearly with acrylamide concentration, with $r^2 = 0.991$. Higher values of V_{eq} (Fig. 3.6) were obtained for hydrogels containing acrylamide. This is attributed to the hydrophilicity of the hydrogels, as a result of the acrylamide added.

Statistical analyses of the effects of polymer ratios on the V_{eq} of P(NIPA)-based hydrogels (Fig. 3.6) revealed no significant differences with p -values greater than 0.05. The variations in the data (Fig. 3.6), standard deviation (SD) and standard error of the mean (SEM) are presented to be 3.05 and 1.53, respectively.

The swelling characteristics of P(NIPA)-based hydrogels are of practical importance. The knowledge of gel swelling kinetics provided the understanding of the network structure of the gels and their capacity to function as drug carriers.

3.3.3 LCSTs of P(NIPA)-based Hydrogels

The LCSTs of the P(NIPA)-based hydrogels are summarized (Table 3.5). The LCST for the homo-polymer soaked with distilled water was $\sim 33^\circ\text{C}$, while 32°C was reported earlier [30] and 34.6°C in recent work [12].

With increasing concentration of acrylamide, the LCSTs of the hydrophilic co-polymer increased from 36.3°C at 5 mol % of AM to 41.7°C at 15 mol% of AM (Table 3.5). This is in agreement with results from prior studies [12, 30, 31, 47]. In contrast, increasing concentrations of hydrophobic co-monomer species, such as BMA (up to about 10 mol%), results in decreasing LCSTs, down to 29.0°C. Hence, the LCSTs depend on the concentration of AM or BMA in the copolymers.

However, PG was also found to greatly increase the LCSTs of P(NIPA)-based hydrogels with *p*-value less than 0.05. This is shown (Fig. 3.7) in which plots of LCST versus P(NIPA)-based gels are presented.

The results on the LCSTs of P(NIPA)-based gels suggest that the release of drugs from the thermo-sensitive hydrogels can be managed with a heat trigger mechanism. Such a mechanism could be used to heat up the soaked gels up to their LCSTs, or nearly above their LCSTs, to control the release of anti-cancer agents. Co-polymers can also be selected to have compositions with LCSTs corresponding to the desired cancer treatment. Such control of the LCSTs makes P(NIPA)-based hydrogels attractive for potential applications in drug delivery systems.

3.3.4 Gel Swelling and PG Release

The mechanism of hydrogel swelling is one of the most essential elements used in controlled drug release. During controlled-swelling, hydrogels experience a swelling-driven phase transition from a glassy state to a rubbery state. This occurs when the transition temperature is lower than the temperature of the fluid that surrounds the polymer matrix. In the glassy state, some drug molecules were trapped. These molecules continue to accumulate, making drug diffusion difficult. However, in the rubbery state, the dissolved drug molecules diffused rapidly

through the swollen polymer. Furthermore, the glassy states of P(NIPA)-based hydrogels were cloudy in appearance, while the rubbery states were transparent.

The fractions of PG released (m_t/m_i) from P(NIPA)-based hydrogels are presented in Figs. 3.8a-3.8d. The release exponent, n , corresponds to the mechanism of drug release. The measured values of the release exponent (n) and the gel geometric constant (k) were obtained from equation (3.9), while the coefficients of diffusion (D_s) were obtained from equation (3.10).

The results for n , k , and D_s were obtained from Figs. (3.8a-3.8d). They are also summarized in Table 3.6. The fractional releases of drugs (from the polymers) were exponentially related to the drug release time. For cylindrical gels, $n = 0.45$ corresponded to Fickian diffusion [48, 49], while the release rate was then dependent on $t^{-0.45}$. This represents diffusion-controlled release. When n lies between 0.45 and 0.89 (i. e. $0.45 < n < 0.89$), non-Fickian diffusional release (anomalous transport) [48, 49] occurs, while $n = 0.85$ corresponds to case-II transport (for a cylindrical sample).

The values of n (Table 3.6) were greater than 0.45, but less than 0.89. The release exponents, n , provided some insights into the mechanisms of PG release from the P(NIPA)-based hydrogels. Such n values (0.62-0.81), therefore, suggest that the fractional release of PG from P(NIPA)-based hydrogels at 37°C occurred by an anomalous transport mechanism. The geometric constants (containing the diffusion term) were between 0.70 and $1.31 \times 10^{-3} \text{s}^{-1}$. The geometric factors decreased with increasing n . Also, the coefficients of PG diffusion from P(NIPA)-based hydrogels were between 4.97 and $9.29 \times 10^{-9} \text{m}^2/\text{s}$. The diffusion rates of P(NIPA)-based hydrogel loaded with PG, in addition to their thermo-response could be used to control the release of drug for localized chemotherapy [50].

3.3.5 Strains (ϵ) Induced in Hydrogels Due to Swelling

The strains, ϵ_s , induced in the hydrogels, due to swelling in the fluids/drug solutions for 72 h at room temperature (29°C), are summarized (Table 3.7). The strain, ϵ , corresponds to the extension in length during swelling. The ϵ_s in the P(NIPA)-based hydrogels soaked in PG varied from 0.44 - 1.73, while those in the gels soaked in DW varied from 0.29 - 1.28. The results show significant elongation in the hydrogels after soaking in PG (44-173%) and DW (29-128%).

The differences in strains induced on the P(NIPA)-based hydrogels (due to swelling in DW/PG) (Table 3.7) were not statistically significant with p -value (of 0.12) greater than 0.05. Also, the effects of polymer ratios (Table 3.7) on increasing the strains was not statistical significant with a p -value (of 0.99) greater than 0.05.

3.3.6 Purity of Extracted Prodigiosin

Single peaks were obtained from the chromatographs for the test sample and the standard sample. The peaks grow and retain symmetry, given a tentative confirmation of the sample (PG) [36, 51].

It is important to note here that the peak areas were used to determine the concentrations of PG in the samples [36, 51]. These were used instead of the peak heights, since the peak heights varied, while the peak areas remained almost constant. The test sample shows good asymmetry, based on the A_s determined to be 1.4.

Other smaller peaks were observed in the test samples due to impurities present. Also, the greatest peak was obtained at 5.01 min of retention time, with a percentage area of 95.42, as compared to 4.87 min for the standard sample, which also had a percentage area of 97.66. The purity of the standard sample was 95 %. This translated by ratio to a sample purity of 92.8 %.

3.4 Summary and Concluding Remarks

The swelling kinetics of P(NIPA)-based hydrogels were studied at temperatures between 28°C to 48°C. P(NIPA) forms a three-dimensional hydrogel, when cross-linked with MBA. The addition of AM and/or, BMA to NIPA improved the swelling behavior of P(NIPA)-based hydrogels. The osmotic pressure or chemical potential balance within and outside the gel network contributes to the swelling properties of the gels. A decrease in the chemical potential of the swelling system directly affects the total volume uptake.

The increase in the SRs of P(NIPA)-based hydrogels (in fluids/drugs at lower temperatures) results in higher solution uptake by the hydrogels during swelling, while the decrease in the SRs at higher temperatures explains the observed reduction of solutes in the hydrogel.

The effects of temperature on the swelling capacity of the gels suggest that drug loading can be done effectively at lower temperatures (room temperature, 29°C), while drug elution can be controlled by regulating the environmental temperature to 37°C, and or above (41, 43 and 45°C). Furthermore, the phase transition results in a mass loss of about 90% in gels containing PG, and even greater mass loss (approx. 95%) in gels containing water or BB.

The co-polymer ratio of the P(NIPA)-based hydrogel (95-5 mol%) with LCST of 36°C results in a more controlled release of PG drug at 37°C. Such a co-polymer ratio should be considered for the localized release of PG in physiological temperature range.

The diffusion coefficients of PG released from the hydrogels were between $4.97 - 9.29 \times 10^{-9} \text{ m}^2/\text{s}$ at 37°C. However, there is a need for further studies for localized release of cancer drugs (such as PG and PT) loaded with P(NIPA)-based gels, while observing their effects on cancer cells. There is also a need for biocompatibility studies of the gels. These are clearly some of the challenges for future work.

The swelling capacities of P(NIPA)-based hydrogels were greatly affected by temperature (swelling environment). The result on the analysis of variance (ANOVA) test of the effect temperature on the swelling ratios revealed that there was a significant difference on the effect of temperature on the swelling. In order to investigate these differences, a post hoc test was carried out using the least significant difference (LSD) test. Moreover, PG was also found to significantly increase the LCSTs of P(NIPA)-based hydrogels.

However, for all the polymer ratios (A, B, C, D); there was no significant difference in the effect of the drugs/fluids on the swelling ratios. Similarly, there was no significant difference in the effect of the different polymer ratio on the SRs as depicted in all the ANOVA tables. Hence there was no need for post hoc test. In addition, there was also no significant differences on the effects of polymer ratios on the equilibrium volume ratios of P(NIPA)-based hydrogels.

The diffusion rates of P(NIPA)-based hydrogel loaded with PG, in addition to their thermo-response, can also be used to control the release of drugs during localized chemotherapy.

3.5 Bibliography

- [1] A. Alwan. Global Status Report on Noncommunicable Diseases in 2010. Geneva, Switzerland: World Health Organization (2011) 164.
- [2] J. Ferlay, H. R. Shin, F. Bray, D. Forman, C. D. Mathers and D. M. Parkin. Estimates of Worldwide Burden of Cancer in 2008: GLOBOCAN 2008. *International Journal of Cancer*. 127 (2010) 2893-2917.
- [3] J. Ferlay, H. R. Shin, F. Bray, D. Forman, C. D. Mathers and D. Parkin. GLOBOCAN 2008, Cancer Incidence and Mortality Worldwide: IARC Cancer-Base No.10 [Internet]. Lyon, France: International Agency for Research on Cancer. 2010.
- [4] D. C. Mathers and D. Loncar. Updated Projections of Global Mortality and Burden of Disease, 2002-2030; Data Sources, Methods and Results. World Health Organization. (2005) 6.
- [5] J. P. Borgstede and B. M. Bagrosky. Early Diagnosis and Treatment of Cancer Series: Breast Cancer: Screening of High-Risk Patients. Philadelphia, PA, United States of America, Saunders Elsevier. (2011) 141-149.
- [6] E-D. Pisano, C. Gatsonis, E. Hendrick, et. al. Diagnostic Performance of Digital Versus Film Mammography for Breast-cancer Screening. *N Engl J Med*. 353 (2005) 1773-1783.

- [7] D. Saslow, C. Boetes, W. Burke, et al. American Cancer Society guidelines for breast screening with MRI as an adjunct to mammography. *CA Cancer J Clin.* 57 (2007) 75-89.
- [8] R-A. Smith, D. Saslow, K-A. Sawyer, et al. American Cancer Society Guidelines for Breast Cancer Screening. *CA Cancer J Clin.* 53 (2003) 141-169.
- [9] N. David and W. D. Mark. The Development and Testing of a New Temperature-sensitive Drug Delivery System for the Treatment of Solid Tumors. *Advanced Drug Delivery Reviews*, 53 (2001) 285-305.
- [10] B. Hildebrandt and P. Wust in: W.P. Ceelen. *Peritoneal Carcinomatosis: A Multidisciplinary Approach*, Springer, New York. (2007) 185.
- [11] Y. Oni, C. Theriault, A.V. Hoek and W.O. Soboyejo. Effects of Temperature on Diffusion from PNIPA-Based Gels in a BioMEMS Device for Localized Chemotherapy and Hyperthermia, *Mater. Sci. and Eng. C.* 31 (2011) 67-76.
- [12] Y. Oni and W.O. Soboyejo. Swelling and Diffusion of PNIPA-Based Gels for Localized Chemotherapy and Hyperthermia. *Mater. Sci. and Eng. C.* 32 (2012) 24-30.
- [13] D. Brain, R. D. Kavanagh, D. K. Brian and D. T. Robert, editors. *Stereotactic Body Radiation Therapy*. Lippincott W. and Wilkins, Philadelphia, PA, USA., 2005.
- [14] J. A. Del Regato. *Radiological oncologists: the unfolding of a medical specialty*. Reston (VA): Radiology Centennial. 268 (1993) 167-176.
- [15] J. Jennifer, D. Kang and F.M. William. Thermoresponsive Hydrogels as a New Ocular Drug Delivery Platform to the Posterior Segment of the Eye, *Transactions of the American Ophthalmological Society*. 106 (2008) 206-214.
- [16] R. H. Todd and S. K. Daniel. Hydrogels in Drug Delivery: Progress and Challenges. *Polymer*. 49 (2008) 1993-2007.
- [17] G. Catarina, P. Paula and G. Miguel. Self-Assembled Hydrogel Nanoparticles for Drug Delivery Applications. *Materials*. 3 (2010) 1420-1460.
- [18] A. Afrassiabi, A. S. Hoffman and L. A. Cadwell, Effect of Temperature on the Release Rate of Biomolecules from Thermally Reversible Hydrogel. *Membrane Sci.* 33 (1987) 191-200.
- [19] T. G. Farmer, T. F. Edgar and N. A. Peppas. *In Vivo* Simulations of pH-Responsive Cationic Hydrogels in Diabetic Patients. *Ind. and Eng. Chem. Res.* 47 (2008), 10053-10063.
- [20] B. Yuan, J. States, C. Sahagun and D. Wicks. Effects of three crosslinkers on colored pH-responsive core-shell latexes. *J. Appl. Polym. Sci.* 107(6) 4093-4099.
- [21] J. D. Schmaljohann, Thermo- and pH-responsive Polymers in Drug Delivery, *Advanced Drug Delivery Reviews*. 58 (2006) 1655-1670.
- [22] B. Jeong and A. Gutowska, Lessons from Nature: Stimuli-Responsive Polymers and their Biomedical Applications, *Trends in Biotechnology*. 20 (7) (2002) 305-311.
- [23] K. S. Soppimath, T. M. Aminabhavi, A. M. Dave, S. G. Kumbar and W. E. Rudzinski. *Drug Development and Industrial Pharmacy*. 28 (2002) 957-963.
- [24] Y. Hu and T. Kaoru. Potential Application of Poly(N-isopropylacrylamide) Gel Containing Polymeric Micelles to Drug Delivery Systems. *Colloids and Surfaces B: Biointerfaces*. 46(3) (2005) 142-146.
- [25] F. Antunes, L. Gentile, L.Tavano and O. C. Rossi. Rheological Characterization of the Thermal Gelation of Poly(N-isopropylacrylamide) and Poly(N-isopropylacrylamide) Co-Acrylic Acid. *Applied Rheology*. 19(4) (2009) 42064-42069.
- [26] N. Bertrand, J. G. Fleischer, K. M. Wasan and J. C. Leroux, Pharmacokinetics and Biodistribution of N-isopropylacrylamide Copolymers for the Design of pH-sensitive Liposomes. *Biomaterials*, 30 (2009) 2598-26059.
- [27] H. A. De Las, C. Alexander and S. Pennadam. Stimuli Responsive Polymers for Biomedical Applications. *Chemical Society Reviews*. 34 (2005) 276-285.

- [28] Q. Yong and K. Park, Environment-Sensitive Hydrogels for Drug Delivery, Wiley Periodicals. Inc. *Appl. Polym. Sci.* 99 (2005) 37-44.
- [29] G. Fu and W. O. Soboyejo. Swelling and Diffusion Characteristics of Modified Poly (N-isopropylacrylamide) Hydrogels. *Mater. Sci. and Eng. C.* 30 (2010) 8-13.
- [30] H. G. Schild. Poly(N-isopropylacrylamide): Experiment, Theory and Application. *Progress in Polymer Science.* 17 (2) (1992) 163-249.
- [31] M. K. Yoo, Y. K. Sung, Y. M. Lee and C. S. Cho. Effect of Polyelectrolyte on the Lower Critical Solution Temperature of Poly(N-Isopropyl Acrylamide) in the Poly(Nipaam-Co-Acrylic Acid) Hydrogel. *Polymer.* 41 (15) (2000) 5713-5719.
- [32] M. C. Wani, H. L. Taylor, M. E. Wall, P. Coggon and A. T. McPhail. Plant Antitumor Agents. VI. The Isolation and Structure of Taxol, a Novel Antileukemic and Antitumor Agent from *Taxus Brevifolia*: *J. Am. Chem. Soc.* 93 (1971) 2325-2327.
- [33] T. Tanaka. Gels. *US National Library of Medicine, National Institutes of Health. Sci. Am.* 244 (1) (1981) 124-138.
- [34] K. D. Kamble, V. D. Hiwarale. Prodigiosin Production from *Serratia Marcescens* Strains Obtained from Farm Soil. *Int. J. Environmental Sci.* 3(1) (2012) 631-638.
- [35] N. Someya, M. Nakajima, H. Hamamoto, I. Yamaguchi and K. Akutsu. Effects of Light Conditions on Prodigiosin Stability in the Biocontrol Bacterium *Serratia Marcescens* strain B2. *General Plant Pathology.* 70 (6) (2004) 367-370.
- [36] LCLGC's CHROMacademy. Crawford Scientific. Quantitative & Qualitative HPLC. Unpublished data.1-31.
- [37] J. W. Dolan (editor). Why Do Peaks Tail? LC Troubleshooting. *LCGC North America.* 21(7) (2003) 612.
- [38] H. G. Schild, M. Muthukumar and D. A. Tirrell: Cononsolvency in Mixed Aqueous Solutions of Poly(N-Isopropylacrylamide). *Macromolecules.* 24 (1991). 948-952.
- [39] O. Okay and Y. Dogu, Swelling–Deswelling Kinetics of Poly(Nisopropylacrylamide) Hydrogels Formed in PEG Solutions. Wiley Periodicals, 2005.
- [40] N. A. Peppas, P. Bures, W. Leobandung and H. Ichikawa. Hydrogels in pharmaceutical formulations. *Eur. J. Pharm. Biopharm.* 50 (2000) 27-46.
- [41] L. Brannon-Peppas and N.A. Peppas. Equilibrium Swelling Behavior of pH-Sensitive Hydrogels. *Chem. Eng. Sci.* 46 (1991a) 715-722.
- [42] A. N. Peppas. Analysis of Fickian and Non-Fickian Drug Release from Polymers. *Pharm. Acta Helv.* 60 (4) (1985) 110-111.
- [43] B. A. Ogunnaike. *Random Phenomena, Fundamentals of Probability & Statistics for Engineers, USA, University of Delaware.* (2009) 1-1055.
- [44] E. Favre, et al. Diffusion of Polyethyleneglycols in Calcium Alginate Hydrogels. *Colloids and Surfaces A: Physicochemical and Engineering Aspects,* 194 (1-3) (2001) 197-206.
- [45] P. J. Flory. Dependence of Elastic Properties of Vulcanized Rubber on the Degree of Cross Linking. *N.R.M.C.S.* (1949) 225-245.
- [46] J. K. Kim, G. B. Cho. Modification of a Cross linked Poly(acrylic acid) Based New Dehumidifying Agent and its Moisture Absorbing Characteristics. *Macromolecular Research.* 17 (7) (2009) 544-548.
- [47] G. Q. Zhang, L. S. Zha, M. H. Zhou, J. H. Ma, B. R. Liang. Preparation and Characterization of pH-and Temperature-Responsive Semi-Interpenetrating Polymer Network Hydrogels based on Linear Sodium Alginate and Cross linked Poly(N-Isopropylacrylamide). *Colloid and Polymer Science* 283 (2005) 431-438.
- [48] M. Grassi and G. Grassi. Mathematical Modelling and Controlled Drug Delivery: Matrix Systems. *Curr. Drug Deliv.* 2 (2005) 97-116.

- [49] R. Zarzycki, Z. Modrzejewska and K. Nawrotek. Drug Release from Hydrogel Matrices. *Ecological Chemistry and Engineering S.* 17(2) (2010) 118-136.
- [50] Y. Danyuo, J. D. Obayemi, S. Dozie-Nwachukwu, C. J. Ani, O. S. Odusanya, Y. Oni, N. Anuku, K. Malatesta and W. O. Soboyejo. Prodigiosin Release From an Implantable Biomedical Device: Kinetics of Localized Cancer Drug Release. *J. of Mater. Sci. and Eng. C.* Vol. 42, (2014) 734-745.
- [51] L.R. Snyder, J. J. Kirkland, and J.L. Glajch, *Practical HPLC Method Development* (John Wiley & Sons, New York, 2nd ed., 1997), p. 180.

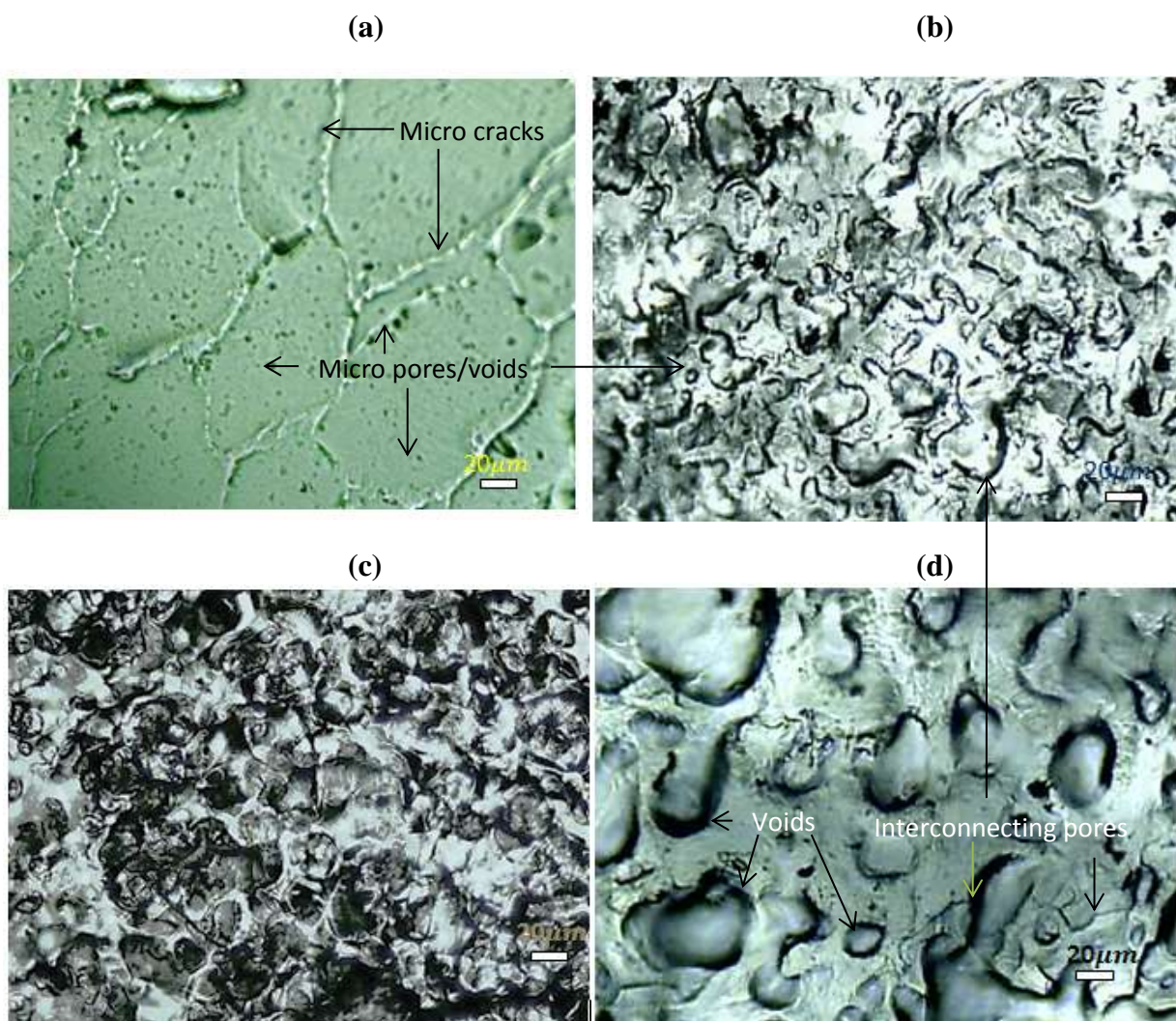
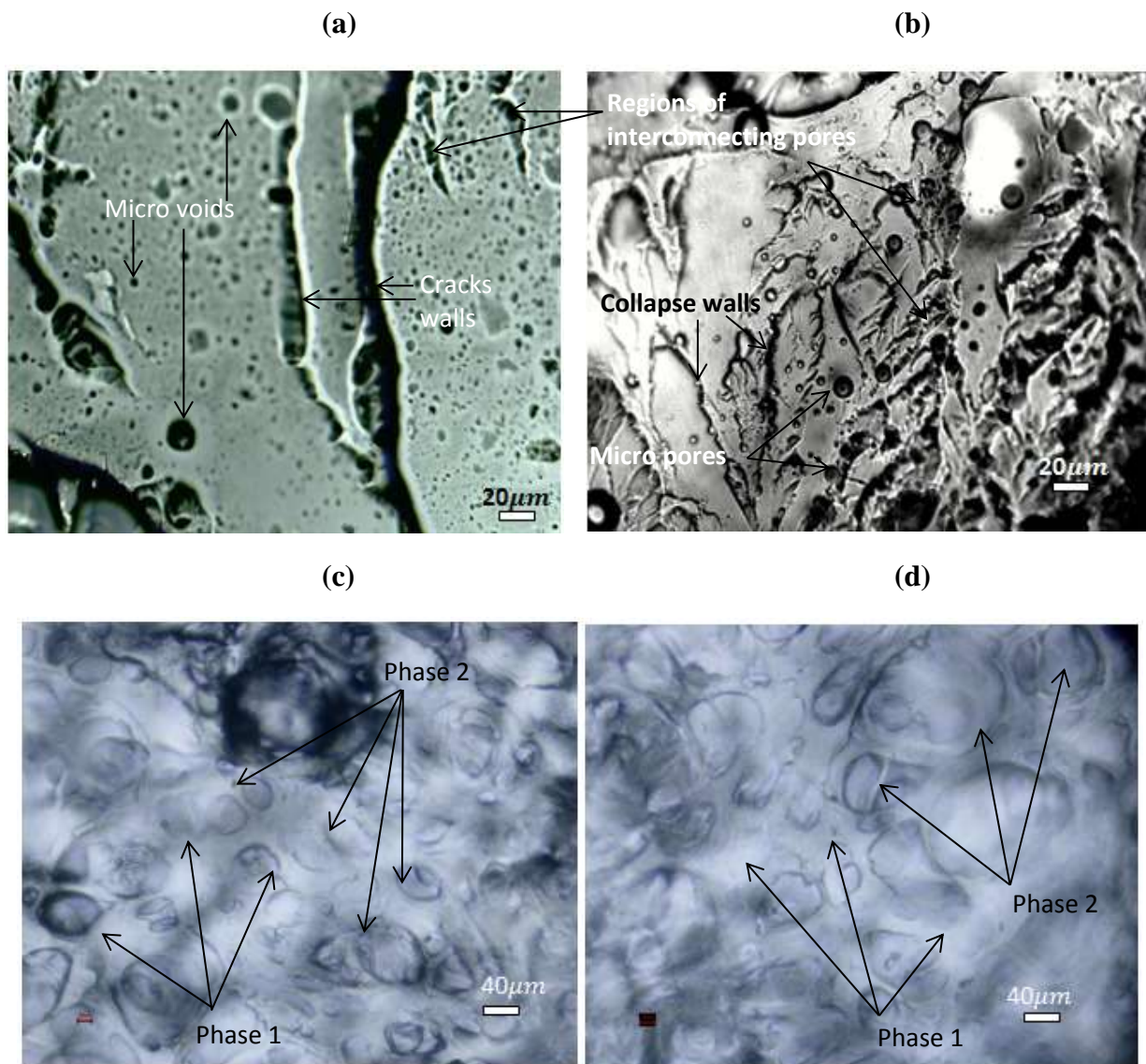
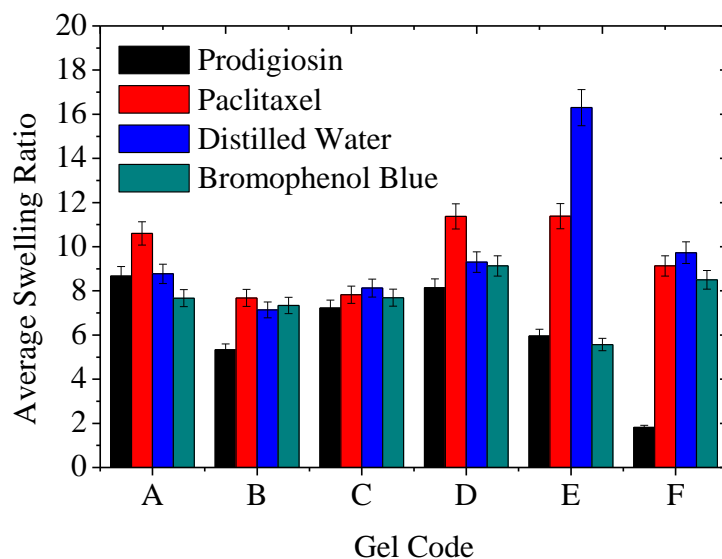


Figure 3.1: LCD Microscopy Analysis of PNIPA-Based Hydrogels: (a) Homopolymer (100 mol% of NIPA and (b) 95 mol% of P(NIPA)-5 mol% of AM; (c) 90 mol% of P(NIPA)-10 mol% of AM; and (d) P(NIPA) with 85 mol% of P(NIPA)-15 mol% of AM.



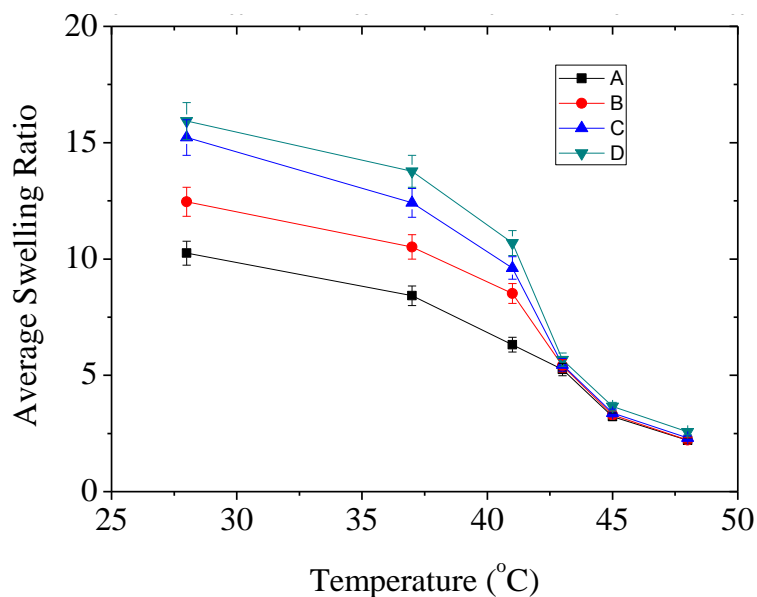
Images (A) And (B) Were Taken With LCD Deluxe Digital Optical Microscope (Celestron, Columbia, St. Torrance, USA), While Images (C) and (D) Were Taken with Nikon Inverted Microscope, TS 100; Supported with Nikon Digital Camera DXM1200F. ^{Phases 1} Interconnecting Matrix Phase, ^{Phase 2} Regions of Micro Pores/ Voids.

Figure 3.2: Microscopy Analysis of P(NIPA)-Based gels: (a) P(NIPA-co-AM-co-BMA) (90:5:5 mol%); (b) P(NIPA-co-AM-co-BMA) (85:5:10 mol%)(imaged with Celestron Microscope); (c) P(NIPA-co-AM-co-BMA) (90:5:5 mol%) and (d) P(NIPA-co-AM-co-BMA) (85:5:10 mol%) (Imaged with Nikon Inverted Microscope).



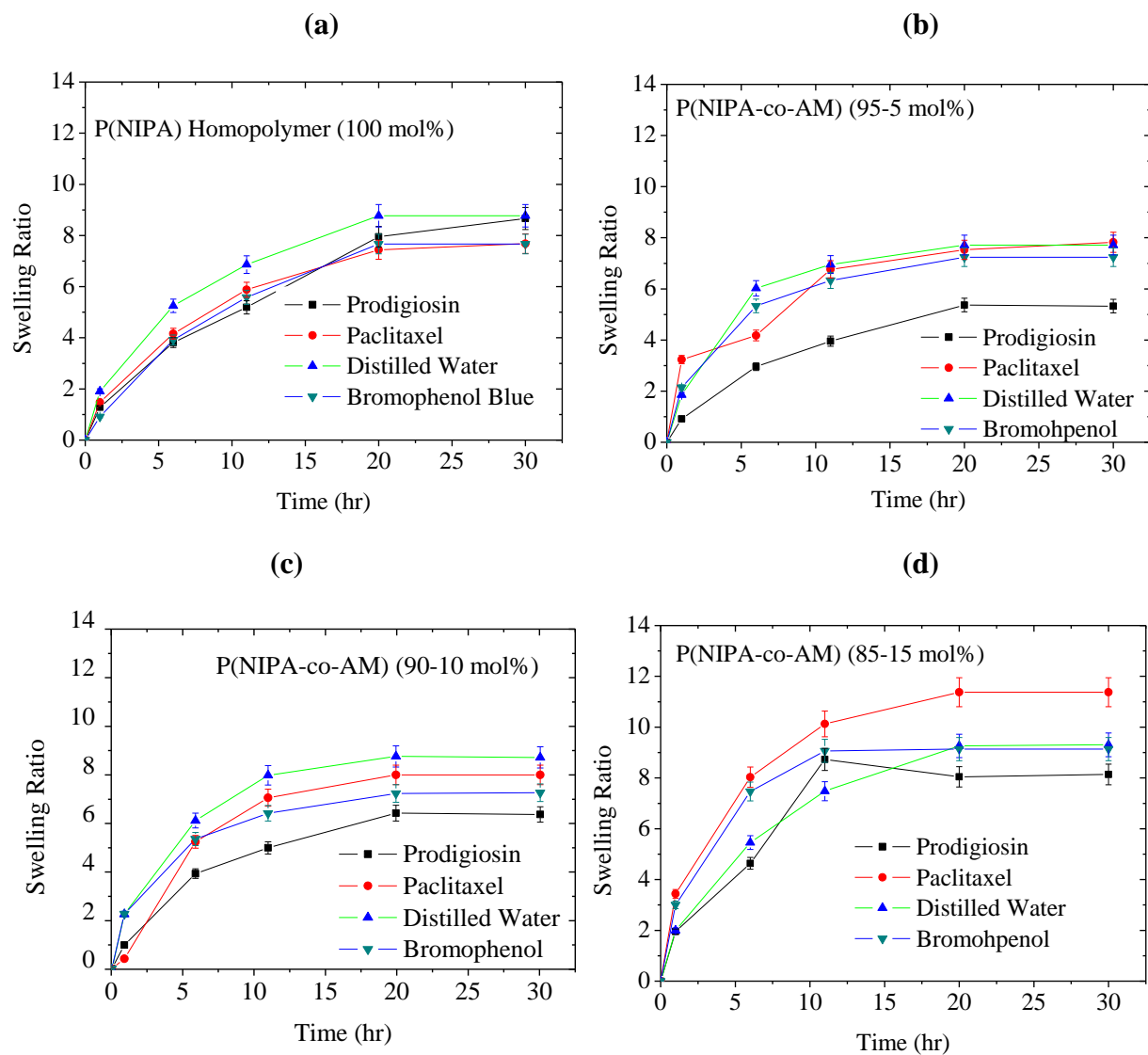
^{P(NIPA)}N-Isopropylacrylamide, ^{AM}Acrylamide, ^{BMA}ButylMethylacrylate, ^{APS}Amonium persulfate, ^{TEMED}N,N,N',N'-Tetramethylethylenediamine; Gel codes; ^AP(NIPA) Homopolymer (100 mol% of P(NIPA)), ^BP(NIPA-co-AM) (95:5 mol%), ^CP(NIPA-co-AM) (90:10 mol%), ^DP(NIPA-co-AM) (85:15 mol%), ^EP(NIPA-co-BMA) (95:5 mol%) and ^FP(NIPA-co-BMA) (90:10 mol%).

Figure 3.3: Average Swelling Ratios of P(NIPA)-based Hydrogels at 28°C (room temperature) for 30 hrs.



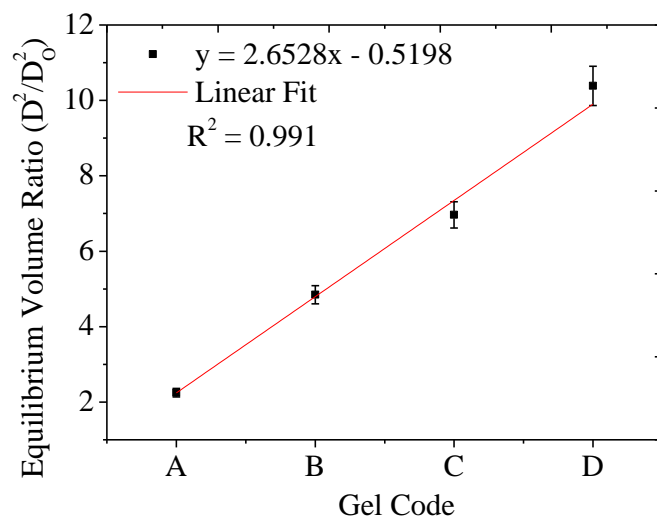
^{PNIPA}N-Isopropylacrylamide, ^{AM}Acrylamide, ^{BMA}ButylMethylacrylate; Gel codes; ^APNIPA Homopolymer (100 mol% of PNIPA), ^BPNIPA-co-AM (95:5 mol%), ^CPNIPA-co-AM (90:10 mol%), ^DPNIPA-co-AM(85:15 mol%).

Figure 3.4: Effect of Temperature on the Average Swelling Ratio of P(NIPA)-Based Hydrogels in 2.5 mg/ml 30 hrs in PG.



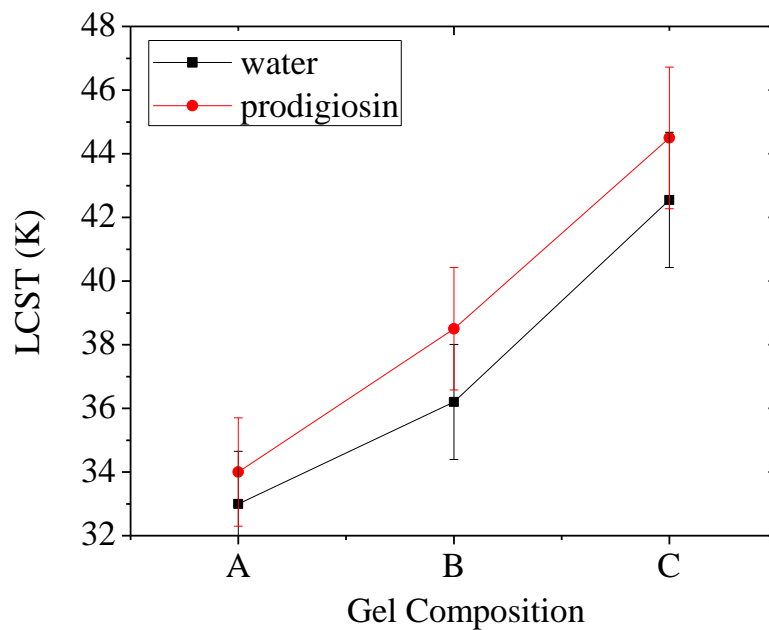
^{P(NIPA)}N-Isopropylacrylamide, ^{AM}Acrylamide, ^{BMA}ButylMethylacrylate, ^{APS}Amonium persulfate, ^{TEMED}N,N,N',N'-Tetramethylethylenediamine; Gel codes; ^AP(NIPA) Homopolymer (100 mol% of P(NIPA)), ^BP(NIPA-co-AM) (95:5 mol%), ^CP(NIPA-co-AM) (90:10 mol%) and ^DP(NIPA-co-AM) (85:15 mol%).

Figure 3.5: Swelling Ratio of P(NIPA)-Based Hydrogels in Different Fluids (5 ml of 2 µg/ml of drug solutions) or distilled water at 28°C.



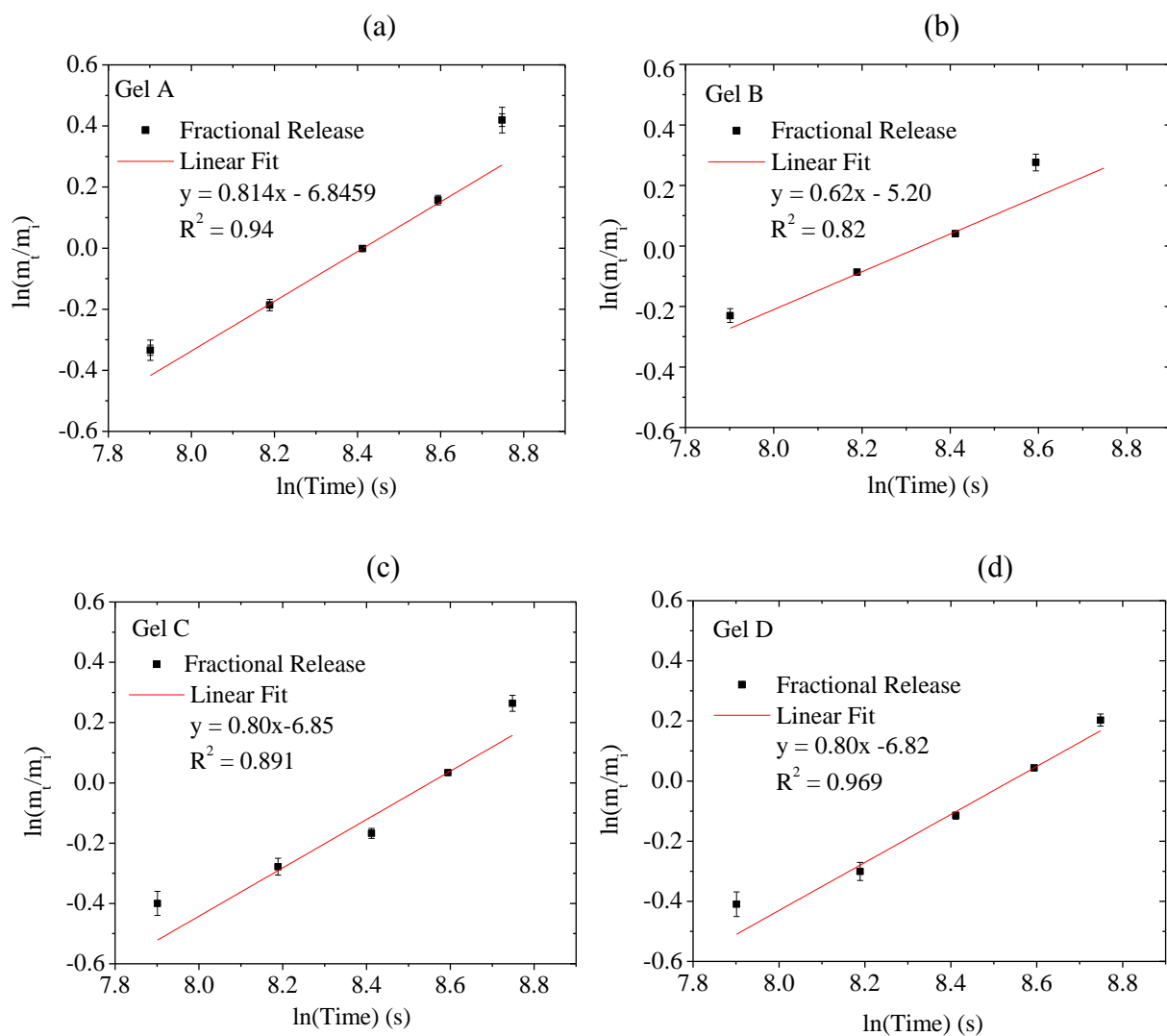
^{P(NIPA)}N-Isopropylacrylamide, ^{AM}Acrylamide, ^{BMA}ButylMethylacrylate, ^{APS}Amonium persulfate, ^{TEMED}N,N,N',N'-Tetramethylethylenediamine; Gel codes; ^AP(NIPA) Homopolymer (100 mol% of P(NIPA)), ^BP(NIPA-co-AM) (95:5 mol%), ^CP(NIPA-co-AM) (90:10 mol%) and ^DP(NIPA-co-AM) (85:15 mol%).

Figure 3.6: Equilibrium Volume Ratio of PNIPA-Based Hydrogels Soaked in Prodigiosin at 28°C.



(a) Homopolymer (100 mol% of PNIPA and (b) 95 mol% of PNIPA-5 mol% of Acrylamide; (c) 90 mol% of PNIPA-10 mol% of Acrylamide

Figure 3.7: Effects of PG on the LCSTs of P(NIPA)-based Hydrogels.



(a) Homopolymer (100 mol% of PNIPA and (b) 95 mol% of PNIPA-5 mol% of Acrylamide; (c) 90 mol% of PNIPA-10 mol% of Acrylamide; and (d) PNIPA with 15 mol% of Acrylamide.

Figure 3.8: Fraction of Drug (20 $\mu\text{g/ml}$ of Prodigiosin) Release from P(NIPA)-Based Hydrogels Versus $\ln t$ (s) at 37°C.

Table 3.1: Gel Materials and their Role in Gel Polymerization.

Gel materials and their reagent grade	Active Role in P(NIPA)-Based Gel Polymerization
N-Isopropylacrylamide (NIPA), 97 %	Monomer
N,N,N',N'-Tetramethylethylenediamine (TEMED), 99 %	Catalytic agent used in conjunction with APS to accelerate the rate of polymerization
N,N'-Methylenebisacrylamide (MBA), 99.5 %	Cross-linker
Ammonium persulfate (APS), 98 %	Radical Initiator
Acrylamide (AM), 99.9 %	Hydrophilic Compound
Butyl Methacrylate, 98.8 %	Hydrophobic Compound

Table 3.2: Displays the ANOVA Test for the Effect of the Different Polymer Ratio on the Swelling Ratios.**ANOVA****Response**

	Sum of Squares	df	Mean Square	F	Sig.
Between Groups	26.350	3	8.783	.419	.741
Within Groups	418.861	20	20.943		
Total	445.211	23			

Table 3.3A: Displays the Analysis of Variance (ANOVA) Test of the Effect of Temperature on the Swelling Ratios.**ANOVA****Response**

	Sum of Squares	df	Mean Square	F	Sig.
Between Groups	19.015	5	3.803	5.738	.001
Within Groups	19.882	30	.663		
Total	38.897	35			

Table 3B: Least Significant Difference (LSD) Test

LSD Multiple Comparisons

(I) Temperature (°C)	(J) Temperature (°C)	Mean Difference (I-J)	Std. Error	Sig.	95% Confidence Interval	
					Lower Bound	Upper Bound
28	37	1.5150*	.4700	.003	.5551	2.4749
	41	.5261	.4700	.272	-.4338	1.4860
	43	1.4638*	.4700	.004	.5039	2.4237
	45	1.8409*	.4700	.000	.8810	2.8007
	48	2.0373*	.4700	.000	1.0774	2.9972
37	28	-1.5150	.4700	.003	-2.4749	-.5551
	41	-.9888*	.4700	.044	-1.9488	-.0290
	43	-.0512	.4700	.914	-1.0110	.9087
	45	.3259	.4700	.493	-.6340	1.2857
	48	.5224	.4700	.275	-.4375	1.4823
41	28	-.5261	.4700	.272	-1.4860	.4338
	37	.9888*	.4700	.044	.0290	1.9488
	43	.9377	.4700	.055	-.0222	1.8976
	45	1.3148*	.4700	.009	.3549	2.2746
	48	1.5113*	.4700	.003	.5514	2.4711
43	28	-1.4638	.4700	.004	-2.4237	-.5039
	37	.0512	.4700	.914	-.9087	1.0110
	41	-.9377	.4700	.055	-1.8976	.0222
	45	.3770	.4700	.429	-.5828	1.3369
	48	.5735	.4700	.232	-.3864	1.5334
45	28	-1.8408	.4700	.000	-2.8007	-.8810
	37	-.3258	.4700	.493	-1.2858	.6340
	41	-1.3147	.4700	.009	-2.2746	-.3549
	43	-.3770	.4700	.429	-1.3369	.5828
	48	.1965	.4700	.679	-.7634	1.1563
48	28	-2.0373	.4700	.000	-2.9972	-1.077
	37	-.5224	.4700	.275	-1.4823	.4375
	41	-1.5112	.4700	.003	-2.4711	-.5514

43	-.5735	.4700	.232	-1.5334	.3864
45	-.1965	.4700	.679	-1.1563	.7634

*. The mean difference is significant at the 0.05 level.

Table 3.4: Repeated ANOVAs for the Swelling Ratios of P(NIPA)-based Hydrogels in Different Fluids (5 ml of 2 µg/mL of drug solutions) or distilled water at 28°C.

Response

Repeated ANOVAS

Polymer Ratio		Sum of Squares	df	Mean Square	F	Sig.
(A) Homopolymer (100 mol% of NIPA)	Between Groups	3.760	3	1.253	.106	.956
	Within Groups	236.446	20	11.822		
	Total	240.206	23			
(B) P(NIPA-co-AM) (95-5 mol%)	Between Groups	8.668	2	4.334	.449	.647
	Within Groups	144.847	15	9.656		
	Total	153.515	17			
(C) P(NIPA-co-AM) (90-10 mol%)	Between Groups	10.290	3	3.430	.316	.813
	Within Groups	216.944	20	10.847		
	Total	227.234	23			
(D) PNIPA-co-AM (85-15 mol%)	Between Groups	16.935	3	5.645	.345	.793
	Within Groups	327.016	20	16.351		
	Total	343.952	23			

^{df} Degree of freedom.

Table 3.5: Activation Energy and LCST of PNIPA-Based Hydrogels in Distilled Water.

Gel Code	Activation Energy (kJ/mole)	Lower Critical Solution Temperature (°C)
A	122 ± 6	33 ± 1.7
B	163 ± 8	36 ± 1.8
C	166 ± 8	38 ± 1.9
D	291 ± 15	42 ± 2.1
E	114 ± 6	29 ± 1.5

^{NIPA}N-Isopropylacrylamide, ^{AM}Acrylamide, ^{BMA}ButylMethylacrylate, ^{APS}Amonium persulfate, Gel codes; ^AP(NIPA) Homopolymer (100 mol% of P(NIPA)), ^BP(NIPA-co-AM) (95:5 mol%), ^CP(NIPA-co-AM) (90:10 mol%), ^DP(NIPA-co-AM) (85:15 mol%) and ^EP(NIPA-co-BMA) (95:5 mol%).

Table 3.6: The Values of n, k and D at 37°C from PG Release.

Compositions of Cylindrical Gel Samples	Release Exponent (n)	Geometric constant k (x 10⁻³s⁻¹)	Diffusion Coefficients D_s (x 10⁻⁹m²/s)
Homopolymer (100 mol% of PNIPA)	0.81	1.15	8.11
P(NIPA-co-AM) (95:5 mol%)	0.62	0.85	6.24
P(NIPA-co-AM) (90:10 mol%)	0.80	0.70	4.97
P(NIPA-co-AM) (90:10 mol%)	0.80	1.31	9.29

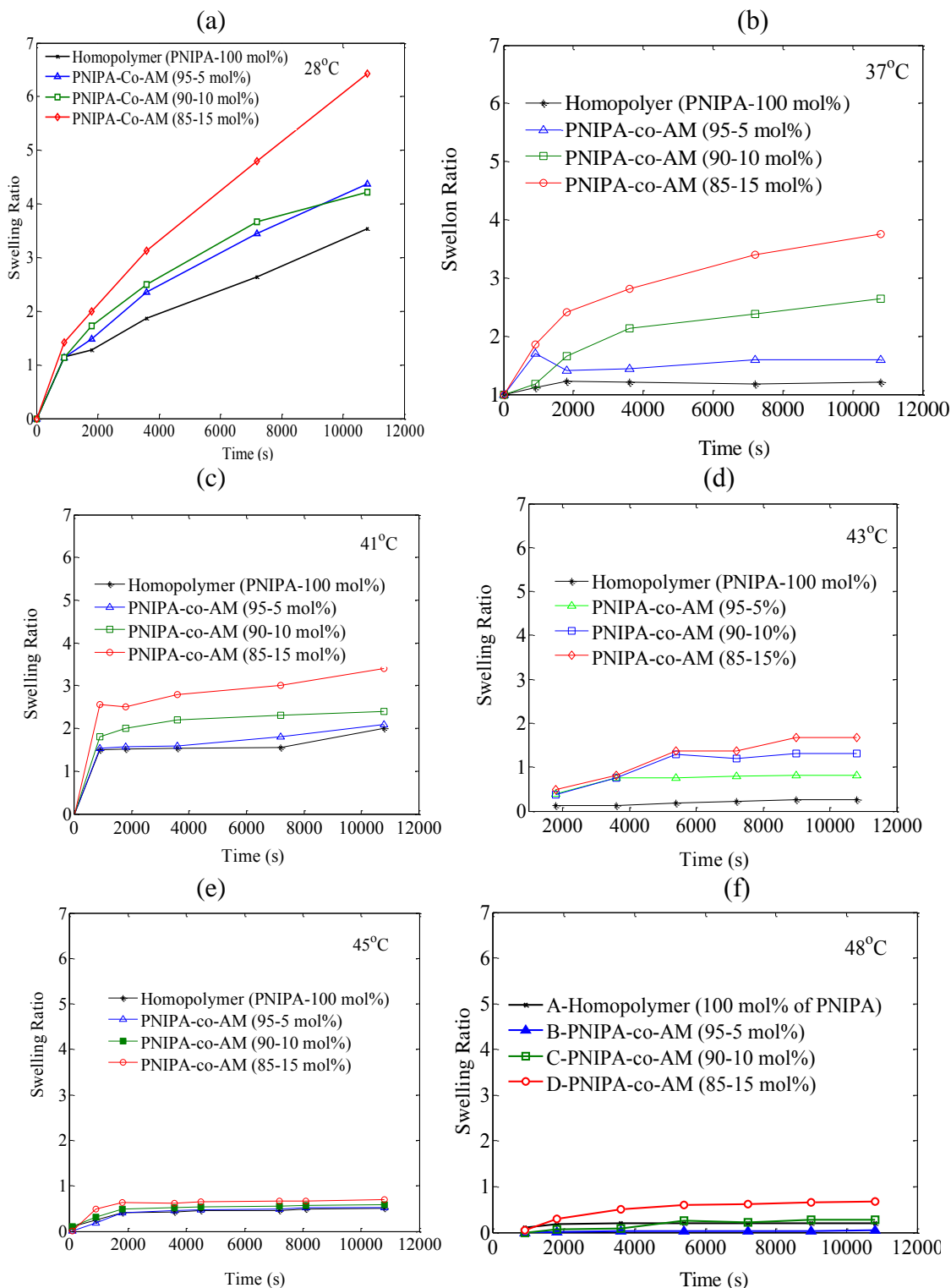
^{P(NIPA)}N-Isopropylacrylamide, ^{AM}Acrylamide

Table 3.7: Strain Induced on Hydrogels Due to Swelling.

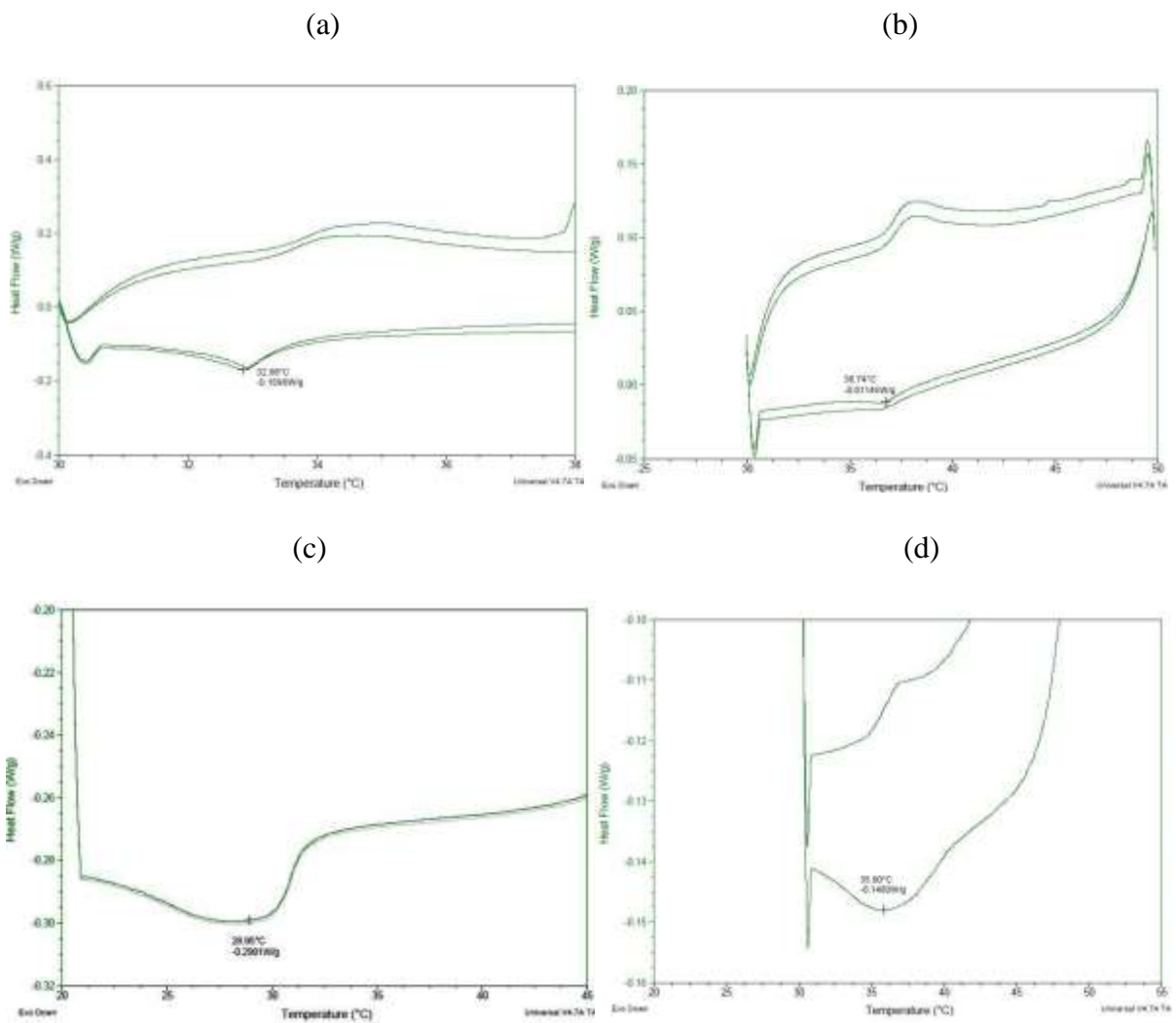
Gel Code	Prodigiosin strain (ε)	Distilled Water (ε)
A	0.44 ± 0.02	0.29 ± 0.02
B	1.08 ± 0.05	1.04 ± 0.05
C	1.35 ± 0.07	1.22 ± 0.06
D	1.73 ± 0.04	1.28 ± 0.06

^{NIPA}N-Isopropylacrylamide, ^{AM}Acrylamide, ^{BMA}ButylMethylacrylate, ^{APS}Amonium persulfate, Gel codes; ^AP(NIPA) Homopolymer (100 mol% of P(NIPA)), ^BP(NIPA-co-AM) (95:5 mol%), ^CP(NIPA-co-AM) (90:10 mol%) and ^DP(NIPA-co-AM) (85:15 mol%).

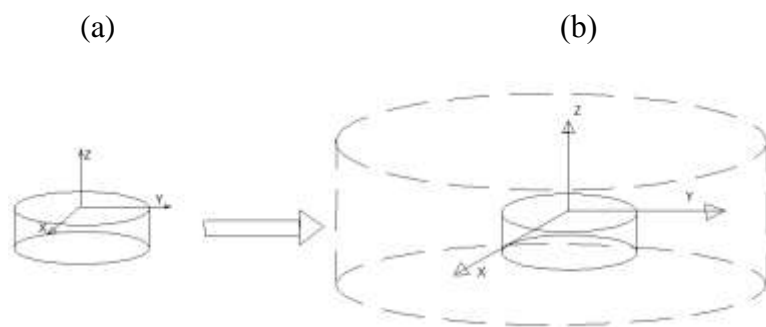
Appendix A. Supplementary Data



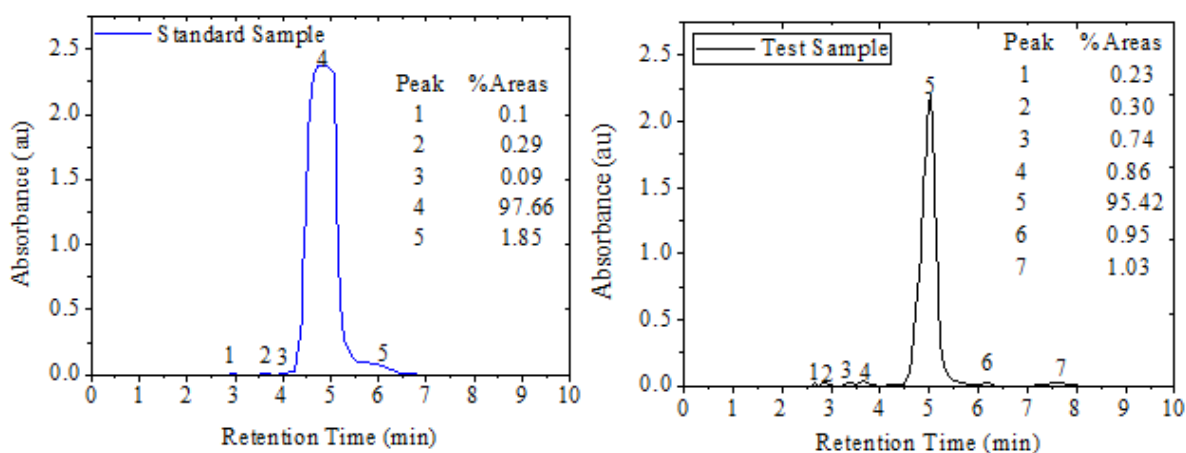
Average Swelling Ratio of P(NIPAA)-Based Hydrogels Soaked in Distilled Water Versus Time (s): (a) at 28°C; (b) at 37°C; (c) at 41°C; (d) at 43°C; (e) at 45°C, and (f) at 48°C.



Original DSC curves of LCST for typical P(NIPA)-based Hydrogels: (a) Homopolymer (100 mol% of NIPA): P(NIPA-co-AM) (85-15 mol%), (c) P(NIPA-co-BMA) (90:10 mol%) and (d) P(NIPA-co-AM-co-BMA) (85:5:10 mol%).



Schematic Illustration of P(NIPA)-based Hydrogel in Glassy and Rubberly State Matrix. (a) Glassy state (appears opaque) and (b) Rubberly state (appears transparent).



HPLC Analysis of Sample Purity: Plots of Standard Prodigiosin and Tested Sample (Prodigiosin), respectively.

P(NIPA)-based hydrogel configuration and their compositions

Gel Code	P(NIPA) (mol%)	AM (mol%)	APS (g)	MBA (mg)	TEMED (μ l)	BMA (mol%)
A	100	-	0.0335	0.0136	5	-
B	95	5	0.0335	0.0136	10	-
C	90	10	0.0335	0.0136	20	-
D	85	15	0.0335	0.0136	30	-
E	95	-	0.0335	0.0136	5	5
F	90	-	0.0335	0.0136	10	10
G	90	5	0.0335	0.0136	20	5
H	85	5	0.0335	0.0136	30	10

^{P(NIPA)}N-Isopropylacrylamide, ^{AM}Acrylamide, ^{BMA}ButylMethylacrylate, ^{APS}Amonium persulfate, ^{TEMED}N,N,N',N'-Tetramethylethylenediamine; Gel codes; ^AP(NIPA) Homopolymer (100 mol% of P(NIPA)), ^BP(NIPA-co-AM) (95:5 mol%), ^CP(NIPA-co-AM) (90:10 mol%), ^DP(NIPA-co-AM) (85:15 mol%), ^EP(NIPA-co-BMA) (95:5 mol%), ^FP(NIPA-co-BMA) (90:10 mol%), ^GP(NIPA-co-AM-co-BMA) (90:5:5 mol%), ^HP(NIPA-co-AM-co-BMA) (85:5:10 mol%).

Preparation of drug/sample solution into working concentrations.

Drug/sample	Initial dissolution	Final dissolution (Topped up with)	Final Concentration
0.1 g of Paclitaxel	2 ml DMSO	38 ml PBS	2.5 mg/ml (DMSO:PBS) (5:95 %)
0.1 g of Prodigiosin	2 ml methanol	38 ml PBS	2.5 mg/ml (Methanol:PBS) (5:95 %)
0.1 g of Bromophenol	2 ml ethanol	38 ml DW	2.5 mg/ml (ethanol:DW) (5:95 %)

4.0 Prodigiosin Release from an Implantable Biomedical Device: Kinetics of Localized Cancer Drug Release

4.1 Introduction

The increasing incidence of cancer [1] has stimulated research on the development of novel implantable devices for the localized treatment of cancer [2-5]. Cancer is currently the second leading cause of death worldwide, after cardiovascular disease [6,7]. Current trends also suggest that cancer will become the leading cause of death by 2030 [6,8]. Furthermore, standard treatment methods, such as bulk systematic chemotherapy [1,4,9] and radiotherapy [10], have exhibited severe side effects. There is, therefore, a need to develop localized cancer treatment methods that mitigate these side effects.

One approach that can be used to reduce the potential side effects of cancer treatments is to use localized chemotherapy to reduce the concentrations of cancer drugs that are needed for effective treatment. This can be achieved by using implantable drug eluting devices for localized drug delivery [4,11]. Such approaches can also be combined with localized hyperthermia in cancer treatment [12-14]. Recent research by Yaoming et al. [15] has also shown that haematoporphyrin based-photodynamic therapy, combined with hyperthermia, provides an effective therapeutic vaccine against colon cancer growth in mice.

This paper presents the results of an experimental study of the kinetics of cancer drug release (bacterial-synthesized prodigiosin (PG)) from an implantable device in which PG is soaked in encapsulated PNIPA gels. The P(NIPA)-based gels are encapsulated in poly-di-methyl-siloxane (PDMS) packages with micro-channels that facilitate the delivery of cancer drugs, such as paclitaxelTM and prodigiosin. The implications of the results are then discussed for the design of implantable biomedical structures for the localized treatment of breast cancer.

4.2 Experimental Materials and Procedures

4.2.1 Materials and Methods

The PaclitaxelTM (PT) that was used in this study was procured from LC Laboratories (Woburn, MA, USA). PaclitaxelTM was dissolved in dimethyl sulfoxide (CH₃)₂SO (DMSO) that was purchased from BDH Chemicals (Poole Dorset, England). DMSO is a polar aprotic solvent that dissolves both polar and nonpolar organic solvents. The prodigiosin (PG) that was used in the study was obtained from the Biotechnology and Genetic Engineering Advanced Laboratory, Sheda Science and Technology Complex (SHESTCO), Abuja, Nigeria. The prodigiosin was extracted from the bacteria, *Serratia marcescens* (SM) *subsp. marcescens* and purified by size exclusion chromatography. It was then characterized with a UV-Vis spectrophotometer (CECIL 7500 Series, Buck Scientific Inc., East Norwalk, USA). Sylgard 184 kit silicon elastomer, with a silicon elastomer curing agent (a cross linker), was used for PDMS encapsulation. The material was obtained from sylgard Dow Corning Krayden Inc. (Midland, Michigan, USA). The materials that were used in the PNIPA gel synthesis (Table 4.1) were purchased from Sigma Aldrich Co. (St. Louis, MO, in the USA).

4.2.2 Preparation of P(NIPA)-Based Hydrogels

The materials that were used in the PNIPA gel synthesis (Table 4.1) were used directly in the powdered form in the as-received condition. The gels were prepared by free radical polymerization [16]. The homopolymer (100 mol% of P(NIPA)) (denoted by gel code A) was prepared by weighing 0.87 g of PNIPA, 0.0136 g of methylene-bis-acrylamide (MBA) and 0.0335 g of ammonium persulfate (APS) with an analytical weighing balance (Mettler AE 100, Mettler-Toledo Ltd., Leicester, UK).

The samples were subsequently topped up with 7.8 mL of distilled water. They were then stirred vigorously until a homogenous mixture was obtained at temperatures $\leq 9^{\circ}\text{C}$ using sonicator water bath (Mettler, Mettler-Toledo Ltd., Leicester, UK). The mixing process was exothermic. The solution was then immersed in ice and sonicated, while nitrogen gas was bubbled through for 20 minutes at 10 bars of pressure to remove all of the dissolved oxygen. Depending on the gel composite, different amounts of the initiator, N,N,N',N'-Tetramethylethylenediamine (TEMED), were added to the solution. The mixture was then swirled gently.

P(NIPA) copolymer hydrogels with 5 or 10 mol% of Butyl-methacrylate (BMA) were initiated with 5, 10 μl of TEMED, respectively, while gels with acrylamide levels of 5, 10 or 15 mol% were initiated with 20, 30, 40 μl of TEMED, respectively. A homopolymer was initiated with 15 μl of TEMED. This reduces the turbidity of the hydrogels and also helps to produce a transparent gel. The solution was poured into cylindrical molds and opened to terminate the free radical polymerization. Samples inside the cylindrical molds were then left at 24°C in a water bath to complete the polymerization process over a period of 12 hours.

P(NIPA) gel composites (denoted by codes B to G to facilitate their presentation in [Table 4.2](#)) were also prepared by the same procedure. However, co-monomer species, acrylamide (AM) and butyl-methacrylate (BMA) were co-polymerized with P(NIPA), as summarized in [Table 2](#). The AM co-monomers were used to produce hydrophilic copolymers, while the BMA co-monomers were used to produce hydrophobic copolymer [4,5]. After co-polymerization, the gels were carefully remolded and washed several times with deionized water to remove any chemical residue. They were then subsequently cut into discs and cylindrical shapes, and soaked in deionized water, while replacing the deionized water for two weeks. The samples were removed after the second week, before air drying to remove any chemical residue. They were

then characterized using optical and scanning electron microscopy techniques described previously in reference [4](#) and [5](#).

4.2.3 Poly (Di-methyl-Siloxane) (PDMS) Fabrication

Molds for the processing of PDMS packages were fabricated from aluminum and bronze metal slabs that were fabricated at Princeton University ([Figs. 4.1a-c](#)). The outer section was fabricated from aluminum (dimensions between 10.12 mm and 15.89 mm), while the internal dimensions varied between 9.66 mm and 13.00 mm. Bronze was machined into cylindrical rods at the middle section that contained the reservoir for the drug carrier polymer (PNIPA). This cylindrical rod had diameters of 4.00 mm to 7.06 mm and heights of about 5.24 mm to 11.20 mm. Holes with a diameter of 1.12 mm were drilled into four locations in the aluminum mold, while similar holes were drilled into the bronze cylindrical rod ([Fig. 4.1a-b](#)). These were introduced to enable the resulting microchannels (obtained after the molding process) to provide a path for drug diffusion from the encapsulated hydrogel. These paths enabled drugs (from the loaded gels) to be delivered to the surrounding tissue in a controlled manner.

PDMS packages with different channel lengths and reservoirs were fabricated by mixing Sylgard 184 kit silicon elastomer with a silicon elastomer curing agent (a cross linker) (Sylgard Dow Corning, Krayden Inc., Midland, Michigan, USA). These were mixed in a ratio of 10:1 by weight. The mixture was stirred vigorously, de-gassed with a GALVAC vacuum oven (LTE Scientific Ltd., Greenfield State) set at -24 mm Hg equivalent, with no heat, for an hour. A complete mold was fixed with the aid of nuts and bolts, while 1.12 mm diameter thick surgical needles were passed through the four faces to produce the micro-channels. In order to induce temperature responsiveness in the gels, 5-10 turns of thin copper wire (0.1 mm diameter) were incorporated into some devices to induce Joule heating. Degassed PDMS was poured gently into

the fabricated molds. The samples were then cured at 60°C for 3 hours and then exposed to room-temperature (28°C) for 12 to 24 hours.

4.2.4 Encapsulation of P(NIPA) into PDMS Capsules

Although P(NIPA)-based hydrogels have been shown to have improved biocompatibility compared to PNIPA solids [17], a special effort was made to encapsulate the non-biodegradable PNIPA-based hydrogels in PDMS, which is a biocompatible polymer that has been approved by the U. S. Food and Drug Administration (FDA) for applications in implantable biomedical devices in humans [18-20], following several toxicity studies [17, 21-23].

The PDMS capsules consisted of Sylgard 184 kit silicon elastomer and a silicon elastomer curing agent of 10:1 ratio by volume (Sylgard Dow Corning, Krayden Inc., Midland, Michigan, USA). Dried P(NIPA)-based hydrogels were then inserted into the reservoir of the PDMS capsules. Before sealing the PDMS packages, the 10:1 ratio by volume mixture of Sylgard 184 kit silicon elastomer and curing agent were applied on both edges of the encapsulate and its cover. The two layers were properly sealed using a clamping device to apply a slight pressure to the axes perpendicular to the edges.

Ten sealed packages were then incubated at 40°C for 24 hours to ensure that the two layers stuck together tightly (i.e. complete polymerization). The devices were later saturated in prodigiosin or paclitaxelTM drug or dye solutions. The microchannels, which were created initially, enabled the P(NIPA) gels to load drugs or dye solution at 28°C. Thus, loading the device after encapsulation allows the gels to load up to the maximum volume of the device. The devices were then subjected to Joule heating at (37, 39, 43, 44, 45°C) (Fig. 4.1e). This was done

to simulate potential exposures to normal body temperature (37°C) and hyperthermic temperature ranges (43-45°C) [24].

The time required for the fluid to flow across the devices with different channel lengths was used to ascertain the diffusion coefficient, D , which is given by:

$$L = \sqrt{Dt} \quad (4.1)$$

where L is the channel length and t is the time taken for the fluid to flow across the channel length.

4.3.0 Results and Discussion

4.3.1 Gel Morphology

An EVO^R analytical scanning electron microscope (SEM) (Oxford Instruments, Tubney Woods Abingdon, Oxfordshire, United Kingdom) was used to study the microstructures of the gels. The scanning electron microscopy (SEM) analysis showed that the porosity increased with increasing acrylamide copolymerization (Figs. 4.2a and 4.2b).

4.3.2 Swelling and Re-swelling Ratios

Although PG, bromophenol blue (BB) and PT are solids, aqueous solvents were used to dissolve them. For example, bromophenol blue was dissolved with ethanol (70%:30% water), while PT was dissolved with methanol (100%) and DMSO (100%) was used to dissolve PT and subsequently topped up with 70:30% of DMSO: phosphate buffer saline (PBS)). The working concentrations were between 1-100 $\mu\text{g/ml}$. The resulting hydrogels (with average diameters of about 4 mm and 2 mm thick each) were then soaked into drug solutions (i.e. PG, PT, distilled

water or BB) to absorb drugs. The swelling and release behavior of the loaded gels were then studied.

The swelling ratios (SR_1) were obtained by soaking the P(NIPA)-based hydrogels in distilled water (DW), PG, PT and BB (at 28 °C below the LCST of the hydrogels). The P(NIPA)-based hydrogels used for the swelling experiments were dried in a vacuum oven at 40°C for 3 days before they were reswelled in DW, PG, PT and BB (at 28 °C below the LCST of the hydrogels). The swelling and reswelling ratios were obtained from equation (4.2a) and (4.2b), respectively. These are given by:

$$SR_1 = (M_t - M_o)/M_o \quad (4.2a)$$

$$SR_2 = (M_t - M_o)/M_o \quad (4.2b)$$

where M_t is the mass of the gel at time t and M_o is the mass of the dried gel at time, $t = 0$.

4.3.3 Swelling and Re-swelling Characteristics

P(NIPA)-based hydrogels were exposed to penetrant solvents (DW, PG/PT (anticancer drugs) or BB). These hydrogels were soaked and allowed to swell for 30 hours to equilibrium conditions ratios. As soon as the hydrogels were exposed to these solvents, they swelled until dynamic equilibrium conditions were reached at saturation. At equilibrium, the thermodynamically driven swelling force is counter-balanced by the retroactive force of the cross-linked structure, leading to an equilibrium state. This swollen state allows for the widening of the gaps between the crosslinks and mesh size. This facilitates the transfer of different solutes through the gels.

Most hydrogels used in biomedical applications have mesh sizes, ranging from 5-100 nm [25], in their swollen state. These size scales are much larger than most small molecular weight

drugs that are used in pharmaceutical formulations, and, therefore, diffusion of these drugs in the swollen matrices was not hindered. The transfer of the solute was controlled by the swelling of the gel. The small hydrodynamic radii of drug molecules then allow the drugs to diffuse through the gel network. Hence, knowledge of gels swelling characteristics enables the understanding of the network structure of the gels and their capacity to function as carriers for drug delivery.

P(NIPA)-based hydrogels swells very well in DW than in PG, BB and PT (Figs. 4.3a-d). Acrylamide and butyl-methacrylate, improves the swelling ratios [26,27,28] (Figure 4). However, the data clearly shows that the swelling ratios of PNIPA-based hydrogels and its copolymers were much higher than the re-swelling ratios. The swelling ratios were greater than the re-swelling ratios (Figs. 4.5-4.8). In comparison with the swelling ratios, the greatest re-swelling ratios were observed in distilled water. These were followed by the re-swelling ratios in BB, PG and PT. There was a very closed patterned of swelling and re-swelling ratios from hydrogels loaded with distilled water, while there exist a wider gap (difference) between swelling and re-swelling ratios of P(NIPA)-based hydrogels loaded with prodigiosin (Figs. 4.5-4.8). The swelling and re-swelling ratios of P(NIPA)-based hydrogels in BB, PG and PT were included for comparison.

4.3.4 Diffusion and Swelling Mechanisms

The fluid release exponent, n , and the diffusion constant, k , were determined from the following expression [29]:

$$\frac{m_t}{m_o} = 4 \left(\frac{D}{\pi \delta^2} \right) t^n = kt^n \quad (4.3)$$

where $\frac{m_t}{m_o}$ is the fluid or drug (prodigiosin/paclitaxelTM) release fraction at time, t , δ is the thickness of the gel and D is the diffusivity. Equation (4.3) suggests that the diffusion coefficient,

D, is independent of the drug concentration. The fractional release of drugs from the polymer is exponentially related to the release time. The release exponent, n, corresponds to the mechanism of drug release. Hence, n = 0.5, corresponds to Fickian diffusion, and the release rate is then dependent on $t^{-0.5}$.

When $n > 0.5$, Non-Fickian diffusional release was assumed and $n = 1.0$, corresponds to case-II transport. In the latter case, the release rate is independent of time (i.e. zero-order release rate kinetics [30]. Equation (4.3) has been applied to systems in which diffusion processes occur within polymeric networks [31]. Increasing porosity, due to copolymerization, leads to $n < 0.5$, since the diffusion mechanism is a combination of partial diffusion through a swollen matrix and partly through fluid/drug-filled pores. Therefore, these shift the release exponent toward smaller values [31]. The measured values of n, k and D are summarized in table 4.3. The constants k and n were obtained from the linear form of equation (4.3). This gives:

$$\ln \left(\frac{m_t}{m_o} \right) = \log k + n \log t \quad (4.4)$$

where k and n are obtained, respectively, from the intercepts and slopes of the plot of $\ln(m_t/m_o)$ versus $\ln t$ (s) (Figs. 4.4a-f). The diffusion coefficient, D, was obtained from:

$$D = \frac{k\pi\delta^2}{4} \quad (4.5)$$

The geometric factor, K, decreases as the release exponent, n, increases. Hence, the diffusivity also increases in response to increasing n. The value of n obtained for gel A suggests Fickian diffusion (i. e. $n = 0.5$), while the values obtained for gels B to D suggest that non-Fickian diffusion dominates (anomalous case, $n > 0.5$) [31].

4.3.5 Modeling of Fluid Release

The drug release from the loaded gels (at temperatures between 28° and 48°C), were modeled using the early-time approximation [32,33]. This model assumes Fickian diffusion. The release rate is then dependent on $t^{-0.5}$. This gives:

$$\frac{dM_t}{dt} = 2M_{total} \left(\frac{D}{\pi\delta^2 t} \right)^{1/2} \quad (4.6)$$

where the above constants have their usual meanings. The release rate is best described by a linear equation of the form:

$$\frac{d(M_t/M_{total})}{dt} = A(t)^{-\frac{1}{2}} \quad (4.7)$$

where $\log A$ corresponds to the intercept of the linear plot from $\log \frac{d(M_t/M_{total})}{dt}$ versus \log time (s), thus, $A = \log \left(\frac{D}{\pi\delta^2} \right)^{1/2}$ and the diffusivity, D , was obtained from equation 4.6. This corresponds to the diffusion coefficient (Figs. 5.4a-b) for gels (C to D). The activation energy for the gels was obtained from the Arrhenius equation. This gives:

$$D = D_o \exp\left(\frac{-E_a}{RT}\right) \quad (4.8)$$

where D is the diffusivity, D_o is the diffusion constant, R is the universal gas constant, T is temperature, E_a is the activation energy for each gel. The activation energies were obtained from the slopes of linear plots of $\ln D$ versus $T^{-1}(K^{-1})$ (Figs. 4.6a-b). The activation energies and LCSTs obtained for the gels are presented in table 4.3. This shows that activation energies and their LCSTs depended mostly on gel composition. The activation energy for the NIPA homopolymer was 122 kJ/mole, while those of the hydrophilic copolymers were between 163 kJ/mole (at 5 mol% of AM) and 291 kJ/mole (at 15 mol% of AM).

These above results are similar to reports from prior work [4], where 124 kJ/mole was reported for the homopolymer and 142.46 kJ/mole for the hydrophilic polymers at (5 mol % of acrylamide (AM)). Similarly, we obtained the LCST for the homopolymer to be at $32.9 \pm 0.01^\circ\text{C}$, while 32°C was reported earlier [30] and $34.6 \pm 0.01^\circ\text{C}$ in recent work [4].

With increasing concentration of acrylamide, the hydrophilic co-monomer resulted in an increase in the LCST from $36.3 \pm 0.01^\circ\text{C}$ at 5 mol % of AM to $41.7 \pm 0.01^\circ\text{C}$ at 15 mol % of AM. Furthermore, Oni et al. [4] reported that increasing concentration of acrylamide resulted in an increase in LCST from 39°C (at 5 mol % of AM), to about 48°C (at 15 mol % of AM). These results are in agreement with those from prior studies [4,11,34,35]. Increasing concentration of hydrophobic co-monomer (at 5 mol % of BMA) resulted in LCST of $28.95 \pm 0.01^\circ\text{C}$. This shows that the LCSTs depend on the composition of the polymer composite.

The release of bromophenol blue, as a function of time, is shown (Figs. 4.7a-b) for gels (A to D). The initial release of the dye was rapid. However, the subsequent release rates of the dye decreased significantly with increasing time. Furthermore, the more porous co-polymers containing the acrylamide co-monomer exhibited higher initial fluid release rates than the PNIPA homopolymer (Figs. 4.7a-b). However, the late time release profiles were similar in all the gels that were loaded with the anti-cancer drug, prodigiosin (Fig. 4.7c).

Table 4 summarizes the diffusion coefficients obtained for P(NIPA) and P(NIPA) co-polymers at different temperatures, while the diffusion coefficients obtained for hydrogels soaked with different fluids at 37°C are presented in Table 4.5. The diffusion coefficients obtained from P(NIPA)-based hydrogels and PNIPA-based copolymers soaked with prodigiosin were $2.1 \times 10^{-12} \text{ m}^2/\text{s}$ and $4.8 \times 10^{-6} \text{ m}^2/\text{s}$, respectively. Similarly, the diffusivity values for P(NIPA)-based gel soaked with BB were $2.0 \times 10^{-17} \text{ m}^2/\text{s}$ and $8.0 \times 10^{-9} \text{ m}^2/\text{s}$, respectively. The diffusivities of fluids released at 37°C , in the copolymer containing 5 mol% AM, were higher

than those of fluids released from the other compositions (10 mol%, 15 mol% AM). This may be due to its LCST (noted at 36°C), which causes it to collapse (phase transformation) by shrinking more quickly than the other compositions (Fig. 4.8).

The above results have shown great improvement and are consistent with prior work [4,16,36]. Furthermore, from recent work [4,5], the diffusion coefficient obtained for Rhodamine dye release from P(NIPA)-based hydrogels, was estimated to be $1.21 \times 10^{-9} \text{ m}^2/\text{s}$ and $6.33 \times 10^{-10} \text{ m}^2/\text{s}$, for copolymers with increasing amounts of acrylamide (i.e. from 5 mol % to 10 mol %). Finally, the diffusivities of paclitaxelTM were found to be $2.38 \times 10^{-16} \text{ m}^2/\text{s}$ and $6.33 \times 10^{-12} \text{ m}^2/\text{s}$ in the P(NIPA) homopolymer and hydrophilic copolymers (with 5 mol % to 10 mol % of BMA), respectively.

4.3.6 Effect of Drug Diffusion across Channel Lengths

Finally in this section, it is important to discuss the effects of drug diffusion across the channel lengths within the PDMS capsules (Figs. 4.1d-e). A plot of L (m) versus \sqrt{t} (s)^{1/2} gives a straight line with an R^2 of 0.98 (Fig. 4.3a). The slope of this line gives the diffusion coefficient of BB at 43°C to be $1.43 \times 10^{-8} \text{ m}^2/\text{s}$. This is higher than the diffusion coefficient of $4.51 \times 10^{-9} \text{ m}^2/\text{s}$ reported previously by Oni et al. [4], for diffusion of rhodamine dye at 37°C.

From equation 4.1, the effective diffusion coefficient, D , across a different channel length, L , can be obtained from $D = L^2/t$, where t is the duration of flow. A plot of L^2 versus t is presented (Fig. 4.3b). This shows the expected linear dependence of L^2 on t , and a slope corresponding to the effective diffusivity of $2.0 \times 10^{-8} \text{ m}^2/\text{s}$ with an $r^2 = 0.97$. Hence, shorter channel lengths facilitated the flow of fluid/drug molecules through the device into the treatment area or vice

versa. Moreover, the shorter channel lengths also require lower pressures to push the drugs through the device into the tumor tissue.

Hence, the current work suggests that flow across the channels (in the PDMS packaging) is well described by a diffusion process, for the range of channel lengths (1.5-7.5 mm) that was used in this study. Similar results have also been reported by Oni et al. [4] for drug elution from PDMS packages. However, it is important to note that such behavior applies to relatively large channels, such as the ones studied in the current work and prior work by Oni et al. [4]. Further work is clearly needed to study possible microfluidic phenomena in smaller channels with micro-scale dimensions.

It is also clear from the current study that the final release rate of drugs into the tumor tissue can be managed by the diffusion across the channels. This is particularly important for the control of initial burst effects during the early stages of drug/fluid from the P(NIPA)-based gels. Such burst effects can be moderated by the flow of drugs across the channel lengths. For example, diffusion across the channel lengths examined in this study resulted in about ~ 8 days of drug diffusion. This is in contrast to ~ 12 hours of direct delivery from encapsulated P(NIPA)-based gels.

4.4 Implications

The studies suggest that, temperature-responsive PNIPA hydrogels encapsulated with a biocompatible polymer (PDMS) can be used for the controlled delivery of prodigiosin or paclitaxelTM cancer drugs to targeted tumors or cancer cells [4,37]. The diffusion times and rates are in the range that is relevant to cancer treatment.

This work demonstrates the potential for the controlled release of prodigiosin (PG) as an anticancer drug. However, *in-vitro* and *in-vivo* experiments are needed to determine the effects of the localized release of prodigiosin on the viability of cancer cells or tissue. The effects of heat shock proteins (in the hyperthermic regime) should also be studied along with the potential for engineering synergy via the controlled release of prodigiosin at hyperthermic temperatures.

In any case, the bacterial synthesis of prodigiosin could greatly reduce the cost of cancer drugs (compared to conventionally synthesized drugs such as paclitaxelTM), while the localized delivery of the cancer drugs could greatly reduce the amount of drugs that are needed for therapeutic cancer treatments. Hence, it is possible to envisage implantable cancer treatment devices, in which prodigiosin produced by bacteria is released at temperatures at which cancer cell viability is also reduced by localized hyperthermia.

The heating of the above devices could be achieved by the use of Joule heating using wound copper wires that are embedded in the PDMS structures [4,5]. The heating could also be controlled with Proportional Integral Differential (PID) controller and *in-situ* sensors that could be used to regulate the local temperatures in the surrounding tissue to levels between 41 and 44°C that are required for typical hyperthermic treatment. These could be achieved using hyperthermic treatment cycles that include heating between 41 and 44°C for ~ 15-30 minutes [38-41], followed by relaxation for duration of ~ 24 hours to manage the effects of heat shock proteins.

The potential device could be used for treating solid tumors (between Stage I and Stage III). Since the treatment is localized, lower drug dosages and higher efficacy are possible [42]. The implantation of the device could be done, after the removal of a tumor for the device to deliver cancer drugs locally to the affected region. The device could then be removed after achieving the desired drug delivery therapy. Alternatively, the device could be left in the body, since PDMS is

biocompatible (U. S. FDA approved) and poses no toxicity threat in long term applications in humans [20].

Further work is clearly needed to develop the local temperature and drug sensors as well as the control systems that are needed to control the delivery of heat and drugs in potential future devices. The system will need to compensate for temperature effects on the drug delivery rates from the PNIPA-based gels and the channels. These are relatively weak for temperatures close to the human body temperature ($\sim 37^{\circ}\text{C}$) in the range between 37 and 39°C , and stronger in the hyperthermic temperature range between 41 and 45°C . Future systems will, therefore, need controllers and local sensors for the management of local drug release and heat diffusion. These are clearly some of the challenges for future work.

4.5 Conclusions

The diffusion kinetics of PNIPA gels has been studied at temperatures of 28°C to 48°C that are relevant to the treatment of cancer via localized heating (hyperthamia) and drug delivery. The drug release rates were governed by the earlier time approximation, while the diffusion rates of drug molecules were strongly influenced by temperature. Fickian diffusion behavior is observed in gel A, while Non-Fickian diffusion dominates the behavior of gels B-D [43]. Furthermore, since PDMS is biocompatible (US FDA), it is recommended as a packaging material for controlled drug release [4].

The porous structures of the PNIPA gel (with mesh size of about $5\text{-}100$ nm) enhances the controlled release of prodigiosin and paclitaxelTM drugs. Furthermore, the gel microstructure does not hinder the flow of drug molecules because of their small hydrodynamic radii, as compared to the polymer mesh size. Since the delivery of the prodigiosin and paclitaxel drugs is localized by the use of the device, the total quantity of drug that is needed for therapeutic

treatment should be much less than that required for bulk systematic chemotherapy. Hence, the potential side effects of localized cancer drug delivery will be reduced by the application of the proposed device.

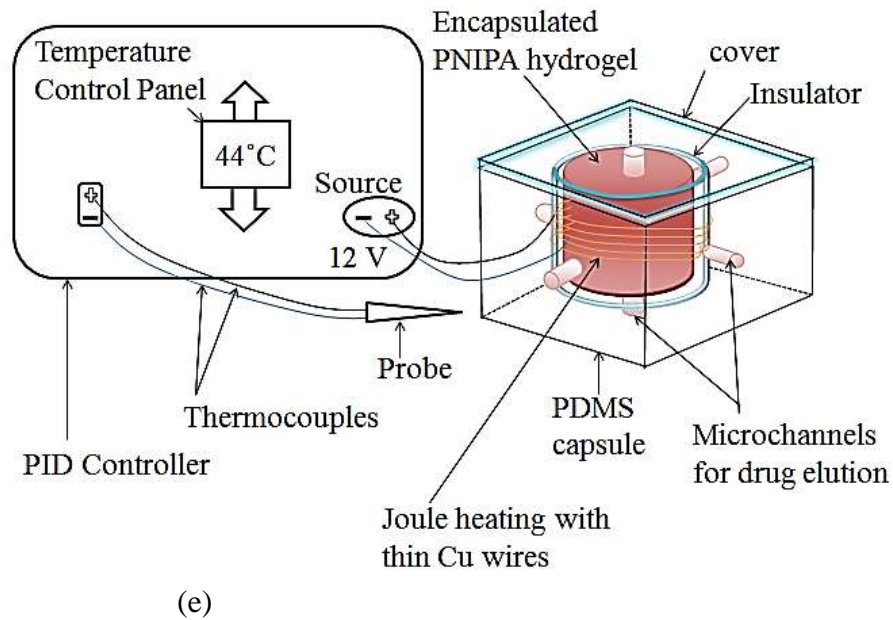
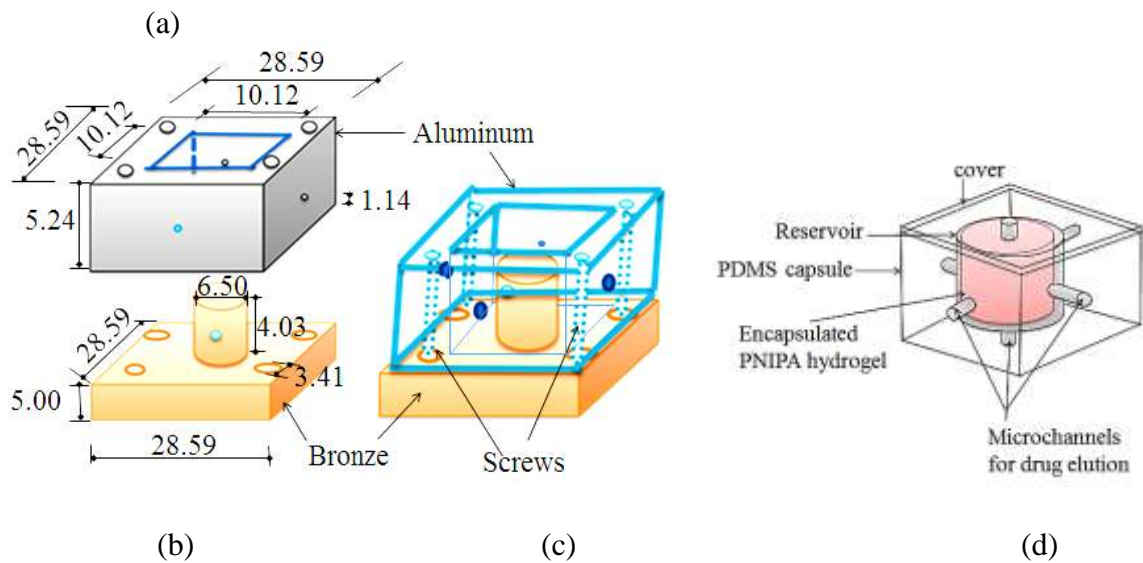
The effective diffusion coefficient, D , across a different channel length, L , was obtained from $D = L^2/t$, where t is the duration of flow. The linear dependence of L^2 and t , gave a slope corresponding to the effective diffusivity of $2.0 \times 10^{-8} \text{ m}^2/\text{s}$ corresponding to an R^2 of 0.97. Since lower pressures are required to drive fluid/drug flow across devices with shorter channel lengths, shorter channel lengths ease the flows of fluid/drug molecules across the device. However, channel lengths can be used to manage the initial burst release of fluid/drug, since the delivery of drugs from the channels (into the tumor tissue) will then be controlled largely by diffusion across the channels. A balanced approach is, therefore, required for the design of optimal channel lengths.

4.6 Bibliography

- [1] B. Hildebrandt and P. Wust in: W. P. Ceelen (Ed). Peritoneal Carcinomatosis: A Multidisciplinary Approach, Springer, New York, (2007) 185.
- [2] A. Afrassiabi, A. S. Hoffman and L. A. Cadwell. Effect of Temperature on the Release Rate of Biomolecules from Thermally Reversible Hydrogel. *Membrane Sci.* 33 (1987) 191-200.
- [3] S. Allan, A. S. Hoffman and J. Heller. *An Introduction to Materials in Medicine*, 2nd Edition. Elsevier Inc. (2004) 628-637.
- [4] Y. Oni, C. Theriault, A. V. Hoek and W. O. Soboyejo. Effects of Temperature on Diffusion from P(NIPA)-Based Gels in a BioMEMS Device for Localized Chemotherapy and Hyperthermia. *Mater. Sci. and Eng. C.* 31 (2011) 67-76.
- [5] Y. Oni and W. O. Soboyejo. Swelling and Diffusion of PNIPA-Based Gels for Localized Chemotherapy and Hyperthermia. *Mater. Sci. and Eng. C.* 32 (2012) 24-30.
- [6] P. Boyle and B. Levin. *The World Cancer Report*. World Health Organization, International Agency for Research on Cancer (IARC) Press, Lyon. (2008) 112.
- [7] J. Mackay and G. A. Mensah. *The Atlas Of Disease and Stroke*, WHO In Collaboration with the Centers for Disease Control and Prevention (2004). ISBN-13 97892415.

- [9] D. Needhama and W. M. Dewhirst. The Development and Testing of a New Temperature-Sensitive Drug Delivery System for the Treatment of Solid Tumors. *Advanced Drug Delivery Reviews*. 53 (2001) 285-305.
- [10] M. C. Perry. Approach to the Patient with Cancer. In: L. Goldman and A. I. Schafer, Eds. *Cecil Medicine*, 24th Ed. Philadelphia, Pa: Saunders Elsevier. (2011) chap 182.
- [8] D. Gutierrez. *Cancer Facts and Figures*. 2nd Edition. America Cancer Society. (2008) 50.
- [11] G. Fu and W. O. Soboyejo. Swelling and Diffusion Characteristics of Modified Poly(N-Isopropyl acrylamide) Hydrogels. *Mater. Sci. and Eng. C*. 30 (2010) 8-13.
- [12] A. Chilkoti, M. R. Dreher, D. E. Meyer and D. Raucher. Targeted Drug Delivery by Thermally Responsive Polymers. *Adv. Drug Delivery Rev.* 54 (2002) 613-630.
- [13] A. Chilkoti, M. W. Dewhirst, G. A. Kong, D. E. Meyer and B. C. Shin. Drug Targeting Using Thermally Responsive Polymers and Local Hyperthermia. *Control Release*. 74 (2001) 213- 224.
- [14] C. Theriault, C. Barkey, R. Chandrasekar, E. Paetzell and Y. Oni, W. O. Soboyejo. An In-Vitro Study of the Effects of Temperature on Breast Cancer Cells: Experiments and Models. *Mat. Sci. and Eng. C*. 32 (8) (2012) 2242-2249.
- [15] H. Yaoming, G. Haiyan and L. Shuping. Haematoporphyrin Based Photodynamic Therapy Combined with Hyperthermia Provided Effective Therapeutic Vaccine Effect against Colon Cancer Growth in Mice, *Int. J. Med. Sci.* 9 (2012) 627-633.
- [16] T. Tanaka. *Gels*. US National Library of Medicine, National Institutes of Health. *Sci. Am.* 244 (1) (1981) 124-138.
- [17] H. Vihola, A. Laukkanen, L. Valtola, H. Tenhu, J. Hirvonen. Cytotoxicity of thermosensitive polymers poly(N-isopropyl acrylamide), poly(N-vinylcaprolactam) and amphiphilically modified poly(N-vinylcaprolactam). *Biomaterials* 26 (2005) 3055-3064.
- [18] P-J. Wipff, H. Majd, C. Acharya, L. Buscemi, J-J. Meister, B. Hinz. The covalent attachment of adhesion molecules to silicone membranes for cell stretching applications *Biomaterials*. 30 (2009) 1781-1789.
- [19] S. A. Visser, R. W. Hergenrother, S. L. Cooper. *Polymers Biomaterials Science: An introduction to Materials in Medicine*. San Diego, Calif: Academic Press. (1996) 50-60.
- [20] Dow Corning Healthcare Product Selection Guide. *Advancing Healthcare through Material Innovations*. U.S. FDA-Registered (CFN 1816403). Form No. 51-988E-01(©2001, 2002, 2003, 2007, 2013 Dow Corning Corporation) 2-19.
- [21] G-H. Hsiue, S-H. Hsu, C-C. Yang, S-H. Lee, I-K. Yang. Preparation of controlled release ophthalmic drops, for glaucoma therapy using thermosensitive poly-N-isopropyl acrylamide. *Biomaterials* 23 (2002) 457-462.
- [22] G-H. Hsiue, R-W. Chang, C-H. Wang, S-H. Lee. Development of in situ thermosensitive drug vehicles for glaucoma therapy. *Biomaterials* 24 (2003) 2423-2430.
- [23] Y. Matsumaru, A. Hyodo, T. Nose, S. Ito, T. Hirano, S. Ohashi. Application of thermosensitive polymers as a new embolic material for intravascular neurosurgery. *J Biomater Sci. Polym Ed.* 7 (1996) 795-804.
- [24] G. Hegyi, G. P. Szigeti and A. Szász. *Hyperthermia versus Oncothermia: Cellular Effects in Complementary Cancer Therapy*. Hindawi Publishing Corporation. Review Article. (2013) 2-12.
- [25] Paul J. Flory, Dependence of elastic properties of vulcanized rubber on the degree of cross linking. *N.R.M.C.S.* (1949) 225-245.
- [26] D. C. Mathers and D. Loncar. *Updated Projections of Global Mortality and Burden of Disease, 2002-2030; Data Sources, Methods and Results*. World Health Organization. (2005) 6.

- [27] N. David and W. D. Mark. The Development and Testing of a New Temperature-sensitive Drug Delivery System for the Treatment of Solid Tumors. *Advanced Drug Delivery Reviews*, 53 (2001) 285-305.
- [28] K. D. Kamble, V. D. Hiwarale. Prodigiosin Production from *Serratia Marcescens* Strains Obtained from Farm Soil. *Int. J. Environmental Sci.* 3(1) (2012) 631-638.
- [29] J. Siepmanna and N. A. Peppas. Modelling of Drug Release from Delivery Systems Based on Hydroxypropyl Methylcellulose (HPMC). *Advanced Drug Delivery Rev.* 48 (2001) 139-157.
- [30] T. T. Wang, T. K. Kwei and H. L. Frisch. Diffusion in Glassy Polymer, III. *Poly. Sci. A27* (1968) 2019-2028.
- [31] A. N. Peppas. Analysis of Fickian and Non-Fickian Drug Release from Polymers. *Pharm. Acta Helv.* 60 (4) (1985) 110-111.
- [32] R. W. Baker and H. K. Lonsdale, in: Tanquary A. C. and Lacey R. E. *Controlled Release of Biologically Active Agents*. Plenum Publishers, New York, 1974, 15-71.
- [33] J. Heller, A. S. Hoffman, B. D. Ratner in, F. J. Schoen and J. E. Lemonsm (Ed). *Biomaterials Sci.* Academic Press, New York. (2004) 629-630.
- [34] H. G. Schild. Poly(N-isopropyl acrylamide): Experiment, Theory and Application. *Progress in Polymer Sci.* 17 (2) (1992) 163-249.
- [35] N. A. Peppas. *Other Biomedical Applications of Hydrogels, Hydrogels in Medicine and Pharmacy. Properties and Applications*, CRC Press, Boca Raton, FL. 3 (1987) 177-186.
- [36] E. S. Matsuo and T. Tanaka. Patterns in Shrinking Gels, *Letters to Nature.* 358 (1992) 482-485
- [37] M. C. Belanger and Y. Marois. Hemocompatibility, Biocompatibility, Inflammatory and In Vivo Studies of Primary Reference Materials Low-Density Polyethylene and Polydimethylsiloxane: A Review. *Biomed. Mater. Res.* 58 (2001) 467-477.
- [38] G. V. Dongen, G. Zoutewelle, J. V. Rijn, et al. Cell Killing and Sensitization to Heat Shock by Hypothermic Incubation of Asynchronous and Synchronized Mouse Neuroblastoma Cell. *Cancer Res.* 45 (1985) 4132-4137.
- [39] E. Kobayashi, M. Yamagishi, T. Kamamoto, et al. Cell Cycle-dependent Heat Sensitization of Murine Granulocyte-Macrophage Progenitor Cells in Regenerating Marrow. *Cancer Res.* 45 (1985) 1459-1463.
- [40] M. R. Dreher, W. Liu, C. R. Michelich, M. W. Dewhirst and A. Chilkoti. Thermal Cycling Enhances the Accumulation of a Temperature-Sensitive Biopolymer in Solid Tumors. *Cancer Res* 67 (2007) 4418-4424.
- [41] G. L. Bidwell III, E. Perkins, Jos Hughes, M. Khan, J. R. James, D. Raucher. Thermally Targeted Delivery of a c-Myc Inhibitory Polypeptide Inhibits Tumor Progression and Extends Survival in a Rat Glioma Model. *PLoS ONE* 8(1) (2013) e55104, 1-12.
- [42] M. A. Moses, H. Brem and R. Langer. Novel Delivery Systems in Cancer Chemotherapy. *Science and Medicine.* 9 (5) (2003) 264.
- [43] M. K. Yoo, Y. K. Sung, Y. M. Lee and C. S. Cho. Effect of Polyelectrolyte on the Lower Critical Solution Temperature of Poly(N-Isopropyl Acrylamide) in the Poly(NIPAAM-co-Acrylic Acid) Hydrogel. *Polymer* 41(15) (2000) 5713-5719.



All the measurements were in mm

Figure 4.1: Schematic Diagrams of Mold and PDMS Components; (a) Aluminium slab; (b) Brass slab with Central Cylindrical rod; (c) Fabricated Mold; (d) Encapsulated Biomedical Device with Microchannels for Drug Elution; and (e) Hyperthermia System with a PID Temperature Controller (Fabricated by Dr. Yusuf Oni).

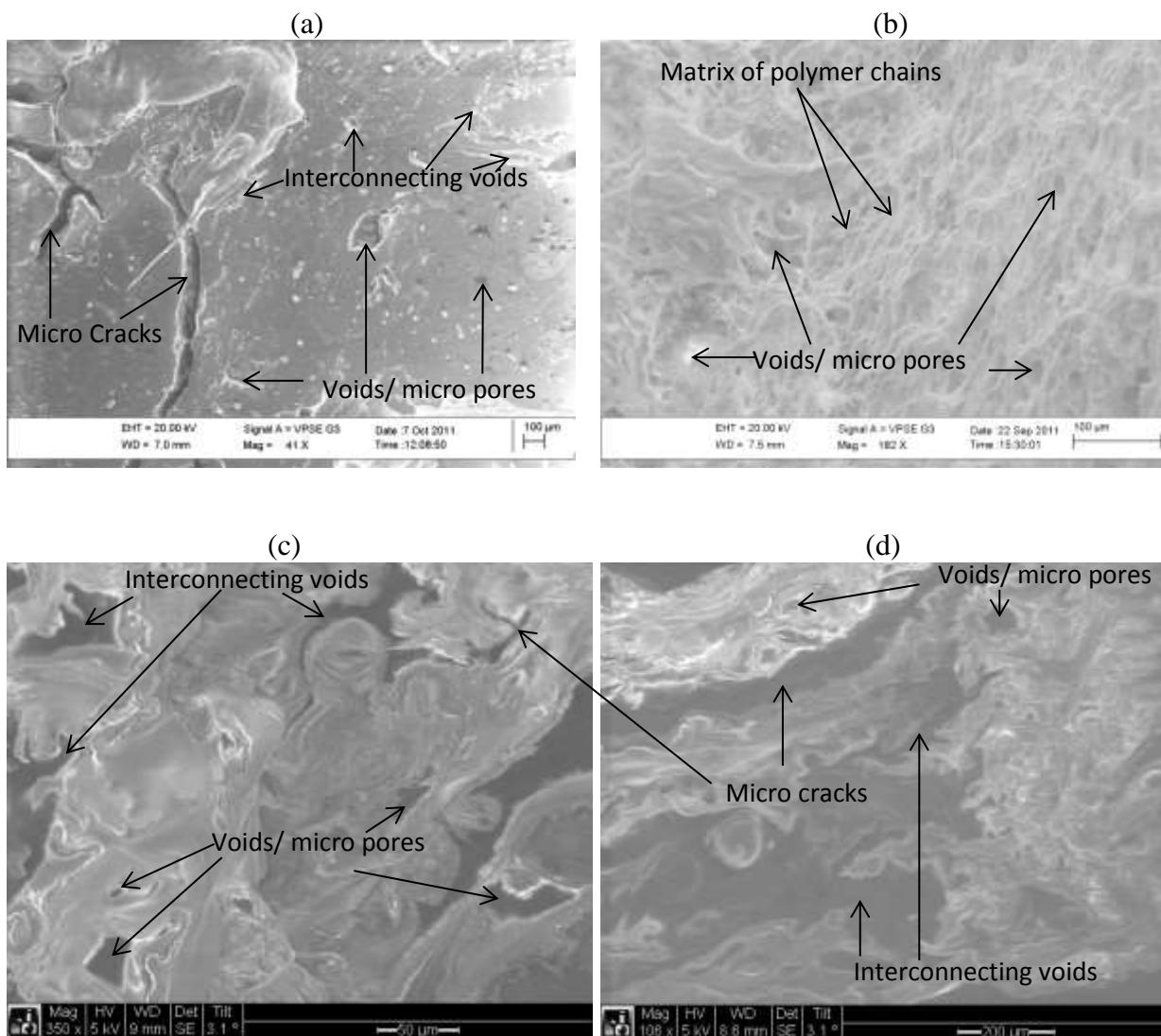
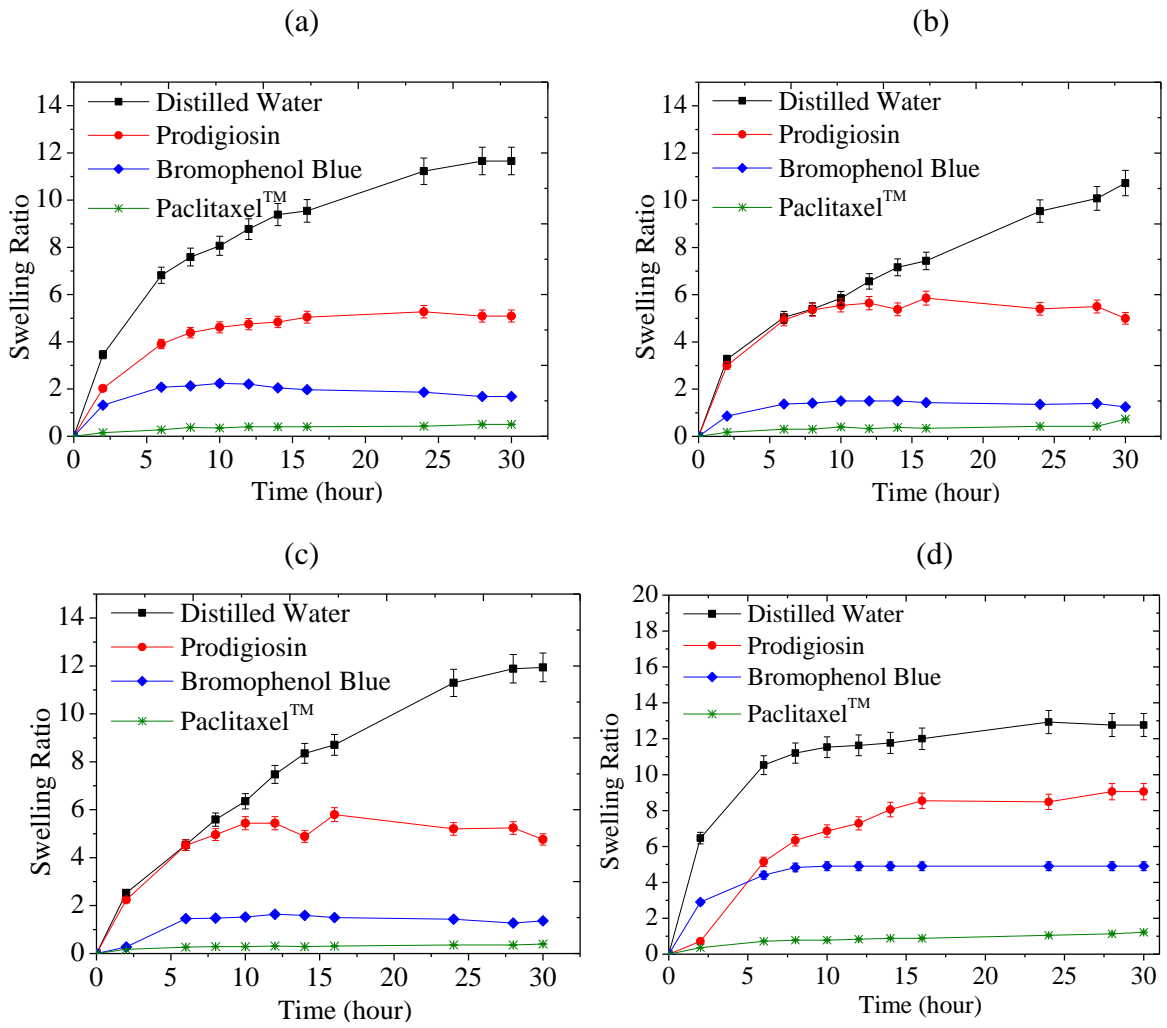


Figure 4.2: SEM Image of P(NIPA)-Based Hydrogels: (a) Homopolymer and (b) P(NIPA)-Composite (With 15 mol% of acrylamide (AM)), (c) P(NIPA)-Copolymer (5 mol% of AM and 5 mol% of BMA) and (d) P(NIPA)-Copolymer (5 mol% of AM and 10 mol% of MA).



(a) Homopolymer (100 mol% of PNIPA and (b) 95 mol% of PNIPA-5 mol% of Acrylamide; (c) 90 mol% of PNIPA-10 mol% of Acrylamide; and (d) PNIPA with 15 mol% of Acrylamide.

Figure 4.3: Swelling Ratio of P(NIPA)-Based Hydrogels and P(NIPA)-Based Copolymers in Different Fluids at 28°C. Error Bars Show 95% Confidence Interval of the Mean.

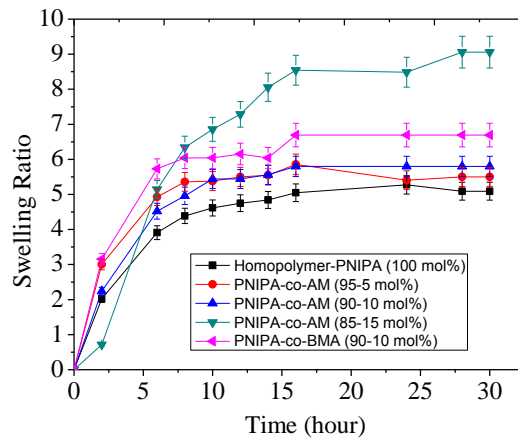


Figure 4.4: Swelling Ratios of PNIPA-based Hydrogels in Prodigiosin at 28°C. Error Bars Show 95% Confidence Interval of the Mean.

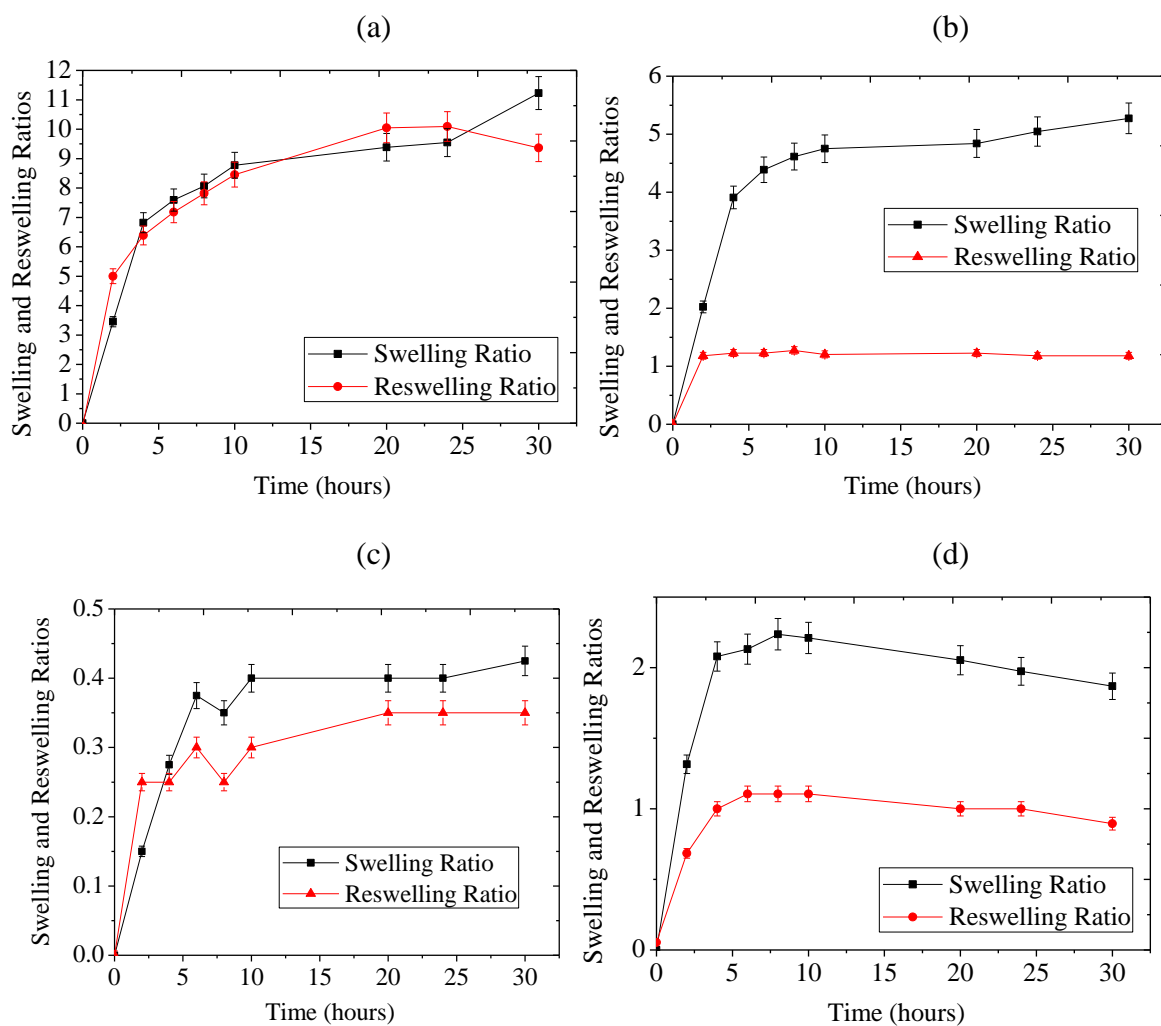
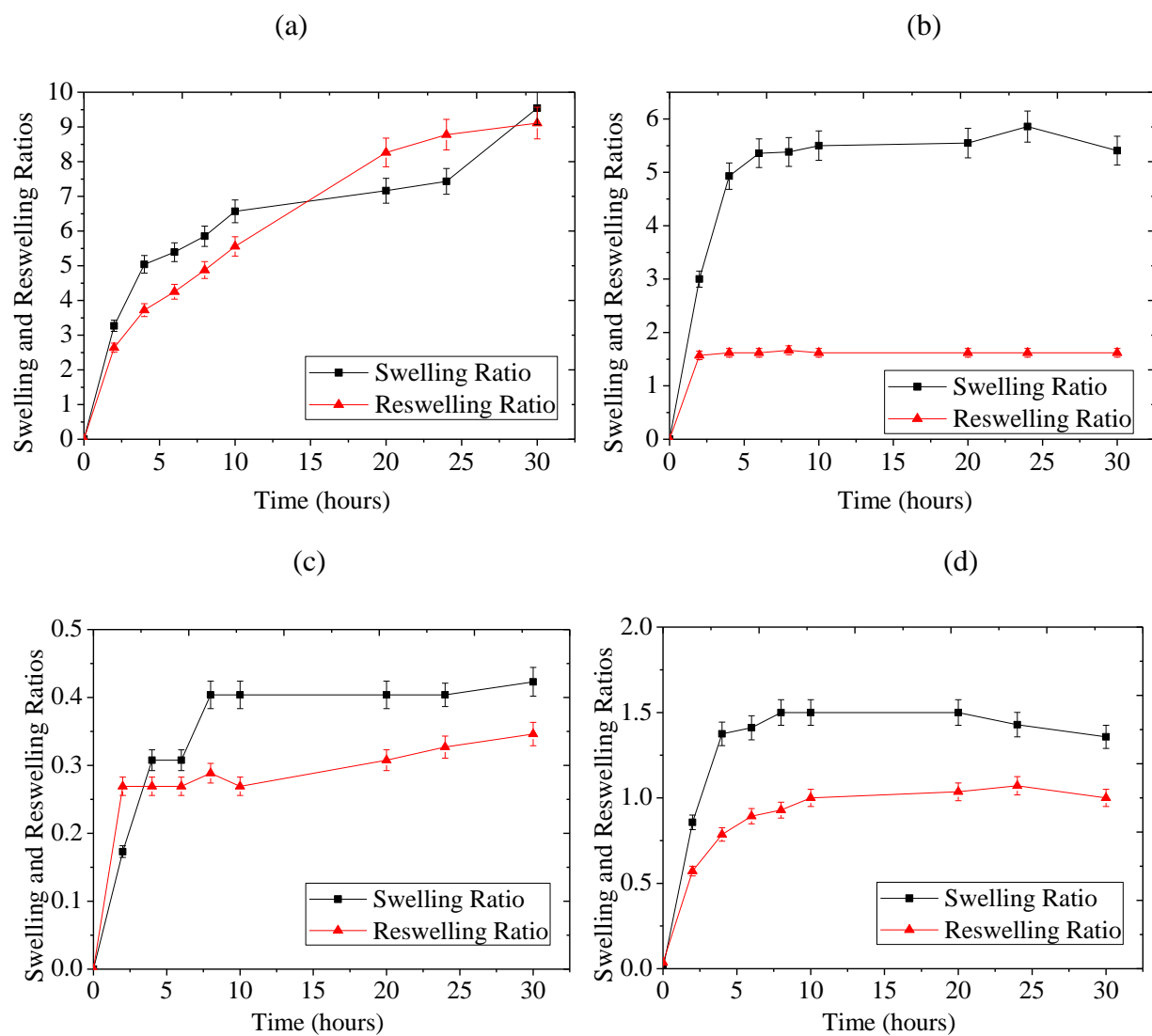
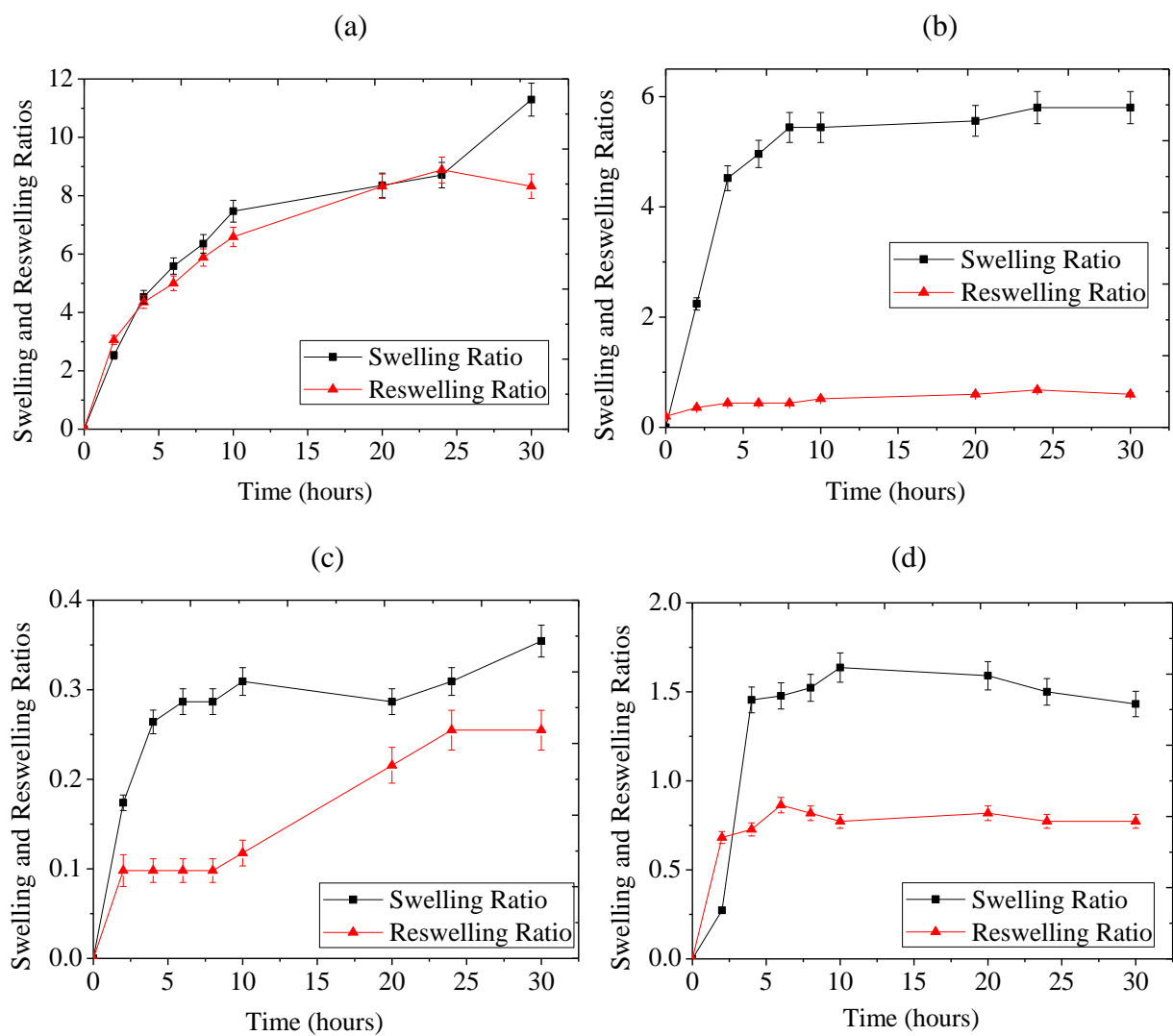


Figure 4.5: Swelling and Reswelling Ratios of P(NIPA)-based Homopolymer in aqueous medium: (a) Distilled Water; (b) Prodigiosin; (c) PaclitaxelTM and (d) Bromophenol Blue. Error Bars Show 95% Confidence Interval of the Mean.



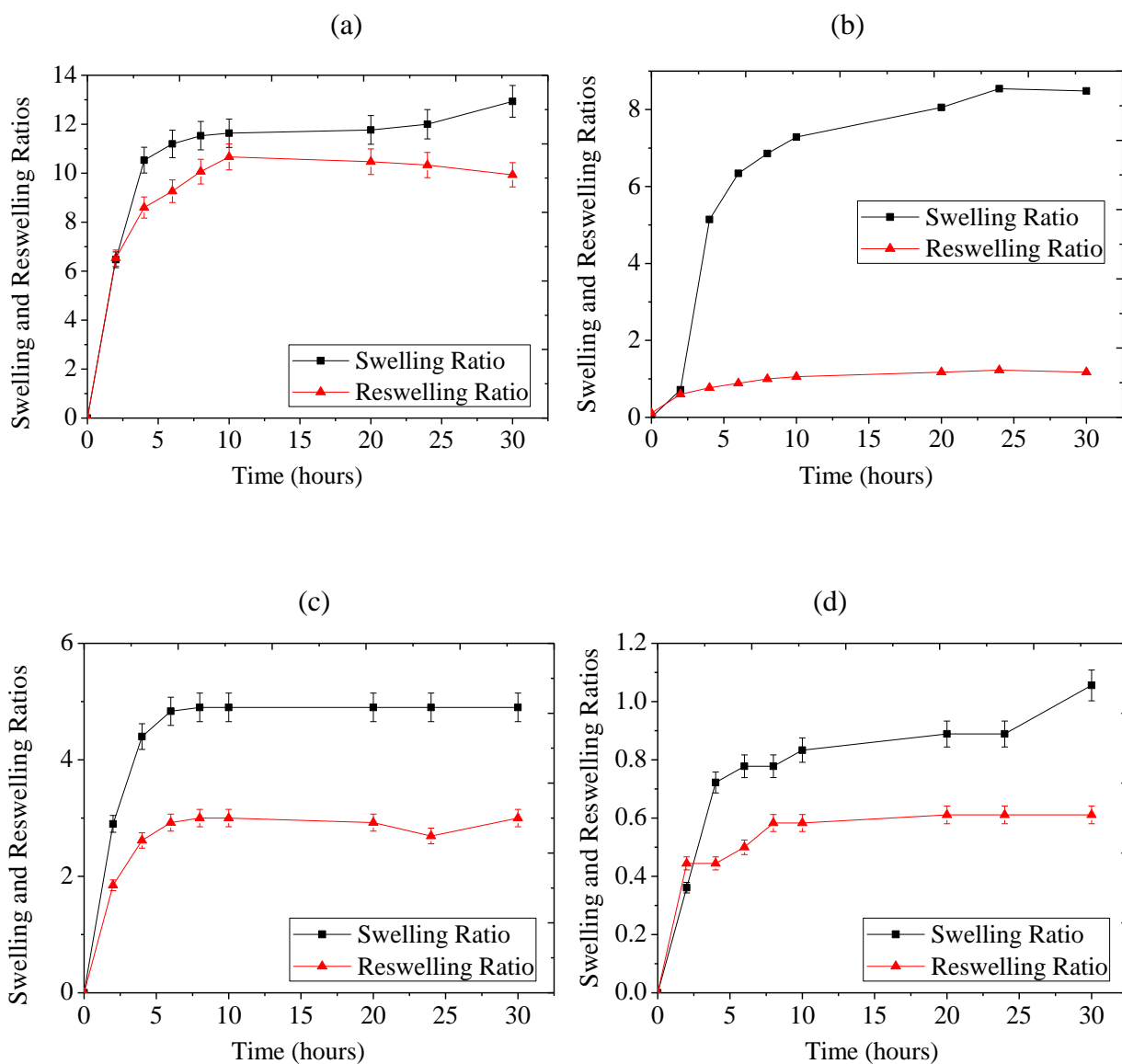
Error Bars Show 95% Confidence Interval of the Mean

Figure 4.6: Swelling and Reswelling Ratios of P(NIPA)-based copolymer (95 mol% of P(NIPA)-co-5 mol% of AM) in aqueous medium:(a) Distilled Water; (b) Prodigiosin; (c) PaclitaxelTM and (d) Bromophenol Blue.



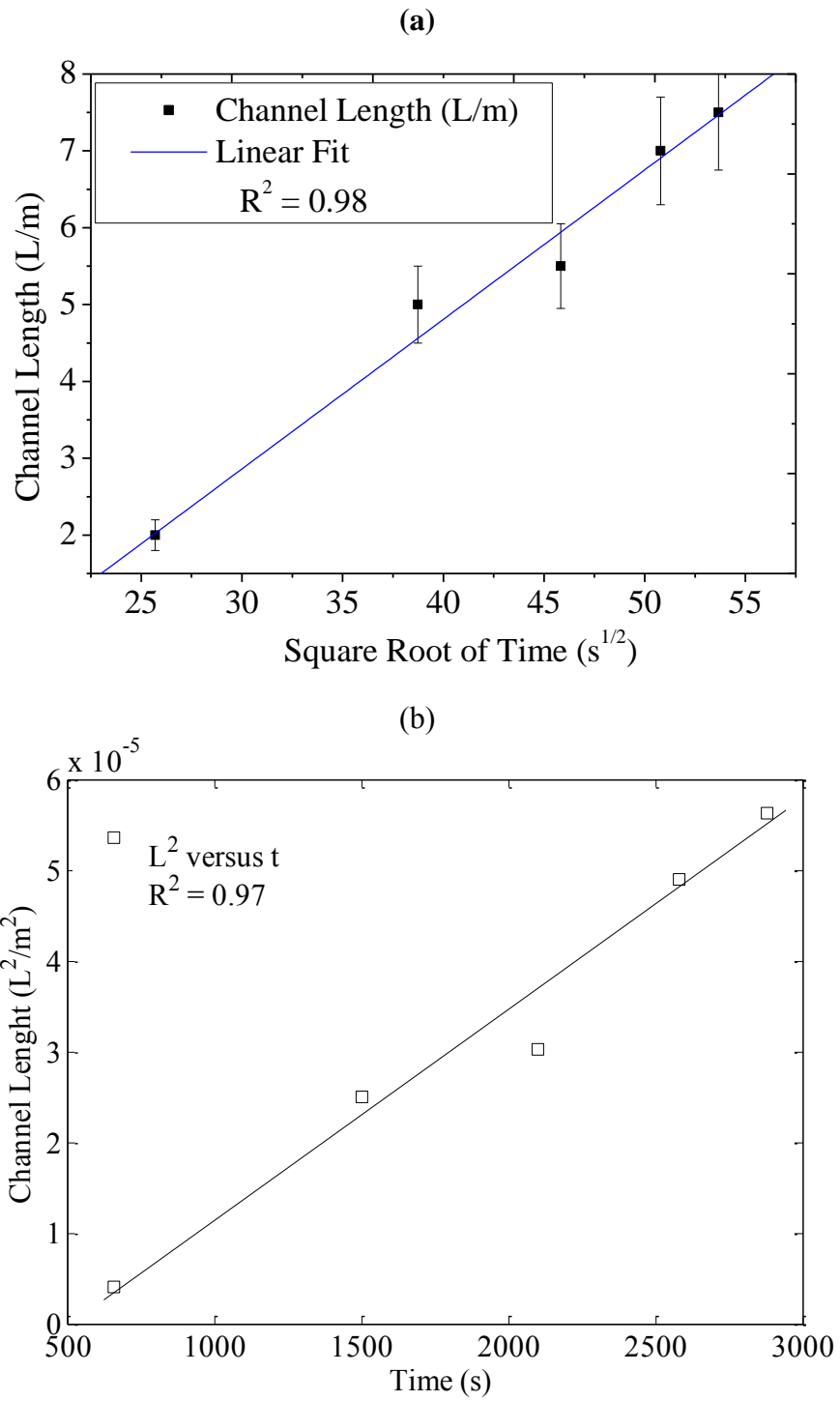
Error Bars Show 95% Confidence Interval of the Mean

Figure 4.7: Swelling and Reswelling Ratios of P(NIPA)-based copolymer P(NIPA-co-10 mol% of AM) in aqueous medium: (a) Distilled Water; (b) Prodigiosin; (c) PaclitaxelTM and (d) Bromophenol Blue.



Error Bars Show 95% Confidence Interval of the Mean

Figure 4.8: Swelling and Reswelling Ratios of P(NIPA)-based copolymer ((85 mol% of P(NIPA-co-15 mol% of AM)) in aqueous medium: (a) Distilled Water; (b) Prodigiosin; (c) PaclitaxelTM and (d) Bromophenol Blue.



Error Bars Show 95% Confidence Interval of the Mean.

Figure 4.9: Plots: (a) Fluid Flow Via Channel Length (cm) Against Travel Time at 43°C; (b) Estimation of the effective diffusivity from L^2 versus Time.

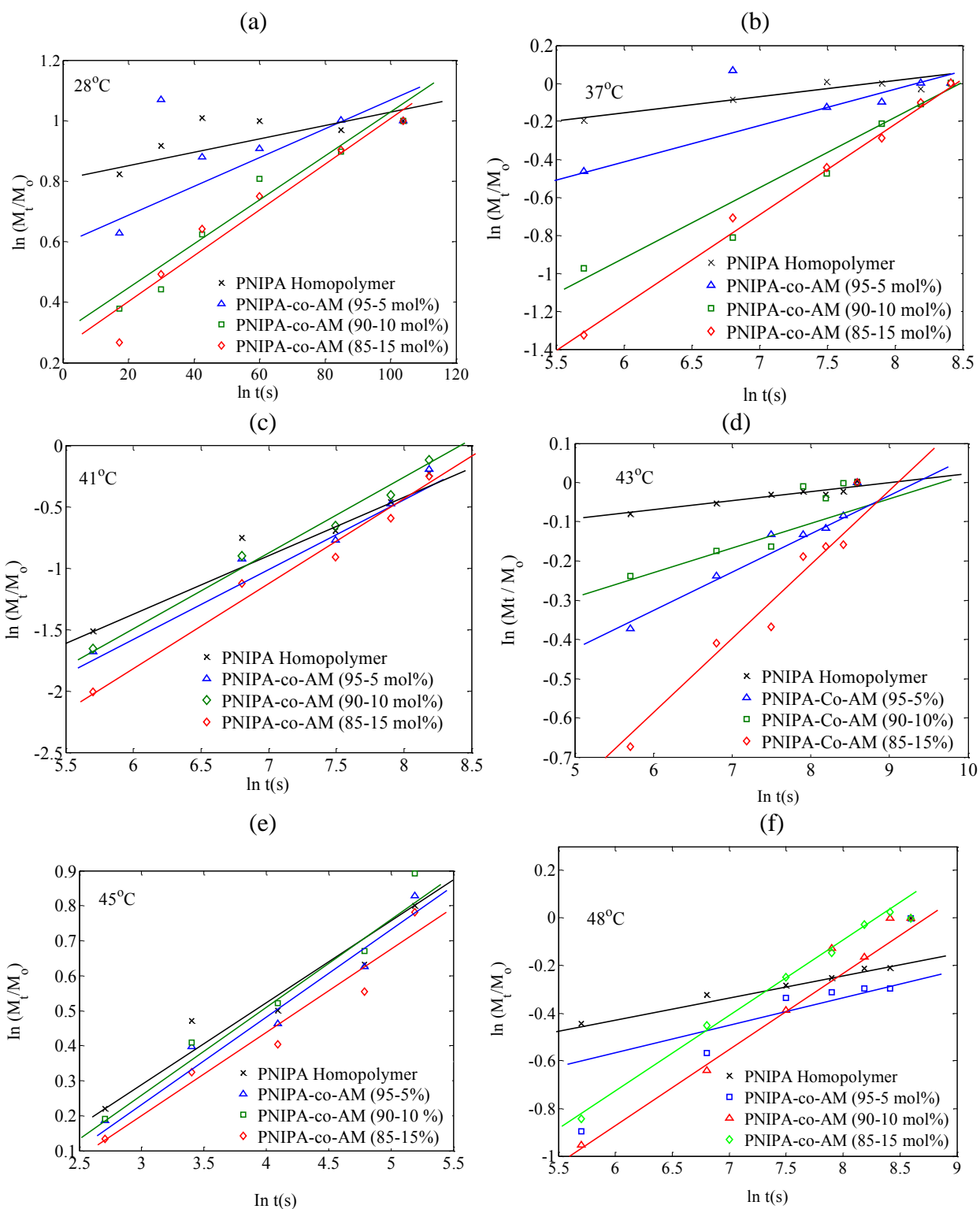
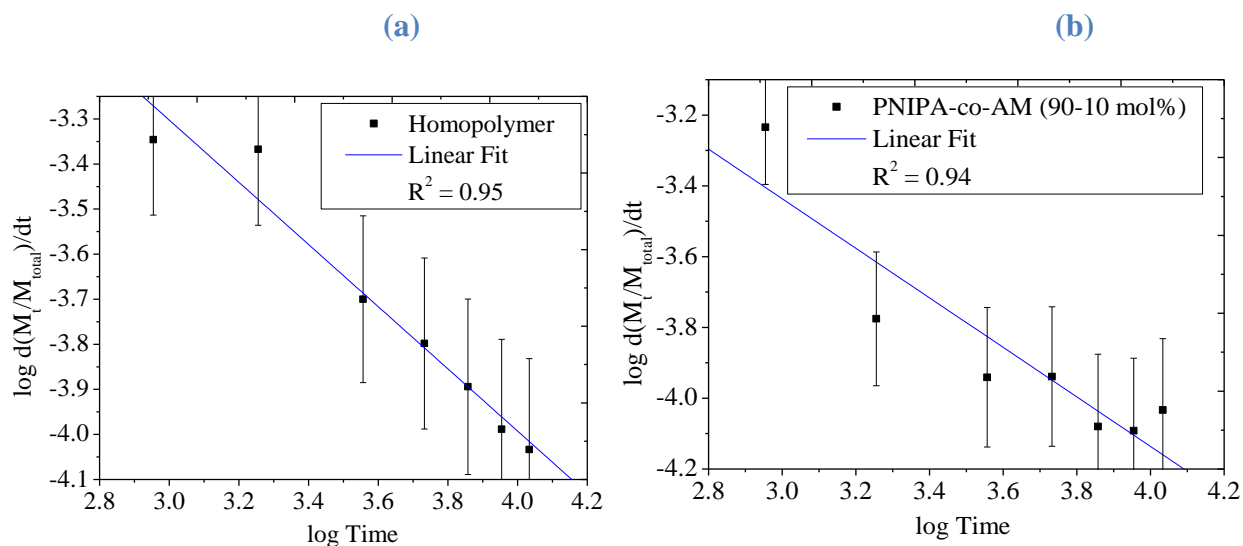
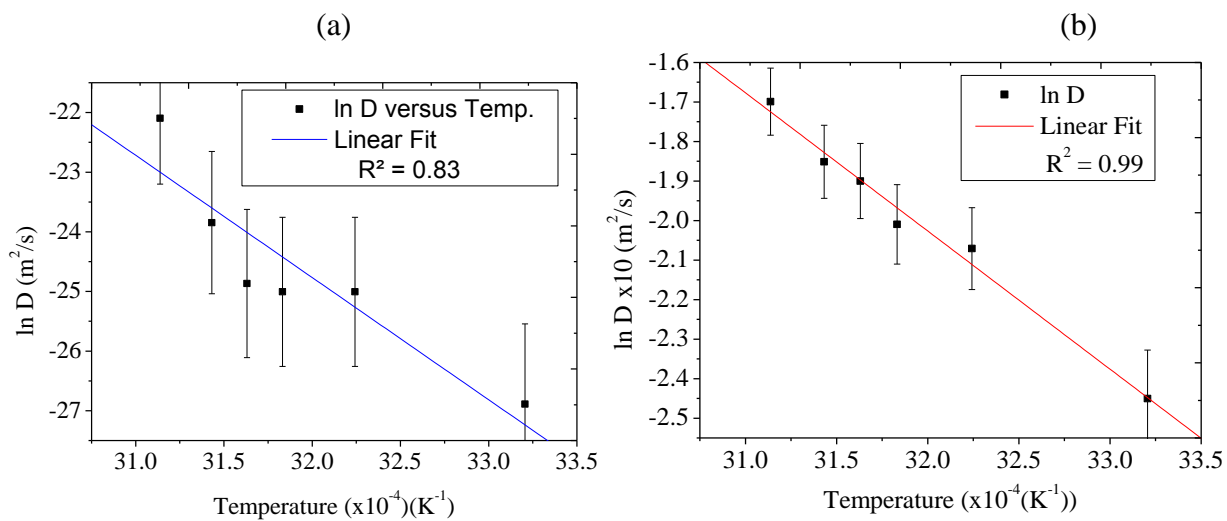


Figure 4.10: Diffusion Fits for Bromophenol Blue Dye Obtained From; Plots of $\ln(mt/m_0)$ Versus $\ln(t)$ (s) for P(NIPA)-Based gels Hydrogels at 28°C, 37°C, 41°C, 43°C, 45°C and 48°C.



Error Bars Show 95% Confidence Interval of the Mean.

Figure 4.11: Release Rates of Bromophenol Blue at 41°C: (a) Homopolymer; (b) Hydrophilic Copolymer (Containing 15 mol% of Acrylamide).



Error Bars Show 95% Confidence Interval of the Mean.

Figure 4.12: Plots of $\ln D$ versus T^{-1} (K^{-1}): (a) Homopolymer, and (b) Co-polymer (With 15 mol % of AM).

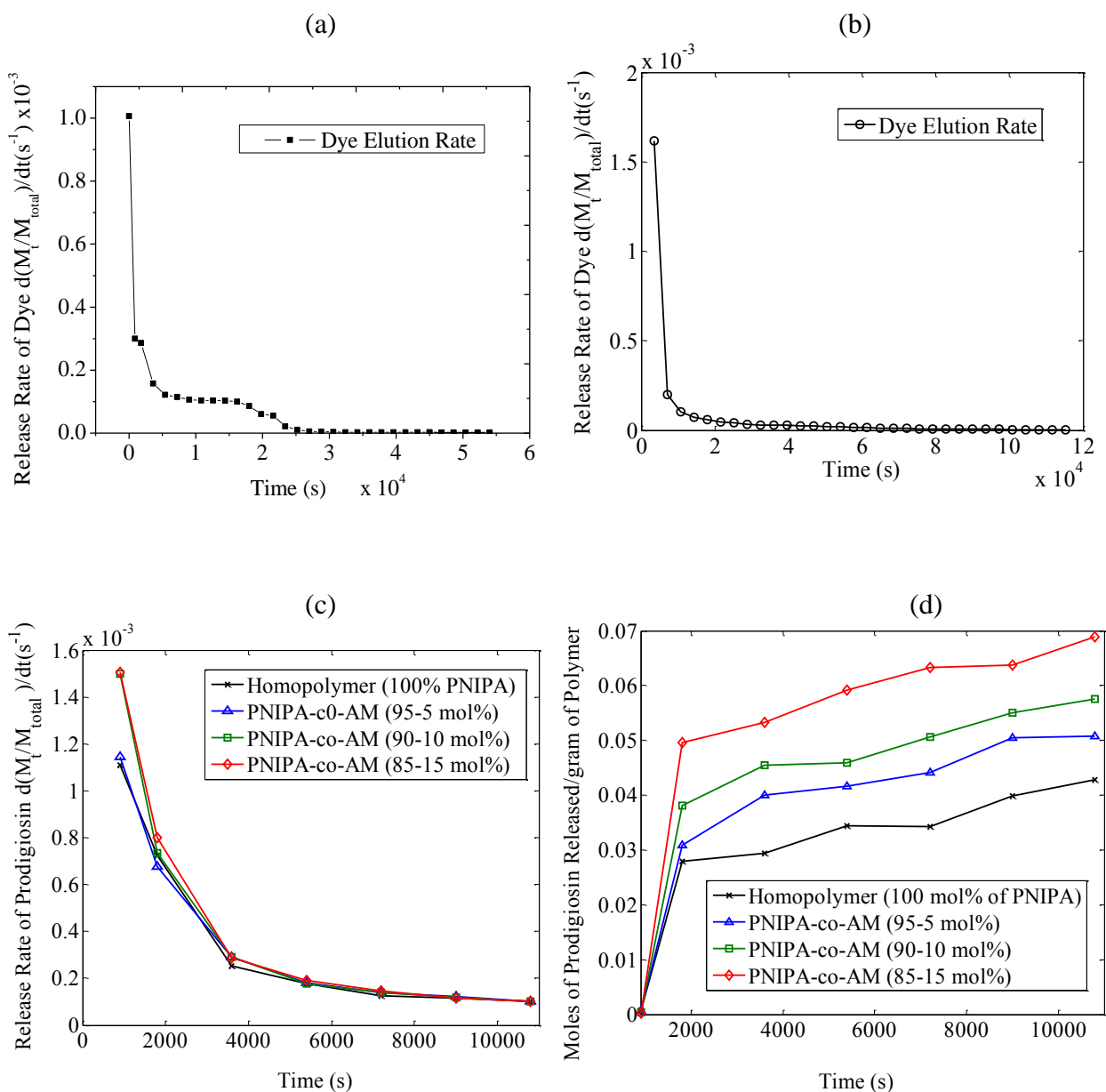
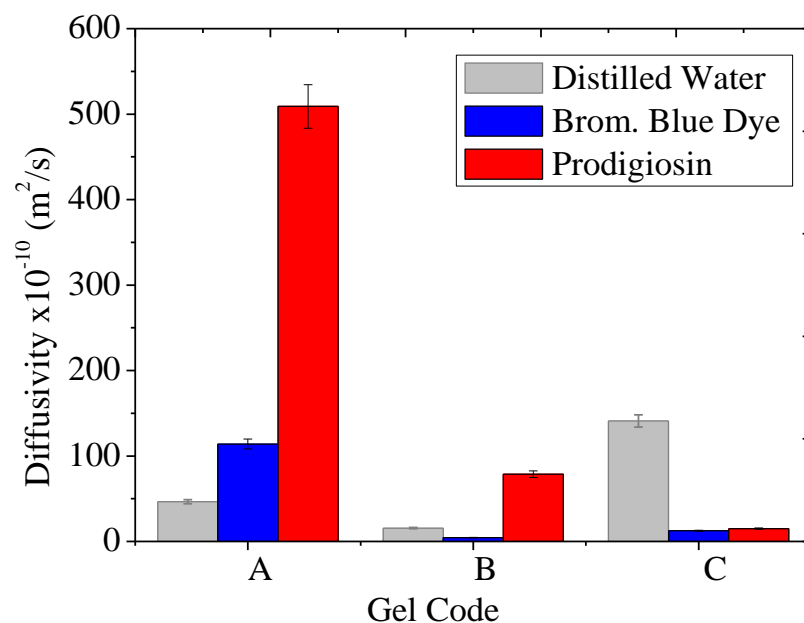


Figure 4.13: Release Rates of Bromophenol Blue Dye at 37°C: (a) Homopolymer, (b) Hydrophilic Copolymer (With 15 mol% of Acrylamide), (c) Release Profiles of P(NIPA)-Based Hydrogels at 41°C and (d) Moles of Prodigiosin Release Per Gram of Polymers (P(NIPA)).



Error Bars Show 95% Confidence Interval of the Mean.

Gel codes; ^AP(NIPA-co-AM) (95-5 mol%), ^BP(NIPA-co-AM) (90-10 mol%) and ^CP(NIPA-co-AM) (85-15 mol%).

Figure 4.14: Fluid/Drug Elution in P(NIPA) Copolymers.

Table 4.1: Gel Materials and their Role in Gel Polymerization.

Gel materials and their reagent grade	Active Role in PNIPA-Based Gel Polymerization
N-Isopropylacrylamide (NIPA), 97 %	Monomer
N,N,N',N'-Tetramethylethylenediamine (TEMED), 99 %	Catalytic agent used in conjunction with APS to accelerate the rate of polymerization
N,N'-Methylenebisacrylamide (MBA), 99 %	Cross-linking Agent
Ammonium persulfate (APS), 98 %	Radical Initiator
Acrylamide (AM), 99.9 %	Hydrophilic Compound
Butyl Methylacrylate, 98 %	Hydrophobic Compound

Table 4.2: P(NIPA)-Based Hydrogel Configuration and their Compositions.

Gel Codes	PNIPA (mol%)	Acrylamide (mol%)	Butyl Methyl Acrylate (mol%)
A	100	-	-
B	95	5	-
C	90	10	-
D	85	15	-
E	95	-	5
F	90	-	10
G	90	5	5
H	85	5	10

Table 4.3: Diffusivity, D, of P(NIPA)-loaded Prodigionsin, Drug Release Exponent (n), and Geometric Constant of P(NIPA)-Based Hydrogels (K) at 37°C (Obtained with Fickian Diffusivity Equations) [29].

Gel Codes	Release exponents	Geometric constants	Diffusion Coefficients
	(n)	(k)	D (m ² /s)
A	0.5 ± 0.025	0.01 ± 0.002	3.6 x 10 ⁻¹⁰ ± 0.18
B	0.6 ± 0.03	0.01 ± 0.010	9.7 x 10 ⁻¹⁰ ± 0.485
C	0.6 ± 0.03	0.01 ± 0.006	9.7 x 10 ⁻¹⁰ ± 0.484
D	0.7 ± 0.035	0.01 ± 0.003	11.4 x 10 ⁻¹⁰ ± 0.57

^{P(NIPA)}N-Isopropylacrylamide, ^{AM}Acrylamide, ^{BMA}ButylMethylacrylate; Gel codes; ^AP(NIPA) Homopolymer (100 mol% of P(NIPA)), ^BP(NIPA-co-AM) (95-5 mol%), ^CP(NIPA-co-AM) (90-10 mol%), ^DP(NIPA-co-AM) (85-15 mol%), ^EP(NIPA-co-BMA) (95-5 mol%), ^FP(NIPA-co-BMA) (90-10 mol%), ^GP(NIPA-co-AM-co-BMA) (90-5-5 mol%), ^HP(NIPA-co-AM-co-BMA) (85-5-10 mol%).

Table 4.4: Diffusion Values of P(NIPA)-loaded Prodigiosin at Different Temperatures. (Obtained with the Early-Time Approximation Equation) [32,33].

Diffusion coefficients (m²/s) at different temperatures					
Gel Code	37°C	41°C	43°C	45°C	48°C
A	1.1x10 ⁻¹⁰	1.9x10 ⁻⁹	1.0x10 ⁻⁹	4.2x10 ⁻⁸	5.6x10 ⁻⁹
B	2.5x10 ⁻¹⁰	1.4x10 ⁻¹¹	1.6x10 ⁻¹¹	4.4x10 ⁻¹¹	1.4x10 ⁻¹¹
C	1.0x10 ⁻⁹	2.1x10 ⁻⁸	5.6x10 ⁻⁹	1.9x10 ⁻⁹	2.8x10 ⁻⁹
D	1.0x10 ⁻⁹	2.1x10 ⁻⁸	5.6x10 ⁻⁹	1.9x10 ⁻⁹	2.8x10 ⁻⁹

^{P(NIPA)}N-Isopropylacrylamide, ^{AM}Acrylamide, Gel codes; ^AP(NIPA) Homopolymer (100 mol% of P(NIPA)), ^BP(NIPA-co-AM) (95-5 mol%), ^CP(NIPA-co-AM)(90-10 mol%), ^DP(NIPA-co-AM)(85-15 mol%).

Table 4.5: Diffusion Coefficients for the Hydrogels in Different Fluids Were Compared at 37°C.

Gel Codes	Diffusion coefficients in distilled Water (m²/s)	Diffusion coefficients (m²/s) in Bromophenol blue	Diffusion coefficients (m²/s) in Prodigiosin
A	1.76 x10 ⁻¹⁰	8.07 x10 ⁻¹⁰	2.45 x10 ⁻¹⁰
B	4.65 x10 ⁻⁹	1.14 x10 ⁻⁸	5.09 x10 ⁻⁸
C	1.56 x10 ⁻⁹	4.51 x10 ⁻¹⁰	7.86 x10 ⁻⁹
D	1.41 x10 ⁻⁸	1.24 x10 ⁻⁹	1.50 x10 ⁻⁹

^{P(NIPA)}N-Isopropylacrylamide, ^{AM}Acrylamide, Gel codes; ^AP(NIPA) Homopolymer (100 mol% of P(NIPA)), ^BP(NIPA-co-AM) (95-5 mol%), ^CP(NIPA-co-AM) (90-10 mol%), ^DP(NIPA-co-AM) (85-15 mol%).

5.0 Prodigiosin Release from an Implantable Biomedical Device: Effect on Cell Viability

5.1 Introduction

The increasing incidence of cancer [1] has stimulated research on the development of novel implantable devices for the localized treatment of cancer [2-5]. Cancer is currently the second leading cause of death after cardiovascular diseases [6-7]. Current trends suggest that cancer will overtake cardiovascular disease as the leading cause of death by 2030 [6,8]. Since standard cancer treatment methods, such as bulk systemic chemotherapy [1,4,9] and radiotherapy [10], have severe side effects, there is a need for alternative cancer treatment methods with reduced side effects. Using bulk systemic chemotherapy for cancer treatment has major challenges. Most of the injected drugs kill or damage healthy cells or tissues that do not require chemotherapy [11]. Generally, chemotherapy damages cells undergoing division. Hence, the parts of the body in which normal cells divide frequently are likely to be affected by chemotherapy (the mouth, intestines, skin, hair, bone marrow are examples). This causes undesirable short and long term side effects [12].

One approach that can be used to reduce the potential side effects of cancer treatments is localized chemotherapy [4,13]. This can reduce the concentrations of cancer drugs that are needed for effective treatments. Localized cancer treatment can be achieved by using implantable drug eluting devices for localized drug release [4,13,14]. This current study demonstrates the feasibility of a regional chemotherapy using approaches from experiments/simulations modules that show increases in the local concentrations, while minimizing systemic exposure from drug eluted from an implantable biomedical devices into a scaffold model (mimicking a surrounding tumor). Efforts have been made to develop drug delivery systems for localized cancer treatment using P(NIPA)-based gels encapsulated with

(PDMS) [5,14].

P(NIPA) forms a three-dimensional hydrogel, when cross-linked with N,N'-methylene-bis-acrylamide (MBA), butyl methacrylate and or both [14]. Previous studies have shown that when PNIPA is heated in water/fluid at temperatures above 32°C, it undergoes a reversible phase transition at its lower critical solution temperature from a swollen hydrated state to a shrunken dehydrated state, losing about 80-90% of its mass [14]. The objective of this work is to develop an implantable device loaded with a biosynthesized drug, prodigiosin (PG) for the localized treatment of breast cancer [14]. The device is tested under *in-vitro* conditions in which controlled levels of cancer drugs, PG and paclitaxel (PT) were released by *in-vitro* experiment into environments containing MDA-MB-231 breast cancer cells. The effects of localized PG and PT are tested using clonogenic assay techniques. Statistical evidence of the effect of PG inhibition on cancer cell viability is also evaluated before discussing the implications for localized cancer treatment.

5.2.0 Materials and Methods

5.2.1 Materials

The PT that was used in this study was procured from LC Laboratories (Woburn, MA, USA). PT was dissolved in dimethyl sulfoxide (CH₃)₂SO (DMSO) that was purchased from BDH Chemicals (Poole Dorset, England). The PG that was used in this study was obtained from the Biotechnology and Genetic Engineering Advanced Laboratory, Sheda Science and Technology Complex (SHESTCO), Abuja, Nigeria. Sylgard 184 kit silicon elastomer, with a silicon elastomer curing agent (a cross linker) were obtained from Sylgard Dow Corning Krayden Inc. (Midland, Michigan, USA). The materials that were used in the PNIPA gel synthesis were purchased from Sigma Aldrich Co. (St. Louis, MO, USA). MDA-MB-231 cell line was procured from American Type Culture Collection (ATCC and Manassas, KS,

USA). Trypsin-EDTA, L15 medium, Fetal Bovine Serum (FBS) and penicillin-streptomycin were procured from Sigma-Aldrich (St. Louis, MO, USA).

5.2.2 P(NIPA)-based Scaffold

Syntheses of P(NIPA)-based hydrogels were presented in our earlier studies [14]. P(NIPA)-based scaffolds were prepared by free radical polymerization [15]. Samples were weighed with an analytical weighing balance (Mettler Model AE 100, Mettler-Toledo Ltd., Leicester, UK) (Table 5.1), followed by mixing 15.56 g of P(NIPA), 0.244 g of methylene-bis-acrylamide (MBA) plus 0.598 g of ammonium persulfate (APS). The samples were dissolved with 140.0 ml of deionized water, shaken until a homogenous mixture was obtained. Samples were placed in ice inside a vacuum oven to degas for 20 minutes at -24 mmHg. This was done to remove the dissolved oxygen. Subsequently, 200 μ L of N,N,N',N'-Tetra-methylethylene-diamine (TEMED) was added to initiate polymerization. Other scaffolds were obtained by similar procedure but this time, copolymerized with 14.78 g, 14.00 g, 13.22 g of acrylamide (AM), representing 5 mol%, 10 mol% and 15 mol%, respectively. These samples were then initiated with 200, 300 and 400 μ L of TEMED, respectively. The solutions were poured into plastic cylindrical molds (4 cm in diameters) and then left at room temperature ($\sim 28^{\circ}\text{C}$) overnight inside a water bath to complete the polymerization process. The samples were carefully remolded and washed several times with deionized water.

5.2.3 Implantable Device

Implantable devices were fabricated from PDMS capsules containing different channel lengths with reservoirs for drug storing as earlier presented [14]. Briefly, PDMS capsules

were fabricated by mixing Sylgard 184 kit silicon elastomer with a silicon elastomer curing agent (a cross linker) (Sylgard Dow Corning, Krayden Inc., Midland, Michigan, USA). These were mixed in a 10:1 ratio by volume, degassed at -24 mmHg under a vacuum oven (Precision Vacuum 19, Artisan Technology Group, Champaign, IL, USA) and then subsequently poured into square aluminum molds. They were cured at room temperature (~28°C) for 24 hours. PNIPA-based hydrogels were prepared as presented earlier [14]. They were then soaked with cancer drugs (PG/PT) and bromophenol blue (BB) before inserting into the PDMS capsules (Fig. 5.1).

5.2.4 Cell Culture

Trypsin-EDTA, L15 medium, Fetal Bovine Serum (FBS) (Sigma-Aldrich, St. Louis, MO, USA) and penicillin-streptomycin were pre-warmed in a water bath to 37°C. The growth medium (L15⁺ medium) contains 10% FBS plus 2% penicillin-streptomycin (i.e. antibiotics). The growth medium was prepared by mixing 45 ml of L15 medium with 5 ml of FBS plus 1 ml of penicillin-streptomycin. MDA-MB-231 cell line was subsequently divided into two. One group was cultured in a T25 flask containing 7 ml of L15⁺ media, while the other group was divided into two T75 flasks containing 10 ml of L15⁺ media. Cells were incubated in a humidified environment containing 5% CO₂-95% air at 37°C (Water-Jacketed CO₂ incubators, Model 6.5W, VWR Scientific Product, San Dimas, California, USA).

Cells were monitored on daily basis with an inverted optical microscope (Nikon ACT-1, TS100 with Nikon Digital Camera, DXM1200F, Melville, NY, U.S.A.). The growth medium (L-15⁺ medium) was changed in every two days by adding 7 mL of a new media. Splitting was carried out when the cells were more than 80% confluent (at least, once every 6 days). The remaining cells were counted and split on the sixth day. 1 ml of cells solution were re-suspended into 6-well plates, diluted with 7 ml growth media to obtain 3×10^2 cells/mL

concentration. These were incubated for 8-10 days. Cells were subsequently detached with trypsin-EDTA. Cells were then centrifuged at 100 rcf (relative centrifuge force) for 8 minutes using an Eppendorf Centrifuge 5804 (Eppendorf, North America, Westbury, NY USA). Subsequently, they were stained with Trypan blue and the numbers of colonies formed were counted. Cell counting was carried out using a hemocytometer. This was used to monitor cell viability and cell growth (proliferation and colony formation).

During cell counting, a mixture of 100 μ l of cell suspension plus 150 μ l of phosphate-buffered saline (PBS) were added to 250 μ l of trypan blue (TB) (in a 1.5 micro-centrifuge tube). Then, 10 μ l of cell-dye was mixed and injected carefully into each chamber of a hemocytometer, allowed to sit for five minutes until the counting was conducted under an inverted optical microscope. Cell counting was conducted in each corner and in the center of the chamber, making a total of 5 squares. Cells within the counting areas were the only cells considered [16]. The total numbers of viable cells were obtained (colorless) as well as the number of dead cells (dyed blue). The cell concentration was determined by counting the number of cells in a specific number of squares, while accounting for the dilution factor. This was used to calculate the original concentration in cells/ml. Note that the cells were usually diluted to make the counting easy.

5.2.5 Clonogenic Assay

Clonogenic assay was used to assess the effects of localized cancer drugs (PG and PT) release on MDA-MB-231 cells. The cells were cultured for ten days in a growth medium without changing the media. On the tenth day, the growth medium was carefully drained from the cells and some of these cells were stained with TB, while the other samples were induced with chemotherapy agents (PG and PT). A cluster of blue-staining cells were

considered a colony, if they comprise of at least 20-50 cells. The number of colonies formed (i.e. the number of clones that evolved from single cells) prior to the number of cells plated were determined. The number of cells per unit volume was also determined with a hemocytometer. The plating efficiency (PE), as well as the surviving fraction (SF), was obtained as follows:

$$PE = \frac{\text{Number of colonies observed on a plate}}{\text{Number of cells plated}} \quad (5.1)$$

$$SF = \frac{\text{Number of colonies observed on a plate}}{\text{Number of cells seeded} \times (PE/100)} \quad (5.2)$$

where $PE/100$ represents the correction term for the plating efficiency.

5.2.6 Scaffold Diffusion Experiment

The biomedical devices consisted of PNIPA-based gels encapsulated in a PDMS capsules (Fig. 5.2). The devices were initially loaded with PG, PT and BB prior to elution into a molded P(NIPA)-based scaffold that mimicked surrounding tumor. The scaffold had an average porosity of ~0.34, compared to the porosity of remnant tumor which was reported to be ~ 0.35 [17]. The transport properties of P(NIPA)-based scaffold are summarized in table 5.2, while considerations were made from the diffusive and permeability data for a remnant tumor (Table 5.3). Fluid/drug releases from the devices were controlled with a Proportional Integral Differential (PID) temperature controller (Fabricated at Princeton University, NJ, USA) (Fig. 5.2). This was set to 37°C to mimic the body temperature. After 12, 48, 72 hours, the molded scaffolds that were used to mimic the tumors were then sliced into 1 mm thick sections along the x-axis. The resulting samples were pre-warmed at 37°C in phosphate buffer saline (PBS) (at a pH of ~ 7.4) in a water bath (Model 2321, Fisher Scientific International Inc., OH, USA). Following that, a tissue tearor (Model 985370, Biospec

Production Inc. OK, USA) was then used to reduce scaffolds into smaller particles. This was done to enhance the release of absorbed dye/drug in the scaffolds. The concentration, C, of PG, PT and BBD were then related to the absorbance via the Beer Lambert Law [18]:

$$C = A / (L\varepsilon) \quad (5.3)$$

where L is the path length (1 cm), A is the absorbance of UV-VIS and ε is the coefficient of absorptivity.

5.2.7 Diffusion Model

The mass transport due to diffusion in isotropic tissue is given by [19]:

$$\frac{\partial C}{\partial t} = D^{eff} \nabla^2 C + \frac{\rho}{\varepsilon} \quad (5.4)$$

where C is the concentration of the medium (drug), ρ is the density of fluid, ε is the average porosity of the tissue/scaffold and t is the time for effective drug delivery from an implantable device into a tissue/scaffold. The effective diffusivity, D^{eff} , was related to the tortuosity (λ) of the tissue and the diffusivity, D, in a porous medium. This is given by [19]:

$$D^{eff} = \frac{D}{\lambda^2} \quad (5.5)$$

The effective viscosity, μ , was also related to the porosity [20]:

$$\frac{\tilde{\mu}}{\mu} = \frac{1}{\varepsilon} \lambda^* \quad (5.6)$$

where $\tilde{\mu}$ is the effective dynamic viscosity of the medium. The tortuosity (λ^*) is also related to the porosity (ε) by $\lambda^* = \sqrt{\varepsilon}$ [21]. In the case of diffusion through anisotropic tissue, the diffusion equation was given by Nicholson [19] to be:

$$D^{eff} = \frac{D}{\lambda_x^2} \frac{\partial^2 C}{\partial x^2} + \frac{D}{\lambda_y^2} \frac{\partial^2 C}{\partial y^2} + \frac{D}{\lambda_z^2} \frac{\partial^2 C}{\partial z^2} + \frac{\rho}{\varepsilon} \quad (5.7)$$

where all the symbols have their usual meanings for a 3-dimension tissue/scaffold.

Diffusion model was used to determine the effective diffusivity of anti-cancer drugs in porous P(NIPA)-based scaffolds. Although the optical micrographs of the P(NIPA)-based scaffolds revealed heterogeneous porosity, the transports through the porous structures were treated using a simplified homogeneous transport models with effective transport properties (Tables 5.2-5.3) [19,22]. The models were implemented using COMSOL Multiphysics Finite Element Analysis Software Package (COMSOL 4.3, Stockholm, Sweden). The models considered the diffusion of PG and BB that were released from the biomedical devices into a surrounded scaffold. Transport of anticancer drug species from an implantable biomedical device adopted an approach that represents the typical tissue by a P(NIPA)-based scaffold model. It was assumed that a tissue is made of cells and body fluid. These cells sort of have an effect on the diffusion of fluid through the tissue. The dimensional version of the diffusion model gives:

$$\frac{\partial C}{\partial t} + \nabla(-D\nabla C) = 0 \quad (5.8)$$

where C is the drug concentration and D is the diffusion coefficient of the solute in the tissue/scaffold. The diffusivities were obtained by procedures earlier presented from previous experiments [14]. The biomedical device had a diffusion coefficient of $9.7 \times 10^{-10} \text{ m}^2/\text{s}$, while the surrounding scaffold showed a diffusivity of $3.6 \times 10^{-10} \text{ m}^2/\text{s}$ [14]. Illustration of the model is shown (Fig. 5.2). The boundary conditions were: $C = C_{\max}$ for the left vertical boundary, where C_{\max} is a given concentration, $3.1 \text{ } \mu\text{mol}/\text{ml}$ (obtained by dissolving 0.1 g of PG in 10 mL of ethanol-water (70:30 vol%). The boundary condition for the right vertical

axis was $(-D\nabla C)n = k_m(C - C_{out})$, while all the other boundaries were insulated according to $(-D\nabla C)n = 0$. Where k_m is the mass transfer coefficient (5 mol/min) and C_{out} is the concentration at the boundaries of the porous structure (Fig. 5.2). The maximum concentration was set at $x = 0$ at a corresponding value of $C = C_{max}$.

This gives:

$$C(t_o) = C_{max}\exp(-ax^2) \quad (5.9)$$

where a is a dimensionless constant (1000).

The second part of this exercise considered homogenized one-dimensional (1-D) model geometry with effective transport properties and an average porosity. The equation for 1-D diffusion was then modified from prior work = [23], by considering the average porosity of the scaffold from

$$\varepsilon \frac{\partial C}{\partial t} + \nabla(-D^{eff}\nabla C) = 0 \quad (5.10)$$

where ε is the average porosity (0.34), C is the concentration and D^{eff} is the effective diffusivity. Simulation was carried out by assuming different release times (0, 1, 6, 12, 24, 48, 72, 96, 192, and 384 hours). The average flux ($F_{average}$) was obtained from:

$$F_{average} = \frac{1}{L_x} \int_0^{L_x} k_m(C - C_{out})dA \quad (5.11)$$

where A is an infinitesimal surface area and L_x is the length of the geometry along the x -axis.

It was then possible to determine the effective diffusivity from:

$$D^{eff} = \frac{F_{average}L_x}{(C_{max}-C_{out})} \quad (5.12)$$

where C_{out} denotes the average concentration (mol/m³) at the flux boundary, and L_x is the length of the geometry along the x -axis. The average concentration, C_{out} , was obtained by:

$$C_{out} = \frac{C_{max}A}{L_x} \quad (5.13)$$

where all the variables have their usual meanings.

5.3.0 Results and Discussion

5.3.1 Cancer Cells and Colony Growth

Cultured MDA-MB-231 Breast Cancer Cells floats in a growth media immediately after detachment (Fig. 5.3a). However, cells begin to adhere to the bottom of the flask after few hours (Fig. 5.3b). When MDA-MB-231 adheres on a flask, growth began after few hours leading to huge proliferation (Fig. 5.3c). The growth curve of MDA-MB-231 breast cancer cells is presented (Fig. 5.4). The growth curve of cells describes the relationship between the proportions of cells surviving over a period of time in a growth medium. MDA-MB-231 cells grows to two folds in three days. When cells reached confluence, some cells began to die because they were competing for nutrients.

Clonogenic assay [24-26] was used to examine MDA-MB-231 cell growth and colonies formed by single MDA-MB-231 cells evolving into large communities of cells (~50 cells)[27,28] (Fig. 5.5). These are cells that retained their reproductive capability to form large clones. Such cells were referred to as clonogenic [29]. When a cell becomes incompetent of synthesizing proteins and DNA, or fails to divide and produce a large number of progeny after going through one or two mitoses, such a cell is considered non-viable [29]. We observed a plate efficiency of ~80-90%. This is in agreement with the literature [30,31]. However, the plating efficiency of cells affects the results and interpretation of colon forming assays [32]. This result may also be affected by bumping the door of the incubator, which may cause cells to shed and settle as new colonies, thereby leading to an increase in the

number of colonies counted. Care was, therefore, taken when opening/closing the door to the incubator as well as proper handling cells.

5.3.2 Effects of Drug Release on Cell Viability

The MDA-MB-231 breast cancer cell line was used to test the effects of cancer drugs released from the biomedical device. The cells were treated with 30 μ M concentrations of (PG) and (PT) for 72 hours. By inducing cells with the various chemotherapy agents, PG and PT, the damage of cells productiveness was elucidated (Fig. 5.6a). It was generally observed that PG and PT prevented colony formation and they contributed greatly to the loss of cell viability. The loss of cells reproductive integrity or their inability to proliferate indefinitely were as a result of the drugs release onto the cells. Lowering cell viability was due to increasing cytotoxicity of cancer drugs and the sensitivity of these drugs to induce apoptosis to diseased cells. PG is a promising anticancer agent because of its effect on inducing apoptosis [33,34]. Tsing-Fen *et al.* [35] have recently shown that prodigiosin down-regulates survivin-protein (member of the inhibitor of apoptosis family). Down-regulation of survivin facilitated the sensitivity of paclitaxel in human breast carcinoma cell lines [35]. PG has also been reported to have a synergistic effect on cell death, especially when it was combined with paclitaxel [35].

5.3.3 Effect of Temperature on Cell Viability

In this study, localized hyperthermia was conducted on cells in a culture plate using a temperature PID controller. The results (Fig. 5.6b) indicated a rapid drop in cell survival associated with the release of heat shock proteins at temperatures close to 43-45°C. Heat shock protein 70 is largely associated with anti-tumor activities induced by heated cancer

cells. Its presence enhances the loss of viable cells as was examined (Fig. 5.6b). The heat associated with hyperthermia induces heat stress on tumor cells, which causes the release of heat shock protein 70 [36]. It was earlier reported that hyperthermia induces heat shock protein 70 expression in treated cells. Similar results have been reported by Theriault *et al.* [37]. At these temperatures, the cells were subjected to heat stresses and they become compromised and then lose the ability to survive. Therefore, cells multiplication breaks down due to the heat at temperatures (43-45°C).

5.3.4 Effect of Temperature and Drug Release on Cell Viability

When cells were subjected to temperatures above 37°C, they were found floating on top of the cultured medium and they fail to adhere to the surface of the culture flask, similar to Figure 5.3a. They were showing the responds to an unfavourable environment. The release of heat shock proteins as a result of hyperthermia temperatures in addition to heat stress significantly induces apoptosis especially when the same cells were subjected to different concentration of cancer drugs (PG and PT at 0.01 µM, 1.0 µM, 10 µM, 20 µM and 30 µM) for 60 hrs. The synergistic effect of hyperthermia and drugs are discussed below. The combined effects of hyperthermia and drugs release were the most effective therapy that was demonstrated (Fig. 5.6c). The effects of temperature (below the melting temperatures (T_m) of drugs) plus drug release were presented (Fig. 5.6c). This result has shown possible improved outcomes and is consistent with earlier results presented in the literature [38]. In the earlier work, the death of cancer cells were attributed to the loss of β -actin detection, when a controlled dose of drugs were released [38]. The control experiments at 37°C without drugs gave a rise in cell viability from 100-200% (Figs. 5.6a-b) in 72 hrs and 100-140 % in 60 hrs (Fig. 5.6c). The effect of drug release/hyperthermia reduces the test samples below 100 % (Figs. 5.6a-c).

The combined effect of 1 μM PG or 1 μM PT with hyperthermia (at 43°C) (Fig. 5.6c) attained ~80 %, ~95 % cell viability, respectively as compared to 1 μM PG and or 1 μM PTx with both yielding ~100 % at 37°C. Similarly, 10 μM PG and or 10 μM PT at 43°C reduces cell survival to ~75 % for PG and ~85 % for PT as compared to ~134 % at 37°C. The results from 100 μM (PG/PT) at 43°C showed a great reduction in cell viability (down to ~35 % for PG and ~20 %) as a result of drug release. This shows that, there was a significant increase in cell death (reducing cell viability) as dose of drug increases with increase in temperature. However, there wasn't a clear difference on the effects of PG and PT on cell death, though the results at one point show a slight increase in cell death due to PT than PG. Drug release at 37°C yielded a reduction of cell death to ~20 folds as compared to the controlled. Similarly, drug release and hyperthermia temperatures reduce cells to ~100 folds.

5.3.5 Cytotoxicity of the PG and PT

Cell death was quantified by flow cytometric analysis of trypan blue dye (TBD), which stain cells that are dead or those undergoing death. Cultured MDA-MB-231 cells were induced with 30.0 μM PG/PT for 72 hrs (Fig. 5.6a). This gave rise to cell death of ~ 80 % (with ~20 % of viable cells remaining). These results show the therapeutic effect of PG and PT at higher dose is highly significant. However, following dosages ≤ 1.0 μM of PG/PT, the total percentage of dead cells and cells undergoing death were ~5 % (i. e. ~95 % of viable cells remaining) for PG and ~20 % (i.e. ~85 % of viable cells) for PTx (Fig. 5.6c). The effect of drug release on cell death at concentrations ≤ 1.0 μM were not greatly significant, while concentrations from 10-100 μM have shown a great effect on reducing cell viability due to increased toxicity of drug agents. The controlled concentration for drug release on cell death was ~30 μM .

5.3.6 Statistical Testing on Cell Viability

Statistical analysis for each experiment was carried out for at least at three independent times and the average values \pm standard errors (SE) were reported [39]. The present data were analyzed using Minitab software package (Minitab16, Minitab Inc., State College, PA, USA). We proposed a synergistic effect of drug (PG) and temperature on the viability of MDA-MB-231 cancer cells. Statistical variations of drugs effects, hyperthermia effect and drug-temperature effect on cell viability were evaluated using student's *t*-test statistic [39] at 95% confidence interval (CI). This is a hypothesis test concerning the mean of the population, when the standard deviation δ , is unknown, and the sample size is small. The test [39,40] gives:

$$T = \frac{\bar{x} - \mu_0}{\sigma / \sqrt{n}} \quad (5.14)$$

where T is the T-test statistical parameter, \bar{x} is the sample mean, μ_0 is the population mean, σ is the population standard deviation and n is the sample size. Thus, the significant difference in the cell viability due to PG/PT and temperature were evaluated (Fig. 5.6). A comparison with a difference of $P < 0.05$ was statistically significant or vice versa.

5.4 Effective Diffusivity of Drug Release into Scaffolds

P(NIPA)-based scaffold is presented in Fig. 5.7. Transparent P(NIPA)-based scaffolds were produced with reduced turbidity. BB was experimentally eluted from an implantable biomedical device onto a P(NIPA)-based scaffold (mimicking a surrounding tumor) after 24 hrs. When BB loaded device was implanted into the scaffold, the contours of the dye eluted from the implantable device into the porous scaffold were observed (Fig. 5.7). The eluted dye into the scaffold (with average porosity of 0.34) shows that the dye was successfully diffused

to ~ 10 mm radially away from the implanted device. This means that a tumour with diameters ≤ 15 mm can be treated with this implantable device with minimal exposure (1×10^{-7} mol/m³) on surrounding tissues. The homogenous distribution of pores in the scaffold permitted the dye to uniformly diffuse into the scaffold. However, some regions of the scaffold have varying porosity and varying tortuosity's which affected dye diffusion at such locations in the scaffold. This creates a visual image of high or low dye concentrations as illustrated (Fig. 5.7).

The diffusivities in the scaffold were found to vary from $1.01-9.74 \times 10^{-8}$ m²/s from 3 hours to 192 hours, respectively. The effective diffusivity increases exponentially with time (Fig. 5.8). This implies that local drug concentrations were high over time in as much as the device continues to elute drug into the surrounding scaffolds. The effective diffusivity of drug eluted from the implantable devices was maintained at $\sim 9.7 \times 10^{-8}$ m²/s from 3-6 days' after implantation (Fig. 5.8). Devices with channel length of ~ 2 mm help to maintain the diffusivity at $\sim 9.7 \times 10^{-8}$ m²/s for over 6 days.

From the simulation result (Figs. 5.9a), it shows that drug diffusion in a surrounding scaffold from the implantable biomedical device is depended on the scaffold/tumor porosity or tortuosity and the delivery time. For instance, contour of drug concentration along the length of the geometry (x-coordinate) were much pronounced at regions closed to the implant, while drug concentrations decreased exponentially along the x-coordinate (1D) at different times: 3, 6, 12, 48, 72, 96 (Fig. 5.9b). The presence of drugs detected along the x-coordinates at 6, 12, 48, 72, 96 hrs, were respectively achieved at 3.5 mm, 4.5 mm, 6 mm, 8 mm, 9.5 mm and 10 mm along the length of a solid scaffold. Implanting the device in the middle section of the scaffold via surgery then suggest that local tumors could be managed/destroyed without affecting surrounding tissues containing useful and viable cells.

From the simulation model, at a steady flow, the average flux becomes 25×10^{-15} mol/ms. Comparism of the simulation with scaffold experiment (Fig. 5.10a) showed that, drug concentration decrease exponentially along the geometry of the x-coordinate, especially during the early time of drug release. This is a characteristic of equation (9), where drug concentration was exponentially dependent on time and position. The earlier time releases exponentially increases with concentration rising high at the immediate boundaries to the drug delivery device as presented (Figs. 5.9b and 5.10a).

From the simulation model, appears to slightly deviate from the experiment (scaffold model) conducted (Fig. 5.10a-b). This is attributed to the fact that the average porosity, 0.34 of the scaffold was used in the simulation. However, the porosity of the scaffold varied, ranging from 0.27-0.70. In fact, some of these pores were interconnected, while others were mesopores, micropores and macropores [14]. However, the experimental results validated the simulation by explaining to us that the heterogeneous network structure of the scaffolds creates a complex pore structures. Knowing that the tortuosity (λ^*) is also related to the porosity (ε) by $\lambda^* = \sqrt{\varepsilon}$. Therefore the tortuosity of fluid/drug within the scaffolds provided different fluid dynamism. The cumulative drug eluted from the implantable biomedical devices into scaffolds from experimental and computational simulation is presented at 37°C (Fig. 5.10b). The scaffold model indicated that ~ 65 % of drugs were eluted from the device after 100 hrs, while ~ 90 % was observed from the simulation results after 100 hrs. The simulation assumed an isotropic scaffold model with an average porosity.

5.5 Implications

From the above results, the biosynthesized PG was comparable to PT on their effects on cell apoptosis. PG is more affordable since it can be processed locally and purified for potential applications. Moreover, this preliminary study was governed by a controlled drug

elution from an implantable biomedical devices delivering drugs/dye at diffusivities between $4.9 \times 10^{-9} \text{ m}^2/\text{s}$ and $9.29 \times 10^{-9} \text{ m}^2/\text{s}$. The implantable device could reduce the amount of drug that is needed for a therapeutic effect. It also reduces the side effects of chemotherapy greatly.

The result shows that hyperthermia also reduces cell viability. The combination of chemotherapy and hyperthermia reduces cell viability which indicates there is a synergy of the combined effect. The studies suggest that, temperature-responsive PNIPA-based hydrogels encapsulated within a biocompatible polymer (PDMS) can be used for the controlled release of PG or PT to targeted solid tumors (at stage I – Stage III) or cancer cells [4,41]. Since the delivery approaches are localized, lower drug dosages and higher efficacy are possible [4,41]. This work demonstrates the potential for the controlled release of PG as an anticancer drug. It is possible to envisage an implantable device in which PG produced by bacteria is released at temperatures in which cancer cell viability is also reduced by hyperthermia. Implantation of the device could be done after the removal of a tumor for the device to deliver cancer drugs locally to the affected region.

The effective concentrations of PG and PT for cell viability were $\sim 30 \text{ }\mu\text{M}$. These concentrations reduced the toxicity of PG and PT as cancer drug agents. Hence, PG and PT or both promoted the loss of cell viability with increasing drug concentration (Figs. 5.6a, 5.6c). Furthermore, temperatures of 41- 45°C also induced the loss of cell viability (Fig. 5.6b). This suggests that a combination of localized hyperthermia and drug delivery can be used to treat breast cancer via controlled delivery of heat and drugs from future implantable devices. This study provides information for relevant mechanism towards the design of a delivery device for potential synergy.

Tumor shrinkage was also demonstrated using the scaffold model. This demonstrated the feasibility of a regional chemotherapy which increases the local concentrations, while minimizing systemic exposure to surrounding tissues. However, there is the need for *in-vitro* studies on multiple human cancer cell lines to further study the effects of cell viability with cancer drugs. There is also the need for toxicity studies on lab animals and human clinical trials to develop the appropriate drug concentrations for future work. These are clearly some of the challenges for future work.

5.6 Conclusions

This current study demonstrates the feasibility of a regional chemotherapy using approaches from experiments/simulations that show increases in the local concentrations, while minimizing systemic exposure from drug eluting devices into cancer tumors/scaffolds (mimicking a surrounding tumor). The scaffold model indicated that ~ 85 % of drugs were eluted from the device within ~ 400 h, while ~ 90 % was observed from the simulation results. The simulation assumed an isotropic scaffold model with the target drug-PG, a tripyrrollel isolated from a soil borne microbe (*Serratia marcescens*, *subsp marcescens*), PG is also an immune suppressor that induces apoptosis in haemotopoietic cancer cells with no marked toxicity in nonmalignant cells. The effects of PG release (on cancer cell viability) were compared with those of PT release over a range of temperatures (37 - 43°C) that are also relevant to hyperthermia-induced loss of cancer cell viability. The results show that localized release of PG reduces the viability of human MDA-MB-231 breast cancer cells. Similar reductions in the viability of MDA-MB-231 human breast cancer cell lines are also observed when cancer drug, PT, was released locally. The results obtained provide a proof-of-concept for the controlled release of PG for the very first time in the management of post-operative tumor removal.

The synergistic effects of temperature and drug agents (PG/PT) on cell death, were tested at $\alpha = 0.05$. The means were compared using the student's T-test and a comparison with a difference of $P < 0.05$ was statistically significant.

The porous structures of the P(NIPA)-based, 3-D scaffold enhanced controlled release of fluid/drugs. Since the delivery of fluid/drugs were localized by the use of the implanted devices, the total quantities of drug that are needed for therapeutic treatment are much less than those required for bulk systematic drug. For these particular models (experiment/simulation solutions), we can conclude that simple diffusion is sufficient for the drugs (PG/PT) to spread through a tissue. In the context of drug delivery systems, it is essential for this to occur so that drugs such as PG/PT can have the proposed effect on the tumor/cancer cells. Hence, the potential side effects of localized cancer drug delivery could be much less than those associated with bulk systemic chemotherapy.

5.7 Bibliography

- [1] B. Hildebrandt and P. Wust in: W.P. Ceelen (Ed), Peritoneal Carcinomatosis: A Multidisciplinary Approach, Springer, New York, (2007) 185.
- [2] A. Afrassiabi, A.S. Hoffman and L.A. Cadwell. Effect of temperature on the release rate of biomolecules from thermally reversible hydrogel. J of Membrane Sci. 33 (1987) 191-200.
- [3] S. Allan, Hoffman and Jorge Heller. An Introduction to Materials in Medicine, 2nd Edition. Elsevier Inc. (2004) 628 - 637.
- [4] Y. Oni, C. Theriault, A.V. Hoek and W.O. Soboyejo, Effects of temperature on diffusion from PNIPA-based gels in a BioMEMS device for localized chemotherapy and hyperthermia, J. Mater. Sci. and Eng. C. 31 (2011) 67-76.
- [5] Y. Oni and W.O. Soboyejo. Swelling and diffusion of PNIPA-based gels for localized chemotherapy and hyperthermia. J. of Mater. Sci. and Eng. C. 32 (2012) 24-30.
- [6] P. Boyle and B. Levin. The World Cancer Report 2008, IARC Press, Lyon, (2008).
- [7] J. Mackay and G.A. Mensah, The atlas of disease and stroke, WHO in collaboration with the centers for disease control and prevention, Non-serial Publication, 2004. ISBN-13 97892415.
- [8] D. Gutierrez. Cancer Facts and Figures. 2nd Edition. American Cancer Society. (2008).
- [9] D. Needhama, W.M. Dewhirst, The development and testing of a new temperature-sensitive drug delivery system for the treatment of solid tumors, Advanced Drug Delivery Reviews, ELSEVIER. 53 (2001) 285-305.

- [10] M. C. Perry. Approach to the patient with cancer. In: Goldman L, Schafer AI, eds. Cecil Medicine, 24th ed. Philadelphia, Pa: Saunders Elsevier. (2011) chap 182.
- [11] D. J. Chaplin, S. A. Hill, K. M. Bell and G. M. Toser. Modication of tumor blood flow: Current states and future directions, *semin. Radiat. Oncol.* 8 (3) (1998) 151-163.
- [12] N. David and W. D. Mark. The Development and Testing of a New Temperature-sensitive Drug Delivery System for the Treatment of Solid Tumors. *Advanced Drug Delivery Reviews*, 53 (2001) 285-305.
- [13] G. Fu and W. O. Soboyejo. Swelling and diffusion characteristics of modified poly (N-isopropyl acrylamide) hydrogels. *J. of Mater. Sci. and Eng. C.* 30 (2010) 8-13.
- [14] Y. Danyuo, J. D. Obayemi, S. Dozie-Nwachukwu, C. J. Ani, O. S. Odusanya, Y. Oni, N. Anuku, K. Malatesta and W. O. Soboyejo. Prodigiosin Release From an Implantable Biomedical Device: Kinetics of Localized Cancer Drug Release. *J. of Mater. Sci. and Eng. C.* Vol. 42, Issue (nul) (2014) 734-745. Doi:10.1016/j.msec.2014.06.008.
- [15] F. Antunes, L. Gentile, L. Tavano and R. C. Oliviero. Rheological characterization of the thermal gelation of poly(N-isopropyl acrylamide) and poly(N-isopropyl acrylamide) co-Acrylic Acid. *Applied Rheology.* 1 (2009).
- [16] C. Yu-Wei and C. Pei-ju. Automatic cell counting for hemocytometers through image processing. *World Academy of Science, Engineering and Technology.* (2011) 58.
- [17] C. Nicholson and M. E. Rice. The migration of substances in the neuronal microenvironment, *Ann. NY Acad. Sci.*, 1986; 181, 55-71.
- [18] S. K. Kohl, J. D. Landmark and D. F. Stickle. Demonstration of Absorbance Using Digital Color Image Analysis and Colored Solutions. *Chem. Educ.* 83 (4) (2006) 644-646.
- [19] C. Nicholson. Diffusion and related transport mechanism in brain tissue, *Rep. Prog. Phys.*, 2001; 64, 815-884.
- [20] J. Bear and Y. Bachmat. *Introduction to Modeling of Transport Phenomena in Porous Media*, Kluwer Academic, Dordrecht, (1990).
- [21] S. Liu and J. H. Masliyah. Non-linear flows in porous media, *J. Non-Newton. Fluid Mech.*, 86 (1999) 229-252.
- [22] H-J. Kuh, S. H. Jang, M. G. Wientjes and L-S. Jessie AU. Computational Model of Intracellular Pharmacokinetics of Paclitaxel. *The Journal of Pharmacology and Experimental Therapeutics by the American Society for Pharmacology and Experimental Therapeutics.* JPET 293 (2000) 761-770, 2252/8243.
- [23] I. Rubinstein and L. Rubinstein. *Partial Differential Equations in Classical Mathematical Physics*, CUP, Cambridge. (1993).
- [24] K. Buch, T. Peters, T. Nawroth, M. Sanger, H. Schmidberger and P. Langguth. Determination of cell survival after irradiation via clonogenic assay versus multiple MTT Assay: A comparative study. *Radiation Oncology.* 7(1) (2012).
- [25] S. E. Jones, J. C. Dean, L. A. Young and S. E. Salmon. The human tumor clonogenic assay in human breast cancer. *Journal of Clinical Oncology.* 3(1) (1985) 92-97.
- [26] G. Kishore, N. Leanna and D. M. Sanford. An improved method for staining cell colonies in clonogenic assays. *Cytotechnology.* 54(2) (2007) 85-88.
- [27] Y. Xiaodong. Clonogenic Assay. *Cancer Biology.* Bioprotocol.org. (2012).
- [28] C. X. H. Xu., J. H. Hendry, N. G. Testa and T. D. Allen. Stromal colonies from mouse marrow: characterization of cell types, optimization of plating efficiency and its effect on radio-sensitivity. *J. Cell Sci.* 61 (1983) 453-466.
- [29] M. Ampama, M. Hobbs and R. E. Meyn. *Methods in molecular medicine*, Vol. 110; Chemosensitivity Vol.1. In vitro assay Humana press Inc., Totowa, NJ. (2005).

- [30] J. P. Mather and P. E. Roberts. *Introduction to Cell and Tissue Culture: Theory and Technique*. Plenum Press. New York and London. (1998).
- [31] Cell Biolabs, Inc., San Diego, CA. USA. Product data sheet. MDA-MB-231/ GFP cell line. (c) 2010-2011.
- [32] J. Pomp, J. L. Wike, I. J. Ouwerkerk, C. Hoogstranten, J. Davelaar, P. I. Schrier, J. W. Leer, H. D. Thames and W. A. Brock. Cell density dependent plating efficiency affects outcome and interpretation of colon forming assays. *J. of Radiother Oncol R.* 40(2) (1996) 121-125.
- [33] N. R. Williams, P. C. Fineran, F. J. Leeper and G. P. Salmond. The biosynthesis and regulation of bacterial prodiginines. *Nat. Rev. Microbial.* 4 (2006) 887-889.
- [34] S. K. Pandi, D. Arul, A. S. G. Smiline, I. V. Hairul. S. V. G. Saravanan and R. Raghuraman. Prodigiosin Induced Apoptosis and Inhibited Proliferation in Carcinoma Hsc-2 Cells. *Int. J. of Current Research.* 3(4) (2011) 151-156.
- [35] H. Tsing-Fen, P. Yu-Ta, C. Show-Mei, L. Shin-Chang, F. Bo-Lin, L. Chien-Hsing, Y. Wan-Ju, C. Jo-Shu and C. Chia-Che. Prodigiosin down-regulates surviving to facilitate paclitaxel sensitization in human breast carcinoma cell lines. *Toxicology and Applied Pharmacology.* 235 (2009) 253-260.
- [36] C. J. Gomer, S. W. Ryter, A. Ferrario, N. Rucker, S. Wong and A. M. Fisher. Photodynamic therapy-mediated oxidative stress can induce expression of heat shock proteins. *Cancer Res.* 56 (1996) 2355-2360.
- [37] C. Theriault, C. Barkey, R. Chandrasekar, E. Paetzell, Y. Oni and W. O. Soboyejo. An in-vitro study of the effects of temperature on breast cancer cells: Experiments and models. *Mat. Sci. and Eng. C.* 32(8) (2012) 2242-2249.
- [38] H. Yaoming, G. Haiyan and L. Shuping. Haematoporphyrin Based Photodynamic Therapy Combined with Hyperthermia Provided Effective Therapeutic Vaccine Effect against Colon Cancer Growth in Mice, *Int. J. Med. Sci.* 9 (2012) 627-633.
- [39] B. A. Ogunnaike. *Random Phenomena, Fundamentals of Probability & Statistics for Engineers..* USA, University of Delaware (2009) 1-1055.
- [40] R. B. Dean and W. J. Dixon. Simplified Statistics for small numbers of observations. *Anal. Chem.* 23 (4) (1951) 636-638.
- [41] T-F. Ho, Y-T. Peng, S-M. Chuang, S-C. Lin, B-L. Feng, C-H. Lu, W-J. Yu, J-S Chang and C-C. Chang. Prodigiosin Down-Regulates Survivin to Facilitate Paclitaxel Sensitization in Human Breast Carcinoma Cell Lines. *Toxicol Appl. Pharmacol.* 235(2) (2009) 253-260.

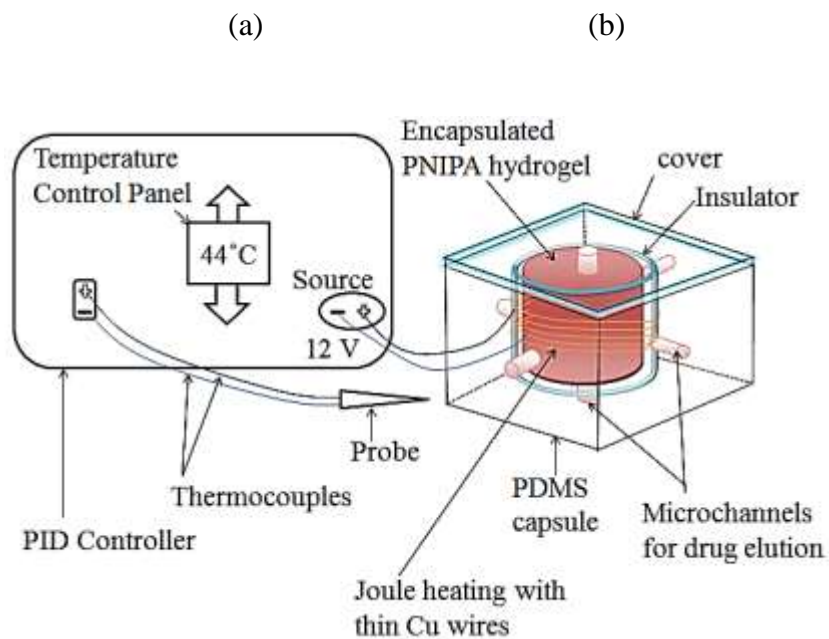


Figure 5.1: (a) Schematic Diagram of Encapsulated Biomedical Device with Microchannels for Drug Elution, (b) PID Temperature Controller (Used to Set and Monitor Local Temperatures).

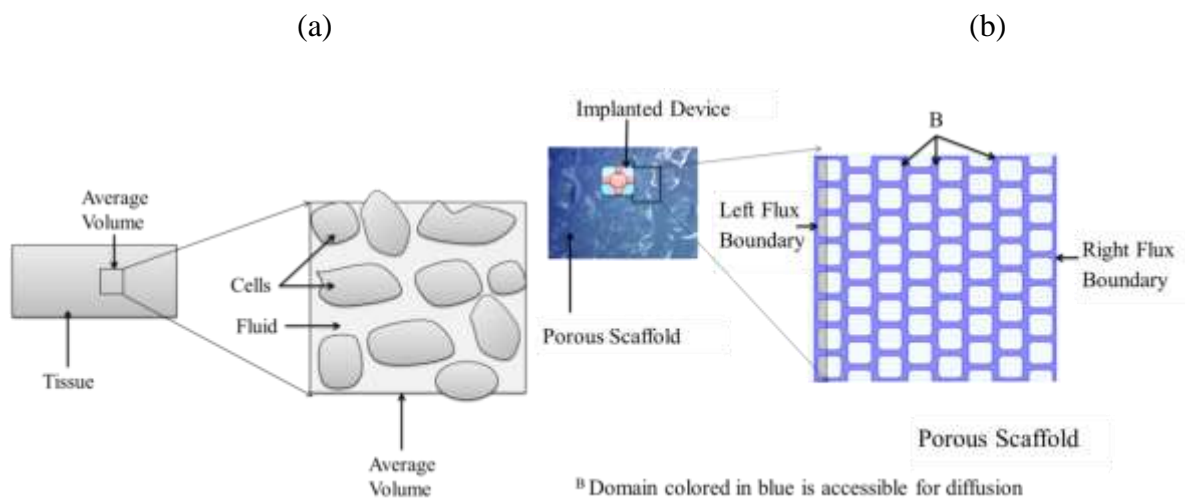


Figure 5.2: Transport of Anticancer Drug Species Delivered from an Implantable Biomedical Device: (a) Schematic Diagram for a Typical Tissue, (b) Schematic PNIPA-based Scaffold Model.

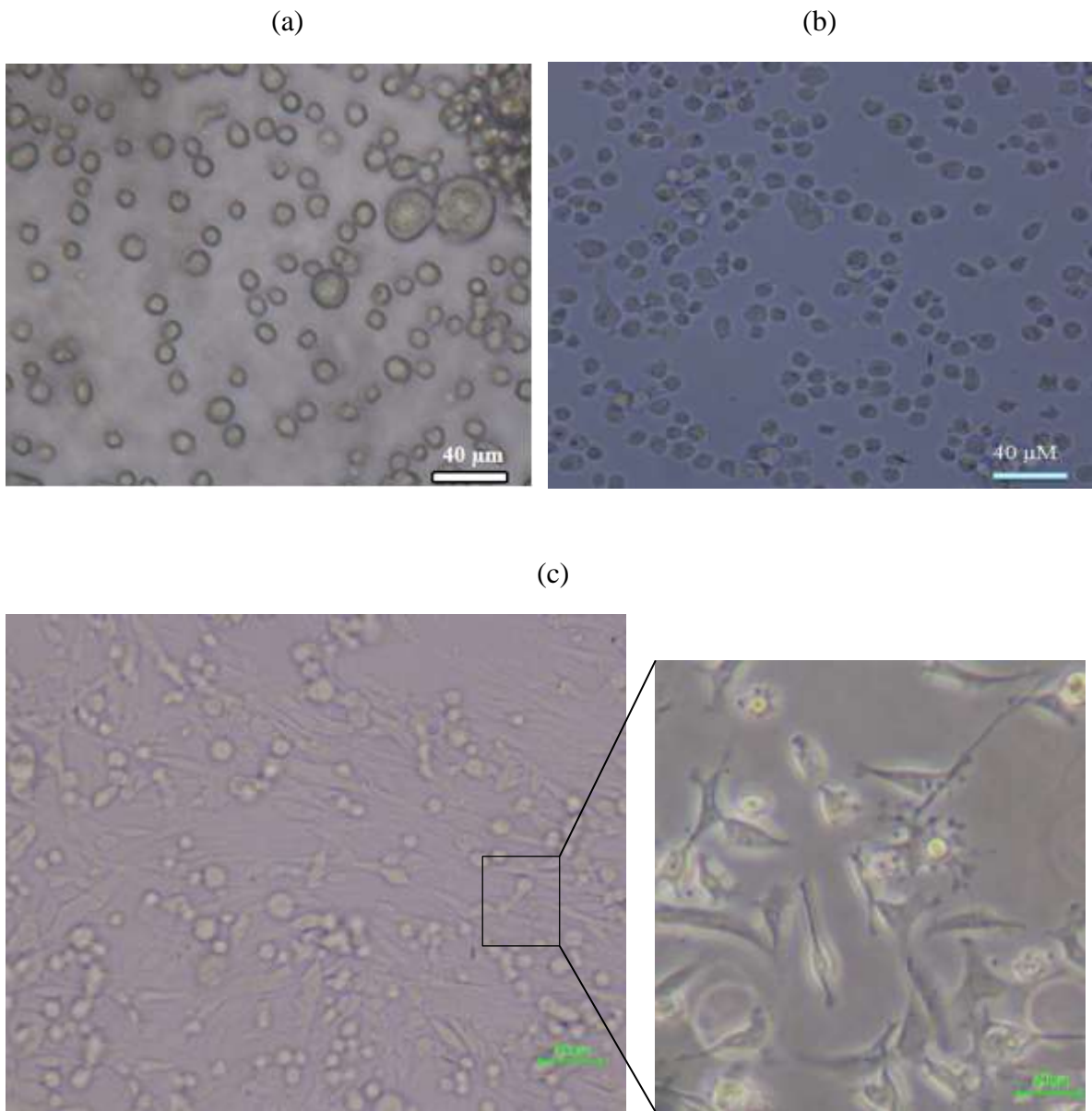


Figure 5.3: MDA-MB-231 Breast Cancer Cells in Culture Flask: (b) Cells Floats on Growth Media Immediately after Detachment; (c) Detached Cells Adhered to Flask after 2 hours; (a) Cells Adhered on the flask after Several Days.

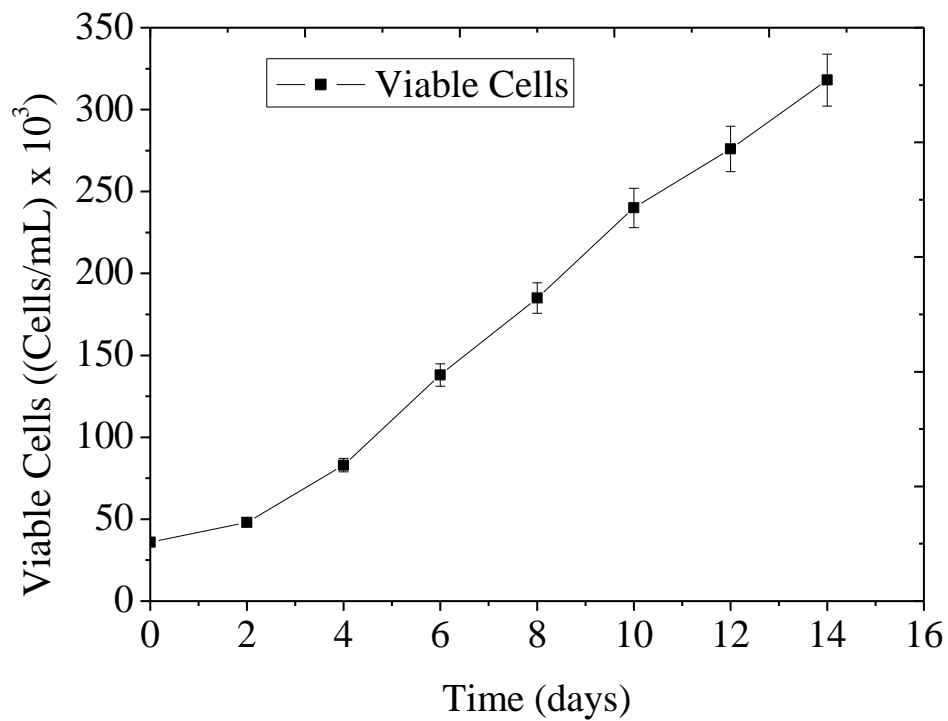


Figure 5.4: Growth Curve of Viable Cells Versus Time (days). Error Bars Show 95% Confidence Interval of the Mean.

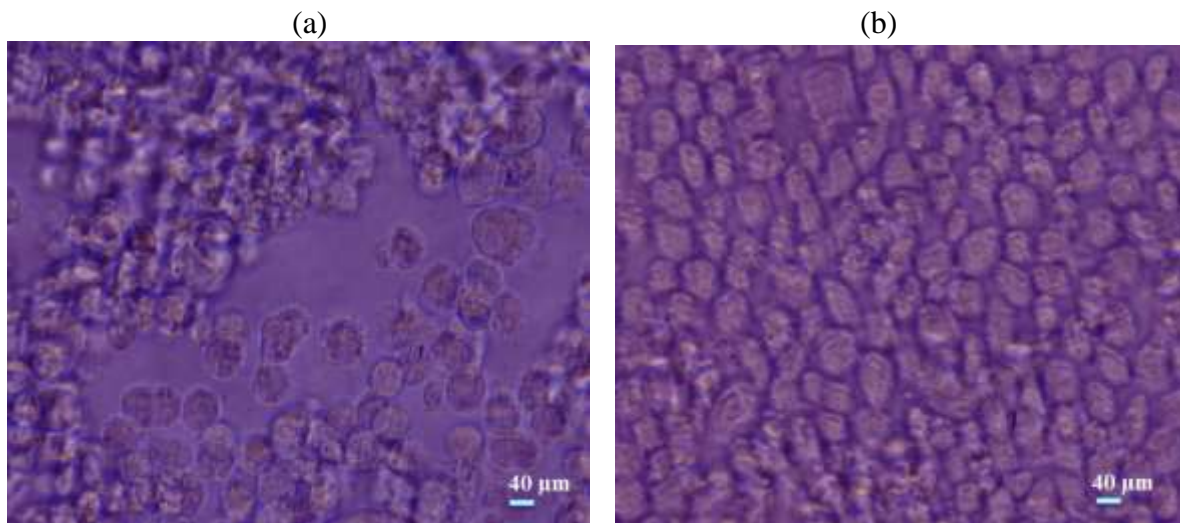
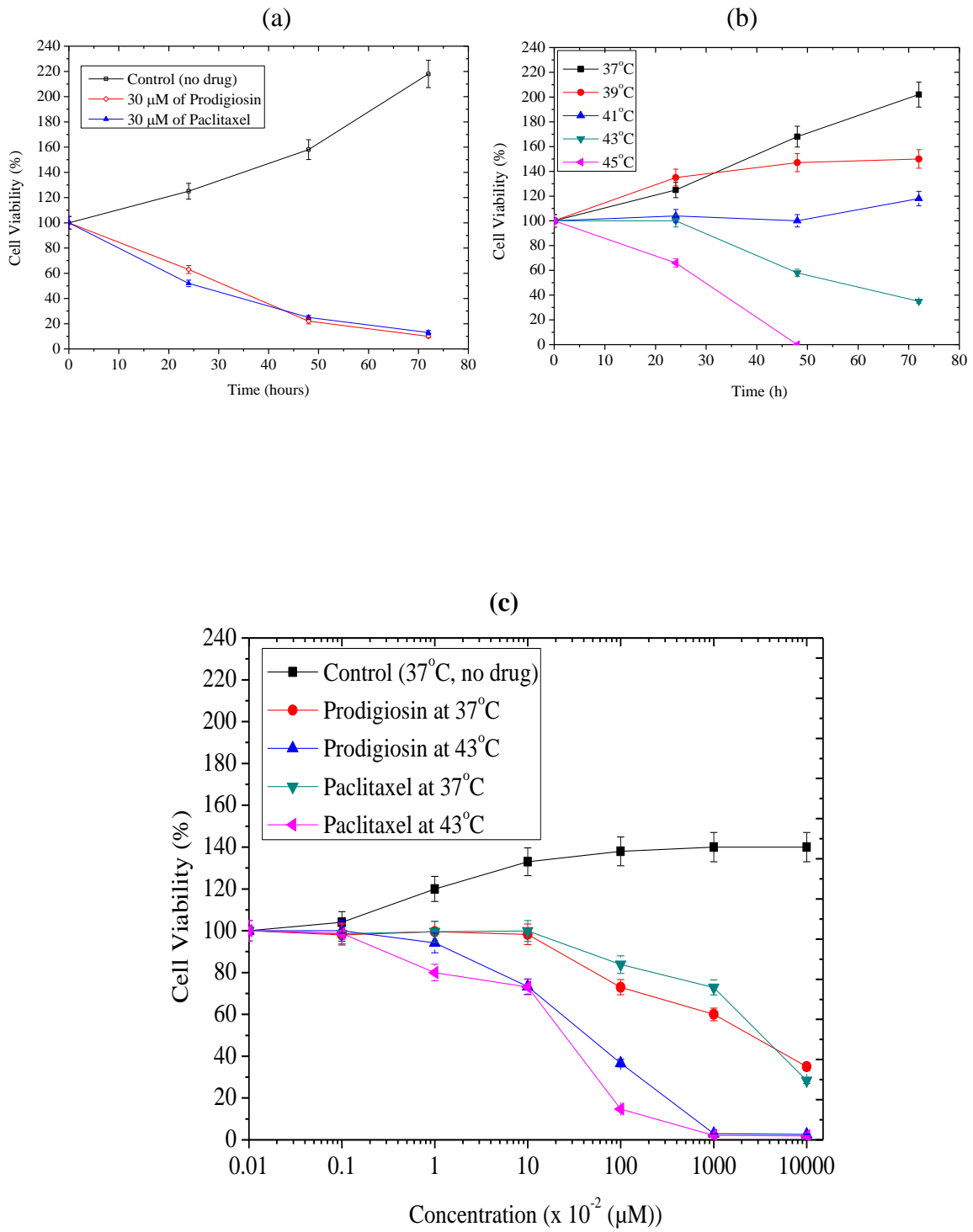


Figure 5.5: Colonies of MDA-MB-231 breast cancer cells on flask: (a) 7 days of culture; (b) 14 days of culture.



Effects of Temperature and Drug Concentration after 60 hrs. Error Bars Show 95%CI of Mean.

Figure 5.6: Cell Viability (MDA-MB-231 Cell Line): (a) Effect of drugs (Prodigiosin and PaclitaxelTM) after 72 hrs; (b) Effect of Temperature on Cell Viability after 72 hrs; (c) Combined Effect of Drug Release and Temperature on Cell Viability.

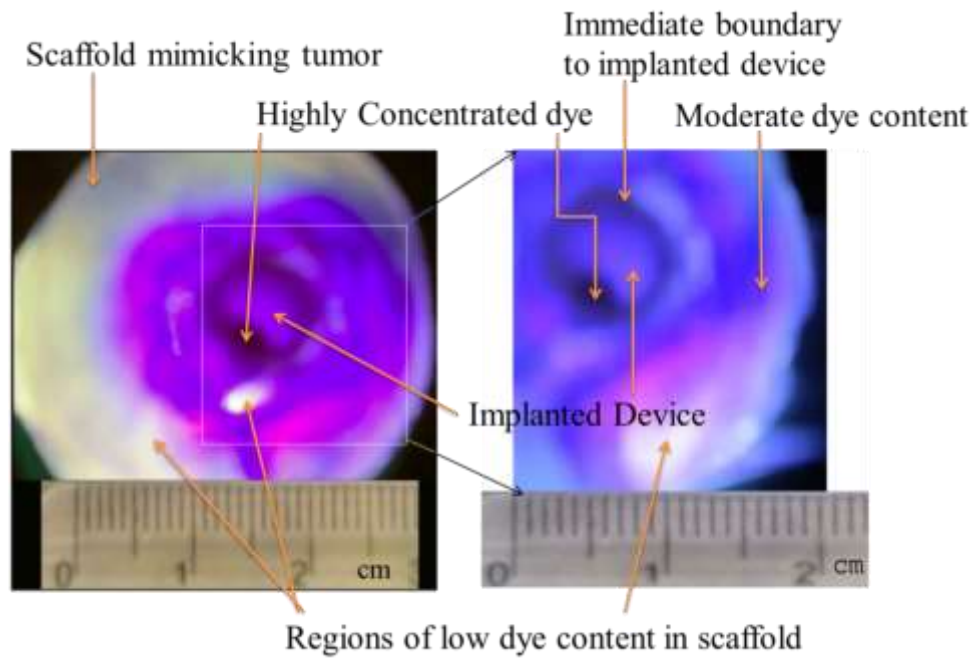
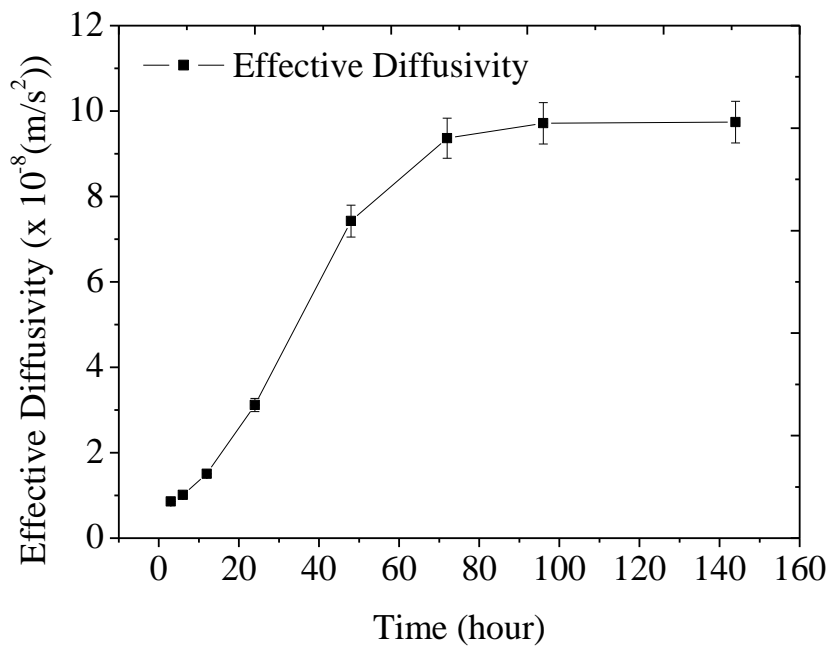


Figure 5.7: Dye Eluted from an Implantable Biomedical Device onto PNIPA-based Scaffold Mimicking Tumor after 24 hrs.



Error Bars Show 95% Confidence Interval of the Mean

Figure 5.8: Effective Diffusivities of Dye Elution versus Time in a P(NIPA)-Based Scaffold.

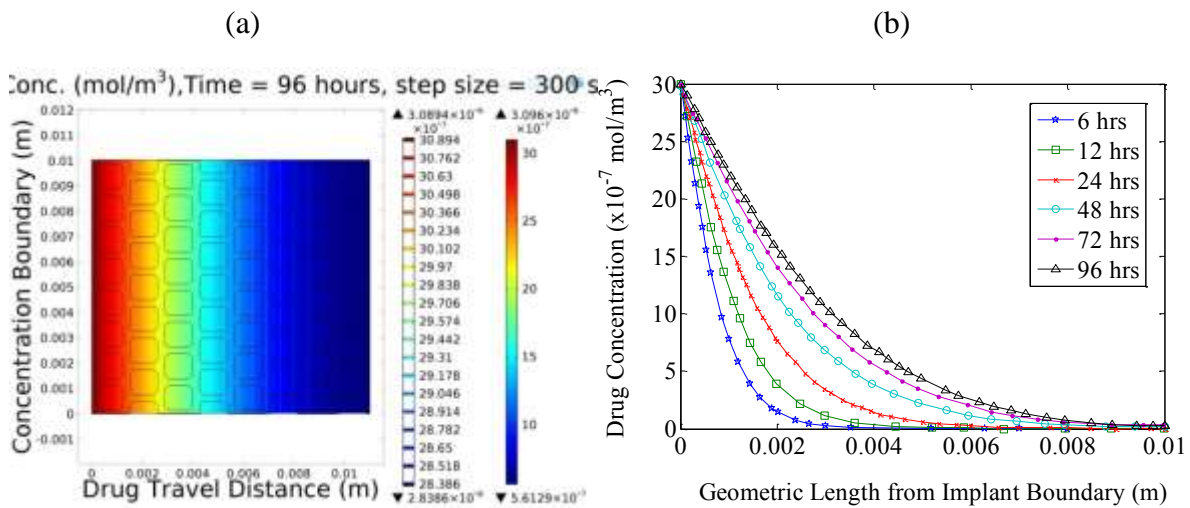
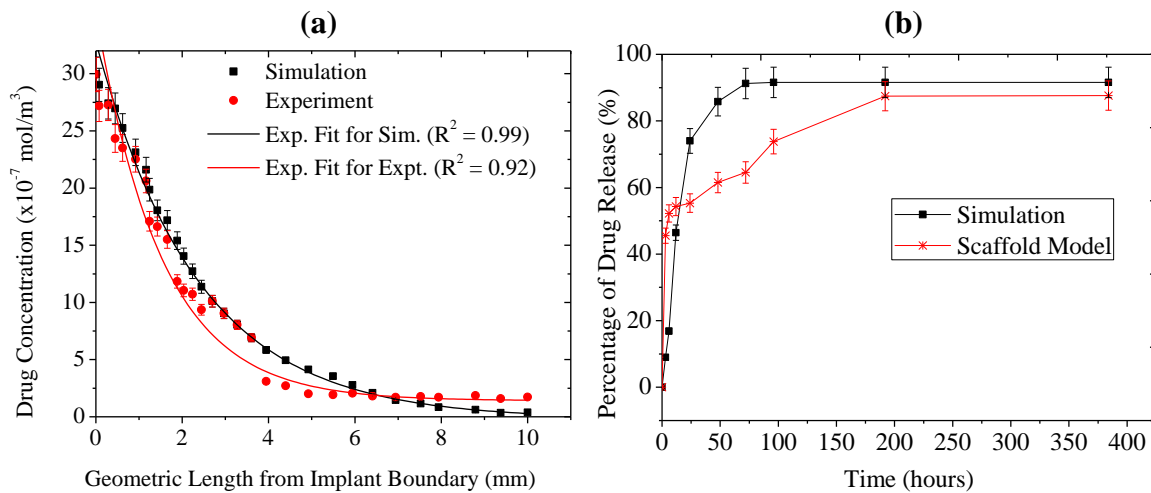


Figure 5.9a-b: (a) Contour of drug concentration along the length of the geometry (x-coordinate) (b) Exponential Decay of Drug Concentration Eluted along the length of the geometry (x-coordinate) at 37°C.



Error Bars Show 95% Confidence Interval of the Mean.

Figure 5.10: Comparing the Experimental and Simulation: (a) Models and Experiment along the Geometry Length from the implanted device boundary at 96 hrs. (b) Percentage of Drug Release from an Implantable Biomedical Device into a Scaffold.

Table 5.1: P(NIPA)-based Scaffolds Configuration and Compositions.

Scaffold Code	PNIPA (g)	AM (g)	APS (g)	MBA (mg)	TEMED (μ l)	Deionized Water (ml)
A	15.56	–	0.598	0.244	100	140
B	14.78	0.78	0.598	0.244	200	140
C	14.00	1.56	0.598	0.244	300	140
D	13.22	2.34	0.598	0.244	400	140

Table 5.2: Transport Properties of P(NIPA)-based Scaffolds.

Scaffold code	Average porosity (ϵ)	Average Tortuosity (λ)	Diffusion Coefficient at 37°C (m^2/s) x 10^{-10}
A	0.34	5.81	8.11
B	0.53	7.27	6.24
C	0.58	7.64	4.97
D	0.67	8.21	9.29

^{PNIPA}N-Isopropyl acrylamide, ^{AM}Acrylamide, ^{BMA}ButylMethylacrylate, ^{APS}Amonium persulfate, ^{TEMED} N,N,N',N'-Tetramethylethylenediamine; Gel codes; ^APNIPA Homopolymer (100 mol% of PNIPA), ^BPNIPA-co-AM- (95-5 mol%), ^CPNIPA-co-AM-(90-10 mol%), ^DPNIPA-co-AM-(85-15 mol%).

Table 5.3: Diffusive and Permeability Data.

Parameter	Cavity	Remnant Tumor	Normal Tissue
Volume fraction of interstitial/Extracellular space	1	0.35	0.2 [19]
Volume fraction of intracellular space	0	0.55	0.65 [19]
Blood vessel exchange area (m^{-1})	N/A	20,000	7,000
Darcy's permeability (m^2)	1×10^{-11}	6.4×10^{-14}	6.4×10^{-15}
Rate of fluid gain from the capillary blood flow per unit volume of tissue	N/A	4.4×10^{-5}	2.8×10^{-7}
Diffusion coefficient in interstitial phase (m^2/s)		9.0×10^{-10} [22]	
interstitial osmotic pressure (Pa)	N/A	1,110	740
Viscosity of the interstitial fluid (Pa-s)			
Density of fluid (kg/m^3)		1,000	

6.0 Pulsated Drug Release from PLGA-Based composites for Extended Delivery

6.1.0 Introduction

There has been higher incidence of cancer in recent years causing high cancer mortality rates across the globe [1]. In 2008, the World Health Organization (WHO) estimated all global deaths arising from cancer to be up to 84 million [2]. It was reported that cancers also gives rise to more deaths than death expected from HIV/AIDS, tuberculosis and malaria all combined [3]. Early detection and treatment are crucial for successful management of cancer [4-7]. However, it is difficult to detect breast cancer at their early stages. This causes late detection and chances of treatment becomes almost unsuccessful especially when the cancer has reached a metastasis stage, before detection.

Meanwhile, reports have shown that the current treatment methods such as bulk systemic chemotherapy [8-11] and radiotherapy [12, 13] have severe side effects. Drug release kinetics as well as the rates of polymer degradation could be used to enhance controlled release of drugs. Localized drug delivery has been fairly successful and gained wider acceptance.

The major goal of localized administration of drugs to tumor-bearing organs is to achieve high drug concentration over time in tumors while sparing the host tissues from drug toxicity. Localized chemotherapy has a greater potential to reach tumor cells. Anticancer drugs may have higher tumor selectivity, while surgery does not offer tumor cell selectivity.

Since the last decade, there have been increasing efforts to develop biodegradable polymers for drug delivery systems [14, 15, 16]. These have flourished because such systems do not require surgical removal, once the drug supply is depleted.

Natural and synthetic polymers are mostly used for drug delivery and they have minimal effect on the biological systems after they have been integrated in the body. *In vivo* degradation is at a well-defined rate, while the degradation products are nontoxic and this has

been long explored to yield readily excreted degradation products [17].

Biodegradable polymers studied in recent times belongs to the polyester family: poly(lactic-acid) (PLA) and poly(glycolic-acid) (PGA). PLA, PGA, and their copolymers (i.e. PLGA) have countless clinical applications [18,19]. PLGA can also be copolymerized with other monomers such as polyethylene glycol for biomedical applications [20-22].

Biodegradable microparticles have also been formulated from PLAs or PLGAs for controlled drug release [23]. PLAs or PLGAs have practicality shown greater biocompatibility and biodegradability [24, 25]. By altering a number of factors such as polymer composition, molecular weight, samples size and surface characteristics, well-defined degradation rates can be achieve to control the release of encapsulated therapeutic agents [26].

The major challenges observed in degradable drug delivery systems are based on a sustained and controlled release of encapsulated agents to achieve long release periods required in cancer treatment. The objective of this work is to develop drug encapsulated PLGA minirods for controlled and sustain drug delivery.

6.2.0 Materials and Methods.

6.2.1 Materials

PLGA with different ratios of lactide to glycolide compositions and molecular weights (50:50 (M_w = 30,000-60,000), 65:35 (M_w = 40,000-75,000), 75:25 (M_w = 66,000-107,000), 85:15 (M_w = 75,000-120,000)) were obtained from Sigma Aldrich (St Louis, MO, USA). The drug paclitaxelTM (anti-proliferative/anti-restenotic/anti-cancer drug) was obtained from LC Laboratories (Woburn, MA, USA), while the prodigiosin (PG) (anticancer drug) was obtained from Sheda Science and Technology Complex (Genetic and Biotechnology laboratory, Abuja, Nigeria). PT was dissolved with dimethyl sulfoxide (CH₃)₂SO (DMSO)

that was purchased from BDH Chemicals (Poole Dorset, England). For the dissolution of PLGAs, dichloromethane (DCM) was obtained from BDH Chemicals (Poole Dorset, England). A binder, polyvinylpyrrolidone (PVP) was also obtained from BDH Chemicals (Poole Dorset, England).

6.2.2 Preparation of Drug Concentrations

Drug samples were weighed with an analytical balance (Mettler AE 100, Mettler-Toledo Ltd., Leicester, UK). 0.1 g of PG was initially dissolved with 2 ml methanol (100%) to give a stock solution of 5 mg/ml. Then, the 5 mg/ml solution was adjusted with PBS to give a final concentration of 2.5 mg/ml. PT drug solutions were similarly prepared. A summary of the drug/sample dissolution is presented in Table 6.1A. However, the initial dissolution of PT was done in 2 ml DMSO, respectively, while 38 ml PBS was used to adjust the stock solution to obtain final concentrations of 2.5 mg/ml. The ratios of DMSO: PBS and methanol:PBS were each 5:95 v/v% in the final drug solutions. The reactions of DMSO with PBS, as well as methanol with PBS, produced turbid solutions. These were filtered twice using Whatman filter paper (number 1) to remove debris.

6.2.3 Dissolution of Polymers

Degradable devices were formed from different polymer ratios as presented above; 50:50 65:35, 75:25 and 85:15. In the first case, 1 g of PLA:PGA (50:50) was dissolved with 1 ml DCM in an airtight plastic container to prevent the DCM from evaporating because of its volatility) for 15 min. Subsequently, the samples were gently stirred with a spatula to form a homogeneous polymer blend. This experiment was then repeated for other PLA:PGA compositions (i.e. 65:35, 75:25 and 85:15).

6.2.4 Formation of PLGA-Based Mini-rods

In forming the degradable mini-rods, 1 ml of drug solutions (2.5 mg/ml of PG or PT) were separately transferred to the PLGA polymer-blends. These mixtures comprised of PLGA-PG and PLGA-PT formulations. The polymer-drugs mixtures were then stirred for homogeneity, while, 1 ml of PVP stock solution (0.2 g/ml of PVP:DCM was used as a cross-linker/binder) was finally added to the polymer-drugs mixtures (PLGA-PG/PLGA-PT) in separate hermetically sealed containers. These were also blended vigorously to form PLGA-PG-PVP or PLGA-PT-PVP. Samples were immediately casted into fabricated cylindrical molds, while casted samples were compressed with 250 N/m^2 on the opposite side of the molds to form devices with diameter of 5 mm and 6 mm thick. Summary of the percentage ratios of polymer-drug-PVP mini-rods formulation is summarized in [Table 6.1B](#). The samples were then dried at room temperature (29°C) for 12 hrs with no immediate heat before they were remolded. They were subsequently dried at 40°C under vacuum for 2 hrs (GALVAC vacuum oven, LTE Scientific Ltd., Greenfield State) set at -24 mm Hg equivalent for 24 hrs to ensure the DCM evaporates and also to provide complete elimination of moisture. This experiment was repeated for other copolymers of PLGA (65:35, 75:25 and 85:15) where PG and PT were used as drugs agents to form different devices.

6.2.3 Characterization of Samples

Prior to optical imaging, samples were washed thoroughly with distilled water to remove soluble products, salts or other impurities and then dried under vacuum conditions until a constant weight was achieved. Proscope HR 640 (Bodelin Technologies, Oswego, USA) equipment and personal scanning electron microscope (PSEM) (ASPEX 3020, ASPEX Corporation, Oregon, USA) were used to observe and monitor structural changes during degradation process.

Samples were clearly viewed from their surfaces, while Proscope image analyzing software (HR 640, Bodelin Technologies, Oswego, USA) was employed to scale and identify features observed on the micrographs.

The experiment was followed by UV-Vis spectrophotometric (UV-Vis) measurements of drugs released at a wavelength of 535 nm for PLGA-PG samples and 210 nm for PLGA-PT samples using a UV-Vis spectrophotometer (CECIL 7500 Series, Buck Scientific Inc., East Norwalk, USA).

Thermal analyses were carried out with DSC equipment (500A Series, Sino. 20130626094, Japan). The glass transition temperatures (T_g), crystallization temperatures (T_c), as well as the melting temperatures (T_m) were investigated. 5 mg of each sample of either PLGA-PG/PLGA-PT, were placed in a small aluminum pan and led into the DSC machine. Samples were heated at 10°C/min from room temperature to 200°C with nitrogen supplied at a flow rate of 50 ml/min. The flow of nitrogen was maintained to establish an oxygen free atmosphere. Thermal properties were then obtained after complete scans.

6.2.4.0 Degradation and Drug Release

6.2.4.1 Polymer Degradation

Initial weights of samples were determined before they were incubated in glass test tubes with each containing 5 ml PBS (pH 7.4). Drug release and hydrolytic degradation were simultaneously carried out in a digital incubator shaker (Innova 4300, New Brunswick Company Inc., NJ, USA) set at 60 revolution per minute (rpm) with temperature at 37°C. This environment assumed physiological conditions for localized drug delivery. The polymer degradation was characterized by weight loss when soaked in PBS. The weight change was observed using:

$$\frac{M_t}{M_i} = \sqrt{t} \quad (6.1)$$

where M_t is the mass of the polymer/sampler at time t , M_i is the initial mass of the sample, and t is the degradation time. It was ensured that, the samples were removed from the PBS each time measurements were to be taken and then placed on a filter paper. They were then dried under vacuum conditions until constant masses on a balance. This was done to avoid residual moisture in the samples during weighing. The rates of polymer erosions were determined from the absorption of PBS over 2-5 months for the different samples:

$$\frac{dM}{dt} = -k \quad (6.2)$$

where M is the change in polymer mass at time, t and k is the kinetic rate constant of the polymer degradation.

6.2.4.2 Determination of Drug Release

The release of incorporated therapeutics agents were observed via UV-Vis measurements over regular time interval. The 5 ml PBS were changed regularly at 7 days interval until the samples finally degraded. The amount of drugs released was examined with the UV-Vis. Moreover, the rate of drug released was estimated from the reaction kinetics:

$$\frac{dC}{dt} = -kC^n \quad (6.3)$$

where k is the reaction rate constant, n is the order of reaction and C is the concentration of drug release at time t . The order of reaction was estimated by plotting a graph of $\ln C$ versus degradation time. This gives a linear relation:

$$\ln C = \ln C_0 - kt \quad (6.4a)$$

where C is the concentration of drug released at time, t , k is the rate of reaction and t is the

drug release time. For a first order drug release, $n = 1$ and at $t = 0$, $C = C_0$. This gives an exponential time dependent of drug concentration and equation (6.4a) becomes:

$$C(t) = C_0 e^{-kt} \quad (6.4b)$$

The drug loading content (DL %) in addition to the drug encapsulation efficiency (DEE %) were given, respectively by:

$$DL \% = W_d / (W_d + W_p) \times 100 \quad (6.5a)$$

$$DEE \% = (W_d / W_i) \times 100 \quad (6.5b)$$

where W_d is the amount of drug loaded, W_i is the initial mass of drug and W_p is the mass of the polymer incorporated.

The effect of the average molecular weight change due to the presents of PBS/moiture causes hydrolytic degradation as presented [27]:

$$M'_n = \frac{M_n}{[1+x(M_n/1800)]} \quad (6.6)$$

where M_n is the initial average molecular weight of the sample, M'_n is the average molecular weight after reaction with PBS and x is the moisture content (weight %).

6.2.4.3 Estimation of Fluid Diffusion in PLGA

Time-dependent power law equation was earlier on developed by Peppas and co-workers [28] for the modeling of drug release from polymeric materials. This is given by:

$$\frac{m_t}{m_i} = 4 \left(\frac{D}{\pi \delta^2} \right) t^n = kt^n \quad (6.7)$$

where $\frac{m_t}{m_i}$ is the fraction of drug release, k is the geometric constant of the release system, n

is the drug release exponent, depicting the release mechanism, m_i is the initial mass of the sample prior to its immersion in PBS, m_t is the mass of the sample at time, t during incubation at regular interval, δ is the thickness/height of the sample and D is the coefficient of diffusion. Equation (6.7) was applied to systems in which diffusion occurred within the polymeric networks [28]. The constants k and n were obtained from the linear form of equation (6.7). This gives:

$$\ln \left(\frac{m_t}{m_i} \right) = \ln k + n \ln t \quad (6.8)$$

k and n were respectively, obtained from the intercepts and slopes of the plots, $\ln(m_t/m_i)$ versus $\ln t$. The intercepts on the $\ln(m_t/m_i)$ were equal to $\ln(k)$. The diffusion coefficients, D_s , were obtained from:

$$D_s = \frac{k\pi\delta^2}{4} \quad (6.9)$$

where k , is the geometric constant of the release system, π is the mathematical constant reflecting the ratio of a circle circumference to its diameter and δ is the thickness of the sample, respectively.

6.3.0 Results and Discussion

6.3.1 Characterization and Morphological Changes

The standard curves for drug released profiles from PLGA-based minirods are presented (Figs. 6.1a-6.1b). The figures all indicated similar relationship between the amounts of drug release versus absorbance from PG and PT encapsulated into PLGA. The relationship between concentration and absorbance showed a gradient of 2.48×10^{-6} ($\mu\text{g}/\text{ml}\cdot\text{au}$).

The proscopie images revealed the microstructures of the degradable PLGA-Based minirods (Figs. 6.2a-6.2c). The microstructures on the first day prior to degradation have shown uniform mixing of drug and polymer with no distinct phases of the two. This indicated that the dissolution method stands a better chance to incorporate polymer and drug for degradable systems made of PLGA-based polymers. The images taken on the 36th and 45th days have shown evidence of surface erosion as well as bulk degradation. There exist a change in color due to the removal of drugs and degradable products. This was more pronounced in (Fig. 6.2b). PLGA (50:50) indicated the presences of polymer chains where the amorphous region absorbs moisture and degraded faster than the crystalline regimes. The other images of PLGA (65:35 PG/75:25 PT) indicated some kind of chain rapture as water penetrates more into the polymer matrix.

Generally, the optical images revealed microfragments of the polymers as degradation time increases. The samples loaded with PT showed brittleness (Fig. 6.2c) as they easily break apart as the incubation time (duration of degradation) extent in PBS especially toward 45 days and above. Despite the long range release of drugs from PLGA with PT loaded as compared to PLGA, the samples containing PT were hard and brittle. This was more pronounced in PLGA (75:25) loaded with PT. They easily fracture and loose the geometry or shape when hydrolysis intensifies.

Porosities of samples were characterized with Gwyddion software package (version 2.40). SEM images of samples are presented (Fig. 6.2d-6.2f). PLGA samples with ratio; 65:35 (loaded with PT) (Fig. 6.2d, left) prior to incubation has pore sizes ranging from 1.3-20 μm (with a mean pore size of 4.75 μm), while PLGA (75:25) loaded with PT (Fig. 6.2e, left) has pore sizes between 0.4-14.8 μm (with a mean pore size of 2.54 μm), whereas PLGA ratio 85:15 loaded with PT (Fig. 6.2f, left) has pores sizes ranging from 0.5-14.80 μm (with a mean pore size of 4.57 μm).

Surface and bulk erosion revealed different pore sizes beginning from the 19th day of incubation in PBS with clear indications of new smaller pores. Microspores were observed ranging from 0.5-12.7 μm (with a mean pore size of 3.19 μm) for PLGA ratio 65:35 loaded with PT (Fig. 6.2d, right), while PLGA (75:25) loaded with PT (Fig. 6.2e, right) revealed pore sizes ranging from 0.2-16.2 μm (with an average pore size of 3.65 μm) and finally, PLGA (85:15) loaded with PT (Fig. 6.2f, right) gave pore sizes between 0.5-14.80 μm (with an average pore size of 4.57 μm). PLGAs samples loaded with PG gave similar results with no significant difference in pore sizes.

These results indicate dominants of micropores with an increase in degradation/incubation time. The porosities of the scaffolds within the internal core of the samples were much greater than that at their surfaces. Though samples loaded with PG and PT revealed more pores structures, the samples loaded with PT showed greater dominance of microcracks as compared to samples loaded with PG. Complete evaporation of DCM/DMSO ended up with a porous structure.

Differents in molecular weights, polymer ratio and the type of drug loaded into polymer, surface erosion and bulk degradation by hydrolysis were responsible for polymer degradation under the *in vivo* conditions at 37°C under a mechanical agitation (60 rpm) in a PBS at pH 7.4. These conditions were considered to simulate physiological conditions. Both the optical and SEM images revealed heterogeneous networks of the polymer matrix which contributes to an autocatalyzed bulk degradation process.

6.3.2 Water Absorption and Mass Loss

Determination of fluid uptake gives an indication of the hydrophilicity/hydrophobicity nature of the PLGA-drug loaded polymer materials and hence, their ability to be degraded by hydrolysis. The rates at which the PBS penetrates into the interior part of the PLGA-based

minirods were very slow (it took few days from day 1-5 and in some case 1-10 days). This gave an understanding about the hydrophobic nature of PLGA-based minirods.

Hence the uptake of PBS was found to increase with the degradation time due to an increase in the permeability of PLGA matrix since porous structures were obtained with porosity becoming more pronounced as a result of degradation products release over time (Figs. 6.2a, 6.2b, 6.2c-6.2e).

An increase in the content of lactide in PLGA-based minirods generally decreased the PBS absorption capacity. It therefore required longer time in water or aqueous environment to breaks the covalent bonds that will improve upon the maximum release of drugs.

6.3.3 Drug Diffusion and Reaction Rates

The results established a first order reaction release profiles which gave an exponential time dependence of drug concentration. The half-life of drug was estimated from the gradient of $\ln C$ versus time as shown (Figs. 6.3a-6.3d). This gives the results as summarized in table 6.2.

The cumulative drug released profiles for PLGA-based minirods are presented (Figs. 6.4a-6.4b) for samples loaded with PG and PT, respectively. The release rates have clearly indicated an initial burst from the polymer matrix. This is also necessary to meet the initial concentration required for therapeutic treatment. However, the release rates were much slower for PLGA (85:15) (Fig. 6.4a) than for the other polymer ratios. The release rates shows that samples incorporated with PG will easily degrade within the 50-100 days as compared to PT loaded which lasted between 100-140 days.

Drug release versus mass loss as a result of polymer degradation at 37°C in PBS at pH 7.4 is presented (Figs. 6.5a-6.5d). These results indicated that the release time is clearly

shorter than the polymer half-life. However, the result for PLGA ratio 50:50 (Fig. 6.5a) has a closer duration of drug release as compared to the polymer half-life.

There were initial exponential decays in drug concentrations with incubation time. However, multi-pulses of drug release profiles were observed over time (Fig. 6.5a-6.5d). This is sometimes preferable to continuous release of drug, which may lead to downregulation of receptors or even development of drug resistance [29]. The results (Fig. 6.5a-6.5d) show that, a novel device can be designed or fabricated with programmed delivery to achieve pulsatile drug delivery over an extended time. Such devices may ensure a programmed off period followed by a prompt and transient drug release in a cycle until the device is completely degraded [29]. Moreover, the release of PG from PLGA-based composites has shown the possibility of fabricating devices with multi-pulse delivery because of its tunable properties.

Diffusion and degradation represents the mechanisms of drug release from PLGA-based minirods. Degradation was associated with water penetration into the interior areas of the PLGAs which was later followed by the hydrolysis of the functional groups and the absorption of water molecules. Further hydrolysis then led to the cleavage of covalent bonds. This causes both surface and bulk erosion.

The half-lives for the different degradable systems are summarized in Table 6.2. The kinetic rate constant (k) for degradation corresponded to the time dependent of polymer mass loss. The plots of mass loss versus time (for PLGA-PG samples) gave an exponential decay (Fig. 6.6a) for the various samples. The k values obtained are also summarized in Table 6.2.

Moreover, the result in Figure (6.6b) has shown an increase in polymer half-life as the degradation rate declined. The degradation rate was quick for the PLGA 50:50 ratio, follow by 65:35, 75:25 and 85:15, respectively. This makes one polymer to degrade more rapidly than the other. The mass loss for the PLGA-PG minirods approached almost 90%; at 170

days for the 85:15 ratio, 120 days for 75:25 ratio, 70 days for the 65:35 and finally, 45 days for the 50:50 ratio.

The mechanism controlling the degradation of PLGA minirods was basically dominated by autocatalyzed bulk degradation within half of the degradation time, while surface erosion subsequently sets in via the hydrolysis of the ester linkages. The crystallinity and intake of PBS including other intrinsic properties affects the rates of the *in vitro* degradation of the polymer. However, the heterogeneous network of the polymer matrix contributes to autocatalyzed bulk degradation. These results provide important insights for the design and selection of biodegradable polymers for biomedical applications.

Summary of drug encapsulation efficiency (DEE) as well as drug loading content are presented in [Table 6.3](#) for PLGA-based polymers. The DEE ranges from 43-92% when PG was encapsulated as compared to the 50-89% DEE when PT was encapsulated. The DL for PLGA encapsulated with PG minirods varied from 2.53-5.43%, while the DL of 3.77-4.82% was reported when PT was encapsulated.

The diffusion coefficients for the initial burst were obtained from equation (6.9) following figure (6.7). The initial diffusion rates for samples encapsulated with PG were between $14.77\text{-}25.11 \times 10^{-6} \text{ m}^2/\text{s}$, while the case for samples encapsulated with PT were also between $2.00\text{-}22.70 \times 10^{-6} \text{ m}^2/\text{s}$. These are summarized in [Table 6.4](#).

6.3.4 Thermal Analysis

The thermal analysis data obtained in the current work includes the; T_g , T_c and T_m . Typical DSC curve for PLA:PGA (50:50) is presented ([Fig. 6.9a](#)). Thermal properties of the polymers decreased drastically with increased in hydrolysis time due to molecular weight loss.

The T_g shows a point at which the mechanical properties of the polymer begins to change from a rubber-like state to a glassy state. Below the T_g , there is limited polymer flow, while above the glass transition more motion occurs. The transition in polymers doesn't suddenly occur but takes place within a range of temperature. For instance the graph for PLGA (50:50) for 24 days of degradation gave T_g within the range of 52.55-73.53°C with the T_g obtained from the middle of the curve (Fig. 6.9a) to be 63.56°C. Thus, the values of the T_{gs} were obtained from the midpoint of the inclined part of the DSC curve.

Above the T_g , the polymer chains possess remarkable mobility. The chains thus, twist and turn, with no change in position until they gain enough energy as temperature gradually increased. The energy gained allows the chains to move into a very ordered manner (crystalline arrangement). During the crystalline arrangement process, heat is given off to the system. T_c was an exothermic process indicated by a lower point of the dip (Fig. 6.9a).

The T_m was represented by an endothermic transition upon which the polymer begins to melt due to heat absorption. The T_m involves a first order transition whereby intermolecular bonds absorb heat energy and the polymer chains then become weak and more relaxed. At this state, the material changes from a solid phase to a liquid phase. Moreover, the samples loaded with PG experienced low melting temperatures as compared to samples loaded with PT. The polymer degradation decreases the thermal properties with increasing incubation period (Fig. 9b).

6.4 Implications

Polymer degradation rates and drug release profiles differed greatly though the same polymer matrix and drug loading (8% by weight) were considered. This implies that, in the design of a biodegradable implant from PLGA for drug delivery device, the amount of drug as well as the type of drug loaded affects drug release and device degradation as expected.

The result on degradation rates and drug release kinetics can be used to design a multimodal device incorporated with different polymer ratios with a desired cancer drugs, while controlling the amount of drug loaded.

The release of PG from PLGA-based composites has shown the possibility of fabricating devices with multi-pulse delivery over an extended time because of its tunable properties. Understanding of polymer erosion and the mechanism of drug release from PLGA-based minirods can be used to design a multimodal device to provide desirable and more controlled drug release kinetics. Moreover, suitable biodegradable polyester with controlled degradation and drug release rate could be selected for controlled drug delivery.

However, thorough studies of biodegradation and mechanical change of polyesters (PLGA) will provide significant understanding into the interactions between polyesters and the biological environments. The size and shape of the implant could also be modeled to achieve the desired treatment model. These are clearly some of the challenges for future work.

6.5 Conclusion

Drug release kinetics as well as polymer degradation mechanisms were studied to provide the basis for the design of implantable biodegradable systems for the localized treatment of cancer. Hydrolysis begins with water penetrating deeply into the interior areas of the polymer. The water molecules caused the functional groups in the polymer chains to hydrolyze and absorb the PBS by a natural diffusion and convection resulting in the cleavage of covalent bonds. Release of degradable products led to mass loss which is a characteristic for polymer erosion. The extent of degradation was determined by the percentage weight loss.

Despite the long range release of drugs from PLGA-PT (paclitaxel loaded) as compared to PLGA-PG (prodigiosin loaded), the samples containing PT were hard and brittle. They easily fracture and lose the geometry or shape. However, the release and degradation of PLGA loaded with PG was faster. The samples containing PG were soft and flexible and could be seen as good scaffolds for implantable devices.

The percentage release of PG from PLGAs ratios; 50:50, 65:35, 75:25, 85:15 gave cumulative releases of 91, 96, 92 and 93.5 %, respectively. On the other hand, the percentage release of PLGAs 65:35, 75:25, 85:15 loaded with PT were 84, 98 and 94, respectively. The PLGA-based minirods revealed distinct structural changes with different degradation rates during the *in vitro* experiments. These results provide important insights for the design and selection of biodegradable polymers for biomedical applications.

6.6 Bibliography

- [1] A. Alwan. Global Status Report on Noncommunicable Diseases in 2010. Geneva, Switzerland: World Health Organization (2011) 164.
- [2] J. Ferlay, H. R. Shin, F. Bray, D. Forman, C. D. Mathers, D. M. Parkin. Estimates of Worldwide Burden of Cancer in 2008: GLOBOCAN 2008. *International Journal of Cancer*. 127 (2010) 2893-2917.
- [3] D. C. Mathers, D. Loncar. Updated Projections of Global Mortality and Burden of Disease, 2002-2030; Data Sources, Methods and Results. World Health Organization. (2005) 6.
- [4] J. P. Borgstede, B. M. Bagrosky. Early Diagnosis and Treatment of Cancer Series: Breast Cancer: Screening of High-Risk Patients. Philadelphia, PA, United States of America, Saunders Elsevier. (2011) 141-149.
- [5] E. D. Pisano, C. Gatsonis, E. Hendrick, M. Yaffe, J. K. Baum, S. Acharyya, E. F. Conant, L. L. Fajardo, L. Bassett, C. D'Orsi, R. Jong and M. Rebner. Diagnostic Performance of Digital Versus Film Mammography for Breast-cancer Screening. *N Engl. J. Med.* 353 (2005) 1773-1783.
- [6] D. Saslow, C. Boetes, W. Burke, S. Harms, M. O. Leach, C. D. Lehman, E. Morris, E. Pisano, M. Schnall, S. Sener, R. A. Smith, E. Warner, M. Yaffe, K. S. Adrews, C. A. Russell. American Cancer Society guidelines for breast screening with MRI as an adjunct to mammography. *CA Cancer J Clin.* 57 (2007) 75-89.
- [7] R. A. Smith, D. Saslow, K. A. Sawyer, W. Burke, M. E. Costanza, W. P. Evans III, R. S. Foster, E. Hendrick, H. J. Eyre and S. Sener. American Cancer Society Guidelines for Breast Cancer Screening. *CA Cancer J Clin.* 53 (2003) 141-169.

- [8] N. David, W. D. Mark, The Development and Testing of a New Temperature-sensitive Drug Delivery System for the Treatment of Solid Tumors. *Advanced Drug Delivery Reviews*, 53 (2001) 285-305.
- [9] B. Hildebrandt, P. Wust in: W.P. Ceelen, *Peritoneal Carcinomatosis: A Multidisciplinary Approach*, Springer, New York, 2007, p185.
- [10] Y. Oni, C. Theriault, A.V. Hoek, W. O. Soboyejo, Effects of Temperature on Diffusion from PNIPA-Based Gels in a BioMEMS Device for Localized Chemotherapy and Hyperthermia, *Mater. Sci. and Eng. C*. 31 (2011) 67-76.
- [11] Y. Oni, W.O. Soboyejo, Swelling and Diffusion of PNIPA-Based Gels for Localized Chemotherapy and Hyperthermia. *Mater. Sci. and Eng. C*. 32 (2012) 24-30.
- [12] D. Brain, R. D. Kavanagh, D. K. Brian, D. T. Robert, editors, *Stereotactic Body Radiation Therapy*. W. Lippincott, Wilkins (eds), Philadelphia, PA, USA., 2005.
- [13] J. A. Del Regato, *Radiological oncologists: the Unfolding of a Medical Specialty*. Reston (VA): Radiology Centennial. 268 (1993) 167-176.
- [14] E. Walter, K. Moelling, J. Pavlovic, H. P. Merkle, Microencapsulation of DNA using Poly(DI-Lactide-Co-Glycolide): Stability Issues and Release Characteristics; *J. Control. Release* 61 (1999) 361-374.
- [15] P. Johansen, Y. Men, H. P. Merkle, B. Gander, Revisiting PLA/PLGA Microspheres: an Analysis of their Potential in Parenteral Vaccination; *Eur. J. Pharm. Biopharm.* 50 (2000) 129-146.
- [16] C. Berkland, M. King, A. Cox, K. Kim, P. W. Pack, Precise Control of PLG Microsphere Size Provides Enhanced Control of Drug Release Rate. *J. Control. Release.* 82 (2002) 137-147.
- [17] C. Berkland, K. Kim, D.W. Pack, PLG Microsphere Size Control Drug Release Rate through Several Competing Factor. *Pharm. Res.* 20 (2003) 1055-1062.
- [18] M. Chasin, R. Langer, *Biodegradable polymers as drug delivery systems*, (1990) 231.
- [19] Y. Qiu, K. Park, Environment-sensitive hydrogels for drug delivery. *Departments of Pharmaceutics and Biomedical Engineering, Purdue University, West Lafayette. USA, Advanced Drug Delivery Reviews.* 53 (2001) 321-339.
- [20] A. G. Hughes, Nanostructure-mediated drug delivery. *Nanomedicine: Nanotechnology, Biology and Medicine.* 1 (2005) 22-30.
- [21] P. A. Gunatillake, R. Adhikari, *Biodegradable Synthetic Polymers for Tissue Engineering. European Cells and Materials.* 5 (2003) 1-16.
- [22] A. T. Metters, C. N. Bowman, K. S. Anseth, Statistical Kinetic Model for the Bulk Degradation of PLA-b-PEG-b-PLA hydrogel networks. *J. Phys. Chem. B.* 104 (2000) 7043-7049.
- [23] A. T. Metters, C. N. Bowman, A Statistical Kinetic Model for the Bulk Degradation of PLA-b-PEG-b-PLA hydrogel networks; Incorporating Network Non-idealities. *J. Phys. Chem. B.* 104 (2001) 8069-8076.
- [24] E. Behraves, A. W. Yasko, P. S. Engel, A. G. Mikos, *Synthetic Biodegradable Polymers for Orthopaedic Applications. Clin, Orthop. Relat. Res.* 367 (1999) 118-125.
- [25] E. Jr. Middleton, C. Kandaswami, T. C. Theoharide, The Effects of Plant Flavonoids on Mammalian Cells: Implications for Inflammation, Heart Disease and Cancer. *Pharmacol Rev.* 52(4) (2000) 673-751.
- [26] A. G. Pathiraja, A. Raju, *Biodegradable Synthetic Polymers for Tissue Engineering. European Cells and Materials.* 5 (2003) 1-16.
- [27] J. V. Koleske, *Blends Containing Poly(ϵ -Caprolactone) and Related Polymers*, in: R. Paul, S. Newman (eds), *Polymer Blends*, Academic press. New York, 1978, pp 369-389.

- [28] A. N. Peppas, Analysis of Fickian and Non-Fickian Drug Release from Polymers. Pharm. Acta Helv. 60 (4) (1985) 110-111.
- [29] H. K. Makadia and S. J. Siegel. Poly Lactic-co-Glycolic Acid (PLGA) as Biodegradable Controlled Drug Delivery Carrier. Polymers (Basel). 3(3) (2011) 1377-1397.

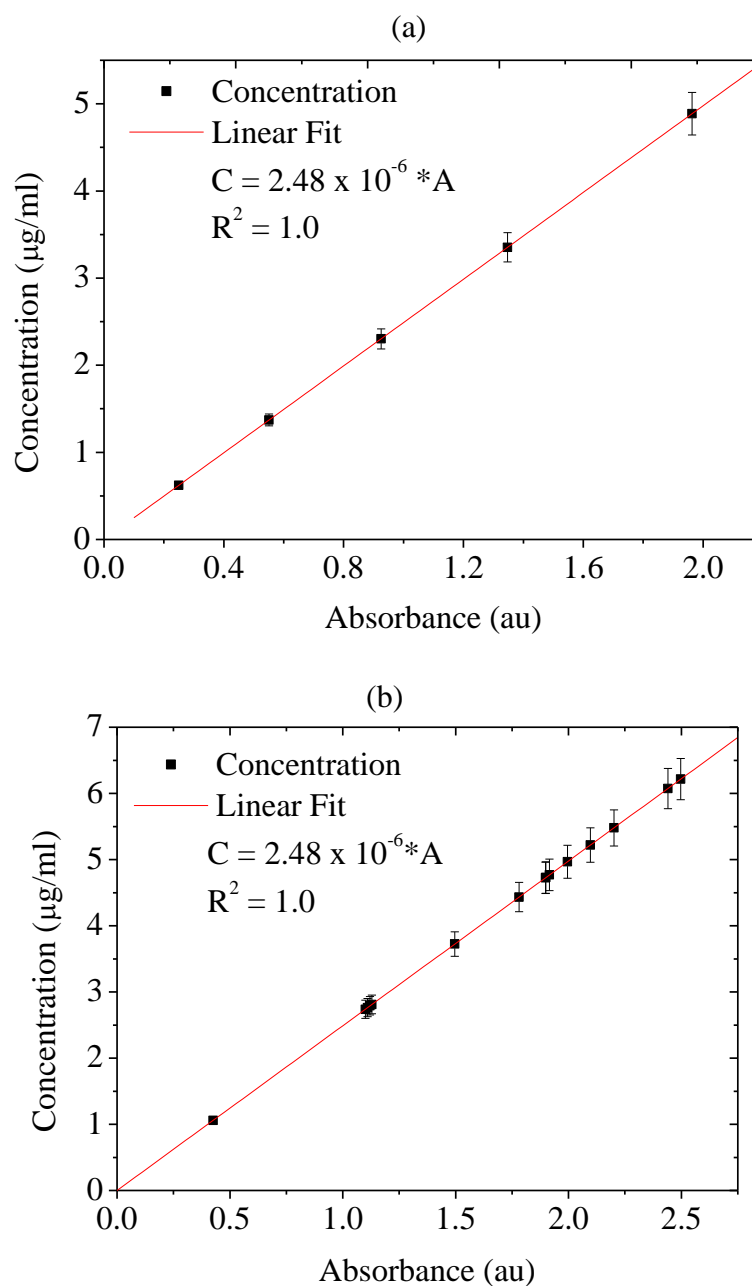


Figure 6.1: Standard Curve for Drug Released from PLGA-based Polymer (PLGA 65:35): (a) PG Released from PLGA-Based millirods and (b) PT Released from PLGA-based Millirods.

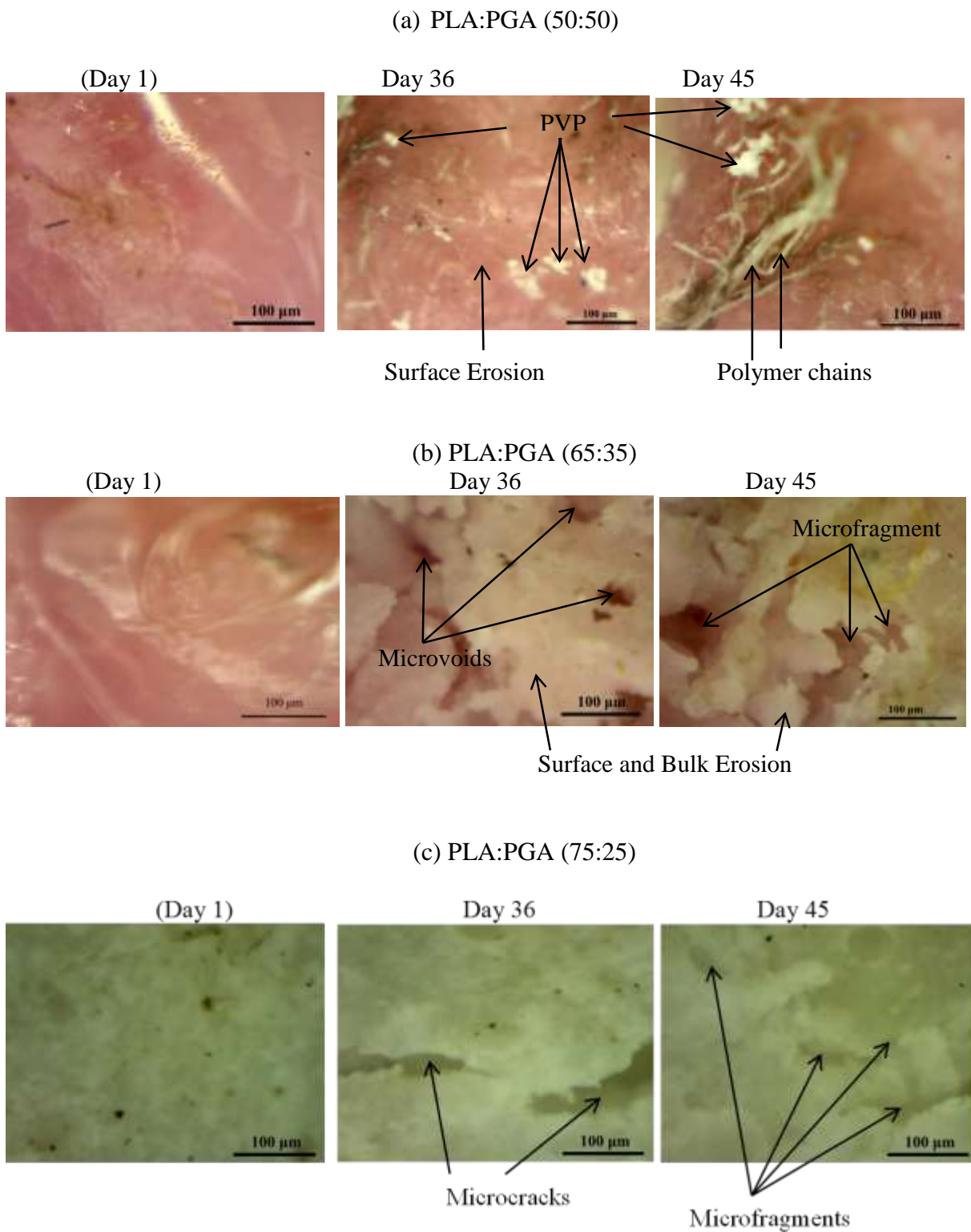


Figure 6.2a-c: Optical Images of PLA:PGA During Degradation and Drug Release at 37°C, pH 7.4, 60 rpm; (a) PLA:PGA (50:50)-Based Minirods Loaded with PG, (b) PLA:PGA (65:35)-Based Minirods Loaded with PG and (c) PLA:PGA (75:25)-Based Minirods Loaded with PT.

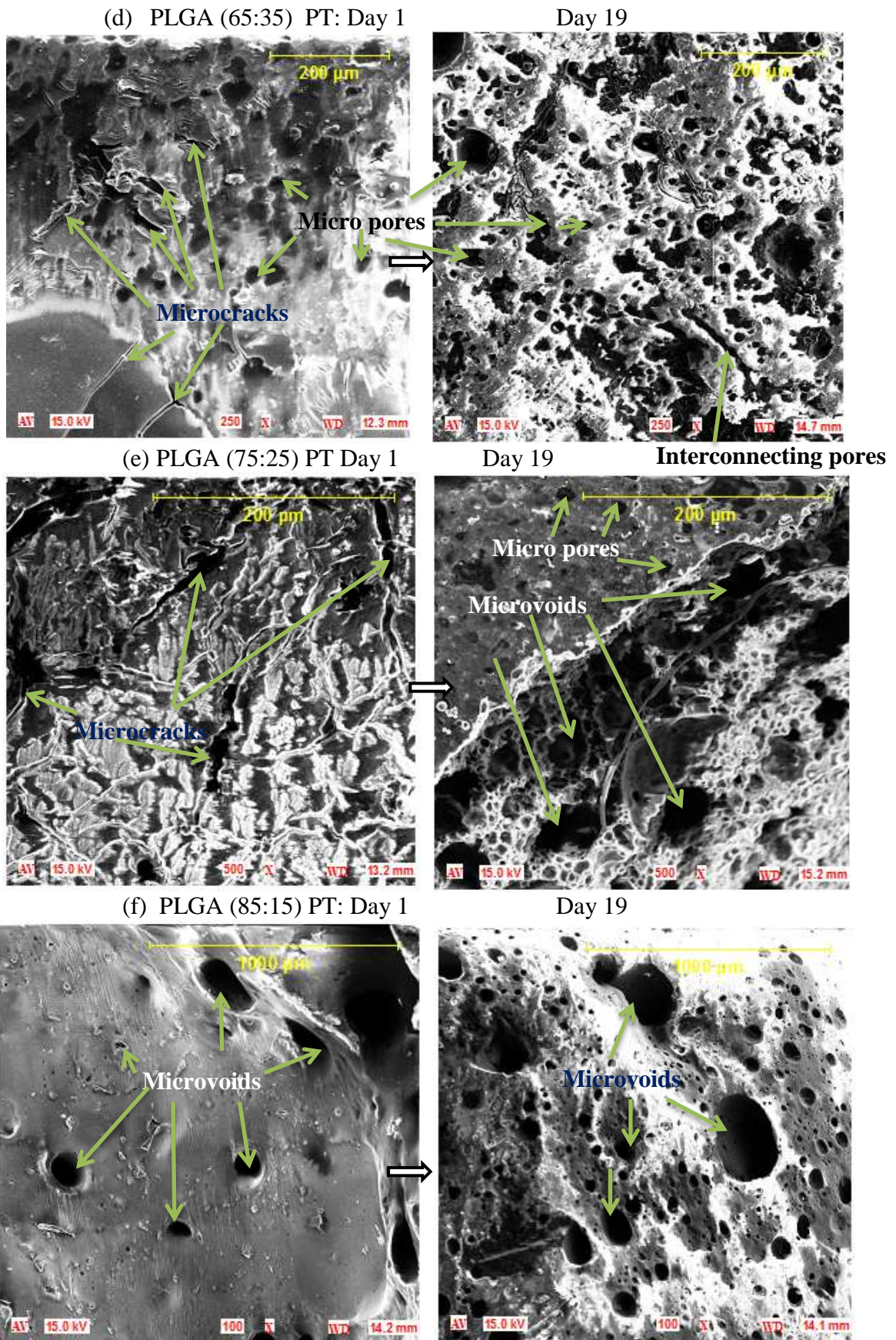


Figure 6.2 (d-f): Poros SEM Images of PLA:PGA During Degradation and Drug Release at 37°C, pH 7.4, 60 rpm Mini-rods Loaded with PT.

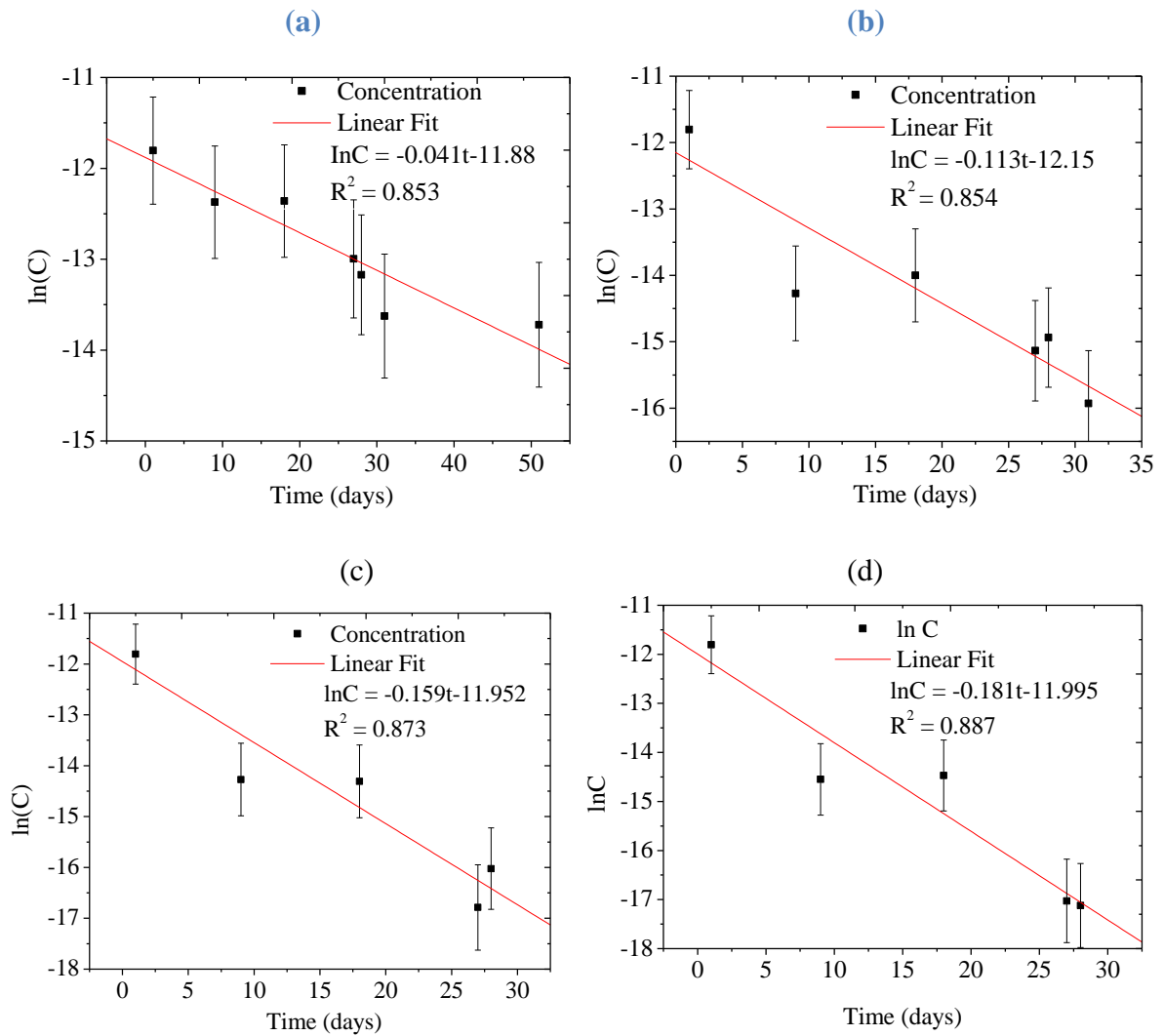


Figure 6.3: First Order Estimation of Rate Constant and Drug half-life from Drug Loaded PLGA-based Minirods: (a) PLGA (50:50)-PG, (b) PLGA (65:35)-PG, (c) PLGA (75:25)-PG and (d) PLGA (85:15)-PG.

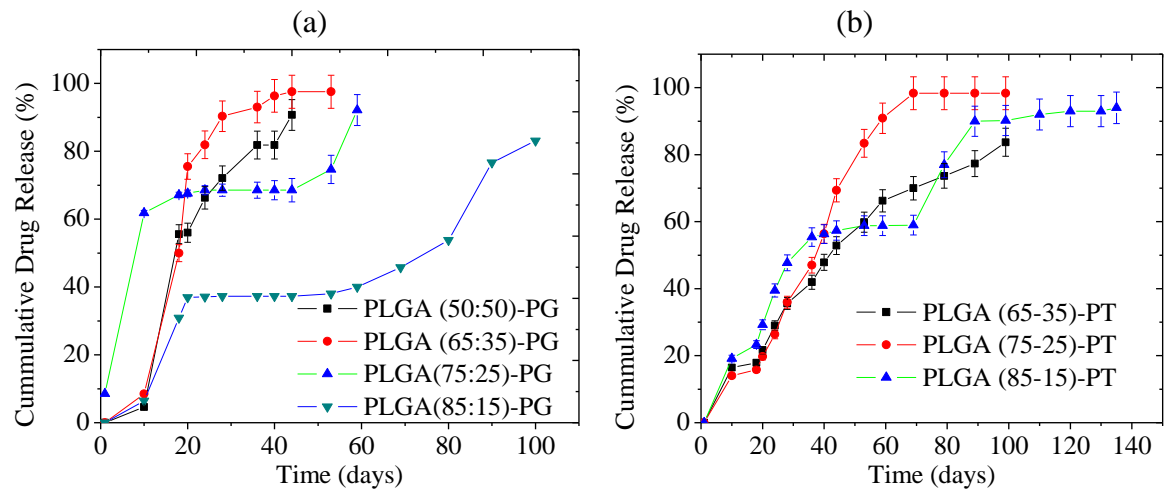


Figure 6.4: Cumulative Drug Release from PLGA, Drug-Based Minirods Incubated at 37°C, pH 7.4 and under a mechanical agitation of 60 rpm.

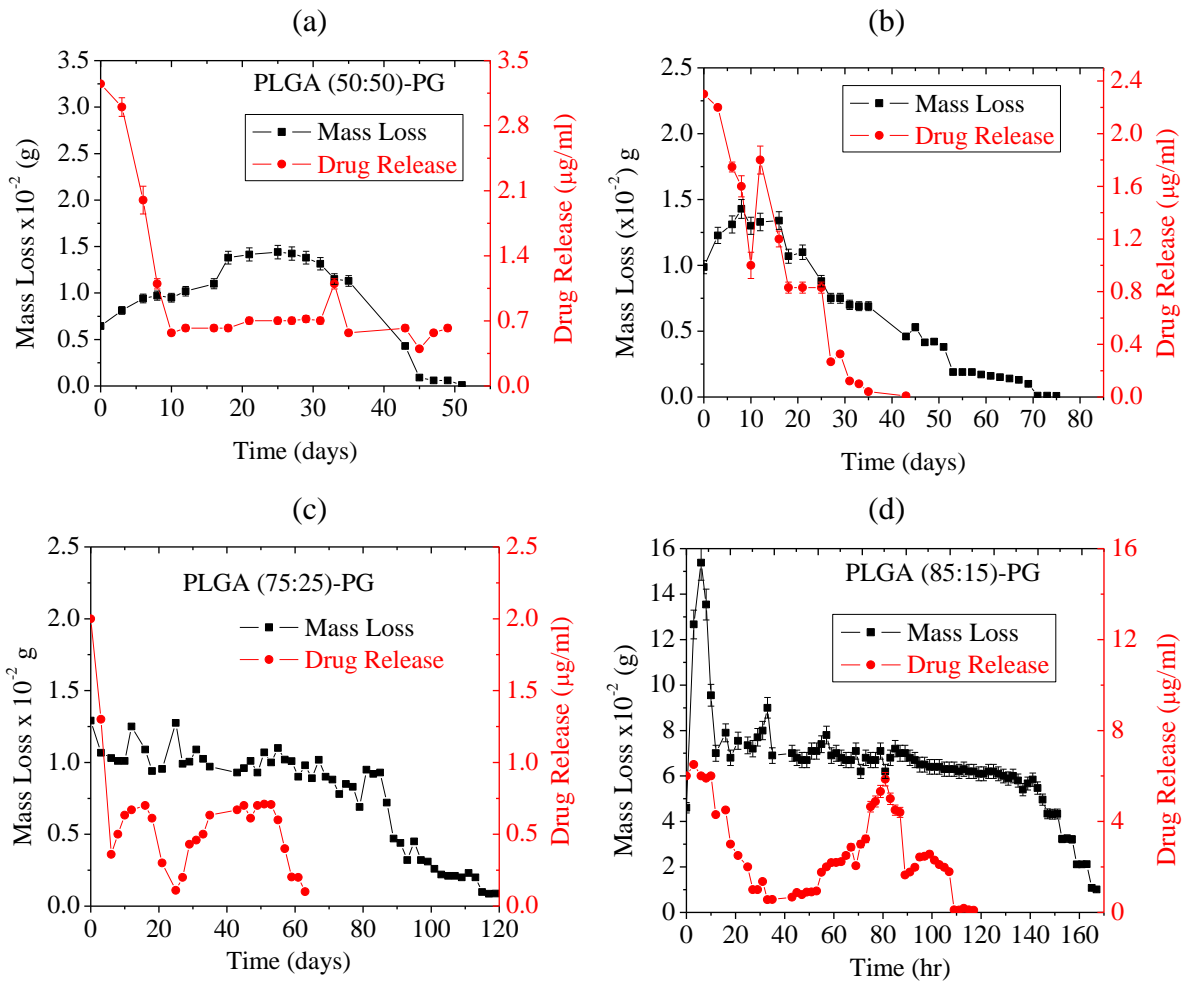


Figure 6.5: Drug Release Versus Degradation of PLGA Drug-based Minirods at 37°C, pH 7.4, 60 rpm.

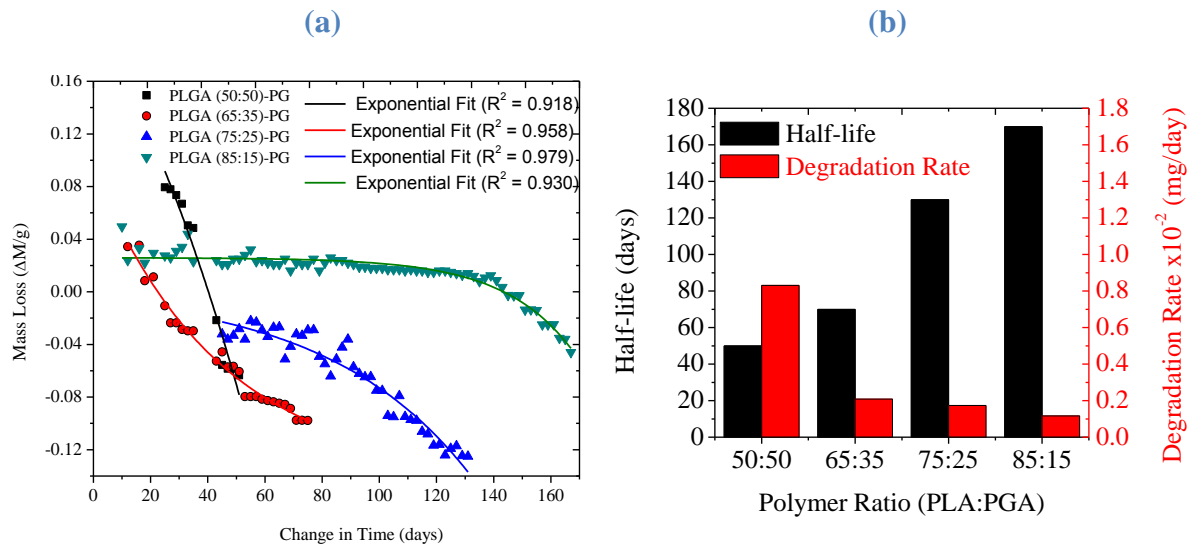


Figure 6.6: Polymer Degradation Rate: (a) Polymer Mass Loss versus Time and (b) Effect of Degradation Rate on Polymer Half-life.

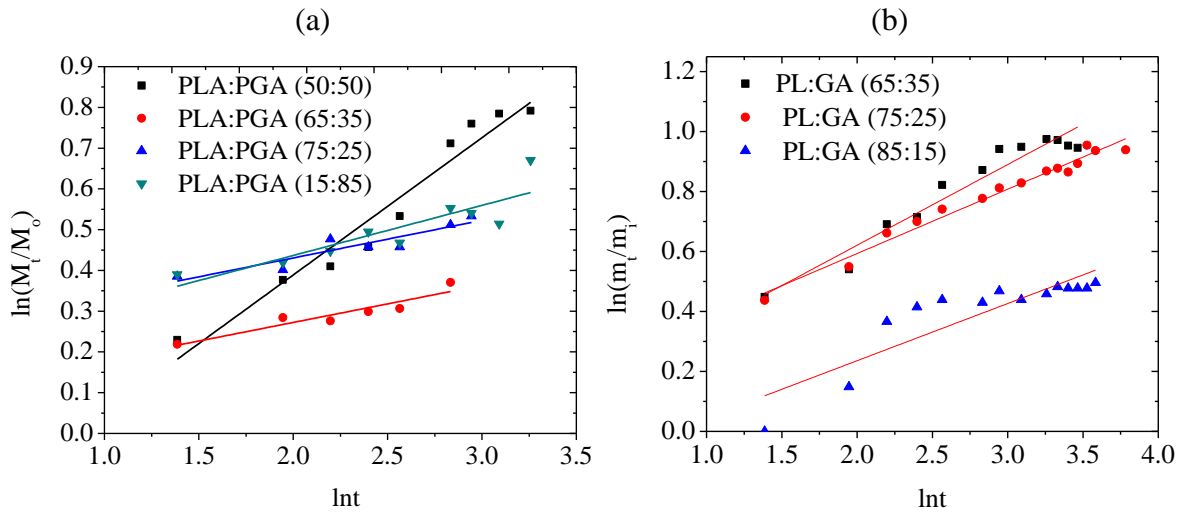


Figure 6.7: Determination of the initial Diffusion Rate from PLGA-based Polymers; (a) Encapsulated with PG and (b) Encapsulated with PT.

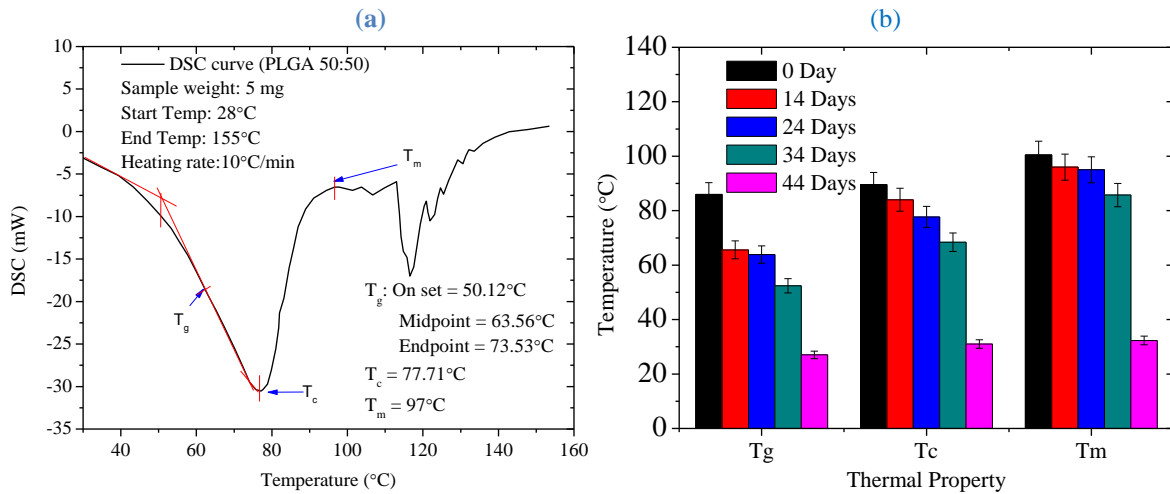


Figure 6.8: Thermal Characteristics of PLGA-based minirods incubated in PBS at 37°C Under Mechanical Shaking (60 rpm): (a) PLGA 50:50 Loaded with PG for 24 days and (b) Decrease in Thermal Properties with Increase in Incubation Time.

Table 6.1A: Preparation of Drugs Solutions into Working Concentrations.

Drug/sample	Initial dissolution	Final dissolution (Topped up with)	Final Concentration
0.1 g of Paclitaxel	2 ml DMSO	38 ml PBS	2.5 mg/ml (DMSO:PBS) (5:95 %)
0.1 g of Prodigiosin	2 ml methanol	38 ml PBS	2.5 mg/ml (Methanol:PBS) (5:95 %)

Table 6.1B: Ratios of Polymer, Drug and PVP Used in PLGA-Drug-Based Minirods Formation.

	Polymer	Drug	PVP
Amount (g)	1	0.1	0.2
Percentage (% w/w)	77	8	15

Table 6.2: Polymer Degradation and Drug Diffusion Terms at 37°C in PBS pH “7.4”.

Polymer Ratio (PLA:PGA)	Decay Term (k_1)	K_2 1/(-k_1)	Half-life of Polymer ($t_{1/2}$)	Offset y_0	Degradation rate, $k = k_2/t_{1/2}$ mg/day	Half-life of Drugs Release
50:50 in PG	-24.05	-0.042	50	0.0259	0.832	16.9
65:35 in PG	-68.799	-0.015	70	0.4621	0.208	6.1
75:25 in PG	44.332	0.023	130	-0.1411	0.174	4.4
85:15 in PG	-50.839	-0.020	170	0.00291	0.116	3.8

Table 6.3: Summary of Encapsulation Efficiencies and Drug Loading for PLGA-Based Polymer.

Polymer Ratio (PLA:PGA)	Drug Encapsulation Efficiency (DEE%)	Drug Loading Content (DL%)
50:50 in PG	92.00	3.8
65:35 in PG	82.10	2.53
75:25 in PG	56.20	3.60
85:15 in PG	43.00	5.43
65:35 in PT	89.10	4.82
75:25 in PT	62.1	3.83
85:15 in PT	50.00	3.77

Table 6.4: Initial Diffusion Terms for the Initial Burst Release of PG and PT from PLGA-based Polymers.

Polymer Ratio in PG	Released Exponent (n)	Geometric Constant (k)	Diffusion Coefficient $\times 10^{-6} \text{ m}^2/\text{s}$
50:50 in PG	0.34	1.33	14.77
65:35 in PG	0.09	1.09	17.95
75:25 in PG	0.09	1.28	25.11
85:15 in PG	0.12	1.21	23.77
65:35 in PT	0.33	0.14	22.70
75:25 in PT	0.25	0.02	2.00
85:15 in PT	0.19	0.15	22.70

7.0 Perspectives and Conclusions

The work in this dissertation was focused on developing strategies for regional cancer drug delivery, especially in localized breast cancer drug delivery. The work demonstrated to a large extent, the significance of polymeric drug delivery systems that are capable of achieving controlled drug release. The materials issues associated with localized drug release have been elucidated and the research was carried out in the following steps:

We presented the results for the swelling kinetics of P(NIPA)-based hydrogels using weight gain experiments with bacterial-synthesized prodigiosin for localized cancer drug delivery (Chapter 3). The swelling due to the uptake of prodigiosin by P(NIPA)-based hydrogels at temperatures between 28-48°C was investigated. This is a temperature range that might be encountered during the implantation of biomedical devices for localized cancer treatment via drug delivery and hyperthermia. The mechanisms of drug diffusion and swelling of P(NIPA)-based hydrogels from the polymer matrices were elucidated.

The swelling kinetics revealed a considerable shift in the swelling ratios of P(NIPA)-based hydrogels. The differences in the swelling kinetics were due to the ionic concentration in the different drug solutions. Moreover, the osmotic pressure or chemical potential energy balance within and outside the gel network was also a contributing factor that affects the swelling properties of the gels. Thus, at equilibrium state, the sum of the osmotic pressure regarding to the mixing, rubber elasticity and ion interaction equals to zero. This implies that a decrease in the chemical potential of the swelling system directly affects the total volume uptake. Statistical analyses were carried out on the variations in data using one-sample T-test and or a paired T-test depending on the data. The implications of the results were then discussed for the design of implantable biomedical devices in which P(NIPA)-based hydrogel can be encapsulated as a drug carrier for localized treatment of breast cancer.

Poly-di-methyl-siloxane packages with well-controlled micro-channels and drug storage compartments were fabricated along with drug storing polymers produced from non-resorbable P(NIPA)-based hydrogels by free radical polymerization (chapter 4). This study considered the kinetics of prodigiosin release from micro-channelled implantable biomedical devices for localized cancer drug delivery. The mechanisms of drug release were studied at temperatures that are relevant to cancer treatment. Combination of diffusion and microfluidics concepts were then used to model the flow of fluid/drug through the micro-channels in the implantable device. The experiments established drug release rates from micro-channels with different lengths. The channel lengths can be used to manage the initial burst release of drugs from the devices into a tumor tissue. Drug release was largely controlled by natural diffusion across the channel lengths. However, a balanced approach is required for the design of an optimal channel length. The implications of the results were then discussed for localized treatment of cancer via hyperthermia and controlled delivery of prodigiosin from encapsulated P(NIPA)-based devices.

Controlled release of cancer drugs (paclitaxel and prodigiosin) from an implantable biomedical device on the effect of cell viability was presented in chapter 5. The cytotoxicity of cancer drugs were studied to developed the dosage ranges required for localized chemotherapy. The effects of localized release of drugs on cell viability were elucidated via clonogenic assay on MDA-MB-231 breast cancer cell line. The results were validated using models to establish the effective diffusivity of fluid/prodigiosin released from implanted device into a surrounded scaffold that mimicked cancer tissue. The trends in the results were analysed using statistical models before discussion their implications for localized treatment of breast cancer via hyperthermia and controlled drug delivery.

Biodegradable and bioresorbable minirods were moulded from polymers: poly(lactic-acid)-co-poly(glycolic-acid) with different ratios. Polyvinylpyrrolidone was used as a cross-linker which also ensured good binding between the drug and polymer (This was presented in chapter 6). The rates of polymer degradation were significantly affected by the polymer ratio and molecular weight. Cumulative release of drugs for an extended duration was achieved via varying the polymer ratio, especially those containing high concentration of lactic-acids. The PLGA-based millirods revealed distinct structural changes with different degradation rates during the *in vitro* experiment. These results provided important insights for the design and selection of biodegradable polymers for biomedical applications. It is therefore recommended that further investigation on the influence of structural changes and mechanical degradation in the design of a multimodal drug delivery system for a sustained controlled release for 4-6 month. These are currently some of the challenges for future work.

The porous structures of the 3-D scaffolds in addition to the encapsulated micro-channel devices enhanced controlled release of drugs. The proposed method of localized drug delivery ensure the total quantities of drug needed for therapeutic treatment of cancer could be much less than those required for bulk systematic drug. Hence, the potential side effects of localized cancer drug delivery could be much less than those associated with bulk systemic chemotherapy.

In conclusion, the research in this dissertation clearly presented the results from *in vitro* experiments from conceptual ideas geared toward *in vivo* biomedical applications.

7.1.0 Recommendations for Future Work

7.1.1 Surface Modification and Cell Adhesion

Previous work on cell culture (chapter 5) indicated poor growth and adhesion of human cancer cells to the surfaces of the biomaterial (PDMS). This call for experiments to be conducted on surface modification of the PDMS in order to examine the surface effects on cell morphology during cell cultures. The substrate could be coated with fibronectin, collagen or Bovine Serum Albumin (BSA) to enhance surface morphology. It is most likely that the adsorption of proteins on the surface of PDMS could increase by achieving improved surface roughness.

The topography and stiffness of PDMS also have an effect on the microenvironment regarding the differentiation of human epidermal stem cells and mesenchymal stem cells. Several techniques exist to modify the surface of the biomaterial. These include: boiling PDMS slabs in deionized water, oxygen plasma treatment, UV-ozone radiation, self-assembled monolayer coating, or polymer/peptide grafting techniques and surface texture with gold (Au) or extracellular matrix (ECM). The modified surface of the biomaterial could enhance cell/surface interaction. Experiments could be conducted to examine pre-stretch effects of PDMS, while coating PDMS with Au, fibronectin, collagen BSA and extracellular matrix (ECM) to enhance cell orientation and adhesion.

7.1.2 Mechanical Characterization of Polymers

Mechanical characterization of the polymers should be well studied to enhance their incorporation into tissues as biomaterials. Even though the P(NIPA)-based hydrogels have shown excellent drug loading competence [1,2,3,4], their use for drug delivery have been mainly imperfed by poor mechanical properties [5]. It is therefore recommended that more

work should be carried out to strengthen these properties while maintaining their porous structures.

7.1.3 Design of a Novel Degradable Implant

Concerning the degradable implants, a multimodal device can be designed to incorporate different copolymer ratios. This will take care of the initial burst effect and as well ensure prolonged and sustained release of cancer drugs. Proposed designs for the multimodal implants are shown below (Figs. 7.1a-c). The copolymers with low PLA ratio (50:50 and 65:75) have higher degradation rate which can ensure the early time concentrations are met as they are susceptible to degrade and release drug quicker (they have low molecular weights), while those polymers with higher amount of lactic acid (eg. PLGA 75:25 and 85:15, they have higher molecular weights) can ensure that an extended time of drug delivery for 4-5 months is ascertain. Future work(s) should also incorporate the activity of enzyme(s) in the degradation process.

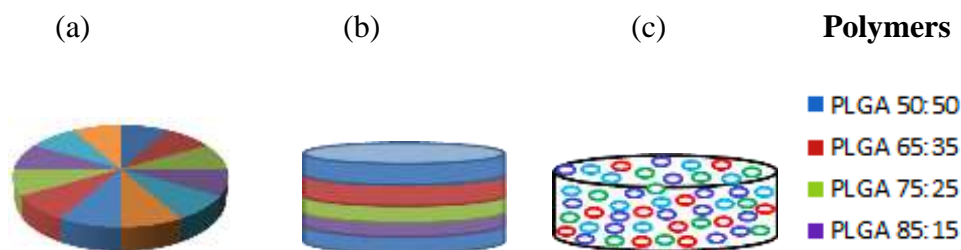


Figure 7.1: Schematics of Novel Biodegradable Drug Delivery Systems.

7.1.4 Animal Trials

In other to develop a system that will model the entire metastatic process, it is recommended that animal trial should be carried out. In doing so one can inject aggressive

basal MDA-MB-231 human breast carcinoma cells orthotopically into the mammary fat pads of severely immunocompromised NOD *scid* gamma (NSG) rats and then, monitor the rats for the development of a primary xenograft tumors. The rats can be sacrificed when a tumors reaches about 10% of body weight (day 53 post-injection) and then study tumor shrinkage with different drug concentrations on loaded biomedical device. The study can then continue to examine tumor shrinkage with loaded biomedical device with chemotherapy drugs at 43°C. This temperature takes care of both hyperthermia and drug delivery. Finally, a histopathology study could be done on the tumor tissues including other organs such as the liver, kidney, etc, to identify the active components of cancer drugs. The results from sections of tumors can further be analyzed with a florescent microscope and HPLC to determine the amount of drug present in sourrounding tissues. These are clearly some of the challenges for future *in-vivo* work.

7.2 Bibliography

- [1] Y. Oni, C. Theriault, A. V. Hoek and W. O. Soboyejo. Effects of Temperature on Diffusion from PNIPA-Based Gels in a BioMEMS Device for Localized Chemotherapy and Hyperthermia. *Mater. Sci. and Eng. C*. 31 (2011) 67-76.
- [2] Y. Oni and W. O. Soboyejo. Swelling and Diffusion of PNIPA-Based Gels for Localized Chemotherapy and Hyperthermia. *Mater. Sci. and Eng. C*. 32 (2012) 24-30.
- [3] Y. Danyuo, S. Dozie-Nwachukwu, J. D. Obayemi, C. J. Ani, O. S. Odusanya, Y. Oni, N. Anuku, K. Malatesta, W. O. Soboyejo. Swelling of poly(N-isopropylacrylamide) P(NIPA)-based hydrogels with bacterial-synthesized prodigiosin for localized cancer drug delivery, *Materials Science & Engineering C* 59 (2016) 19-29. (Available online 28th September 2015).
- [4] Y. Danyuo, J. D. Obayemi, S. Dozie-Nwachukwu, C. J. Ani, O. S. Odusanya, Y. Oni, N. Anuku, K. Malatesta and W. O. Soboyejo. Prodigiosin Release from an Implantable Biomedical Device: Kinetics of Localized Cancer Drug Release. *J. of Mater. Sci. and Eng. C*. Vol. 42, (2014) 734-745.
- [5] E. Vallés, D. Durando, I. Katime, E. Mendizábal and J. E. Puig. *Polymer Bulletin*. 44 (2000) 109-114.